RCA Engineer
Vol. 27 No. 3 May/June 1982

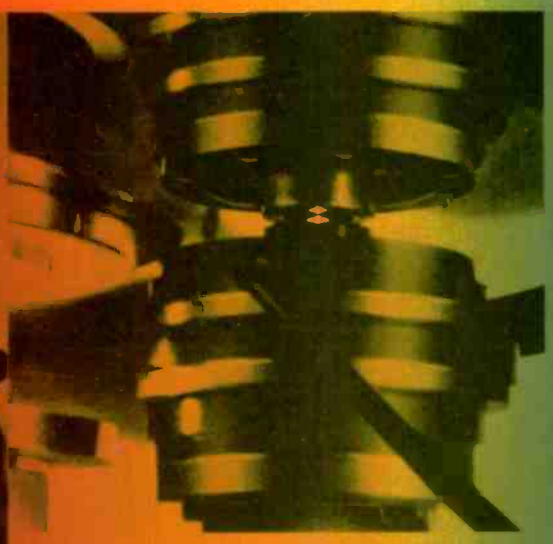

# ELECTRO-OPTICS
## Covering the Spectrum

**Cover design** by Phil Montella, RCA Automated Systems

Our cover shows RCA technologies that span the electro-optics spectrum from the infrared, through the visible to the ultraviolet wavelengths. Depicted technologies are the infrared-camera system from RCA Laboratories and RCA Automated Systems, developed to use the infrared charge-coupled-device staring focal-plane array; the optical video disc system, from RCA Laboratories and Government Systems Division's Advanced Technology Laboratories, that uses argon laser light for ultra-high data rate, high-density-storage applications; and photomultiplier tubes (C31000 and C31000M), from Solid State Division, that are sensitive in the ultraviolet end of the spectrum.

People throughout the Corporation contributed their resources to this cover, including: Automated Systems' Ken Palm, Paul Seeley, Dale Sherman, Charlie Morrissey, and John Phillips; Britt Bailey (New York); Don Reed and Jim O'Brien (Lancaster); Don Norton (Cherry Hill); and Ed Masters (Camden).

*—MRS*


# RCA Engineer

A technical journal published by
RCA Research and Engineering
Bldg. 204-2
Cherry Hill, NJ 08358
TACNET: 222-4254 (609-338-4254)





• To disseminate to RCA engineers technical information of professional value • To publish in an appropriate manner important technical developments at RCA, and the role of the engineer • To serve as a medium of interchange of technical information between various groups at RCA • To create a community of engineering interest within the company by stressing the interrelated nature of all technical contributions • To help publicize engineering achievements in a manner that will promote the interests and reputation of RCA in the engineering field • To provide a convenient means by which the RCA engineer may review his professional work before associates and engineering management • To announce outstanding and unusual achievements of RCA engineers in a manner most likely to enhance their prestige and professional status.

C. David Decker

# Electro-optics: Insight into the future

The union of optics, quantum physics, and electronics known generically as electro-optics is one of the most active and fruitful areas of modern research and development. In the twenty-two years since the first laser was demonstrated, the development of coherent optical sources has spawned a vast array of new applications.

Since laser sources can be focused to spot sizes corresponding to the wavelength of light, high-density digital optical-disc memories are possible. Wide-bandwidth low-loss optical fibers are a reality and, together with solid-state semiconductor lasers and photodetectors, they make possible high-capacity optical-communications links possessing great protection against electromagnetic interference. Materials with certain nonlinear optical properties can switch states in $10^{-14}$ to $10^{-15}$ seconds—far faster than pure electronic processes. Devices based upon optical bistability may in the future permit all-optical logic and data processing.

Continued development of both passive and active electro-optical sensor systems is making possible new capabilities in imaging systems and remote detection devices. "Active" laser radar, or lidar, systems based upon Raman scattering or differential absorption are being developed for satellite operation. "Passive" infrared detector arrays are being incorporated into camera systems for a multitude of applications.

The entire RCA community can take great pride in our past contributions to this highly competitive field. The articles in this issue are a sampling of some of the current efforts in electro-optics. The future of RCA rests on the development and exploitation of disciplines like electro-optics, to discover the wonders of nature and to apply these discoveries in creative ways to satisfy human needs.

*C. David Decker*
Director, Advanced Technology Laboratories
Government Systems Division

RCA Engineer

Vol. 27 | No. 3 May | June 1982

## in this issue ... electro-optics

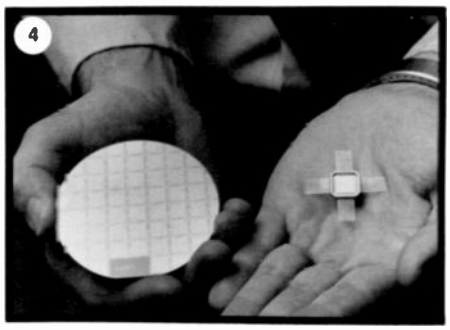


■ **Ettenberg:** *"The common link between the systems and devices described in this issue is not only that they use light to produce individual systems superior to their magnetic or electronic counterparts, but that they provide an integrated system of information storage and retrieval."*

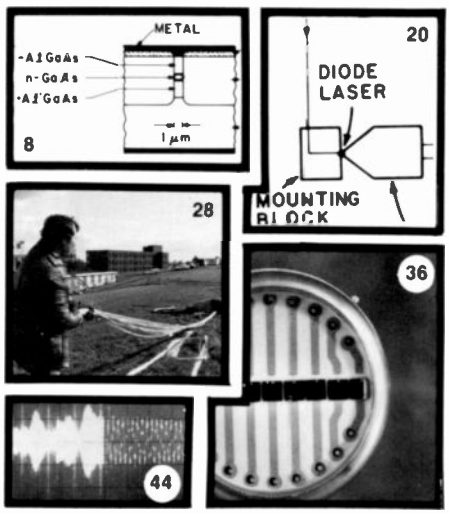


■ **Botez:** *"Diode lasers have come a long way since their discovery two decades ago."*

■ **Bartolini:** *"The development of the high-power single-mode diode laser and compatible optical recording media has increased the probability of an optical disc product in the mid-1980s time frame."*

■ **Ainsbury:** *"RCA Systems Services tendered for a Ministry of Defense contract to design and install a fiber-optic communications system, to link computers in three separate buildings."*

■ **Ammon/Reno:** *"The high storage densities associated with diffraction-limited optical systems provide a cost per recorded bit that is an order-of-magnitude lower than with any other media."*

■ **Altman, *et al.*:** *"Remote sensing by lidars makes possible many important measurements that cannot be adequately carried out by presently used passive sensors."*

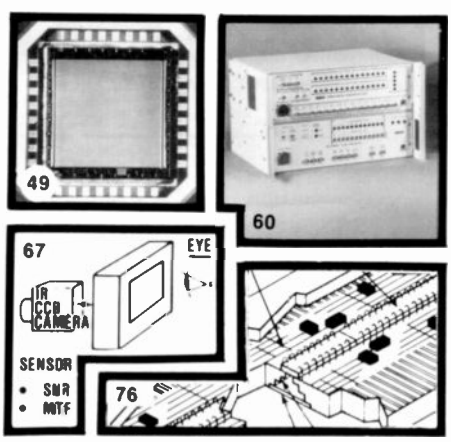


■ **Kosonocky, *et al.*:** *"The monolithic Schottky-barrier IR-CCD focal-plane arrays represent the only infrared array technology that is compatible with standard IC processing."*

■ **Klein, *et al.*:** *"The sensor has successfully demonstrated that it can 'see' through smoke, haze and dust."*

■ **Cantella:** *"Theoretically and experimentally demonstrated characteristics of Schottky-barrier focal-plane arrays indicate great potential for Government and commercial applications."*

■ **Warren, *et al.*:** *"The high yield and maturity of this silicon-based technology may make it the only viable choice for the next generation of NASA earth-resource satellites."*

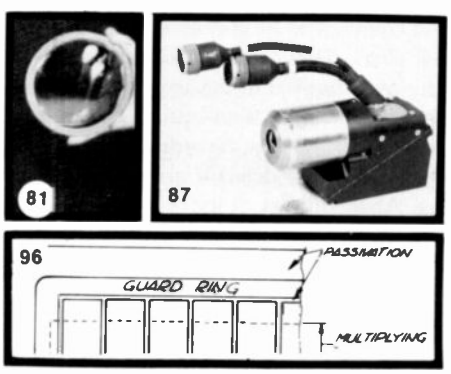


■ **Neuhauser:** *"In 1981, RCA entered into its first venture in Saticon-tube manufacture when it developed the 13-mm (1/2-in) Hawkeye camera tube—the BC4398."*

■ **Arlan:** *"The first-generation electro-optical multiplexer developed for the U.S. Army Night Vision Laboratory formed the basis for a low-power, miniaturized, high-performance TV sensor."*

■ **Webb/McIntyre:** *"One advantage of the reach-through avalanche photodiode structure is that it can be made with a high quantum efficiency for wavelengths ranging from the near ultraviolet to beyond one micron."*

## in future issues...

anniversary issue
microwave technology
modelling, simulation, and analysis

M. Ettenberg

# Some of the new optoelectronic systems

*A plethora of imaging devices, coupled with the microcomputer revolution, has created a need for very large data- and image-communications and storage systems.*

**Abstract:** *This article describes some of the new optoelectronic systems RCA is developing. Described in some detail—their operation, limitations, competition, and commercial and research status—are optical recording and fiber-optical communications.*

A major portion of RCA's businesses involves optoelectronics, which may broadly be defined as the conversion of electronic energy into light energy or back again. This introductory article deals with solid-state devices and systems that employ this conversion, and therefore omits conventional television. Instead, it emphasizes some of the newer devices and systems that are going to become large military and commercial businesses within the next few years. These systems and their applications, discussed in this issue of the *RCA Engineer*, include fiber-optical communications, optical disc recording, and imaging by means of detector arrays and ranging. Also, authors of independent articles discuss two of the more important devices—high-power diode lasers and avalanche photodetectors—that are the newest and key ingredients for these coming systems. The driving force creating this new technology is the demand for systems with greater sensitivity, speed, and reliability at lower cost and with some functions not heretofore achievable.


Final manuscript received March 9, 1982.
Reprint RE-27-3-1

## Imaging detector arrays

The switch from vacuum tubes and mechanically scanned linear arrays to CCD (charge-coupled device) focal plane arrays for imaging was obviously a step in that direction. A focal plane array is a two-dimensional array of detectors set in the focused plane of an optical system (film in a camera is located in the focused plane of *that* optical system). The CCD allows the collected charges (electrons generated by the light) in the detectors to be transferred to collector lines along the periphery of the device, replacing wire pairs that would otherwise be required for each of the thousands of detectors. This development was a natural combination of VLSI and detector technology; its success depended on the fine control of silicon and its processing steps to create a large-area device containing tens of thousands of individual devices. Each device not only works as it must in an integrated circuit, but it must operate with the uniform linear analog properties of a detector. Unlike integrated circuits for digital applications, where the circuit element is either on or off (1 or 0), the detector element in a CCD array must transfer a charge proportional to the impinging light intensity.

Inexpensive solid-state imaging devices sensitive to the visible and infrared wavelengths allow us not only to sense but to reproduce images of both moving and stationary objects. Moreover, solid-state devices can operate in environments otherwise inaccessible to vacuum imaging tubes because of tube size, cost, or reliability.

The availability of a plethora of imaging devices, coupled with a microcomputer revolution that places very large processing power at everybody's fingertips, has created a need for large data- and image-communications and storage systems. For example, a digitized color television channel communicates over 200 Mbits/s and requires a storage medium with a terabit ($10^{12}$ bits) of capacity for one hour of such information. This need can, and will, be satisfied by optical fiber communications and optical disc recording. In this article, I discuss optical fiber and optical disc technologies; how they work, their limitations, the competition, and the commercial and research status.

## Optical fiber technologies

In essence, optical fiber communication is simple: Signals are sent through a transparent glass or plastic fiber by turning a light on and off and detecting the light's presence at the other end of the fiber. This system operates best digitally because of the nonlinearity between the electrical signal input and the light-source intensity. Frequency-modulated (FM) signals can also be transmitted by modulating the length of time the light is on. The fibers are thin (about the thickness of a human hair) to conserve the relatively costly pure silicon dioxide ($SiO_2$) from which they are

**The ultimate storage medium.** On a single 12-inch disc, the entire *Encyclopaedia Britannica* or 50,000 still photographs can be recorded and stored for instant access. To make an optical disc recording, a bright beam of laser light is focused onto a spinning disc, melting a pattern of tiny "pits" in the disc material. The recorded information is played back not with a diamond stylus, but with a weaker beam from the same laser. Such factors as the minuteness of the recorded bytes, and a turntable speed of 1,800 rpm, allow for at least 100 times the storage capacity of magnetic tape.

made and because the fatter the fiber, the more the light pulse spreads as it travels in the fiber. This spreading or pulse dispersion arises when light reflects at various angles along the fiber so that, within the same fiber length, light reflecting at relatively large angles (higher-order modes) takes longer to arrive at the detector at the other end than light traveling at lower angles or going straight through (lower-order or fundamental mode).

The ultimate fiber systems, which are not yet commercially available, use single-mode fibers whose light-carrying core is only about one wavelength wide ($\sim$4 $\mu$m). In a single-mode fiber the light can travel only straight through, and no light-pulse broadening occurs. Many gigabits/second ($10^9$ bits/s) can be transmitted over tens of kilometers with such fibers. Of course, coupling light from a source and connecting such fibers are extremely difficult mechanical tasks and thus the common commercial application of single-mode fiber systems is still in the future.

Solid-state light sources and detectors were being developed before the advent of low-loss fibers, but compatible size and reliability made them natural partners. Detectors, primarily silicon devices, are of two types: *pin* and avalanche. In a *pin* detector, light is transformed into electrons, as in a solar cell. A bias of a few volts is applied to help speed up the electron removal. The avalanche detector, the ultimate solid-state detector, is operated with a high bias. The high electric field within the detector causes electrons created by photons to bang into other electrons, creating a multiplication of electrons, and thereby achieving internal gain. Such detectors are almost ideal and can detect photons nearly down to the one-photon level. Both detector types are quite sensitive and, depending on the data rate, can accurately determine the presence of a pulse with nanowatts of light power and at pulse lengths of a nanosecond ($10^{-9}$ s) or less. The limitation of the avalanche detector is that it requires more expensive and complicated circuitry that accurately maintains relatively high voltages (100 to 300 V) and that must track the avalanche voltage region with temperature.

Light sources also come in two types, LEDs or diode lasers. LEDs can couple about 100 $\mu$W or so into a fiber; lasers can couple many milliwatts into the fiber. Both LEDs and lasers are diodes of III-V

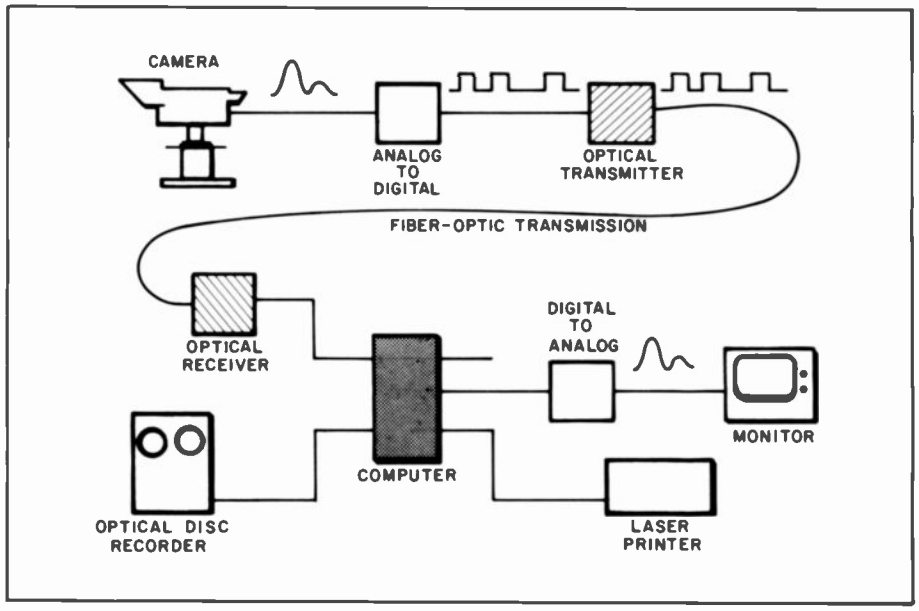


**Fig. 1. Total systems concept for the future use** of optical components in broadcast studios or offices (the studio would not need a printer).

(GaAs, AlGaAs, InGaAsP, InP) channel compounds that, when forward biased, create photons. The driving electronics for these sources are somewhat complicated, and current-controlled rather than common-voltage-source circuitry must be employed due to the LED's or laser's *diode*-type current-voltage relationship. In addition, diode lasers have a threshold current so that the driving circuitry must not only be current controlled but must also provide a modulated current containing the information signal, riding on a dc-current bias that just exceeds the threshold. Finally, the threshold current of diode lasers are temperature sensitive so that feedback- or temperature-control circuitry is required. Because of their high light intensity, only diode lasers can couple enough light to be useful for single-mode fibers; and because of their narrow spectrum width (potentially much less than 1 angstrom versus 300 angstroms to 1000 angstroms for an LED) and fast switching capability (less than 1 nanosecond versus a few nanoseconds for an LED), only lasers can be employed for systems operating at data rates exceeding 100 Mbits/s. The spectral width of the source is important because of light-pulse-width broadening in the fiber. This effect is called wavelength or material dispersion, since different wavelengths "see" different indices in $SiO_2$ and thus travel at different velocities within the fiber.

Finally, to complicate the situation, fiber-optics applications exist in two wavelength regimes: one at approximately 0.8 $\mu$m, which uses (AlGa)As light sources and Si detectors; and one in the 1.3- to 1.6-$\mu$m regime, where emitters and detectors are made of the III-V compound InGaAsP. Although the (AlGa)As-source and Si-detector combination at 0.8 $\mu$m was developed first, improvements in fiber purity have allowed lower losses at the longer wavelengths. For example, at 1.55 $\mu$m, fiber losses of only 0.2 dB/km have been achieved. In such fibers, the light is not yet diminished 3 dB (half intensity) after a 10-km run. Such low losses allow for repeaterless runs exceeding 100 km. Sources at various wavelengths within the wide spectral window of the fibers also permit wavelength multiplexing within the same fiber. Wavelength multiplexing is potentially a powerful tool allowing simultaneous, multiple high-bandwidth channels to flow down the same fiber without the need for even faster multiplexing electronics. This expensive and power-consuming electronics is replaced with simple light sources at various wavelengths and with filters in front of the detectors.

Fiber-optics-based systems compete now with metal-coaxial-cable-based systems and in the future, when costs are further reduced, they will compete even with twisted-pair systems. Fiber optics is a more complicated system than coaxial cable due to the addition of active optoelectronic components at the ends. In addition, connectors and taps are not fully developed and require more mechanical precision than their coaxial counterparts. However, fiber-optics systems are immune to electromagnetic interference and radiofrequency interference, provide electrical isolation and, because of their low leakage loss, are relatively secure from tapping. Because they are small in diameter and have low leakage, many fibers can be placed in a single cable without cross talk. These features are important for many applications, but the major reasons that fiber optics will dominate the cable communications field is their broad bandwidth and low loss. Current commercial multimode fiber-optic links have a bandwidth-distance product of a GHz-km or better, with losses as low as 1 dB/km, while single-mode fiber can have distance-bandwidth products 100-times larger with even lower losses. The ultimate bandwidth of fiber-optics systems is limited only by the frequency of light, approximately $10^{14}$ Hz/s (~1-billion telephone circuits).

## Optical disc technologies

The basic principles of optical disc recording systems are also simple. The system uses conventional microscope optics to focus a laser spot and create a mark on a rotating disc surface. This mark can be read later by the same or similar laser at lower power. Again, we require a light source and detector. Because the system is larger, we can afford to employ a large helium-neon or argon laser but the solid-state (AlGa)As diode laser is the preferred source. Silicon avalanche or *pin* diodes are the detector elements. The smallest bit element (usually a melted pit on the disc surface) is basically set by the diffraction-limiting resolution of the light, of the order of 0.5 $\mu$m, so that $2 \times 10^4$ bits/cm can be recorded along a track at a density of greater than $10^8$ bits/cm$^2$ (more than $10^{10}$ bits for a 30-cm-diameter disc). If we spin a 30-cm disc at 30 rps, then a data rate of approximately 50 Mbits/s is achieved. In addition, anyone who has looked through a microscope knows that the field of view is many hundreds of micrometers so that multiple spots can be observed and/or recorded at one time. Multichannel recorders are being developed (as discussed in this issue) with the same optics as in the single-channel modes but with individually addressable linear arrays of light sources and detectors. For a system which uses a high-power argon-laser light source, this means separating the one beam into multiple paths by diffraction and then sending the multiple beams through a multichannel acousto-optic modulator. For diode lasers, multichannel recording can be done by employing an array of individually ad-

dressed diode lasers, and progress toward such an array is being made. Arrays of up to 20 devices imaged through the same optics are reasonable, and gigabit/s ($10^9$ bit/s) recorders are now in the design stage.

The optical disc medium consists of a flat plate of aluminum, glass, or plastic on which a thin coating (a few hundred angstroms) or multilayer coatings of organic, inorganic, or metallic materials are applied. The coatings are designed to melt, blister, or vaporize when approximately 10 mW of laser power is focused into a 1-$\mu$m spot on their surface (the temperature reaches approximately 1000°C when the laser is writing, depending somewhat on the power directed into the spot and the heat loss in the media). Due to losses in the optics, 20 to 40 mW is required at the source. The hole or bubble is a permanent mark that can be read at a much lower power level (approximately 1 mW). The approximately 10-mW recording level is required because the recording-layer materials are stable at room temperature and, more important, at the ~1-mW readout power levels that may heat the disc locally to about 100°C. The use of magneto-optic effects or crystalline-to-amorphous phase changes also makes erasable recording possible.

Because of the thinness and the relatively low melting points (for good sensitivity) of the films forming the active media, the disc shelf life with respect to corrosion or other similar degradation is still a problem and an active area of development.

Today, optical discs have recording densities and per-track data rates approximately 100 times that of the highest-density magnetic-disc recorders. To record and read back such small spot sizes, the lens must focus on the disc and the particular track within the tolerance of the pit size, which is about 0.5 $\mu$m. This focusing is done by active servos, that is, a voice coil for the focus lens and a galvonometer mirror for the spot mirror. In the case of magnetic recording, the density is achieved by direct mechanical tolerances and flying heads almost in contact with the disc. Due to these close mechanical spacings and tolerances, the high-density magnetic discs are not removable and must be sealed in the so-called Winchester configuration to exclude dust. Dust in the optical system can be kept out of focus by applying an overcoat to the disc surface.

Although magnetic-disc-based systems could theoretically approach optical recording speeds and densities, the increased mechanical complexity and the restrictions on the disc materials and preparative techniques to produce mechanically smooth and defect-free magnetic discs at the required density favor the optical technique for very-high-data-rate, high-density storage. In addition, the permanence, removability, ease of handling, storing and transporting, as well as lower ultimate cost of optical-disc recordings have attracted most major computer and electronic companies to start developing such systems. Detailed descriptions of RCA efforts in this area, where we are a technical leader, are included in this issue.

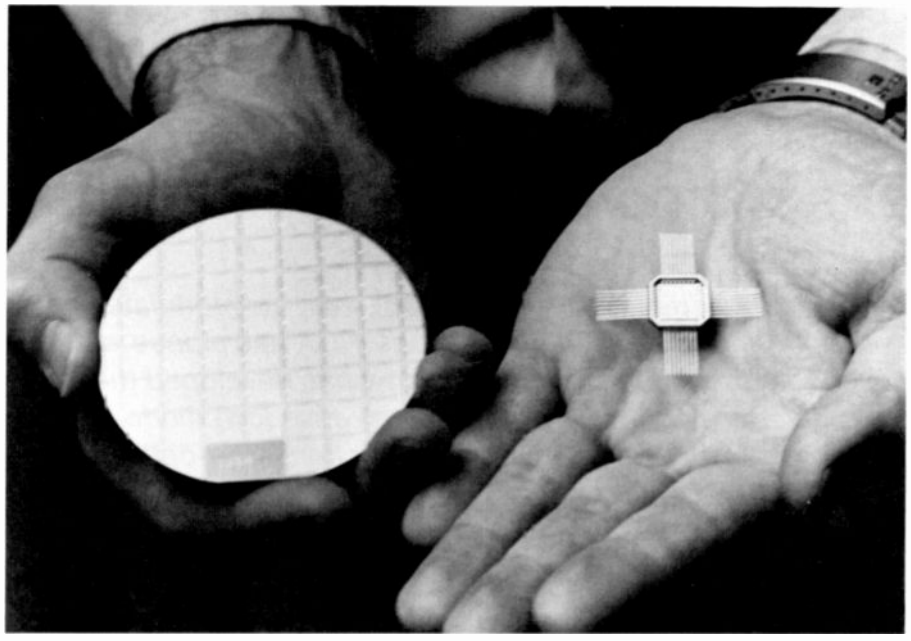

**A processed 3-inch silicon wafer** and a packaged 64- by 128-element IR-CCD array chip.

The common link between the systems and devices described in this issue is not only that they use light to produce individual systems superior to their magnetic or electronic counterparts, but that they provide an integrated system of information storage and retrieval. A CCD solid-state camera for information input, together with a fiber-optic connection to the optical disc recorder (whose stored information can then be printed out on a laser printer connected by a fiber-optic link), describes the key elements of the office of the future without letters, memos, or filing cabinets.

**Michael Ettenberg** is Head, Optoelectronics Devices and Systems Research Group, at RCA Laboratories. He joined the Laboratories in 1969, and has made major contributions in the area of III-V compound synthesis and devices. In the area of material synthesis, he was codeveloper of the multibin liquid-phase epitaxial technique used widely for the growth of multiple-layer heterojunction structures. He has made important contributions to the development of cw injection lasers, which include studies leading to the reductions in laser threshold and the development of dielectric facet coatings. His work on the reliability of laser diodes has included high-temperature degradation studies, reduction of mirror damage by facet coating, the study of the effect of growth conditions on long-term operating reliability, and some of the first studies of reliability in long-wavelength electroluminescent devices. This research has been instrumental in making possible very long-lived LEDs and cw laser diodes for optical communications. He has authored or coauthored more than 90 papers on his work.

Contact him at:
**RCA Laboratories**
**Princeton, N.J.**
**TACNET: 226-3149**

D. Botez

# Single-mode diode lasers for systems-oriented applications

*Single-mode diode lasers are compact, easy-to-modulate light sources for a vast array of applications. RCA has pioneered semiconductor laser research, and now has developed the most powerful single-mode continuous-wave (cw) diode in the world, the constricted double-heterojunction large-optical-cavity (CDH-LOC) laser.*

**Abstract:** *This paper discusses the various ways of achieving single-mode stabilization in diode lasers. Both low-power and high-power devices are presented and discussed with relation to their use in systems applications such as optical recording and optical communications. Emphasis is placed on the operational characteristics of the CDH-LOC laser, an RCA product unmatched in high-power capability.*

Ever since their discovery in 1962, semiconductor diode lasers have been thought of as ideal light sources for a multitude of applications, because of their small size and ease of modulation when compared to gas lasers. The realization of heterojunction devices[1] and proofs of reliable and long-lived continuous-wave (cw) operation[2] (1976-1980) have paved the way toward the use of diode lasers in systems-oriented applications. The simplest cw diode lasers are composed of a multilayered planar geometry with an oxide-defined stripe for current confinement (Fig. 1a). When the diode is forward biased, carriers are injected from *p*- and *n*-type layers into a recombination region where they recombine to give light. Stimulated recombination and cleaved-end mirrors provide light amplification in a resonator. Lasing action occurs when enough carriers are injected to provide the electronic gain needed to overcome the cavity's internal and external losses.

For cw operation at room temperature, low lasing-threshold currents are required, which implies a thin recombination region. In turn, the lasing transverse spot size—which is rather small (0.5 to 1 $\mu$m)—provides a divergent beam of 30° to 40° full-width half-power (FWHP) in the plane perpendicular to the junction. In the plane of the junction, light confinement is controlled by the current flow, and thus the lasing spot is comparable in size to the stripe-contact width. The laser emission is then elliptical (Fig. 1a) with typical transverse and lateral beamwidths, at half power, of 40° and 10°, respectively.

The emitting area on the cleaved facet is defined by the built-in dielectric profile; the emitted light can therefore be thought of as an optical mode of a two-dimensional dielectric waveguide. For use in systems it is important that a single Gaussian-like beam be obtained at all drive levels of interest (that is, stable fundamental optical-mode operation). In reality, stripe-geometry devices, with a few exceptions, generally have an unstable optical mode.

Serious efforts for diode-laser mode stabilization were started in the late 1970s.[3] The basic thrust was to achieve lasers that will operate in a stable fundamental spatial mode to a specified output-power level. With spatial stabilization, it was found that cw oscillation in a single mode in frequency can be obtained as well. That is, the laser oscillates in only one mode of the lasing cavity composed of mirror facets and the two-dimensional built-in dielectric waveguide. Such "single-mode" devices are a definite requirement for long-distance high-data-rate optical communications and other applications such as fiber sensors, holographic printing, and guided-wave signal processing.

Our discussion will cover both single-frequency lasers as well as devices that operate in a stable, single spatial mode. The latter category includes: low-power (3-to 5-mW/facet) lasers for short, low-data-rate optical communication links and, especially, high-power (15- to 50-mW/facet) lasers for optical recording, single- and multimode-fiber data-distribution systems, analog signal transmission, high-speed printing, and space communications.

We shall treat primarily aluminum gallium arsenide (AlGaAs) single-mode devices (0.75- to 0.9-$\mu$m emission region) as they cover very large potential markets: optical recording, short high-data-rate optical links (for example, computer networks), data-bus distribution systems, printing and space communications. The other class of commercially available diode lasers are indium gallium arsenide phosphide (InGaAsP) devices (1.2- to 1.7-$\mu$m emission region) that emit in the low-attentuation-loss and low-pulse-dispersion regions of silica-based fibers,[3] and therefore are needed for long-distance high-data-rate optical communications. InGaAsP single-mode diodes will be briefly discussed with respect to the performance of their AlGaAs counterparts. We start by pre-


Final manuscript received February 26, 1982
Reprint RE-27-3-2

senting the stripe-geometry laser, its problems, and the various principles of lateral-mode stabilization. Then we proceed to describe low-power (3- to 5-mW) and high-power (15- to 50-mW) laser structures and their electro-optical characteristics. Finally, the devices' dynamic behavior as related to their use in systems is briefly discussed.

## Lasing mode stabilization

The simplest type of practical laser diode is the stripe-geometry double-heterojunction (DH) laser[4] (Fig. 1b). Atop a GaAs substrate, four layers are deposited: *n*-type $Al_xGa_{1-x}As$; an *n*, *p*, or undoped "active" layer, $Al_yGa_{1-y}As$; *p*-type $Al_xGa_{1-x}As$; and a $p^+$-GaAs layer for contact. The compositions are such that $x$ is greater than $y$, which gives an active layer of lower energy bandgap ($\Delta E_g \geq 0.3$ eV) and higher refractive index ($\Delta n = n_1 - n_2 \geq 0.2$). Consequently, carriers injected from the *n*- and *p*-$Al_xGa_{1-x}As$ layers are confined to the active layer, where they recombine to produce light. The generated radiation is trapped in the one-dimensional dielectric guide formed by the active layer of thickness $d$ and index $n_1$, and the confining layers of index $n_2$. This waveguide in the plane perpendicular to the junction (the transverse direction) supports only the fundamental mode as long as $d$ is less than 0.4 $\mu$m and $\Delta n$ is greater than 0.2 (see equation (1) below).

For practical diodes, $d$ is typically 0.05 to 0.2 $\mu$m and $\Delta n$ is greater than 0.2, and thus a stable fundamental transverse mode (that is, in the plane perpendicular to the junction) is always the case. By contrast, along the active layer (the lateral plane) the mode confinement is provided by the current flow alone, which, for standard stripe-contact (10- to 15-$\mu$m wide) devices, often results in a series of instabilities:[3, 4] strong nonlinearities ("kinks") in the light-current (L-I) characteristics; pulsations; excess noise; and optical-mode beam shifts. Such behavior can seriously affect or even prevent the use of stripe-contact diode lasers for optical communication systems. As a result, current state-of-the-art laser diodes represent tremendous efforts in recent years to achieve laser-mode stabilization by changing the basic planar-DH stripe-geometry structure.[3]

Two general approaches to stabilization via structural changes have been pursued: tight current confinement; and the creation of a built-in real-index wave-confining structure (waveguide or antiwaveguide as shown in Fig. 2). Tight current confinement to narrow stripes (3 to 7 $\mu$m) results in lasers with "kinkless" L-I characteristics, up to at least 10 mW cw; wide, non-Gaussian beams; and multimode spectra.[5, 6] Only structures with built-in lateral wave confinement have resulted in single-mode lasers; that is, devices that operate over wide ranges of drive current in a stable fundamental spatial mode as well as in a single frequency mode. In a positive-index guide, the guided mode is "proper" or "trapped" in the sense that it is totally internally reflected at the dielectric boundaries (bottom of Fig. 2a). The amount of refractive-index change, $\Delta n$, and the spatial extent of the index variation, $w_0$, are chosen such that the structure supports only one mode—the fundamental one. The first-order-mode cutoff condition is

$$\left(\sqrt{\Delta n}\right) w_0 \leq \lambda / \sqrt{8n} \qquad (1)$$

where $n$ is the averaged refractive index.[4] Equation (1) holds for passive waveguides. In active waveguides, gain-loss considerations can allow stable fundamental-mode oscillation at $w_0$ values that are twice the one given by equation (1).[4] Also, $\Delta n$ should be larger than approximately $10^{-3}$ to overcome the effect of current-induced guiding.

The negative-index guide or antiguide differs from a positive-index guide in that the "guided" modes are "improper." In other words, upon reflections at the dielectric boundaries, part of the light is refracted in the outer regions (bottom of Fig. 2b), and thus the mode will vanish after propagating a finite distance in a passive guide. The refracted light can be thought of as radiation loss, $\alpha_R$:[7]

$$\alpha_R \cong \frac{m^2\lambda^2}{2\, w_0^3 n^2 \sqrt{2\,|\Delta n\,|/n}} \qquad (2)$$

where $m$ is the mode number. The losses for the first-order mode ($m = 2$) are four times the losses for the fundamental mode ($m = 1$). In a passive guide, "leaky" modes cannot be supported for long distances, but in active structures the elec-

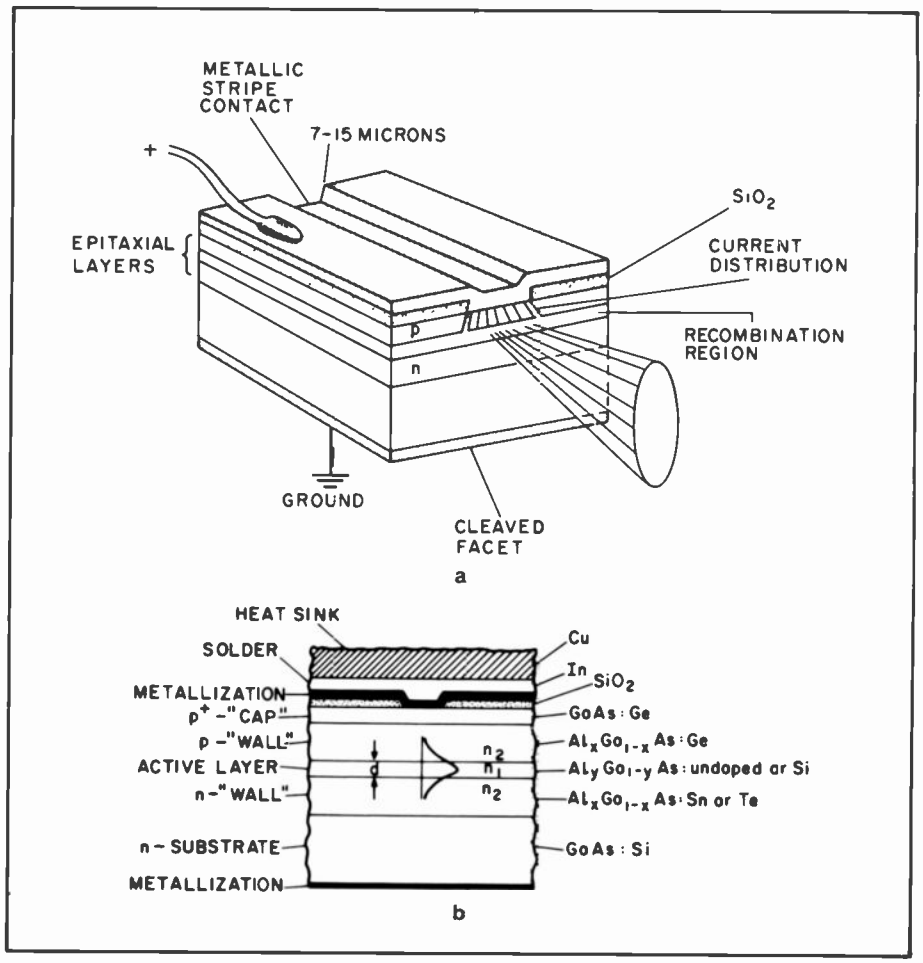


**Fig. 1. Simple cw diode lasers.** Schematic representations of: **(a)** the stripe-geometry double-heterojunction laser structure; **(b)** the cross section of a heterojunction AlGaAs laser ($x - y > 0.25$; $n_1 - n_2 > 0.2$) for cw room-temperature operation. The active layer of thickness $d$ (0.05 to 0.2 $\mu$m) is placed 2 to 3 $\mu$m away from the contact stripe.

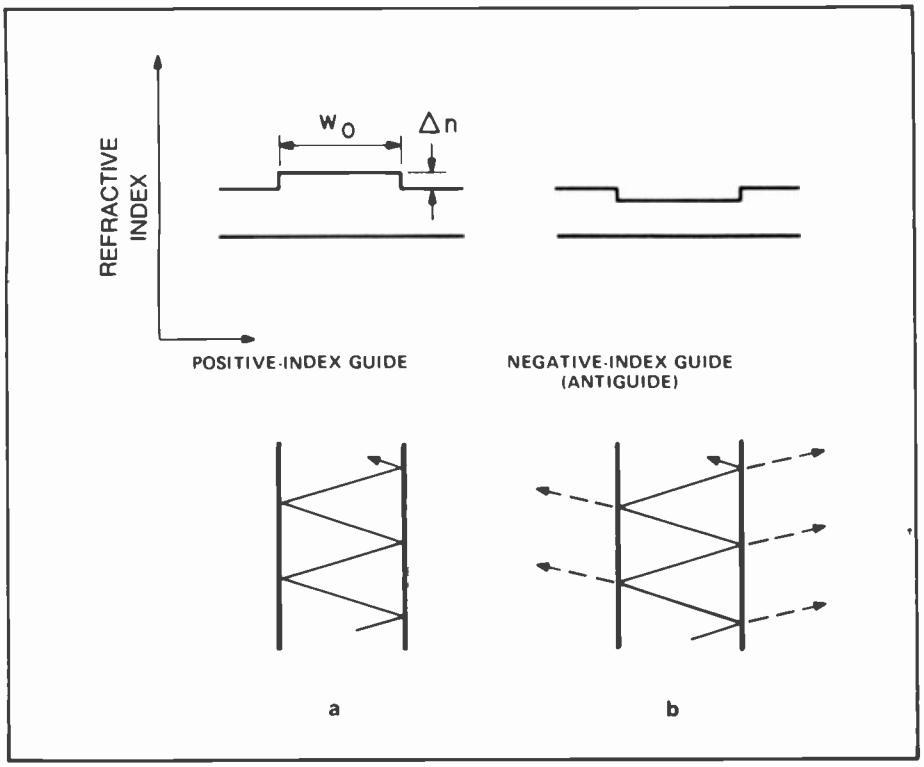


**Fig. 2. Laser-mode stabilization is attempted via changes to the basic planar-DH stripe-geometry structure.** Refractive-index variation in the lateral plane and ray-optic representation of light propagation for: **(a)** positive-index guide; **(b)** negative-index guide (antiguide).

tronic gain can overcome the radiation losses and allow sustained propagation and oscillation of leaky modes. The strong dependence of the radiation loss on the mode number provides discrimination against high-order mode oscillation in some high-power single-mode devices. More complex leaky guides (for example, a combination of Figs. 2a and 2b) can have even stronger discrimination against high-order modes than indicated by formula (2). Variations in refractive index of the types shown in Fig. 2 are "built into" the lateral direction by etch and regrowth techniques,[8] controlled deep Zn diffusions,[9] and one-step liquid-phase epitaxial (LPE) growth over channeled substrates.[10, 11]

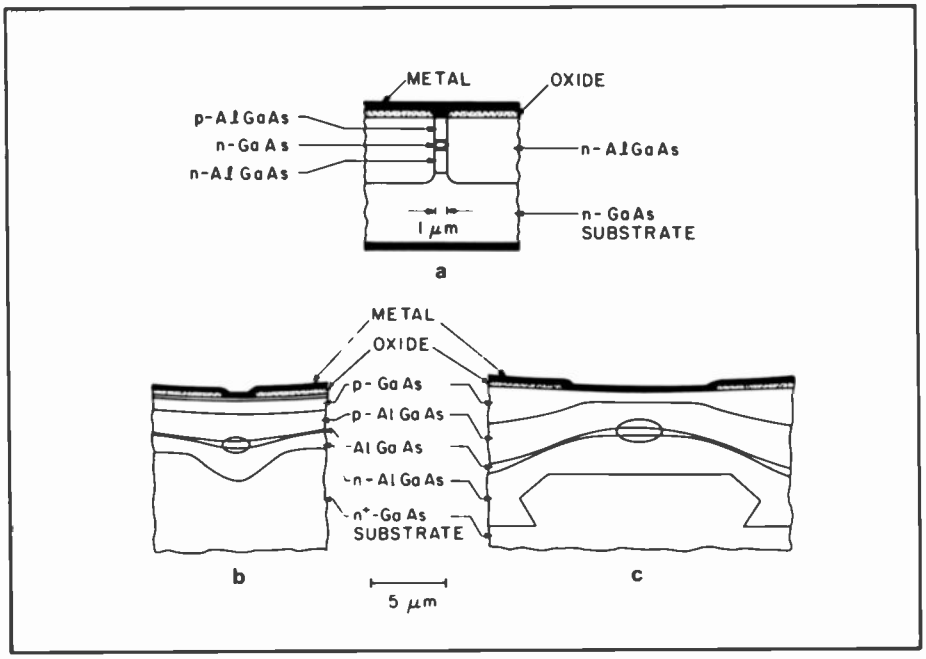


**Fig. 3. Available power is directly related to the size of the lasing spot.** Schematic representations of low-power single-mode laser types: **(a)** buried-heterostructure (BH); **(b)** channeled-narrow-stripe (CNS); and **(c)** constricted double-heterojunction (CDH). The lasing spots are shown to scale in the lateral direction.

## Low-power single-mode lasers

Low-power lasers are devices that can operate reliably at cw output-power levels in the 1- to 5-mW range. The amount of available power is directly related to the size of the lasing spot, since for AlGaAs structures at high powers, the degradation is a function of the power density.[2] As shown in Fig. 3, the spot sizes for various low-power lasers can differ from one device to another; this in turn affects their respective maximum output powers. Three typical cw single-mode lasers are displayed in Fig. 3: (a) the buried-heterostructure (BH) laser;[8] (b) the channeled-narrow-stripe (CNS) laser;[12] and (c) the constricted double-heterojunction (CDH) laser.[13] Mainly due to their spot size, these AlGaAs devices have the following maximum powers for reliable operation: approximately 1 mW for the BH laser; and 3 to 5 mW for the CNS and CDH lasers. Low-power single-mode devices are successfully used for optical disc and audio/video disc readout, optical communications, and guided-wave signal processing.

The BH laser is obtained by first etching a mesa of DH laser material (Fig. 1b) and then "burying" the mesa by LPE growth of low-index high-resistivity *n*-type material. A positive-index guide (Fig. 2a) is then achieved in the lateral direction. Due to very good current confinement, BH lasers have the lowest thresholds (approximately 10 mA) of any type of mode-stabilized device. As a result of the relatively large lateral index differential, however, the mesa width for fundamental-mode operation is rather small (approximately 1 μm). The resulting lasing spot not only limits the device power capability but also provides wide (40° to 50° FWHP) lateral and perpendicular far-fields.

CNS and CDH lasers are devices grown by one-step liquid-phase epitaxy (LPE) over a nonplanar substrate. Due to the LPE-growth dependence on local surface curvature,[13] the active layer assumes a convex-lenslike shape above a substrate channel (Fig. 3b) or above a mesa (Fig.

3c). These lateral variations in thickness are equivalent to lateral variations in refractive index and thus positive-index guides are formed. Since the lateral variation in refractive index is much milder than in BH devices, lasing spots 3-$\mu$m wide are easily attainable. Threshold currents are in the 30- to 70-mA range, and the far-fields are Gaussian and typically 12° by 35° at half power. Single-mode powers up to 10 mW have been reported, and in general, such devices can be operated reliably in the 3- to 5-mW/facet cw-power range. Below we illustrate electro-optical characteristics for the CDH laser, which is an RCA commercial product.

Figure 4a displays cw light-current characteristics and Fig. 4b shows 3-mW spectra for CDH lasers at various heat-sink temperatures. Up to 100°C the threshold current and the slope efficiency vary little with temperature, making the CDH device the least temperature-sensitive commercially available single-mode diode laser. Due to these remarkable characteristics the CDH diode has achieved cw lasing and single-mode operation to the highest ambient temperatures—170°C and 150°C, respectively—ever reported in the literature.

Typical room-temperature cw spectra and lateral far-field patterns as a function of drive are shown in Figs. 5a and 5b, respectively. Single-longitudinal-mode operation occurs at power levels above approximately 1 mW. Mode "hopping" to longer wavelengths as the current is increased above threshold is a consequence of joule heating in the device junction. The transition from one mode to another is not a monotonic function of drive, but occurs rather suddenly (over only 1 to 2 mA in drive current). Between jumps the mode shifts slightly with temperature: 0.5 to 0.8 angstroms per Kelvin. To control mode "hopping" or mode shifting due to ambient temperature changes, one could use thermoelectric cooling. However, at constant heat-sink temperature, shifts due to joule heating can be controlled only by using feedback from external or internal grating structures. The lateral far-field pattern is Gaussian up to approximately 8 mW. Above 8 mW the onset of high-order spatial modes can be observed. Their stability and lack of astigmatism make CDH lasers useful for highly efficient coupling (to 70 percent with no cross-lens) up to 4 mW into single-mode fibers (Fig. 6). By combining a single-mode CDH laser, a single-mode fiber and a GaAs MESFET amplifier, a 500-MHz transmitter module for optical communications has been realized.[14]

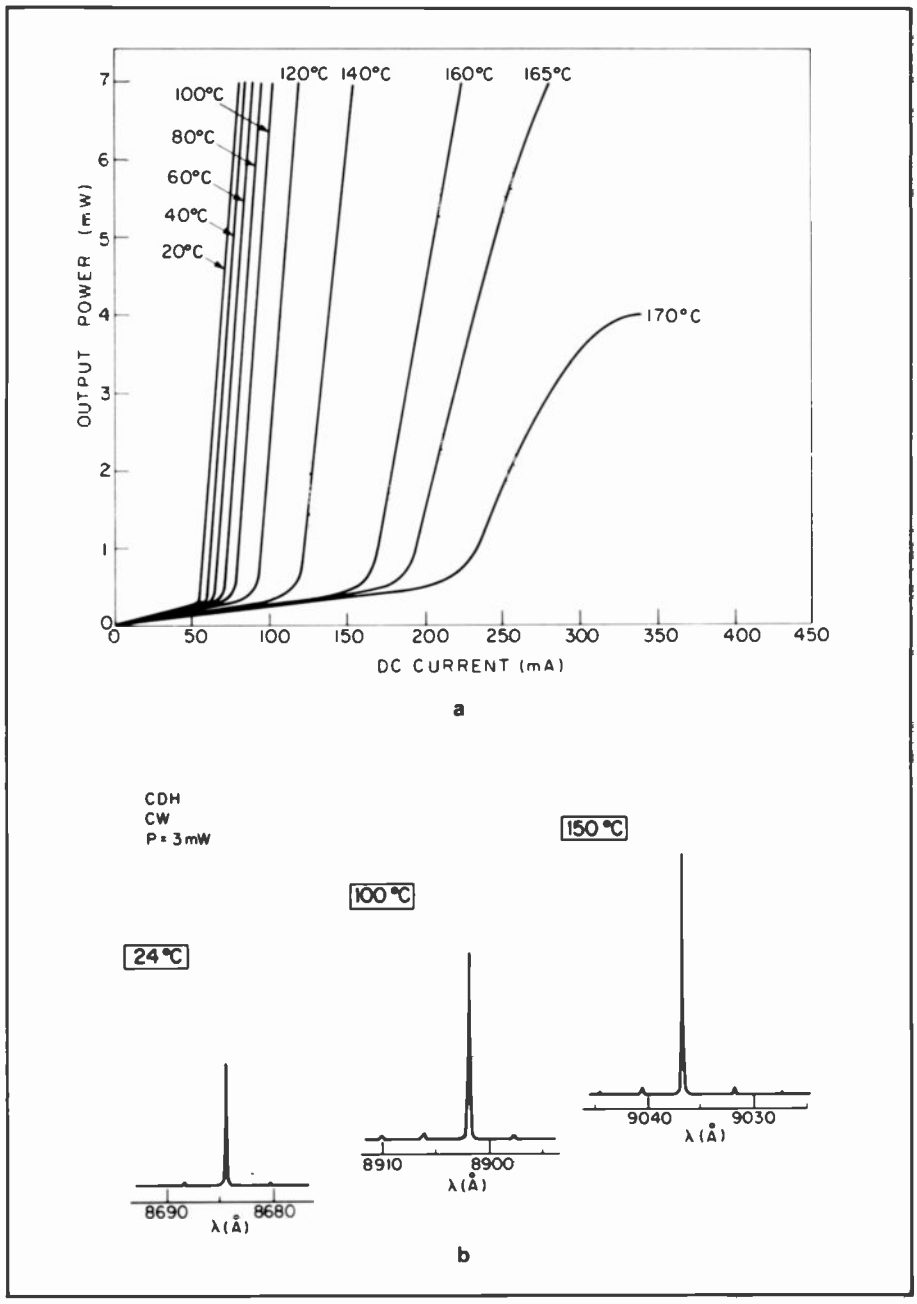


**Fig. 4. The CDH device is the least temperature-sensitive commercially available single-mode diode laser.** Cw light-current characteristics **(a)** and spectra **(b)** of CDH lasers at various heat-sink temperatures. At 150°C ambient temperature, the junction temperature is ≅170°C.

For the 1.2- to 1.7-$\mu$m wavelength region, lasing-mode stabilization has been achieved mainly by the fabrication of buried heterostructures. The active layer is then InGaAsP, while the confining and burying layers are made of *n*- and *p*-type InP.[15] Maximum mesa width for fundamental-mode operation is 2 to 3 $\mu$m. Just as for AlGaAs devices, low lasing thresholds (approximately 10 mA) and rather wide beam patterns (50° by 30°) are obtained. However, the power capabilities of InGaAsP devices are much higher than for AlGaAs BH lasers since facet-induced degradation does not seem to occur. Fundamental-mode operation to cw powers as high as 25 mW has been reported,[16] while single-mode operation is obtained only up to between 6 and 7 mW. InGaAsP mode-stabilized devices are currently used in field trials of optical communication systems at 1.3- and 1.55-$\mu$m wavelengths. Because of low fiber attenuation and virtually zero pulse dispersion, information could be transmitted at gigabit rates over distances as long as 100 km.[3]

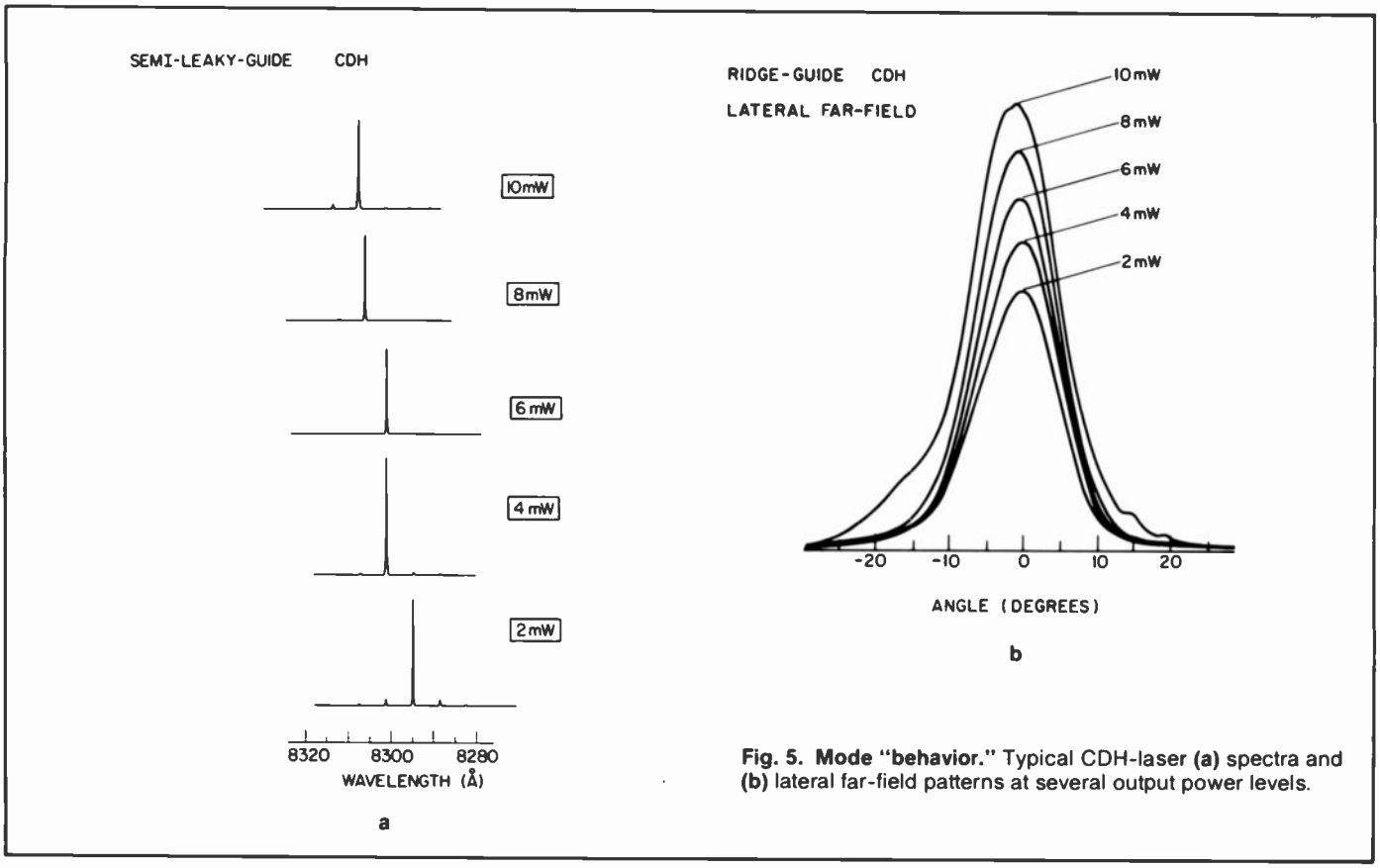


**Fig. 5. Mode "behavior."** Typical CDH-laser **(a)** spectra and **(b)** lateral far-field patterns at several output power levels.

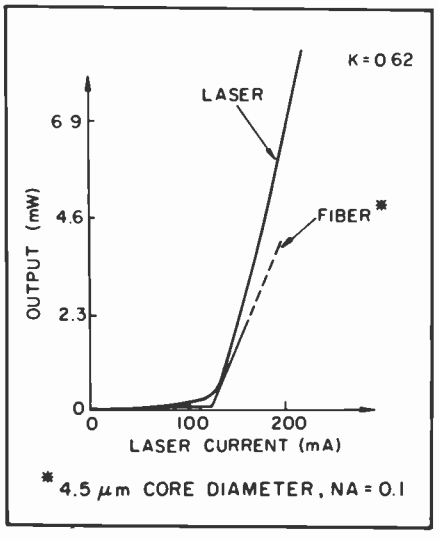


**Fig. 6. CDH-laser coupling to single-mode fibers is highly efficient.** The coupling efficiency is ≅62 percent (Ref. 14).

## High-power single-mode lasers

### *Means of achieving high-power single-mode operation*

As pointed out in the previous sections, for low-power devices the single-mode power that can be obtained reliably is limited by the mode spot size. At the same time, the mode lateral width is limited by the condition for fundamental-mode operation in a positive-index guide (equation (1) ). Thus, reliable single-mode operation could not be achieved at powers above 5 mW/facet. To overcome these limitations, two basic approaches have been taken:

1. Increase the lasing spot size both perpendicular and parallel to the junction, *plus* introduce a mode-dependent loss mechanism (lateral antiguiding,[11, 17, 18] lateral absorption, [18, 19] or scattering[20]) to discriminate against high-order-mode oscillation.
2. Eliminate facet degradation by making nonabsorbing-mirror (NAM) laser structures.[21, 22]

The most successful devices to date, the constricted double-heterojunction large-optical-cavity (CDH-LOC)[13] and the channel-substrate-planar (CSP),[19] use the first approach. In either case, the first step is to increase the mode spot size in the transverse direction. As shown schematically in Fig. 7, there are two ways to achieve large transverse spot size: by growing DH structures of very thin active layers, and by growing large-optical-cavity (LOC) structures. Thinning of the active layer from a standard value of approximately 0.15 μm to between 0.05 and 0.06 μm causes the mode transverse spot size to virtually double (that is, from 0.6 μm to 1 μm at $1/e^2$ points in intensity).[23] The LOC concept, originally developed at RCA, implies the growth of an additional cladding layer of refractive-index intermediate between that of the active layer and that of the *n*-AlGaAs confinement layer.[24] The optical mode then propagates mostly in the guide layer, while obtaining electronic gain from the active layer. Mode transverse sizes as large as 2 μm can thus be achieved. The second step is to provide, in the lateral direction, weak-mode confinement and a mode-dependent lateral loss mechanism. High-power CDH-LOC structures have a LOC geometry coupled with lateral antiguiding losses.[13, 25] By contrast, CSP structures have a DH geometry of very thin active layer, coupled with lateral absorption[19] and antiguiding losses.[18] Each device will be discussed in the next subsection.

Another key concept is that of using nonabsorbing-mirror facets (Fig. 8). In conventional diode lasers, intense nonradiative recombination at the facet depletes the minority carriers and, in turn, the effective bandgap narrows.[21] Lasing light is thus heavily absorbed at the facet, a process that eventually results in catas-

trophic mirror damage. To prevent such effects at the mirror facets, one has to create regions there of higher bandgap than in the lasing region (Fig. 8). Such nonabsorbing-mirror (NAM) structures can be obtained either by "burying" the facets in high-bandgap material or by using preferential Zn diffusion,[21, 22] and the devices' reliable power level is then increased fivefold.

## *Types of high-power single-mode lasers*

We show in Fig. 9 four major types of high-power single-mode devices: (a) CDH-LOC;[11] (b) channel-substrate-planar[19] (CSP); (c) "crank"-type transverse junction stripe[22] (crank-TJS); and (d) buried-heterojunction large-optical-cavity[20] (BH-LOC). Such devices have been shown to operate single-mode cw to at least 10 mW/facet, while having the capability (that is, large spot size or nonabsorbing mirrors) for reliable operation at output power levels above 10 mW/facet.

The CDH-LOC device (Fig. 9a) is fabricated by one-step liquid-phase epitaxy (LPE) above a mesa separating a pair of substrate-channels. Standard 10-$\mu$m-wide oxide-defined contact stripes are used for current confinement. Due to the LPE dependence on local surface curvature,[13] an optical cavity is formed above the mesa: a convex-lens-shaped active layer ($Al_{0.07}Ga_{0.93}As$) atop a concave-lens-shaped guide layer ($Al_{0.21}Ga_{0.79}As$). The combination of the two provides a large spot size and discrimination against high-order-mode oscillation via lateral antiguiding losses in the guide layer[11] and/or mode-dependent lateral gain-region overlap.[26] The cw threshold currents have values in the 60- to 100-mA range, high external differential quantum efficiencies (30 to 40 percent from one facet) and narrow beams (6° by 25° at the half-power points in planes parallel and perpendicular to the junction). The most notable feature is single-mode cw operation to 40 mW/facet,[11] the highest power into a single-mode device ever reported.

The CSP laser (Fig. 9b) is made by one-step LPE above a substrate-channel, and by a preferential Zn diffusion to ensure uniform current flow across the channel region.[19] Lateral-mode control and selection are realized via lateral absorption and antiguiding losses to the substrate regions on both sides of the channel. Typical beamwidths are 10° by 27°. The transverse far-field pattern is relatively narrow because very thin active layers (500 to 600 angstroms) ensure large transverse spot size (Fig. 7a). The maximum reported single-mode cw output power is 20 mW/facet.

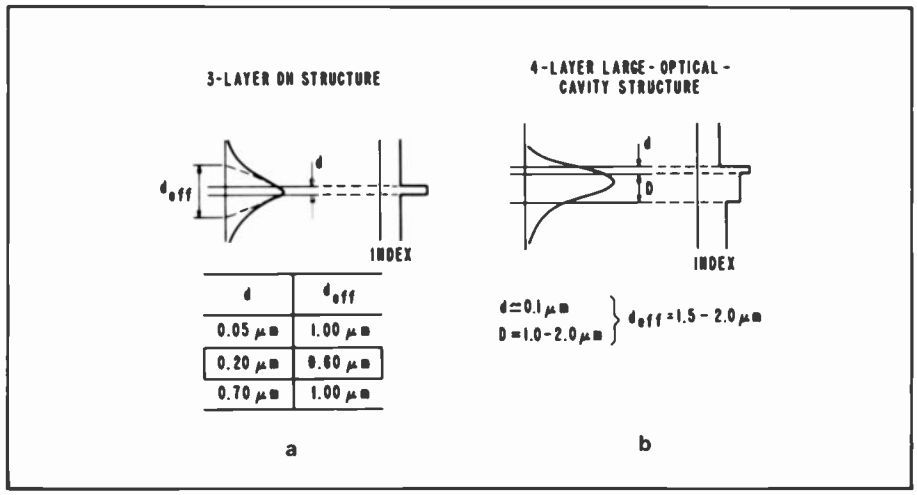


**Fig. 7. Two ways to achieve large transverse spot size.** Transverse-mode-spot size and refractive-index profiles for: **(a)** standard double-heterojunction (DH) structure; **(b)** large-optical-cavity (LOC) structure.

The crank-TJS laser (Fig. 9c) is a nonabsorbing-mirror structure (Fig. 8). Lateral-mode control is realized by two Zn-diffusion fronts. Zn is preferentially diffused in the longitudinal direction such that one can cleave mirrors through nondiffused areas. Since heavy Zn doping narrows the bandgap, light generated in the diffused areas will not be absorbed in the mirror-facet regions. This approach has increased tenfold the power capabilities of TJS-like structures[22] and "window-stripe" Zn-diffused structures.[21] The crank-TJS device has relatively low thresholds (30 to 40 mA), large beamwidths, and a maximum cw single-mode power of 20 mW.

The BH-LOC structure (Fig. 9d) is made by a two-step LPE process during which a 2- to 3-$\mu$m-wide mesa of planar LOC material is embedded in high-resistivity material. Mode control and selection is due on the one hand to the mode-cutoff properties of the buried lateral waveguide and on the other hand to mode-dependent scattering losses off the walls of the buried mesa.[20] Due to tight current confinement, very low thresholds (10 to 20 mA) and very high overall power-conversion efficiencies (30 to 50 percent) are achieved. Cw operation has been reported up to 10 mW/facet in a single mode, and up to 20 mW/facet in the fundamental spatial mode.

A comparison of the major types of single-mode cw devices yields several conclusions. With the exception of nonabsorbing-mirror devices, all other high-

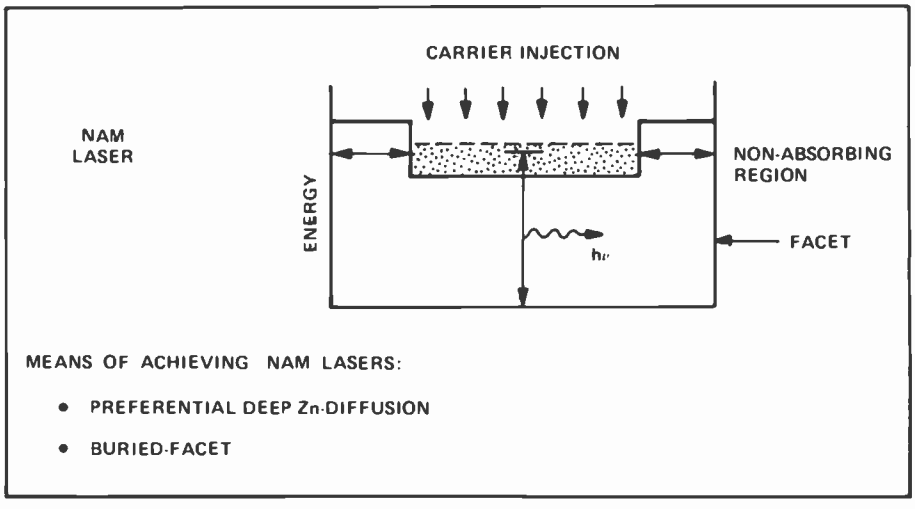


**Fig. 8. Preventing mirror damage—the nonabsorbing-mirror (NAM) laser structure.** The material at the mirror facets is transparent to the light generated in the current-pumped region.

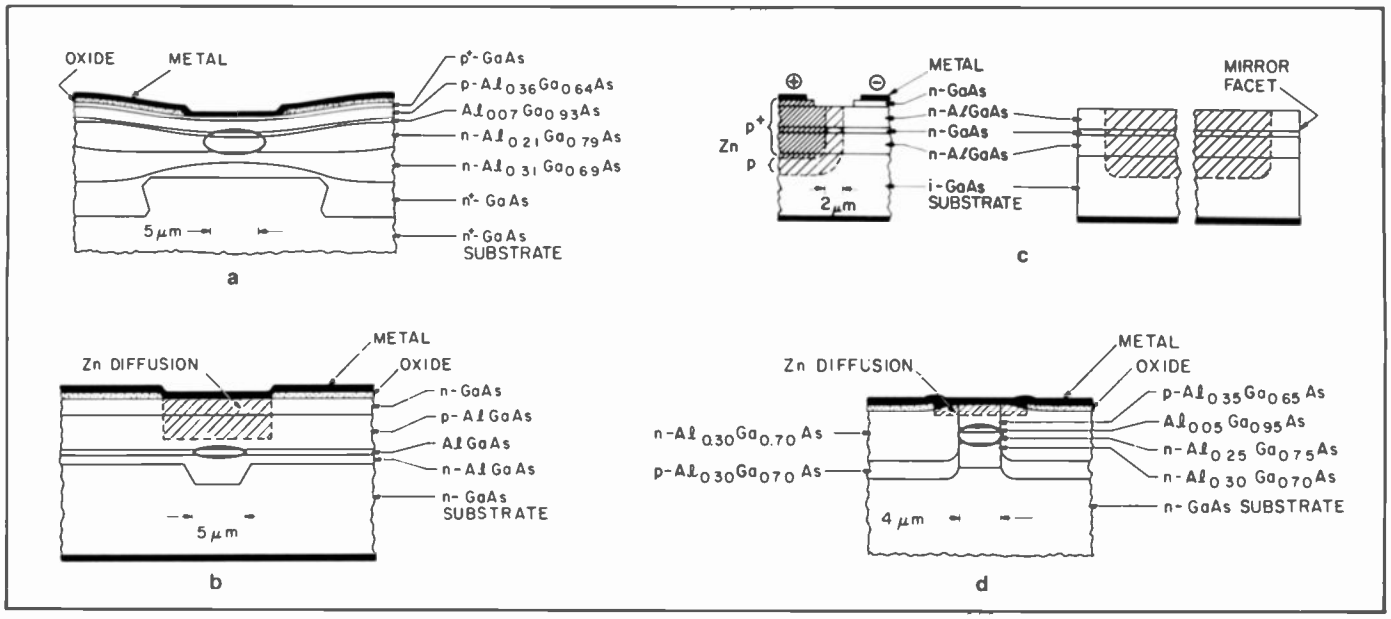


**Fig. 9. High-power single-mode laser types: (a)** constricted double-heterojunction large-optical-cavity (CDH-LOC); **(b)** channeled-substrate-planar (CSP); **(c)** "crank"-type transverse junction stripe (crank-TJS); and **(d)** buried-heterojunction large-optical-cavity (BH-LOC). The lasing spot sizes are shown to scale.

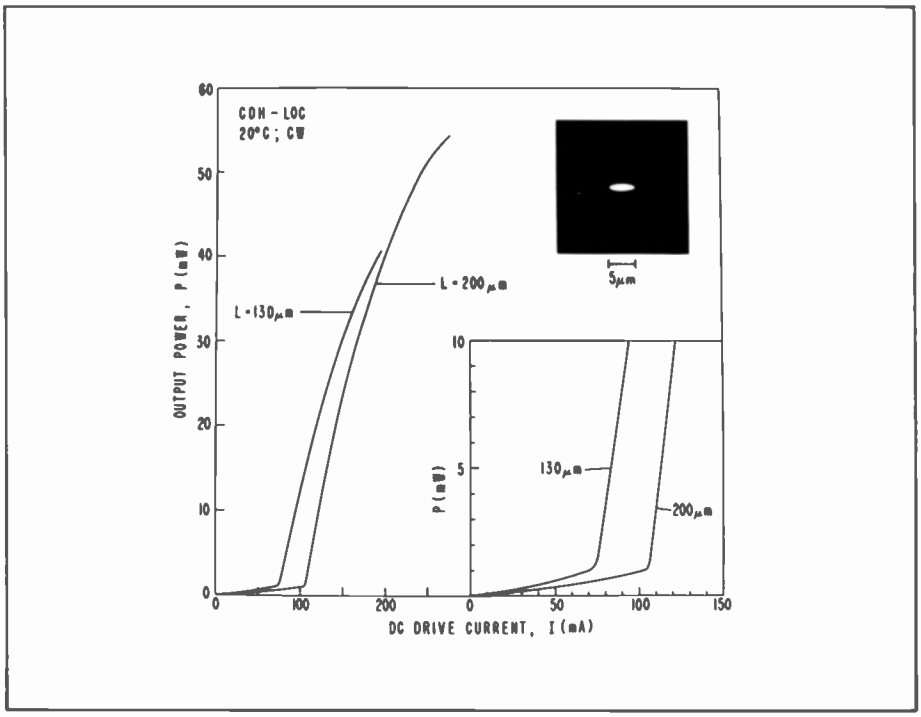


**Fig. 10. Typical cw light-current characteristics of CDH-LOC lasers.** The upper insert is a high-resolution photomicrograph of the near-field pattern.

power lasers rely on some sort of mode-dependent loss mechanism to discriminate against high-order-mode oscillation. Another relevant feature is that the larger the mode-spot size, the higher the single-mode power capability. High-power single-mode AlGaAs devices are currently used for optical recording,[27] high-speed printing, and data-bus fiber distribution systems.[28] As for long-wavelength (that is, InGaAsP) lasers, high-power device operation will be needed for long-distance high-data-rate optical communications. Powers as high as 25 mW cw have been demonstrated in the fundamental mode alone, while reliable operation has been obtained only at 5-mW power levels. Below we discuss results obtained from the most powerful device to date, the CDH-LOC laser.

## *Electro-optical characteristics of CDH-LOC lasers*

Typical cw light-current (L-I) characteristics are shown in Fig. 10. The L-I characteristics are very linear up to moderate powers (20 mW) and "kinkless" up to the maximum diode drive as limited by heating (for example, 55-mW cw for 200-μm-long devices). The slight bending of the L-I characteristics with increasing current above 25 mW is due to heating. In spite of this, both diodes are single mode up to at least 40 mW from one facet (Fig. 11). The devices can operate cw to heat-sink temperatures as high as 70°C. In the upper-right-hand corner of Fig. 11 we show a high-resolution near-field photograph of the laser emission. The photograph is taken by using an optical arrangement with high magnification and with a numerical aperture of 1.25. The lasing spot is large (2 μm by 7.3 μm at $1/e^2$ points in intensity) and thus allows burn-out powers (that is, catastrophic facet-damage levels) as high as 500 mW/facet in low-duty-cycle pulsed operation.

The lasers' spectra are recorded with a 1-meter double-grating spectrometer of 0.1- to 0.15-angstrom resolution. Typical diode spectral behaviors are shown in Fig. 11. Virtual single-longitudinal-mode oscillation is recorded from approximately 1.1 to 2.5 times the threshold current value. With increasing drive above the threshold, mode hopping occurs because the gain envelope shifts in wavelength in reaction

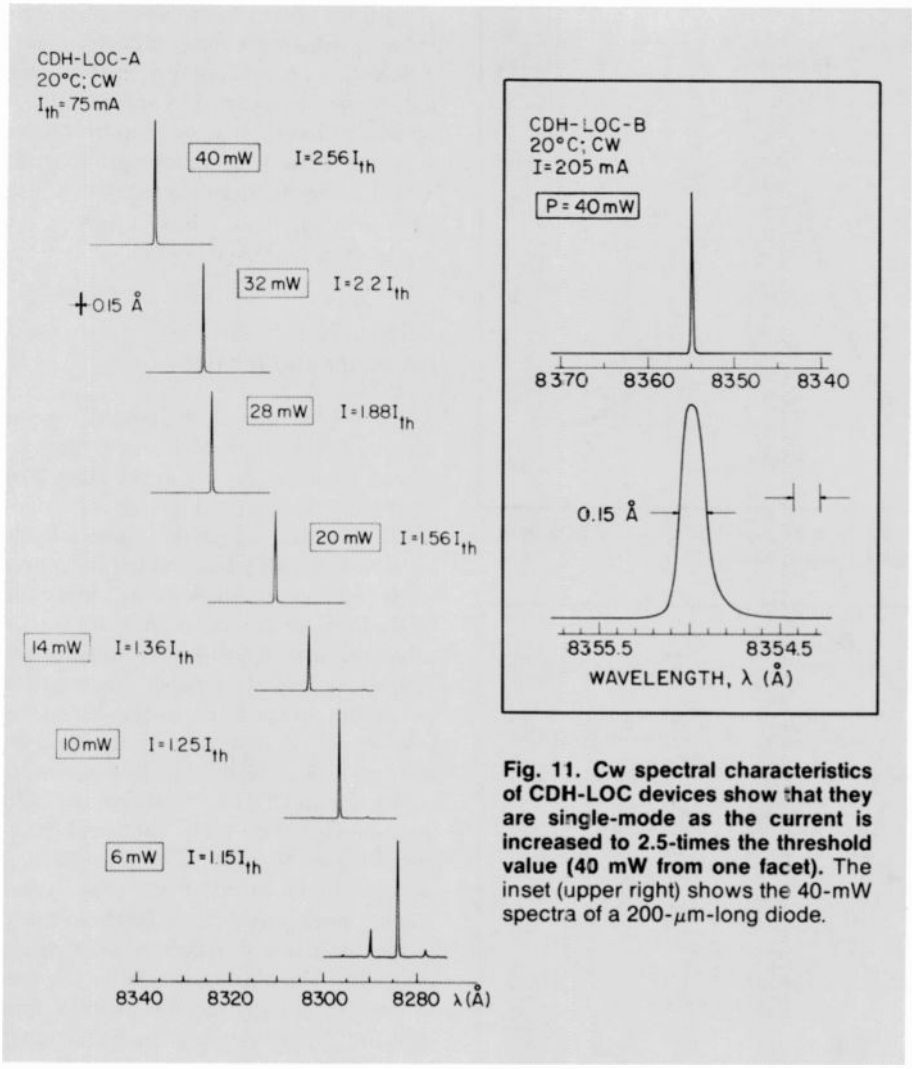


**Fig. 11. Cw spectral characteristics of CDH-LOC devices show that they are single-mode as the current is increased to 2.5-times the threshold value (40 mW from one facet).** The inset (upper right) shows the 40-mW spectra of a 200-$\mu$m-long diode.

to joule heating, and the single-longitudinal-mode nature of the diode becomes stronger. Thus, above the 20-mW cw-power level no other longitudinal modes are distinguishable on the linear recording scale. Using decibel (dB) scales (Fig. 12), one can see that at 30 mW, the main mode is at least a thousand times stronger than the satellite modes.[29] The maximum single-mode power of 40 mW is the highest room-temperature cw power into a single longitudinal mode ever reported in literature for a diode laser.

Typical cw far-field patterns to 40 mW (perpendicular and parallel to the junction) are shown in Fig. 13. As expected, the presence of the LOC structure gives relatively narrow transverse beamwidths ($\theta_\perp \simeq 25°$). The lateral far field is also narrow ($\theta_\parallel = 6°$ as it reflects a large lateral spot width. The major application of the CDH-LOC device is in high-data-rate optical recording as described by R.A. Bartolini in this issue.[27] There, the diodes are driven under high-duty-cycle (50 percent) conditions (50-ns-wide pulses and 10-MHz repetition rate) or near-cw conditions (dc bias at 90-percent threshold plus 50-percent duty cycle). Stable single-lobe operation is then obtained to 50 and 60 mW/facet as shown in Figs. 14 and 15. Such devices are used regularly in optical recording. It must be stressed that the beam shape and position are virtually the same in cw and pulsed driving conditions. This quality is quite important since it means that "reading" and "writing" can be performed without need for adjusting the optics. Although 50 to 60 mW in a single lobe at 50-percent duty-cycle operation can be obtained regularly, some devices can be driven single-lobe to powers as high as 100 mW/facet, as shown in Fig. 16.

Aside from optical recording, high-power CDH-LOC lasers have been used for coupling record-high powers into multimode fibers[28] and single-mode $LiNbO_3$ waveguides.[30] Such results are

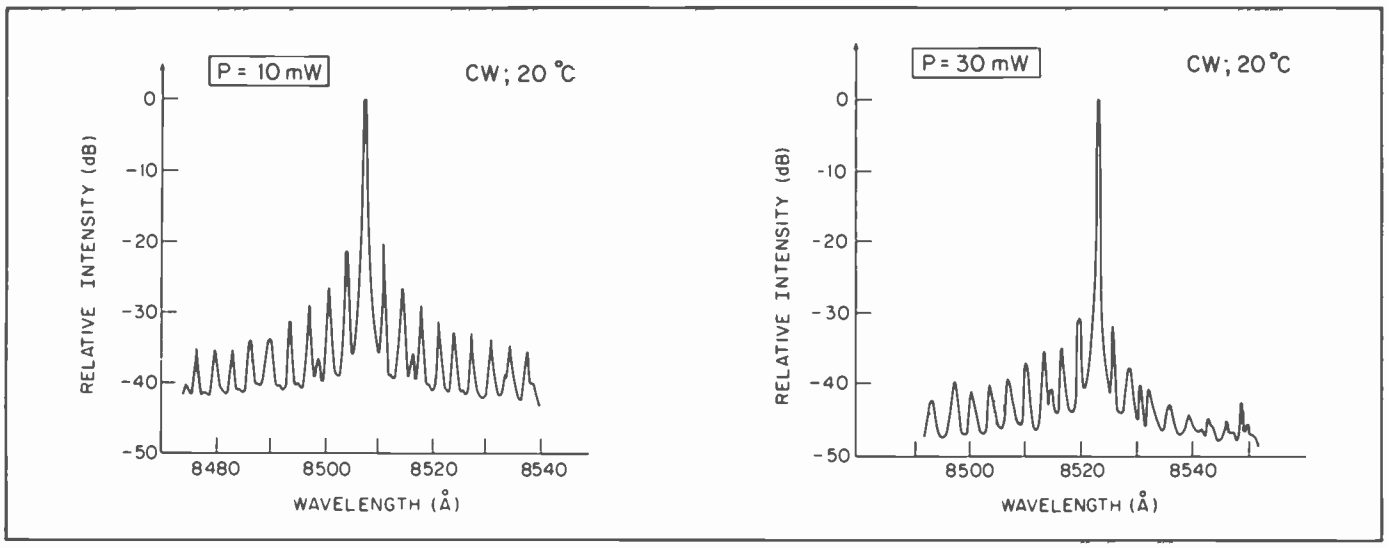


**Fig. 12. Typical cw spectra of CDH-LOC lasers.** These are given at 10 mW/facet and 30 mW/facet, on a decibel (dB) scale.

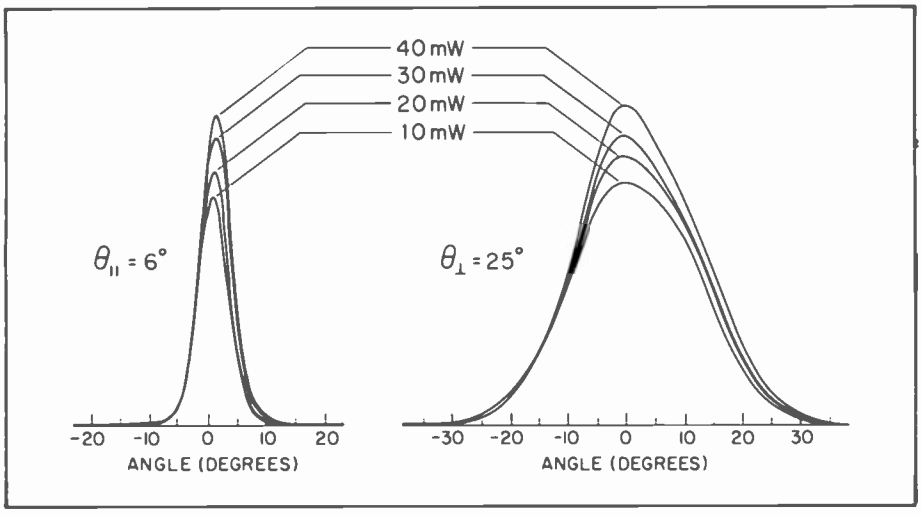


**Fig. 13. CDH-LOC-laser far-field patterns** in the plane of the junction ($\theta_{\parallel}$), and in a plane perpendicular to the junction ($\theta_{\perp}$), at several cw output-power levels.

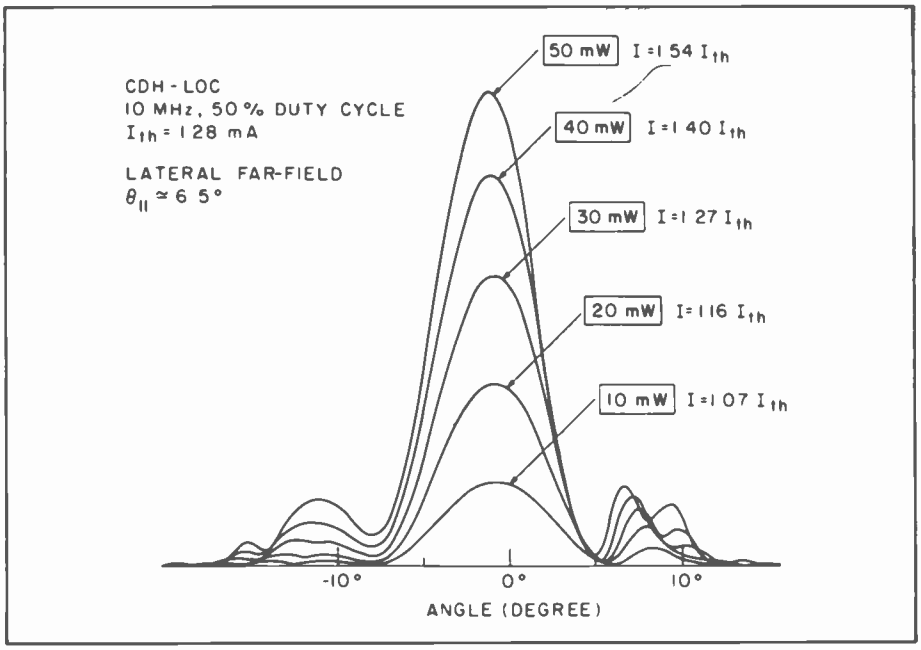


**Fig. 14. Typical CDH-LOC-laser lateral far-field patterns** as a function of drive level above threshold when operated at 50-percent cycle.

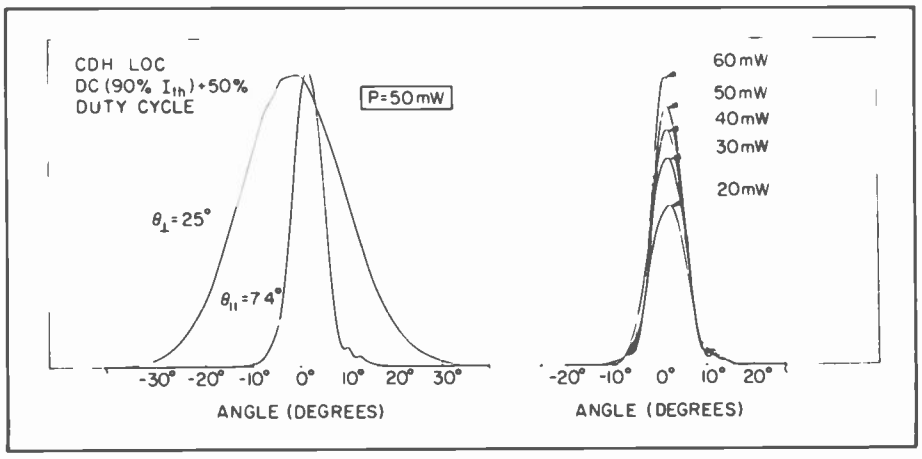


**Fig. 15. Typical far-field patterns of CDH-LOC lasers** driven at (90% $I_{th}$) dc + 50-percent duty cycle.

relevant for fiber data-distribution systems and for guided-wave signal processing, respectively. For such systems, fiber-attenuation losses are dwarfed by splice/connector and/or insertion losses, and thus there is no need for long-wavelength sources. In fact, better thermal characteristics and lower cost will favor AlGaAs high-power devices over InGaAsP devices.

## *CDH-LOC device reliability and arrays*

As mentioned previously, reliable operation in AlGaAs diode lasers is directly related to power density at the facet. For mode-stabilized coated devices of "standard" spot size, 0.5 $\mu$m by 3 $\mu$m, reliable operation can only be expected for power levels in the 3- to 7-mW range.[2] Since the CDH-LOC device has a spot size 6 to 8 times the size of low-power single-mode lasers, one expects reliable operation at cw output-power levels in the 20- to 30-mW range. Preliminary results tend to confirm such expectations. Life tests were performed on CDH-LOC devices operated at 50-percent duty cycle, with peak powers of 40 to 50 mW/facet. Two diodes, which emitted 40 mW/facet peak power initially, have passed the 10,000-hour mark on the life test with relatively small drops in output. The maximum relative changes in beam shape, as recorded with a split detector, are ±5 percent. Such characteristics satisfy well the requirements for optical recording systems.[31]

For the future, one can envision the fabrication of independently addressable arrays of high-power diode lasers for use

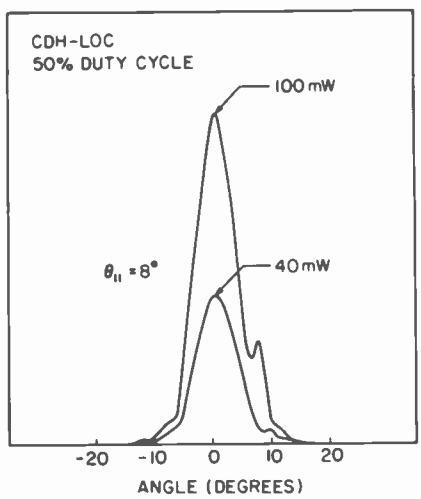


**Fig. 16. Lateral far-field patterns of CDH-LOC lasers** driven at 50-percent duty cycle (10 MHz).

in multichannel optical recording. Preliminary results of our work in CDH-LOC laser arrays are shown in Figs. 17a to 17c. A ten-diode monolithic array has been fabricated (Fig. 17a) with CDH-LOC devices on 150-$\mu$m centers. The devices lase in relatively large spot sizes, as seen from the near-field profile of a single device (bottom Fig. 17a), and have remarkably similar threshold currents (80 to 90 mA) and lateral far-field patterns ($\theta_{\parallel} \simeq 8°$). These features show the reproducibility of liquid-phase epitaxy over channeled substrates. In cw operation, the monolithic CDH-LOC array delivered up to 300 mW (Fig. 17b), while in low-duty-cycle pulsed operation 3.5 W of power could be obtained (Fig. 17c). Both results represent the highest powers ever achieved, cw and pulsed, from monolithic arrays of mode-stabilized lasers.

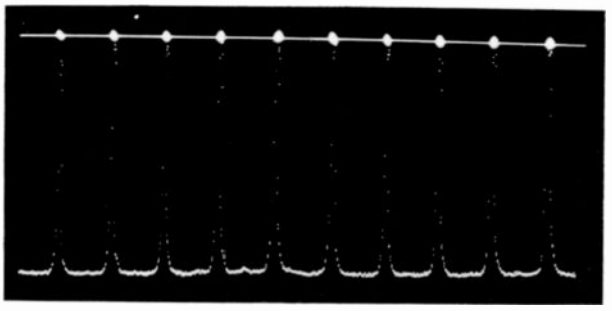

150 $\mu$m

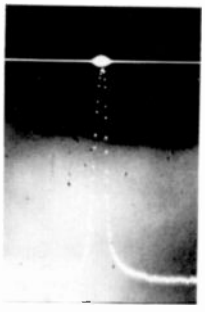

15 $\mu$m

a

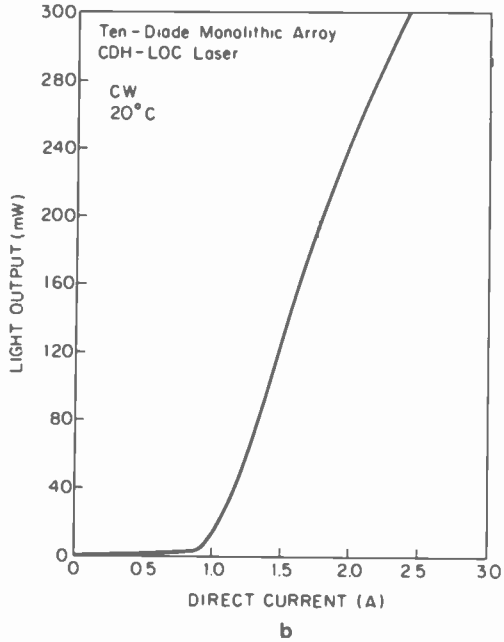


b

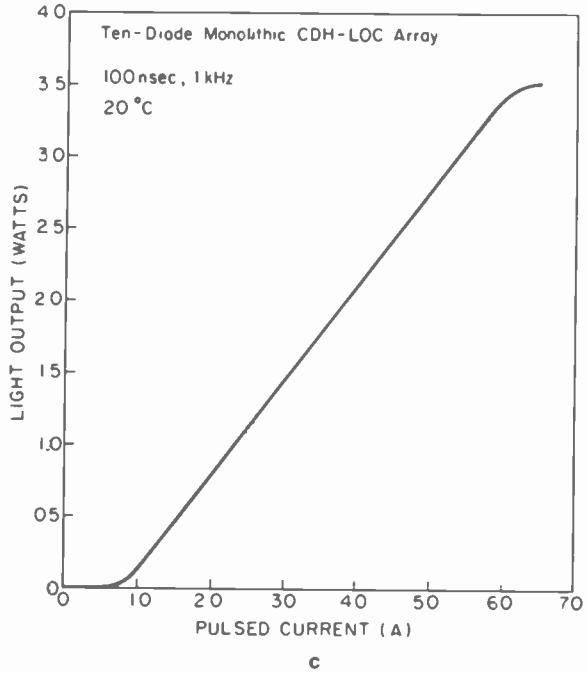


c

**Fig. 17. Ten-diode monolithic array of CDH-LOC lasers:** (a) near-field patterns of the array (top) and of an array unit (bottom); (b) cw light-current characteristics; (c) pulsed (low-duty-cycle) light-current characteristics.

## Dynamic behavior

As far as their use in systems, four types of diode-laser modulation characteristics are of interest: light-pulse response to a current pulse; frequency response; noise performance as a function of current drive; and single-mode stability. Spatial-mode stability in the near and far field is already assured for single-mode lasers, since the optical mode is defined by a built-in dielectric waveguide.

The diode's pulse response is characterized by turn-on and turn-off response times as well as by dynamic features such as relaxation oscillations[4] (RO) and, sometimes, self-sustained oscillations (SSO).[12] Most single-mode laser types have fast (subnanosecond) turn-on response times, after an initial drive-level-dependent delay time.[4] That, however, does not follow for the turn-off response time. Observed pulse "tailing" effects cause intersymbol inter-

ference for (return-to-zero) RZ-format modulation at data rates above 400 Mbits.[28] Relaxation oscillations are rapidly damped oscillations that can affect system performance at data rates above 100 Mbits. For most single-mode lasers, ROs are heavily damped and thus do not affect system operation. By contrast, the occurrence of self-sustained oscillations, observed sometimes in aged devices, spells the end of the diode's useful life in high-speed (≥200 Mbit) applications. Fortunately, SSOs occur relatively infrequently in high-quality single-mode facet-passivated diodes.

The diode's frequency response consists mainly of a drive-level-dependent resonance peak in the gigahertz range.[4] For high-frequency diode operation, the device should be driven at high current levels above the threshold. Tied in with the frequency response is the diode's (intrinsic) noise response. For well-behaved, isolated single-mode diodes, the noise spectrum peaks at lasing threshold and then drops significantly with current drive above threshold.[33] However, reflections back into the diode or operation in a mode-"hopping" region are serious sources of noise and should be avoided.[33] For instance, reflections into the device can be minimized by using fibers with angle-polished ends, or eliminated by using optical isolators.[34]

Probably the most serious problem in the use of single-mode diodes is the instability of the single longitudinal mode. Mode "hopping" generally occurs in a random way as a function of time at fixed temperature and as a function of ambient temperature at fixed output-power level. For many systems—such as optical recording, multimode-fiber communications, and printing—this random longitudinal-mode hopping is of no concern. However, if stable operation in a single-frequency mode is necessary—such as in single-mode fiber-optical communications, space communications and holographic printing—mode stabilization by external means has to be implemented. Methods for achieving single-frequency-mode stabilizations include the use of external cavities with diffraction gratings[35] or hemispherical mirrors,[36] and injection locking.[37] The single mode is thus selected via stable external means, and can be tuned by adjusting the external cavity components or by changing the ambient temperature. For the future, one can envision single-frequency-mode stability by the monolithic incorporation of submicrometer gratings in the laser structure.[3, 38] The stabilization of the frequency mode, together with tight temperature control and/or external reflection for spectral line narrowing ($\Delta\nu < 1$ MHz), will eventually open the way for heterodyne detection and thus the potential for terahertz (THz) bandwidth communications.[39]

## Conclusions

Diode lasers have come a long way since their discovery two decades ago. Both low- and high-power single-mode diodes operating continuously and reliably at room temperature are commercially available. The CDH-LOC laser, a culmination of research efforts at David Sarnoff Research Center, provides the highest single-mode power ever achieved from a semiconductor injection laser. The device opens new horizons in optical recording, fiber-optical communications, and space communications.

## References


1. Kressel, H. and Nelson, H., "Close Confinement Gallium Arsenide *p-n* Junction Lasers with Reduced Optical Loss at Room Temperature," *RCA Review*, Vol. 30, pp. 106-113 (1969).
2. Ettenberg, M. and Kressel, H., "The Reliability of (AlGa)As cw Laser Diodes," *IEEE J. Quantum Electron.*, Vol. 16, pp. 186-196 (1980).
3. Botez, D. and Herskowitz, G., "Components for Optical Communication Systems: A Review," *Proceedings IEEE*, Vol. 68, pp. 689-732 (1980).
4. Kressel, H. and Butler, J.K., *Semiconductor Lasers and Heterojunction LEDs*, Academic Press, New York (1977).
5. Kobayashi, T., *et al.*, "Lasing Characteristics of Very Narrow Planar Stripe Lasers," *Japan J. Appl. Phys.*, Vol. 16, pp. 601-607 (April 1977).
6. Marschall, P., *et al.*, "New Diffusion-Type Stripe-Geometry Injection Laser," *Electron. Lett.*, Vol. 15, No. 1, pp. 38-39 (January 1979).
7. Engelmann, R.W.H. and Kerps, D., "Leaky Modes in Active Three-Layer Slab Waveguides," *IEEE Proceedings*, Vol. 127, pp. 330-336 (1980).
8. Tsukada, T., "GaAs-$Ga_{1-x}Al_xAs$ Buried Heterostructure Injection Lasers," *J. Appl. Phys.*, Vol. 45, No. 11, pp. 4899-4906 (November 1974).
9. Ueno, M. and Yonezu, H., "Stable Transverse Mode Oscillation with Deep Zn Diffusion," *IEEE J. Quantum Electron.*, Vol. QE-15, No. 10, pp. 1189-1195 (October 1979).
10. Botez, D., "Single-Mode CW Operation of 'Double-Dovetail' Constricted DH (AlGa)As Diode Lasers," *Appl. Phys. Lett.*, Vol. 33, No. 10, pp. 872-874 (November 15, 1978).
11. Botez, D., "CW High-Power Single-Mode Operation of Constricted Double-Heterojunction AlGaAs Lasers with a Large Optical Cavity," *Appl. Phys. Lett.*, Vol. 26, No. 3, pp. 190-192 (February 1980).
12. Kirkby, P.A., "Channeled-Substrate Narrow-Stripe GaAs/GaAlAs Injection Laser with Extremely Low Threshold Currents," *Electron. Lett.*, Vol. 15, pp. 824-825 (1979).
13. Botez, D., "Constricted Double-Heterojunction AlGaAs Diode Lasers—Structures and Electro-Optical Characteristics," *IEEE J. Quantum Electron.*, Vol. QE-17, No. 12, pp. 2290-2309 (1981).
14. Ladany, I., *et al.*, "A 500-MHz Driver for Single-Mode Fiber-Optic Communication Systems," *Digest of Int. Elec. Dev. Mtg.*, Paper 25-2, pp. 630-633, Washington, D.C. (December 1978).
15. Ladany, I., private communication.
16. Hirao, I., Doi, A., Tsuji, S., Nakamura, M., and Aiki, K., "Fabrication and Characterization of Narrow Stripe InGaAsP/InP Buried Heterostructure Lasers," *J. Appl. Phys.*, Vol. 51, pp. 4539-4540 (August 1980).
17. Botez, D., Spong, F.W., and Ettenberg, M., "High-Power Constricted Double-Heterojunction AlGaAs Lasers for Optical Recording," *Appl. Phys. Lett.*, Vol. 36, No. 1, pp. 4-6 (January 1, 1980).
18. Ishikawa, H., Hanamitsu, K., Tagaki, N., Fujiwara, T., and Takusagawa, M., "Separated Multiclad-Layer Stripe Geometry GaAlAs DH Laser," *IEEE J. Quantum Electron.*, Vol. QE-17, No. 7, pp. 1226-1233 (July 1981).
19. Aiki, K., Nakamura M., Kuroda, T., Umeda, J., Ito, R., Chinone, N., and Maeda, M., "Transverse Mode Stabilized $Al_xGA_{1-x}As$ Injection Lasers with Channel-Substrate-Planar Structures," *IEEE J. Quantum Electron.*, Vol. QE-14, No. 2, pp. 89-87 (February 1978).
20. Chinone, N., Saito, K., Ito, R., Aiki, K., and Shige, N., "Highly Efficient (GaAl)As Buried-Heterostructure Lasers with Buried Optical Guide," *Appl. Phys. Lett.*, Vol. 35, No. 7, pp. 513-516 (October 1, 1979).
21. Yonezu, H., Sakuma, I., Kamejima, T., Ueno, M., Iwamoto, K., Hino, I., and Hayashi, I., "High Optical Power Density Emission From a 'Window-Stripe' AlGaAs DH Laser," *Appl. Phys. Lett.*, Vol. 34, No. 10, pp. 637-640 (May 15, 1979).
22. Kumabe, H., Nita, S., Seiwa, Y., Tanaka, T., Sogo, T., Horiuchi, S., and Takamiya, S., "Continuous-Wave 15-mW Operation Test of Single-Mode High-Power Crank Structure TJS Laser Diodes," *Tech. Digest IEEE/OSA Conf. Lasers and Electrooptics '81, Paper FA4*, Washington, D.C. (June 10-12, 1981).
23. Botez, D., "Near- and Far-Field Analytical Approximations for the Fundamental Mode in Symmetric Waveguide DH Lasers," *RCA Review*, Vol. 39, pp. 577-603 (1978).
24. Lockwood, H.F., Kressel, H., Sommers, H.S., and Hawrylo, F.Z., "An Efficient Large Optical Cavity Injection Laser," *Appl. Phys. Lett.*, Vol. 17, pp. 499-502 (1970).
25. Botez, D., Butler, J.K., and Connolly, J.C., "Mode Control in High-Power CDH-LOC Diode Lasers: The W-Shaped Lateral Waveguide," *Proc. 3rd Int. Conf. on Integrated Optics and Optical Fiber Communication Paper MB5*: 10-11, San Francisco, Calif. (April 1981).
26. Butler, J.K., private communication.
27. Bartolini, R.A., *RCA Engineer*, Vol. 27, No. 3, (this issue) (May/June 1982).
28. Channin, D.J., Botez, D., Connolly, J.C., Schroeder, J.O. Bednarz, J.P., and Ettenberg, M., "High-Power Optical Fiber Data Transmission Using

CDH-LOC AlGaAs Laser Diodes," *Tech. Dig. Intern. Electron. Dev. Mtg., Paper 18.5*, pp. 452-455, Washington, D.C. (December 1981).

29. Sommers, H.S., Jr., private communcation.
30. Hammer, J.M., Botez, D., Neil, C.C., and Connolly, J.C., "High-Efficiency High-Power Butt-Coupling of Single-Mode Diode Lasers to Indiffused $LiNbO_3$ Optical Waveguide," *Appl. Phys. Lett.*, Vol. 39, pp. 943-945 (December 15, 1981).
31. Ettenberg, M. and Botez, D., "High-Power Diode Lasers for Optical Recording with Operating Lifetimes in Excess of 10,000 Hours," to be published.
32. Channin, D.J., Ettenberg, M., and Kressel, H., "Self-Sustained Oscillations in (AlGa)As Oxide-Defined Stripe Lasers," *J. Appl. Phys.*, Vol. 50, No. 11, Part 1, pp. 6700-6706 (November 1979).
33. Jäckel, H. and Melchior, H., "Fundamental Limits of the Light Intensity Fluctuations of Semiconductor Lasers with Dielectric Transverse Mode Confinement," *Fifth European Conf. on Optical Communication, Paper 2.5*, Amsterdam (September 1979).
34. Seki, M., *et al.*, "0.8 μm Band Optical Isolator for Fiber-Optic Communication," *Tech. Digest of the Topical Meeting on Optical Fiber Communications, Paper WD2*, pp. 56-59, Washington, D.C. (March 1979).
35. Sommers, H.S., Jr., "Performance of Injection Lasers with External Gratings," *RCA Review*, Vol. 38, pp. 33-59 (March 1977).
36. Preston, K.R., Woollard, K.C., and Cameron, K.H., "External Cavity Controlled Single Longitudinal Laser Transmitter Module," *Electron. Lett.*, Vol. 17, pp. 931-932 (November 1981).
37. Kobayashi, S. and Kimura, T., "Injection Locking in AlGaAs Semiconductor Laser," *IEEE Quantum Electron.*, Vol. QE-17, pp. 681-689 (May 1981).
38. Utaka, K., Akiba, S., Sakai, K., and Matsushima, Y., "Room-Temperature CW Operation of Distributed-Feedback Buried-Heterostructure InGaAsP/InP Lasers Emitting at 1.57 μm," *Electron. Lett.*, Vol. 17, pp. 961-963 (December 1981).
39. Okoshi, T. and Kikuchi, K., "Heterodyne-Type Optical Fiber Communications," *J. Opt. Comm.*, Vol. 2, pp. 83-88 (September 1981).

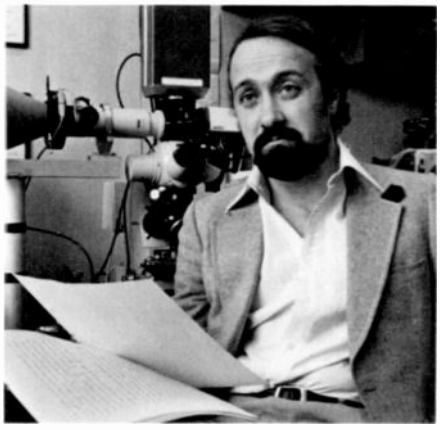

**Dan Botez** joined the Technical Staff at RCA Laboratories in 1977. His work resulted in "thick-window" high-radiance surface-emitting LEDs; and the development of a novel type of single-mode stabilized cw diode laser, the constricted double-heterojunction (CDH) laser, which has demonstrated cw and pulsed operation to the highest ambient temperature ever reported, and which represents the least temperature-sensitive commercially available diode laser. Recent work has resulted in the constricted double-heterojunction large-optical-cavity (CDH-LOC) laser, to date the most powerful single-mode cw semiconductor laser, and thus has allowed optical recording of information at the highest data rates ever achieved. He received a 1979 RCA Outstanding Achievement Award for contributions to the development of a high-density optical recording system employing an injection laser. Dr. Botez is the author or co-author of over 40 scientific papers and has published a major review *(Proceedings IEEE*, June 1980) on components for optical communication systems. In 1982, he was appointed a Research Leader in the OptoElectronics Research Group.

Contact him at:
**RCA Laboratories**
**Princeton, N.J.**
**TACNET: 226-2526**

R.A. Bartolini

# High-density optical recording using laser diodes

*High-power single-mode diode laser and compatible optical recording media developments are providing a basis for future optical disc recording system products.*

**Abstract:** *Optical recording systems capable of information storage and retrieval by the use of a highly focused laser beam as the recording and playback source have been developed to a point where product introduction in the mid-1980s is highly probable. The product potentials range from video information-storage applications to large archival digital data mass memories. This article presents the features of an optical disc data-storage-and-retrieval system based on a semiconductor diode laser as the recording source.*

Optical disc recording systems capable of information storage and retrieval by means of a highly focused laser beam as the recording and playback source have been under investigation at RCA Laboratories for the last 10 years. The product potentials for this technology range from broadcast video applications[1, 2] to random-access large archival digital data mass memories for government applications.[3, 4, 5] The two key elements for any optical disc recording system application are the recording laser source and the recording media. The ideal recording laser source is the semiconductor diode laser.[6–10] The details of such a device are presented on pages 8 to 19 in this issue in another article, by D. Botez. My article describes the results when such a device is used in optical disc recording applications and gives the latest results on optical disc recording media development, which is compatible with this recording source.


Final manuscript received February 9, 1982
Reprint RE-27-3-3

## Recording and playback system

Optical disc recording systems provide the following advantages:

1. Very high information density of $10^{10}$ to $10^{11}$ bits per disc have been demonstrated.
2. Very high data rates of up to 50 Mbits/second in a single-channel recorder have been demonstrated.
3. Rapid random access to the data ($<<1$ second) has also been demonstrated.
4. The cost of the media has been projected to be $5 \times 10^{-8}$ cent/bit.
5. The media has the potential for archival storage (10 years or more) of the data.

Figure 1 shows a block diagram of a typical optical disc recording and playback system. For recording, the output of the laser is directed through a modulator (both electro-optic and acousto-optic devices have been used) that modulates the intensity of the light, in response to an input electrical signal. The modulated laser beam is enlarged by the recording optics so that it will fill the aperture of the focusing lens. This lens focuses the laser beam into a small (less than 1-$\mu$m diameter) area on the recording medium so that the intensity modulation of the beam results in the information being stored as a series of "spots" along a track in the surface of the recording medium. For readout, an unmodulated, less intense (so that further recording will not take place) laser beam from the same laser follows the same path as that followed by the recording beam to the recording medium. The light is reflected from the recorded "spots" and passes back, through the focusing lens and a quarter-wave plate (not shown). The light, now rotated by 90° in polarization by the two passes through the quarter-wave plate, passes through a polarizing beam splitter (not shown) and is directed by the optics to a photodetector. The photodetector converts the reflected light beam (modulated by the recorded "spots") to an electrical output signal representative of the original input recording signal to the modulator. The radial position of the laser's spot on the disc is determined by the position of the motor-driven translation stage and the track mirror. The control system can move the translation stage so that either spiral or concentric circular tracks can be recorded. During readout, the translation stage is used to determine the approximate track location while the track mirror provides fine tracking control to lock on and read the desired information.

When recording data, two important performance parameters are the total data capacity of the storage media and the rate at which the data can be stored and retrieved. It is desirable to have both of these parameters as large as possible, for example $10^{10}$ to $10^{11}$ bits total capacity and 20 to 50 Mbits/s data recording rates.

The total data capacity of an optical disc depends on the number of data bits that can be stored on a single revolution (track) of the disc and the total number of revolutions (tracks). The primary factors that determine the bit density along the track are the minimum recorded area size and the modulation-encoding scheme (that is, the number of bits per recorded area). The major factors that determine total number of tracks are the size of the

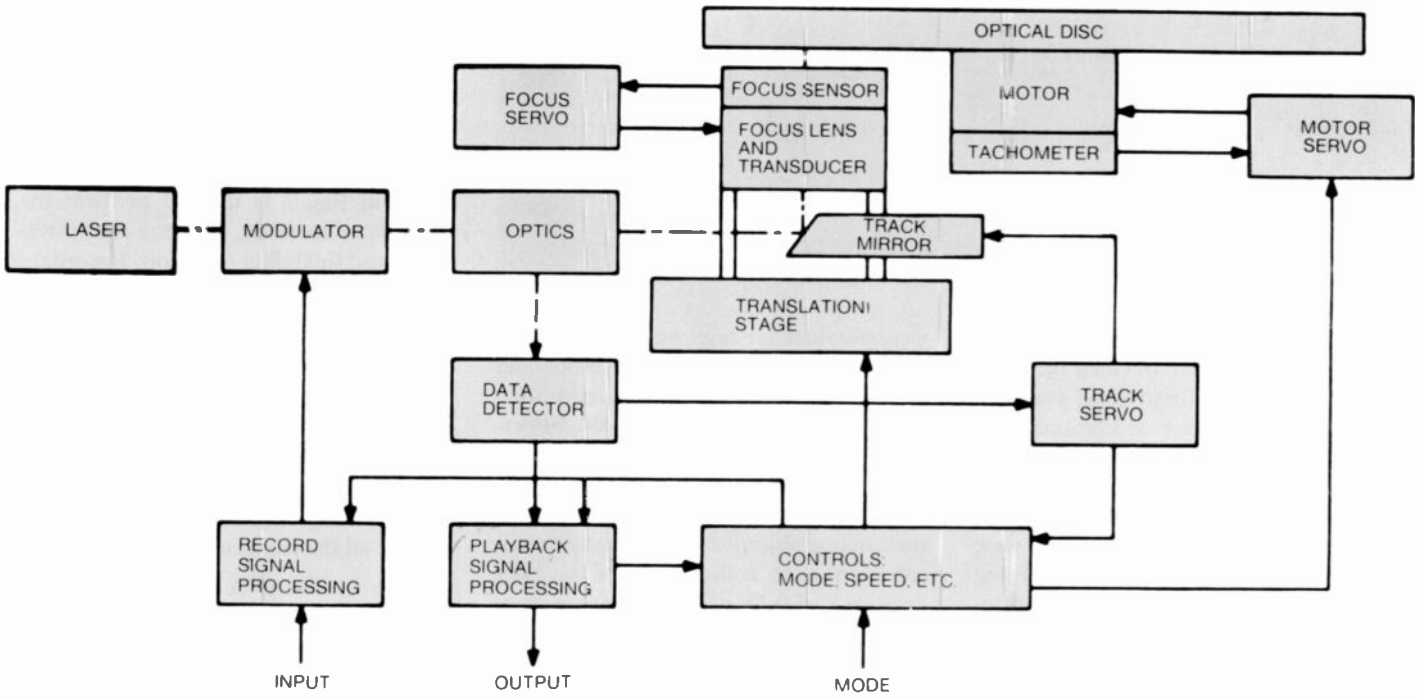


**Fig. 1. The major components of the optical disc recording and playback apparatus.** The laser and disc media are the key items in such a system.

disc and the track-to-track spacing, which must be sufficient to reduce cross talk below an acceptable level.

When a modulation-encoding scheme is assumed that requires one bit per recorded area and a track-to-track cross-talk limitation that requires the track density to be one-third the bit density along the track, then the total number of bits ($C_o$) that can be stored on an optical disc rotating at constant angular velocity is

$$C_o = \frac{\pi}{6d_o^2}(D_oD_i - D_i^2), \qquad (1)$$

where $d_o$ is the recorded area diameter, $D_o$ is the disc's outer recording diameter, and $D_i$ is the disc's inner recording diameter. For $C_o$ to be a maximum, $D_i$ equals $D_o/2$. Assuming $D_o$ is 30.5 cm, equation (1) reduces to

$$C_o = \frac{1.2 \times 10^{10}}{d_o^2}, \qquad (2)$$

where the units of $d_o$ are in micrometers.

The data recording rate ($R$) is given by

$$R = \frac{\pi D_i}{d_o} S, \qquad (3)$$

where $S$ is the disc rotation rate in rps. The disc rotational velocity is limited by mechanical properties of the disc substrate and by focusing and tracking-servo performance. For many different substrates and the present servo systems, a disc rotational velocity of 30 rps is practical and, with $D_i$ equal to $D_o/2$, equation (3) reduces to

$$R = \frac{14.4 \times 10^6}{d_o} \text{ bits/s}, \qquad (4)$$

where the units of $d_o$ are in micrometers.

Equations (2) and (4) show the dependence of the disc data capacity and data rate on the recorded area size which, in turn, depends on the laser spot size. The laser spot size is a function of the laser wavelength ($\lambda$) and the numerical aperture (NA) of the recording focusing lens; that is,

$$d_{1\,2p} = 0.56\,\frac{\lambda}{\text{NA}}, \qquad (5)$$

where $d_{1\,2p}$ equals the spot diameter at the half-power points (1/2p) for a Gaussian beam truncated by the lens at the $1/e^2$ points.[11] The recorded area is typically of the order of this half-power-spot diameter and thus equations (2) and (4) become

$$C_o = 3.8\left(\frac{\text{NA}}{\lambda}\right)^2 \times 10^{10} \text{ bits} \qquad (6)$$

and

$$R = 25.7\left(\frac{\text{NA}}{\lambda}\right) \times 10^6 \text{ bits/s} \qquad (7)$$

Focusing lenses with NAs from 0.6 to 0.85 and lasers with wavelengths of 0.442 to 0.82 $\mu$m have been used in optical disc recording systems. Table I compares the disc capacity and data rate for these ranges.

As Table I shows, the use of a longer wavelength laser requires a sacrifice in both disc capacity and data rate even when compared to a shorter wavelength system using an NA of 0.6.

Table II lists some of the commercially available lasers (with relevant properties) that have been extensively used as recording sources in optical disc systems. The choice of the proper laser depends on the particular optical recording application. For example, the helium-cadmium (HeCd) laser produces the shortest wavelength beam and, thus, produces the smallest recording element which provides for the highest disc-data capacity and highest single-channel recording rate. The argon ($Ar^+$) laser on the other hand, due to its high output power, can have its output beam split into a number of sub-beams (up to nine have been reported[12]) that can be independently modulated and used to

**Table I. Disc capacities and data rates** for some typical optical disc recording systems.

| $\lambda$ ($\mu$m) | NA | $C_o$ (bits) | $R$ (Mbits/sec) |
|---|---|---|---|
| 0.442 | 0.6 | $7 \times 10^{10}$ | 35 |
| 0.442 | 0.85 | $1.4 \times 10^{11}$ | 50 |
| 0.82 | 0.6 | $2 \times 10^{10}$ | 19 |
| 0.82 | 0.85 | $4 \times 10^{10}$ | 27 |

**Table II. Optical recording lasers** (cw, single mode).

| *Type* | λ (nm) | $d_{1/2p}$ (μm); NA = 0.85 | $P_{output}$ (max) |
|---|---|---|---|
| HeCd | 442. | 0.29 | 40mW |
| $Ar^+$ | 488. | 0.32 | 1 – 4W |
| HeNe | 633. | 0.42 | 50mW |
| AlGaAs | 820. | 0.54 | 40mW |

simultaneously record data at *n* times the single-channel data rate (*n* being the number of sub-beams). Commercial availability and proven lifetime characteristics have made the helium-neon (HeNe) laser an attractive optical disc recording source.

The HeCd, $Ar^+$, and HeNe lasers are all gas lasers, and until recently, they were the only lasers used for optical recording applications. But the development of optical recording media with increased sensitivity, and the continued improvement of the modal characteristics and output power capabilities of the aluminum-gallium arsenide (AlGaAs) semiconductor diode lasers has allowed recording of video and digital information with these semiconductor sources. This is a major development in the field of optical recording because the diode laser permits the design of extremely compact systems with significant reductions in the size and cost of the record and playback system. Because the output power of the diode laser can be modulated directly by the input signal, the external light modulator common to all gas-laser optical recording systems can be eliminated, and diode-laser arrays will ultimately permit extremely high data rate (hundreds of Mbit/s) systems. The high efficiency of the diode laser also permits the electrical input power to the system to be reduced drastically compared to gas-laser systems. Finally, the diode laser is potentially more reliable than its tube counterpart.

Diode-laser requirements for optical recording applications are operation at peak powers of 40 mW or more, at 50-percent duty cycle, and at rates up to 30 MHz. In addition, the laser should exhibit stable fundamental spatial-mode operation in both transverse and lateral directions. "Lateral" and "transverse" designate planes respectively parallel and perpendicular to the junction plane, both being perpendicular to the direction of beam propagation, that is, the longitudinal direction.

A newly developed diode-laser structure, the constricted double-heterojunction large-optical-cavity (CDH-LOC) device, provides for high output power (up to 100 mW) in a single stable mode and the promise of good lifetime (more than 10,000 hours to date at 40 mW, 50-percent duty cycle, and 10 MHz).[13]

Figure 2 shows the diode-laser optical recording system, which begins with a microscope objective of sufficient numerical aperture to collect most of the laser light (NA of 0.35). This objective is positioned to collimate the light, but further beam conditioning is required because of the asymmetric beam spreading in the lateral and transverse planes. This conditioning of the beam is accomplished by a combination of two simple plano-convex cylindrical lenses that function as a beam expander in one dimension. The positions of the cylindrical lenses are adjusted for common focus in both lateral and transverse directions. When the optical system is aligned, an approximately symmetrical beam just fills the focusing objective lens (NA of 0.85) producing a spot size of 0.6 μm (half-power diameter) in both the lateral and transverse directions.

Also shown in Fig. 2 is the readout path and readout elements of the optical-disc system (tracking mirror, quarter-wave plate, polarizing beam splitter, and photodetector).

Since the data is written in real-time with an instantaneous playback capability, a read-after-write (RAW) scheme can be used to verify that the data has been recorded without errors. A separate laser (lower power) can be used for this purpose, as shown in Fig. 3. In addition to the diode laser and optics of Fig. 2, the HeNe in Fig. 3 is used to perform the function of focusing, tracking, read-after-write, and final data detection. Recording results from the use of this system will be presented later in this article.

## Recording media

The key component of the optical disc system for data storage and retrieval is the recording media. Ideally, it should provide all the characteristics listed below.

*High sensitivity.* A few milliwatts incident onto the recording surface is a practical value based on existing lasers if one considers optical efficiencies, reflections, and other system losses.

*High resolution.* Since high-density optical recording systems require 1-μm (or smaller) spots, the material must have a resolution capability that is greater than 1000 *l*p/mm.

*High SNR.** The signal, to be useful, must be recorded with sufficient SNR (the limit on SNR is dictated by system considerations; that is, digital versus analog, data recording rate, disc capacity, and so on).

*Real-time recording and instant playback.* The material must have real-time recording characteristics and allow immediate retrieval of the stored in-

* SNR is the peak-to-peak signal-to-RMS-noise ratio in a 4.2-MHz bandwidth.

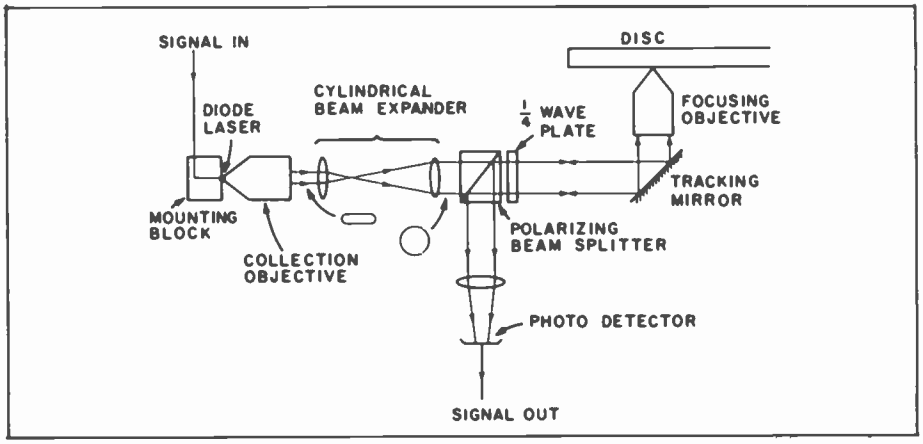


**Fig. 2. The optical components of the diode-laser optical disc recording and playback system.** The major items are the cylindrical beam expander and the focusing objective lens.

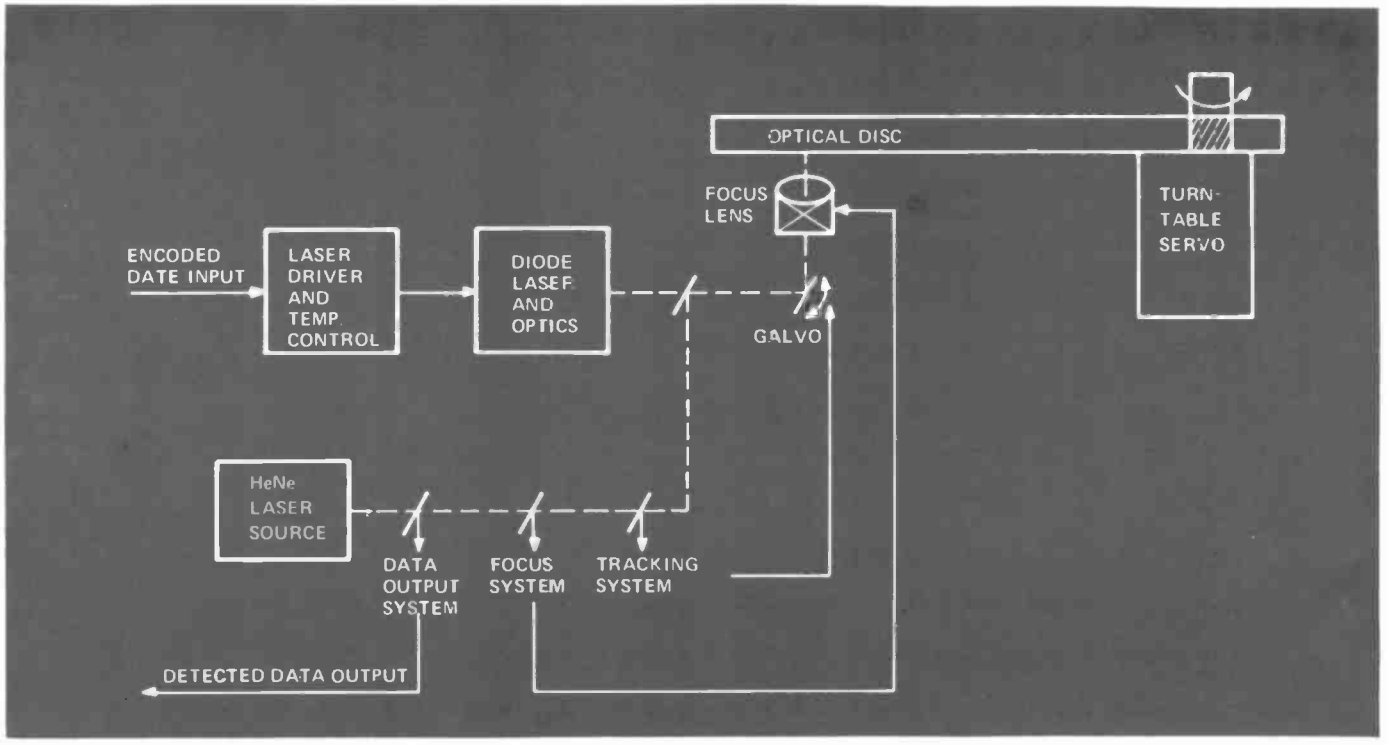


**Fig. 3. The overall diode-laser optical disc recording and playback apparatus.** The HeNe laser is used for readout of data as well as for focusing and tracking functions.

formation; that is, there should be no processing steps required.

*Immunity to defects.* Material pinholes, dust, and other surface contaminants can prevent the recording of many signal elements, or obscure them after recording; thus, the material must allow for protection from this source of "noise."

*Archival storage.* The material should allow permanent recording of the data and should not degrade under ambient conditions or prolonged readout.

There are many classes of materials in which changes in the optical properties may be induced by the absorption of light from the recording laser beam.[14]

The class of materials that were found to satisfy all of these conditions are ablative (melted or vaporized) thin films.[15 - 17] The highly focused laser beam serves as an intense and extremely localized source of heat. The thin film is locally heated by the focused laser beam, and surface tension opens a hole (pit) in the melted area. To read the data, an unmodulated laser beam (with intensity below the recording level) is scanned across the pits by the rotating disc, and the change in reflectivity from pit to land is detected as the data output signal.

In general, for thermal types of recording media where the pit formation process proceeds via melting of the layer of recording medium, the energy ($E$) which is required to form the pit and, therefore, the power required in the incident recording beam depend on three major parameters, as shown in equation (8).

$$E \propto \frac{Q_m}{\eta_{optical}\,\eta_{thermal}} \qquad (8)$$

$Q_m$ is the amount of energy required to melt the pit in the layer of recording medium, neglecting any heat losses to the substrate or overcoat layers. $\eta_{optical}$ is the optical efficiency of the structure in which the recording medium is placed, that is, the fraction of the incident recording beam which is coupled into and absorbed by the layer of the recording medium. $\eta_{thermal}$ is the thermal efficiency of the recording process, being that fraction of the heat generated within the layer of recording medium that does not diffuse into the substrate or overcoat materials, which are in contact with the layer of recording medium.

The simplest ablative recording medium that has been used for optical recording is a single 30- to 50-nm vacuum-deposited layer of metal. This type of optical recording structure reflects about 40 percent of the incident light and also absorbs about 40 percent (the rest is transmitted). The optical efficiency ($\eta_{optical}$) of this structure is, thus, 40 percent. A metallic optical recording structure that has been found to improve significantly on this factor is a thin-film multilayer antireflection (AR) structure called the trilayer optical recording structure.[18]

The trilayer structure is shown schematically in Fig. 4. The substrate is first coated with a reflective layer of aluminum, followed by a layer of transparent dielectric material, and finally a very thin layer of the metallic recording medium. By choosing the thickness of the dielectric and the thin metal layer appropriately, it is possible to create an antireflection condition for light of the recording wavelength. This results in a very high fraction (up to 90 percent) of the incident beam being absorbed by the thin metallic layer. The optical coupling of the trilayer structure can, thus, be up to twice that which can be achieved by use of a single layer of the recording material due to the losses by reflection and partial transmission through the single layer. The trilayer design thus provides for the highest value for $\eta_{optical}$ in equation (8).

The trilayer structure also provides an advantage over the single-layer approach during readout where the signal contrast is enhanced because the pits formed during recording exhibit a high reflectivity to the presence of the exposed aluminum reflection layer, while the AR condition is maintained in the unrecorded areas.

The amount of energy, $Q_m$, required to melt the pit in the metallic recording layer

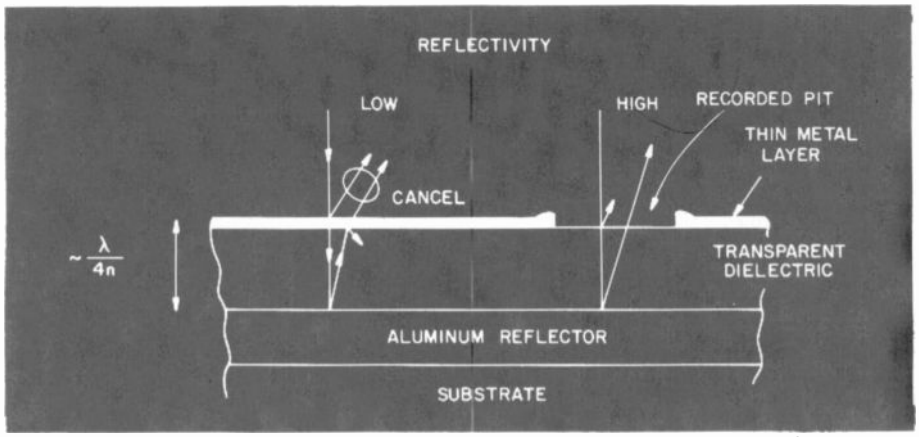


**Fig. 4. Details of the optical characteristics and operation of the trilayer optical disc structure.** The antireflection condition achieved by the quarter-wave optical thickness, $\lambda/4n$, is the key to this structure.

**Table III. Recording characteristics** of metal trilayers.

| Metal | $T_m$ (°C) | $P_T$ (mW) | SNR (dB) |
|---|---|---|---|
| Te | 450 | 3 | 54 |
| Pb | 327 | 3 | 36 |
| Bi | 271 | 3 | 41 |
| In | 156 | 5 | 40 |

$T_m$ = melting point temperature
$P_T$ = threshold incident recording power
SNR = playback signal-to-noise ratio

of Fig. 4, is heavily dependent on the melting point temperature of the metal itself. Of a large variety of low-melting-point metals tested, tellurium (Te) has been found to provide the highest playback signal-to-noise ratio (SNR) (see Table III).[19]

The choice of Te as the absorbing layer in the trilayer structure consequently provides for an optimum value for $Q_m$ in equation (8).

The thermal efficiency, $\eta_{thermal}$, depends not only on the thermal properties of the recording medium and material in contact with this layer, but also on the duration of the pit-formation process, which is determined by system-related factors such as recorded signal bandwidth, laser-output duty cycle, turntable speed, and laser-spot size.

The presence of the aluminum-reflector layer in the trilayer structure represents a potential heat sink that may reduce the thermal efficiency of the recording process. The heat generated in the tellurium layer by the absorption of the incident recording beam will diffuse through the dielectric layer, and after some characteristic time, dictated by the thickness and the thermal properties of the dielectric layer, it will reach the aluminum-reflector layer. Since aluminum is a good thermal conductor, once this layer is thermally coupled into the process of pit formation, the thermal efficiency of the recording can be substantially reduced, leading to a corresponding reduction in the recording sensitivity.

In general, in order to eliminate the deleterious effects of the heat losses to the aluminum layer, the parameters of the dielectric layer must be specified such that the thermal time constant for heat to diffuse from the layer of recording medium to the aluminum layer exceeds the duration of the pit-formation process. A polymeric dielectric material, for example, was found to provide a twofold improvement in recording sensitivity over an $SiO_2$ dielectric layer.[7] Thus, the choice of materials for the dielectric layer can optimize the value of $\eta_{thermal}$ in equation (8).

Besides the ablative pit-forming mode of optical recording (Fig. 5a) in a trilayer structure, two new interesting modes of recording have been reported recently. The first is a bubble-forming mode[20, 21] (Fig. 5b). In this mode, the absorbing layer is a high-melting-point metal (such as titanium) instead of a low-melting-point metal (such as tellurium), and the dielectric layer material is chosen to have a vaporization temperature well below the melting temperature of the absorbing layer. Upon exposure to the highly focused laser beam, bubbles are formed as the top absorbed layer bulges due to the gas pressure from the vaporized dielectric layer beneath (Fig. 5b). The bubble disrupts the AR condition and, thus, the readout is similar to the pit-forming mode (that is, high-reflectivity recording regions and a low-reflectivity unrecorded region). The other new mode is a reversible recording mode[22] (Fig. 5c). In this mode, no topographical (pit or bubble) disruption of the trilayer structure occurs during recording. Instead, the optical properties of the recorded region

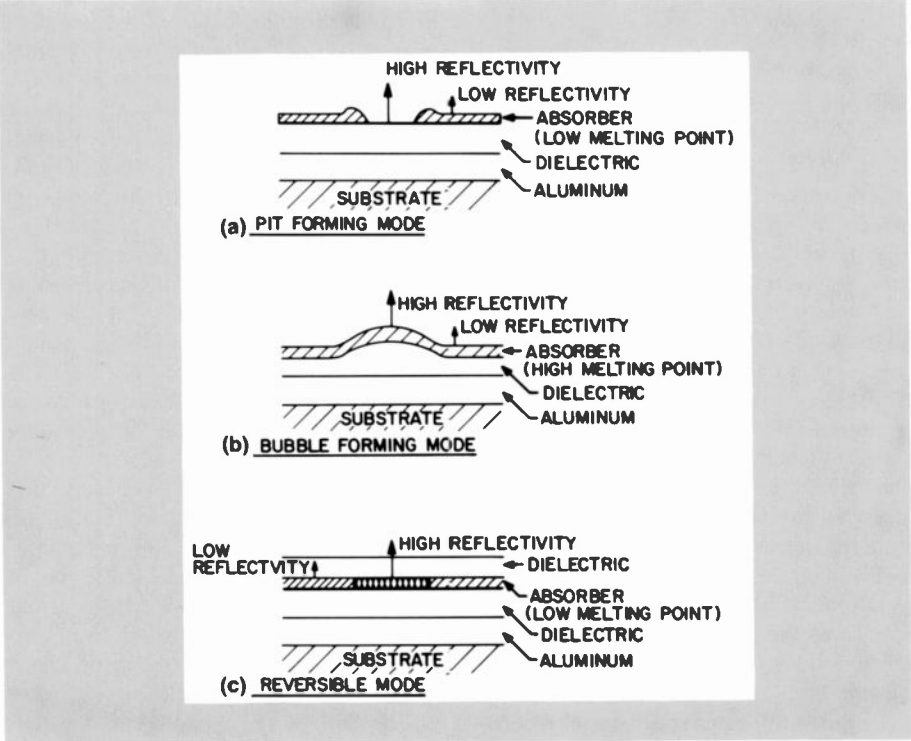


**Fig. 5. Three different recording modes of the trilayer optical disc structure.** By varying materials and number of layers, significantly different recording effects can be produced.

are changed when the material switches between the crystalline and amorphous phases.

The pit-forming mode in this case is inhibited by the use of a dielectric capping layer (Fig. 5c). The recorded region can be erased (restored to the original phase) by continuing the high-power readout (but with less power than the recording beam) of the recorded information. The areas can then be re-recorded and erased many times (up to 50 record/erase cycles have been reported[22]).

Thus far in the discussion of the materials aspects of the design of the recording structure, the effects of defects on the quality of the playback signal have been neglected. Since the density of information is so high, even defects which have sizes in the range of 1 $\mu$m will result in a significant loss of information. There are basically three sources of such defects, and the overall design of the optical recording disc must take all of them into account.

The first and probably most important source of defects is that of precipitated dust particles, which accumulate on the surface of the recording medium. These particles may obscure a number of recorded pits, or even prevent their formation if the particle is present during the recording step. A relatively thick (180-$\mu$m) transparent overcoat or encapsulation layer will protect against signal degradation due to dust particles by placing them out of focus.[21] Figure 6 shows such an overcoat in contact with the Te-trilayer structure.

The second source of defects depends on the intrinsic quality of the evaporated coatings that form the recording structures. These coatings *must* be free of pinholes to a very high degree, and this necessitates the most rigorous standards for cleanliness during the evaporation steps.

The third source of defects is due to intrinsic surface defects present in the substrate disc. Even the most carefully polished glass substrate will have a finite density of cavities and microscratches on its surface; in the case of an inexpensive plastic substrate the defect density is likely to be considerably higher. The surface defects intrinsic to the substrate can be hidden relatively easily by pre-coating the substrate with a thin layer of plastic material applied by coating from a solution. Such a layer is applied by spin coating and, as it dries, surface tension causes the uppermost surface to harden and form an almost defect-free surface for coating with

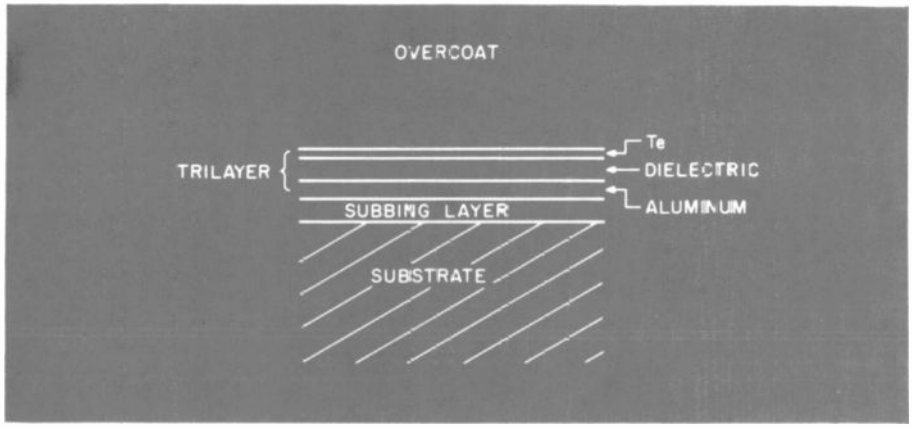


**Fig. 6. A cross-sectional view of the overcoated Te-trilayer optical recording disc with a subbed substrate.**

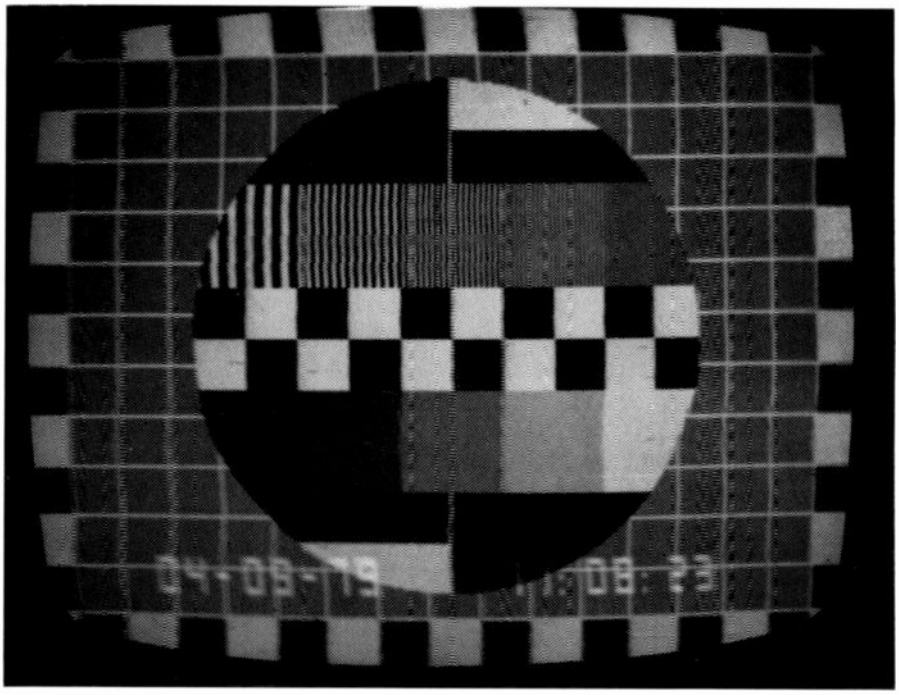

**Fig. 7. A TV monitor displaying a video-signal test pattern recorded and read out from a Te-trilayer optical disc, using a diode laser as the recording and playback source.**

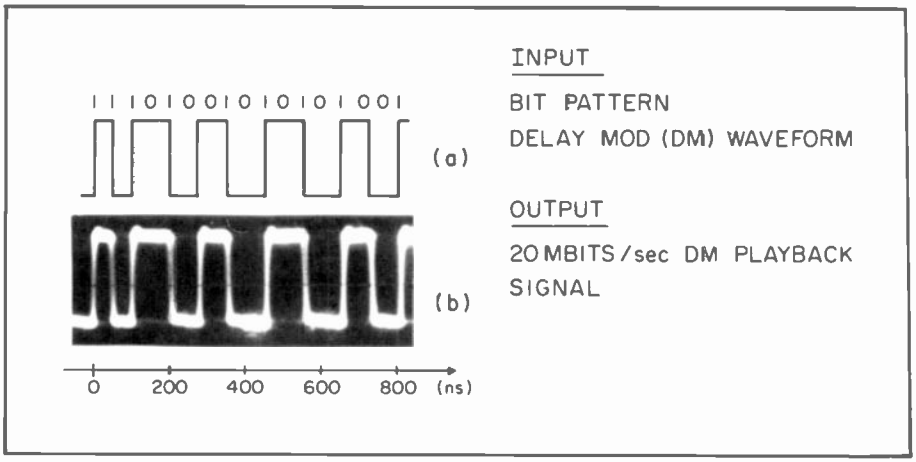


**Fig. 8. Diode-laser recording and playback of a 20 Mbit/s DM digital signal. (a)** Input bit pattern and DM waveform. **(b)** Output DM signal recordings.

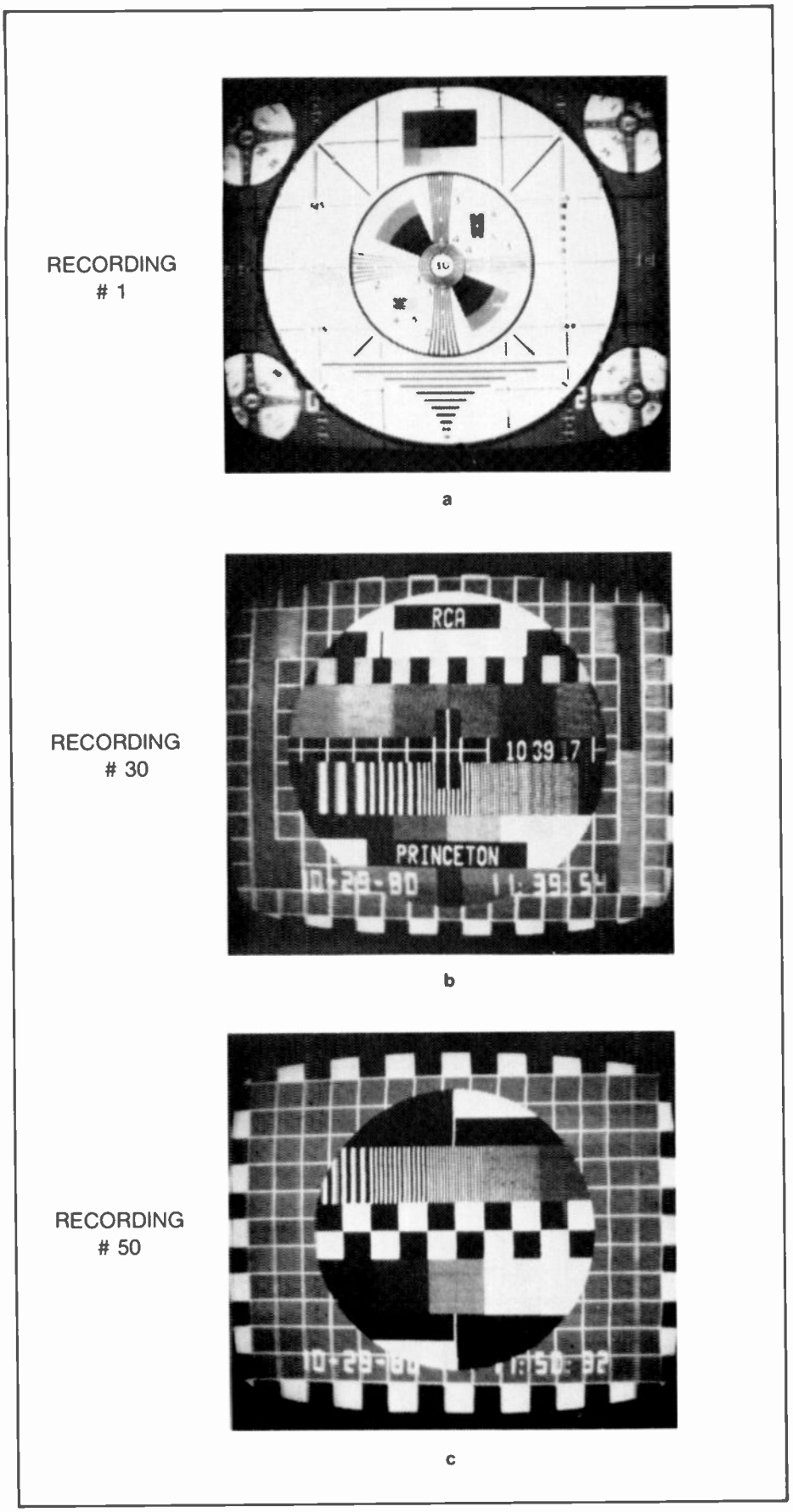


**Fig. 9. Photograph of TV monitor playback of reversible recordings: (a)** recording #1, **(b)** recording #30, and **(c)** recording #50.

the recording structures. This surfacing or subbing layer is shown in Fig. 6. Recording results obtained for some of these structures are discussed in the following section.

## Recording results

Recording results from the diode laser in the recording arrangement of Fig. 3 and the optical disc structure of Fig. 4 are shown in Figs. 7 and 8.

Figure 7 is a photograph of the TV monitor displaying the playback video signal that was recorded and read out by use of the diode-laser recording system.[7] The SNR is approximately 45 dB.

Figure 8 shows digital recording results obtained with the diode-laser recording system. Figure 8a shows the input bit pattern and corresponding delay-modulation (DM) 20-Mbits/s digital encoding waveform that was used to directly modulate the diode laser. The output signal during playback is shown in Fig. 8b.

Using the optical disc structure of Fig. 5c, reversible video optical recording has been demonstrated.[22] Figure 9 shows photographs of the playback of video information displaying the first, thirtieth, and fiftieth successive recordings made on one track of a disc during the record/erase/re-record sequence.

## Conclusions

The development of the high-power single-mode diode laser and compatible optical recording media has increased the probability of an optical disc product in the mid-1980s time frame. The product potentials range from video information applications to large archival digital data mass memories. The key to success in any of these application areas is the emergence of a useful recording media product.

## Acknowledgment

The author would like to thank J.P. Bednarz and C.J. Kaiser for their excellent technical assistance in many aspects of this work.

## References

1. Bartolini, R.A., Bell, A.E., Flory, R.E., Lurie, M., and Spong, F.W., "Optical Disk Systems Emerge," *IEEE Spectrum*, Vol. 15, pp. 20-28 (August 1978).

2. Lurie, M. and Flory, R.E., "Developing a Broadcast Quality Optical Video Disc System," CLEOS, San Diego, Calif. (February 1978).
3. Kenville, F.F., "Optical Video Disc for Very Large Digital Memories," *RCA Engineer*, Vol. 24, No. 1, pp. 27-31 (June/July 1978).
4. Ammon, G.J., Reno, C.W., and Tarzaiski, R.J., "Digital Optical Video Disc," *Final Report Government Contract F30602-78-C-0050*, Rome Air Development Center (April 1979).
5. Ammon, G.J. and Reno, C.W., "Optics for Multi-Beam Optical Disc Systems," *Proc. SPIE*, Vol. 299 (1981).
6. Botez, D., Spong, F.W., and Ettenberg, M., "High-Power Constricted Double-Heterojunction AlGaAs Diode Lasers for Optical Recording," *Appl. Phys. Lett.*, Vol. 36, No. 1, pp. 4-6 (1980).
7. Bartolini, R.A., Bell, A.E., and Spong, F.W., "Diode Laser Optical Recording Using Trilayer Structures," *J. Quantum Electronics*, Vol. 17, No. 1, pp. 69-77 (1981).
8. Asbeck, P.M., Cammack, D.A., Danicle, J.J., Lou, D., Heemskerk, J.P.J., Klouters, W.J., and Ophey, W.H., "High-Density Optical Recording with (GaAl)As DH Lasers," *Appl. Phys. Lett.*, Vol. 34, No. 12, pp. 835-837 (1979).
9. Bulthuis, K., Carasso, M.G., Heemskerk, J.P.J., Kivits, P.J / P.J., Kleuters, W.J., and Zalm, P., "Ten Billion Bits on a Disk," *IEEE Spectrum*, Vol. 16, pp. 26-33 (August 1979).
10. Botez, D., "CW High-Power Single-Mode Operation of Constricted Double-Heterojunction AlGaAs Lasers with a Large Optical Cavity," *Appl. Phys. Lett.*, Vol. 36, No. 3, pp. 190-192 (1980).
11. Olaofe, G.O., "Diffraction by Gaussian Apertures," *J. Opt. Soc. Am.*, Vol. 60, pp. 1654-1657 (1970).
12. Ammon, G.J. and Reno, C.W., "Optical Disc Recording at 300 Mbit/sec.," This issue of the *RCA Engineer*.
13. Botez, D., "Single-Mode Diode Lasers for Systems-Oriented Applications," This issue of the *RCA Engineer*.
14. Bartolini, R.A., Weakliem, H.A., and Williams, B.F., "Review and Analysis of Optical Recording Media," *Optical Engineering*, Vol. 15, pp. 99-108 (1976).
15. Harris, A.L., "Continuous Wave Laser Recording on Metallic Thin Film," *Image Technology*, pp. 31-35 (April/May 1970).
16. Maydan, D., "Micromatching and Image Recording on Thin Film by Laser Beams," *Bell System Tech. J.*, Vol. 50, pp. 1761-1789 (1971).
17. Corcoran, J. and Ferrier, H., "Melting Holes in Metal Films for Real-Time High Density Permanent Digital Data Storage," SPIE 21st International Tech. Symposium and Instrument Display, San Diego, Calif. (1977).
18. Bell, A.E. and Spong, F.W., "Antireflection Structures for Optical Recording," *J. Quantum Electronics*, Vol. 14, pp. 487-495 (1978).
19. Bell, A.E. and Bartolini, R.A., "High Performance Te-Trilayer for Optical Recording," *Appl. Phys. Lett.*, Vol. 34, No. 4, pp. 275-276 (1979).
20. Cornet, J., Lehureau, J.C., and Le Carvennec, F., "Characteristics and Performance of a Novel Recording Material," Conference on Lasers and Electro-Optics (CLEO), Washington, D.C. (June 1981).
21. Robbins, W., Freese, R., Smith, T., and Willson, R., "Bubble-Forming Media for Optical Recording: A New Approach," Conference on Lasers and Electro-Optics (CLEO), Washington, D.C. (June 1981).
22. Bell, A.E. and Spong, F.W., "Reversible Optical Recording in Trilayer Structure," *Appl. Phys. Lett.*, Vol. 38, pp. 920-921 (1981).
23. Bell, A.E., Bartolini, R.A., and Spong, F.W., "Optical Recording with the Encapsulated Titanium Trilayer," *RCA Review*, Vol. 40, pp. 345-362 (1979).

**Bob Bartolini** joined the technical staff of RCA Laboratories, Princeton, in 1966 where his work has included among other things: holography, which included development of novel optical recording materials for relief-phase and volume-phase holograms; integrated optics, which involved development of organic material for integrated optic devices; optical data storage applications, which has included development of systems for high-data-rate and high-density-data-storage applications using solid-state diode lasers. Currently, he is a Research Leader in the Optoelectronic Devices and Systems Research Group with responsibility for the research and development of optical information recording materials and systems. Dr. Bartolini has received three RCA Laboratories Achievement Awards, he holds 21 U.S. Patents, and he has published or presented over 50 technical papers.

Contact him at:
**RCA Laboratories**
**Princeton, N.J.**
**TACNET: 226-3129**

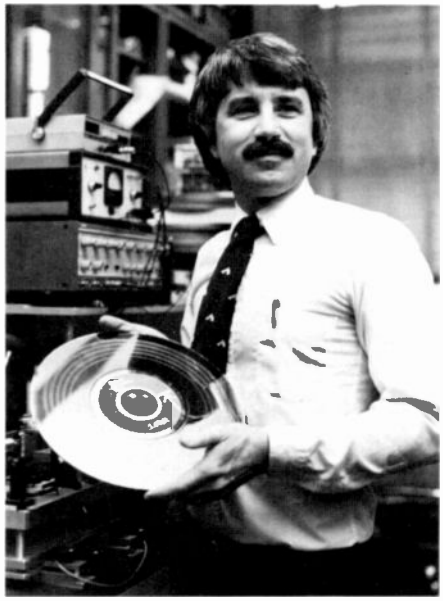

D.C. Ainsbury

# Design, development and installation of a fiber-optic communications system

*The fiber-optic system installed by RCA Systems Services provides the Royal Signals and Radar Establishment in England with a secure, versatile and reliable communications link between computers in several widely dispersed locations on the site.*

**Cable pulling.** The cable bundle is pulled through the duct and is guided over sharp edges to prevent damage to the fibers.

**Abstract:** *Under contract to the Ministry of Defense, RCA Systems Services designed and installed a fiber-optic communications system to link computers in three separate buildings. The network has five nodes and comprises a mixture of parallel, serial synchronous, and serial asynchronous data links. The longest link is approximately 440 meters and the shortest link is approximately 55 meters. Non-multiplexed methods are used to transmit parallel data. Five parallel data links and three serial data links were provided. The author reviews the components required, the design, and the system-installation process.*

Malvern, in Worcestershire, England, is a small spa town built on the slopes of the Malvern Hills; for many years it has been famous for its waters and hand-built Morgan Sports Cars. But Malvern is also the home of the Royal Signals and Radar Establishment (RSRE), an organization engaged in research and development for the Ministry of Defense.

RCA Systems Services tendered for a Ministry of Defense contract to design and install a fiber-optic communications system, to link computers in three separate buildings. Fiber-optic links were required to provide secure, interference-free communications over long distances. RCA was awarded the contract in August 1981 with the completion date fixed for the end of December, a contract duration of only 20 weeks.

The task was assigned to the Microprocessor Group, a small team in Systems Services specializing in the design and production of industrial and military microsystems, with skills in the fields of hardware, software, and computer interfacing.


Final manuscript received January 27, 1982.
Reprint RE-27-3-4

## Background to RCA Systems Services

Located in Guisborough, Cleveland, this small close-knit group concentrates on the

supply of services to customers who use computers to monitor, log, or control processes and operations. The services may be viewed in the following ways, although an individual customer's needs often embrace more than one of these subdivisions.

### *Contract programming*

The wide cumulative experience of our staff enables us to supply programmers and analysts with an appropriate background for most projects. Contracts may be arranged for any length of time for work either on the customers' own premises or at RCA premises. This service allows customers to supplement existing teams to ensure timely project completion, with RCA supplying special skills, or providing independent project control. It is also a cost-effective way of managing the maintenance of computer systems when occasional changes are outside the scope of the original team. RCA contract programmers have contributed to projects within, for example, ICI and British Steel, and are now contributing to Ministry of Defense projects.

### *Turnkey computer systems*

RCA's well-established project management skills enable the group to undertake full responsibility for building computer systems that meet stated functional objectives. Feasibility studies and research studies also fall into this category. The group's skills extend beyond writing real-time applications programs to include operating-system design and modification and also involvement with language processors. The group has its own computing facilities.

### *Microelectronic design*

This part of the group specializes in the design and construction, to customers' individual requirements, of special purpose interfaces, controllers, monitors, and so on. The use of CMOS microcomputer components is common when so many industrial applications require low power consumption, high reliability, and noise immunity. Prototype devices are designed and built at Guisborough. Small-scale production runs can be accomplished within RCA resources. The development of these devices is often a cooperative process in which RCA staff members work closely with customers' own research workers to achieve a satisfactory solution. The group has already constructed microprocessor-based equipment for many applications within public bodies such as the Navy, a Royal Ordnance Factory, and Nationalized Industries.

**Table I. Computer links and interfaces.**

| | | | |
|---|---|---|---|
| Dual DEC 10 (DR01-CL) | to | DEC 10 (DR01-CL) | Parallel |
| Dual DEC 10 (DR01-CL) | to | GEC 4065 (special I/F) | Parallel |
| Dual DEC 10 (DMR11-AB) | to | DEC 10 (DMR11-AB) | Serial V35 |
| Dual DEC 10 (DR01-CL) | to | VAX 11/780 (DR11W) | Parallel |
| Dual DEC 10 (DR01-CL) | to | PDP 11/34A (DR11W) | Parallel |
| Dual DEC 10 (DZ11A) | to | Modular One (DZ11A type) | Serial V24 |
| VAX 11/780 (DZ11A) | to | Modular One (DZ11A type) | Serial V24 |
| Dual DEC 10 (differential) | to | Line printer (differential) | Parallel |

## System requirements and objectives

The fiber-optic communications network was to have five nodes to connect the computers listed in Table I. The network, shown in Fig. 1, would comprise a mixture of parallel, serial asynchronous, and serial synchronous data links, and all the links would be bidirectional. The longest link (between buildings) would be approximately 440 meters, and the shortest link (inside the building) would be approximately 55 meters.

The data rates for the V24 serial asynchronous links would be 9600 baud, and the data rate for the V35 serial asynchronous link would be 56 Kbaud. The data rates for the high-speed parallel data links are a function of the types of interface boards used and the distance between interfaces, and rates range between 250,000 and 500,000 words per second, depending on the type of link. Two word lengths would be transmitted by the system, the lengths being 16 bits and 18 bits, again dependent on the type of interface used.

The contract requirement was for RCA to provide everything between the on-site computers. This included the copper cables between the computer interfaces and the data-link equipment cabinets, the cabinets including data-link electronics and power

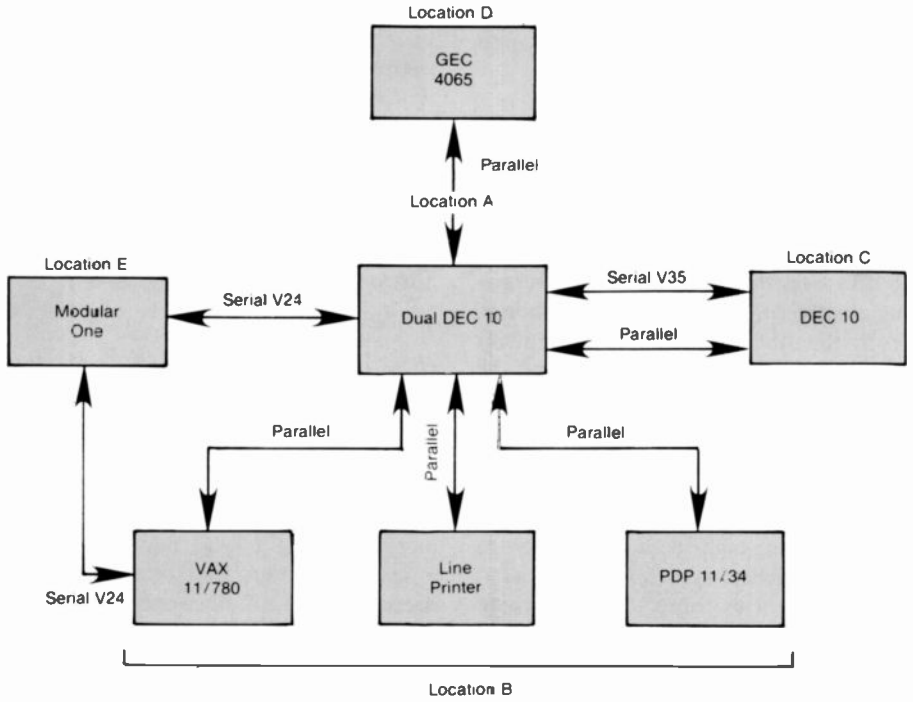


**Fig. 1. Fiber-optic communications network.** The diagram shows the distribution of data links and computers in the five locations.

**Table II. Data transmission rates,** using multiplexed and non-multiplexed approaches.

| *Approach* | *Data-transmission rate (words/second)* |
|---|---|
| Non-multiplexed, 300 meters | 250 K |
| Multiplexed, 300 meters | 217 K |
| Non-multiplexed, 30 meters | 454 K |
| Multiplexed, 30 meters | 357 K |

supplies, and the fiber-optic cables between data-link cabinets.

It was decided that RCA would be responsible for the system design, equipment production, installation, and contract management. The equipment production would include the cabinets, racks, power supplies and line driver/receiver cards, but not the fiber-optic components. A subcontractor, Focom Systems, was appointed to supply the fiber-optic transmitter/receiver cards, connectors and cables, and to assist with cable installation and termination.

The main design aims were for the equipment to be modular in construction for ease of maintenance, and to facilitate future modification and expansion. Standard commercial parts of good quality were to be used where possible, to minimize the design and production costs of the system. The equipment was to be self-contained, requiring connections only to the computer interface boards, the building power supplies, and the fiber-optic cables.

## Background to Focom Systems Limited

Focom Systems was formed in late 1979 to take over the Rank Optics fiber-drawing plant when Rank decided to withdraw from the fiber-optic business. Focom started trading in January 1980 and the majority of personnel within the company are from the original team that developed the Rank low-loss fiber-manufacturing process. Focom rapidly developed a range of optical fiber cables and terminal equipment including high-speed multiplexers to meet the practical needs of the computer, process-control and closed-circuit-television market.

This practical approach to the fiber-optic market has allowed Focom to contract for a wide variety of installations for both parallel high-speed data-transmission and multiplexed computer systems. Approximately 50 percent of the current installations are direct or associated Ministry of Defense equipment, the remainder being with major commercial companies.

Focom is among the market leaders in fiber-optics for short-haul and computer interconnection in the United Kingdom, and it is estimated that they currently supply more than 60 percent of this market. Focom mainly supplies short-haul fiber-optic systems with transmission distances of a few meters to 2 km. But installed at English Clays in Cornwall is a 256-channel system operating over some 4 km, and transmission over 12 km has been demonstrated with the standard Laser Transmitted and Avalanche Photodiode Receiver in Focom's 1600-series range of equipment. A number of tests have been carried out by RSRE on Focom and Rank natural fused-silica and synthetic silica fibers, mainly in the areas of low-temperature and high-radiation levels. We understand from the reports that the Plastic-Clad Silica fibers, which have been used for the current contract, have proved most successful in these tests.

## Design considerations—parallel links

Two methods of implementing the high-speed parallel data links were considered. The first method was to link all the control- and data-signal lines directly, with one fiber-optic cable per line. This method was considered to be expensive on components, using a large number of fiber-optic transmitters and receivers, and a large quantity of fiber-optic cable. The second method was to multiplex some of the signals, and transmit them serially down one or more fiber-optic cables. This method was initially considered less expensive on components, but introduced a time delay in data transmission and thus reduced the maximum transmission speed.

Both methods were examined in detail. The study was based on data-link distances of 30 meters and 300 meters, which were the original estimates provided by the customer. It was concluded that multiplexing data on the parallel data links between computers was feasible. However, this conclusion was based on a limited assessment of the data available and a theoretical design study, and not on a practical demonstration of a working system. The following paragraphs consider the relative merits of the multiplexed and non-multiplexed approaches, with reference to data-transmission rates, cable requirements, and data-link components.

The transmission rates in Table II were based on the following system parameters:

1. Back-to-back data-transmission time, including handshaking protocol, was 2 microseconds.
2. Transmission time for 30 meters of cable was 0.1 microsecond.
3. Multiplexing time for 8 bits was 0.6 microsecond.

The total amount of four-fiber cable required to implement four data links (excluding spare fibers) was as follows: non-multiplexed data links required 9720 meters; and multiplexed data links required 4800 meters. The multiplexed systems would therefore reduce the cable requirement by 4920 meters.

The reduction in fiber-optic cables required for the system would give a corresponding reduction in the labor requirements for cable installation, termination, and testing. This reduction was estimated to be approximately 5 man weeks.

If the multiplexed data links were adopted, the number of standard fiber-optic transmitter/receiver modules required would be reduced from 216 to 74, a saving of 142 modules. However, the data links would require 18 high-speed transmitter/receiver modules for the serial transmission of the data bits. These high-speed modules were considerably more expensive than the standard low-speed modules.

The multiplexed data links would also require 18 special multiplexer boards and 8 special control and synchronization boards. The design, development, and manufacture of these boards would incur a labor cost that would not be incurred if

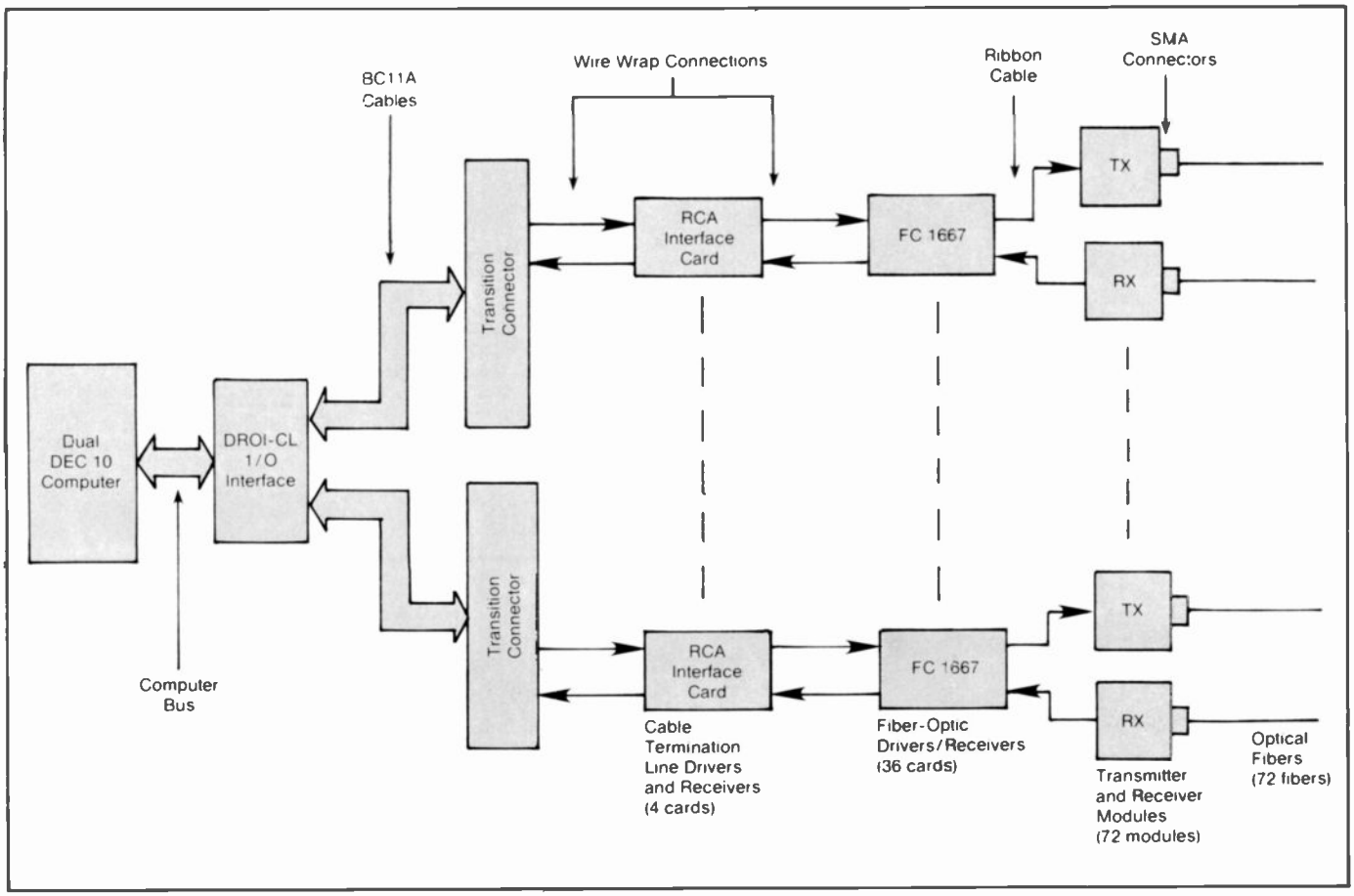


**Fig. 2. Typical configuration of parallel-data-link equipment.** This diagram illustrates part of the Dual-DEC-10-to-DEC-10 link.

the non-multiplexed data links were to be implemented.

Costs for the two parallel transmission schemes were estimated and it was found that the non-multiplexed method was only 10 percent more expensive than the multiplexed method. The saving in materials by multiplexing was almost balanced by the extra design and development labor costs. The results of the study were presented to the customer and it was decided to adopt the low-risk non-multiplexed method of transmitting parallel data. The block diagram of this method is shown in Fig. 2.

## Parallel link descriptions

Five parallel data links were provided. These include three different types, listed in Table III.

The first type is the Dual DEC-10-to-DEC-10 data link, which has a DR01-CL interface unit at each end. This interface unit allows back-to-back parallel communication between two DEC 10 computers by means of two BC11A ribbon cables, which plug directly into the interface-unit back-plane bus. The maximum back-to-back distance is approximately 10 meters. The data-link interface equipment supplied by RCA was designed to accept two BC11A cables and provided the correct termination and signal buffering, so as to appear electrically identical to a DR01-CL interface unit. A parallel interface card with line drivers, line receivers, and terminating resistors was constructed to provide the correct computer interface. This interface card was designed to accommodate 12 input and 12 output signals. The other side of this interface card was linked to the fiber-optic transmitter/receiver cards. A total of 72 signal lines were provided for this data link, 36 for data and 36 for control and parity signals.

The second type of parallel data link had a Dual DEC 10 at the local end and three different computers at the remote end, the different computers being a GEC 4065, a DEC VAX 11/780 and a DEC

**Table III. Link fibers and distances.**

| *Link* | *Number Fibers* | *Distance (meters)* |
|---|---|---|
| Dual DEC 10/DEC 10 (parallel) | 72 | 440 |
| Dual DEC 10/GEC 4065 (parallel) | 44 | 440 |
| Dual DEC 10/DEC 10 (serial V35) | 4* | 440 |
| Dual DEC 10/VAX 11/780 (parallel) | 44 | 55 |
| Dual DEC 10/PDP 11/34A (parallel) | 44 | 55 |
| Dual DEC 10/MOD ONE (serial V24) | 4* | 175 |
| VAX 11/780/MOD ONE (serial V24) | 4* | 150 |
| Dual DEC 10/Line Printer (parallel) | 20 | 55 |

*Including 2 spare fibers.

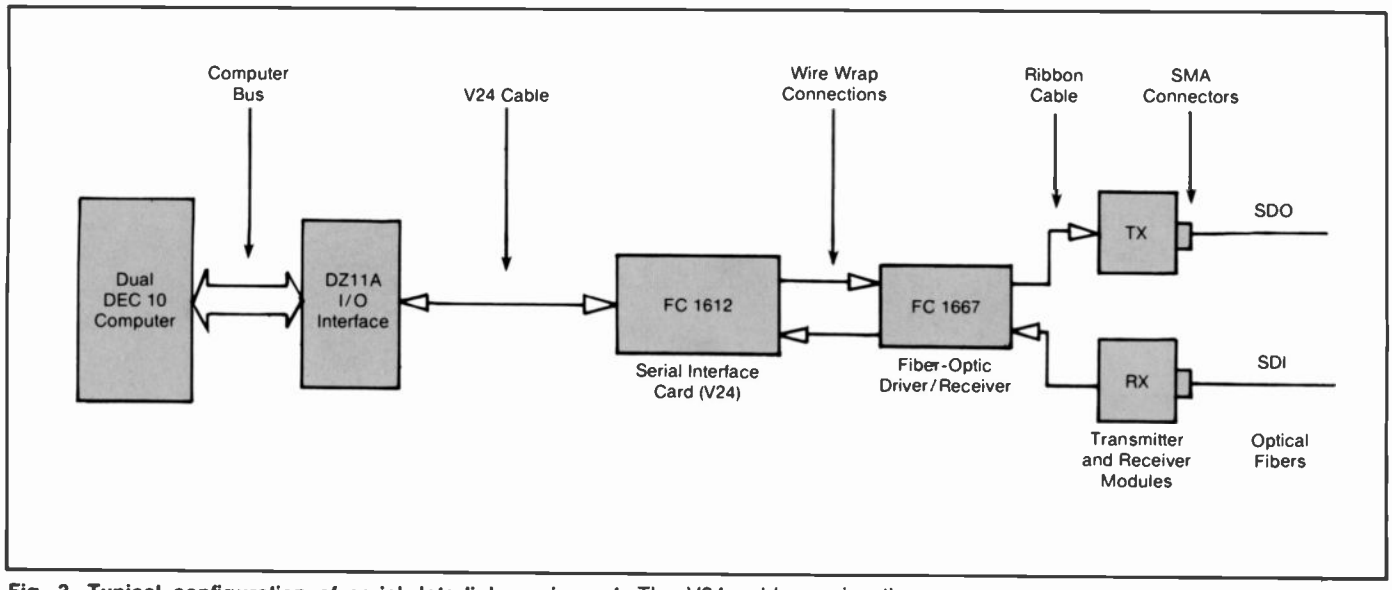


**Fig. 3. Typical configuration of serial-data-link equipment.** The V24 cable carries the normal RS232 data and handshaking signal lines.

PDP 11/34A. The Dual DEC 10 interface units were all the DR01-CL type; the VAX 11/780 and the PDP 11/34A had DR11W interfaces; and the GEC 4065 had an interface unit configured to look like a DR11B interface. These three data links were designed to accept a simple BC11A cable at the local end, and two BC08S-type cables at the remote end. The links used the same type of parallel interface cards as the DEC-10-to-DEC-10 link, to terminate the cable signals and connect them to the fiber-optic transmitter/receiver cards. A total of 43 signal lines were provided for each of these three data lines—32 for data and 11 for control and parity signals.

The third type of parallel data link was between the Dual DEC 10 and a line printer, which are normally connected by a multi-core twisted-pair cable. The data-link-interface equipment was designed to accept the standard DEC cables at the computer end and at the line-printer end. The equipment required another type of interface card because the signals are almost all differential; this card was designed to transmit and receive six differential signals and one TTL signal, and provide an interface between the twisted-pair cables and the fiber-optic transmitter/receiver cards. A total of 18 signal lines were provided for this data line—8 for data and 10 for control and parity signals.

## Serial link descriptions

Three serial data links were provided. The serial block diagram is shown in Fig. 3. These are in two different types and are also listed in Table III.

The first type is between a CTL Modular One computer at the remote end and two different computers at the local end, these computers being a Dual DEC 10 and a VAX 11/780. These computers all have DZ11A-type interface cards that provide full-duplex asynchronous serial communication at a rate of 9600 baud, by means of a V24 interface. The asynchronous serial-data-link equipment comprises a Focom FC 1612 V24 interface card and a fiber-optic transmitter/receiver card, and is connected to the computers at either end by standard V24 screened cables. The digital V24 signal is fed in and out of the system through a standard 25-pin D-type connector mounted on the rear of the equipment. This connector provides all data and protocol connections between the FC 1612 interface card. The card serializes the Request-to Send, Clear-to-Send data and feeds this at TTL levels to the optical transmitter. The signal, received at TTL levels from the optical receiver, is separated into data and protocol signals, and fed at V24 levels to the output pin on the 25-pin D-type connector. The interface card has a front panel on which is mounted light-emitting-diode (LED) status indicators and switches to control local and remote loop-back tests on the data link. Each serial data link has a total of two cables, one for transmitted data and one for received data.

The second type of serial data link is between the Dual DEC 10 computer and the DEC 10 computer. These computers both have DMR11-AB interface cards that provide full-duplex synchronous serial communication by means of a V35 interface at a rate of 56 Kbaud. The synchronous serial-data-link equipment comprises a Focom FC 1612D V35 interface card and a fiber-optic transmitter/receiver card, and is connected to the computers at either end by screened twisted-pair cables with MRAC connectors. The FC 1612D interface card is very similar to the V24 interface card described above, except that it accepts the differential inputs required by the V35 convention.

## Fiber-optic components

The fiber-optic components purchased from the subcontractor included all fiber-optic transmitter/receiver cards, serial interface cards, cables, and connectors.

The transmitter/receiver cards, shown in Fig. 4, were developed specifically for this application, using existing circuit designs but re-packaged to make optimum use of the space available. RCA components were used in both the logic and electro-optic circuits on this card. The transmitter/receiver system is in two parts. The first part is a single eurocard printed-circuit board with a TTL-level input and output and some of the fiber-optic driver/receiver circuitry. The second part is the fiber-optic transmitter/receiver modules containing the high-gain driver/receiver circuits and fiber-optic connectors, which are mounted on a special plate on the rear of the card frame, and connected to the card's back-plane by means of a ribbon cable.

The transmitter-input signal passes through a buffer and drives a transistor

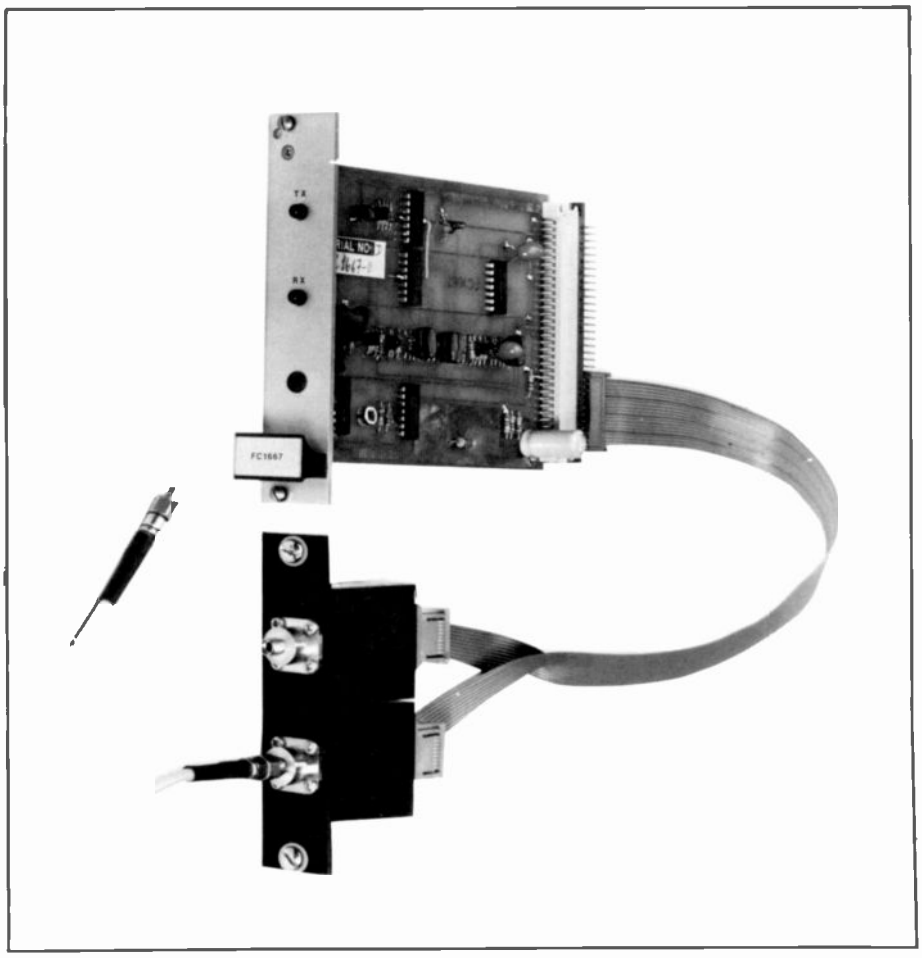

**Fig. 4. Fiber-optic transmitter/receiver modules,** which provide an interface between the fibers and the rack-mounted eurocard.

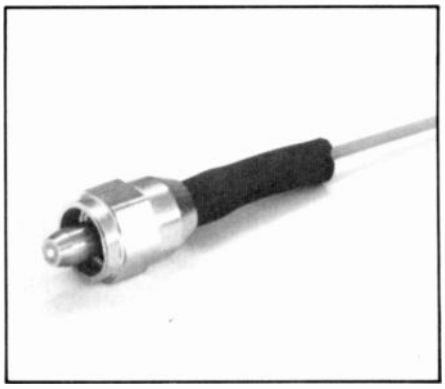

**Fig. 5. SMA connector.** This type of connector is widely used in Europe and provides a simple method of terminating the fiber and cable sheath.

stage, where the bias and feedback are added to produce the drive to the output transistor, which in turn modulates the output LED. The LED current is monitored to prevent current overdrive, thereby ensuring maximum life in the optical transmitter. Controls on the card allow for the independent adjustment of both bias and modulation. The LED works in the infrared spectrum with an emission wavelength of 820 nm and a minimum output of 200 $\mu$W into a 200-$\mu$m-core fiber. The data-transmission baudwidth is dc to 5 MHz (10 Mbit/s, non-return-to-zero).

The receiver module uses a *pin* diode as the optical detector and requires a minimum signal level of 0.7 $\mu$W to give a $10^{-9}$ bit-error rate. The photocurrent from the *pin* diode is amplified in a first-stage FET integrated circuit, where an automatic gain control (AGC) voltage is derived, which controls the amount of photocurrent reaching the second-stage high-gain amplifier. The signal is then fed to a dual-threshold Schmitt trigger to recover the data. The maximum transmission distance with this system is 800 nm, using 25-dB/km optical fiber.

The front panel of the transmitter/receiver card has two LED indicators that display the status of the transmitter and receiver circuits and indicate correctly operating data links. These status-indication signals are also taken off the card and used by the data-link monitoring equipment.

The cable used in this installation contains four 200-$\mu$m-core plastic-clad silica fibers, with an attenuation of less than 25 dB/km. Each fiber has a silicone cladding to 380 $\mu$m and a Tefzel™ jacket with an overall diameter of 600 $\mu$m. The four fibers are laid in a 6-mm flame-retardant polyethylene sheath that is reinforced with three Kevlar™ strength members, which gives the overall construction a tensile strength in excess of 90 kg. This cable can be pulled into earthenware, plastic, or metal ducting in straight pulls of up to 1 km. The fibers have a 3-dB bandwidth of 25 MHz-km, a minimum static-bend radius of 90 mm and a temperature rating from −10°C to +70°C.

Each optical fiber terminates in a single SMA-style optical connector, shown in Fig. 5, manufactured in France by Radiall. The connectors are crimped to the 200-$\mu$m-core fiber and then cleaved to provide the optically finished face. The crimp-and-cleave connector has several advantages over the earlier connectors, which were potted and then ground and polished. With the crimp-and-cleave connector, the termination time for each fiber end has been reduced from something like 20-to-30 minutes to a matter of 5-to-10 minutes depending on the accessibility of the cable. In addition, the repeatability of the fiber end has been considerably increased, because the crimping and cleaving is controlled by the crimp tool and cleaving jigs. Because the tooling, rather than the technician, now controls the termination of the cable, relatively unskilled operators can terminate fiber-optic cables quickly and easily.

An advantage in this particular installation was that the cables could be pulled through wet and dirty ducts with the minimum of protection on the cable ends, the cables were then terminated after installation in a clean environment. Factory-terminated cable would have required a large degree of protection during the cable-pulling operation, and would most certainly have suffered connector damage.

## Cabinet design

The data-link equipment at each of the five nodes in the network is contained in a standard commercial 19-inch cabinet. The five cabinets vary in height according to the number of card frames required for each location, the smallest being 3-U high and the largest 39-U high (the U unit is the European standard measurement for

cabinet height, and is approximately 1¾ inches). The four largest cabinets (33 U and 39 U) have front and rear doors that allow easy access to both card frames and cables. These cabinets also contain 19-inch rack-mounting power-supply subassemblies, which were specially constructed to provide the power for the card frames. The power distribution is by means of heavy-duty bus bars attached to the side of each cabinet; the bus bars accept push-on spade connectors at half-inch intervals, and were incorporated in the design to keep the cabinet wiring as simple as possible.

The data-link printed-circuit boards are all single eurocard size, 100 mm by 160 mm, with a 25-mm front panel and a European DIN standard 41612 two-part edge connector at the rear. Two sizes of DIN connectors were used, 32 pins in a 64 shell and 64 pins in a 96 shell. These connectors all had wire-wrap pins and covered the pin-out requirements on all the different boards in the system. The front panels were used to mount LED indicators and test switches. The panels also had locking screws to fasten the cards into the card frames.

The printed-circuit boards for each data link were plugged into standard 19-inch rack-mounting card frames. The most complex link (DEC 10 to DEC 10) required three frames, bolted together using tie-bars to create a subassembly that was wired as one unit before installation in the cabinet. The simple serial-data-link node required only one card frame, which held the cards for two V24 links and the rack-mounting power-supply cards. Each card frame was fitted with a seven-line printed-circuit-board back-plane mounted on the rear of the DIN card. The remaining three tracks were for two fault signals and a board-in-place signal. The computer-interface cable connectors were also mounted on the rear of the card frame. Small printed circuit boards were built to mount the two types of parallel connectors, with tracks taken to wire-wrap pins, to facilitate wiring to the wire-wrap pins on the DIN sockets.

A special mounting plate was constructed to hold 12 fiber-optic transmitter/receiver modules and serial interface connectors. This plate was attached to the rear of the card frame and was designed to hinge down, thus providing access to the back-plane and computer-interface connectors. The transmitter/receiver modules were mounted one above the other on a one-inch panel, and attached individually to the mounting plate by quick-release fasteners. The modules were connected to their associated driver/receiver boards by short ribbon cables, which plugged onto the wire-wrap pins on the rear of the DIN connector. Viewed from the rear, the rack layout was such that computer cables were routed up the right side of the cabinet, and the fiber-optic cables were routed up the left side of the cabinet.

**Fig. 6. Installation of the cable ducts.** This shows the cable sock that attaches the draw rope to the cable bundle.

Each data-link subassembly of one, two, or three card frames included a specially designed monitor card. The function of this card was to monitor the three power-supply voltages, the board-in-place signal from the cards in the racks, and the transmitter and receiver fault signals from the fiber-optic driver/receiver cards. The object of the card was to provide a system normal signal that could be displayed locally on each data-link subassembly, summarized on the front panel of each cabinet, and displayed remotely as a link-alarm signal.

The power-supply subassemblies were specially constructed in 6-U high 19-inch rack-mounted card frames, and four units were built and mounted in the rear of the four large cabinets. These units were designed to accommodate three types of commercial power supplies; these were 5-volt and 12-volt linear supplies and 12-volt high-current switched-mode supplies. The numbers of each type in the four power-supply subassemblies varied according to the needs of the individual cabinets. This modular approach to the construction of the power supplies meant that only three different types were used in the whole system and, therefore, the number of spare power supplies could be kept to a minimum. The 5-volt and 12-volt supplies were plug-in boards and were used for the TTL logic and the fiber-optic receiver bias. The 12-volt switched-mode supplies (10-amp versions) were used to provide the fiber-optic transmitter drive current, and the largest cabinet required approximately 25 amps. All the power-supply units were fitted with filters, to ensure that transmitted interference from the building power supplies was kept to a minimum. The power-supply subassemblies were fitted with a front panel with the cabinet mains switch and LED indicators for each voltage rail. The two largest cabinets were also fitted with fans to provide forced air cooling.

## System installation

The system installation was in two parts, the first being the cable installation, termination and test. The fiber-optic cable runs between buildings were laid underground in 4-inch plastic ducts, with inspection pits where the ducts change direction (Fig. 6). The longest run between nodes was 440 meters and required 31 four-way cables. The cables were pulled in the same way as normal electrical cable, using a cable sock and draw ropes in the ducts. Care was taken where the cable changed direction, and it was important to maintain a certain minimum bend radius so as not to damage the optical fibers. Inside the buildings, the cable was laid in standard trunking. The installation team fortunately chose a dry day for the job, and in that day laid over 13½ km of cable.

At each computer location, the cables were brought in under a false floor and terminated in die-cast-aluminum splitter boxes The purpose of these boxes was to clamp the outer sheath of the four-way cable, split the optical fibers into four individually sleaved cables, and clamp the outer sheaths of of these single-fiber cables (Fig. 7). These cables were then terminated with the SMA-type connectors described previously. Every fiber and connector in the network was tested for continuity first of all and then attenuation, to ensure that all optical fibers were continuous and correctly terminated. In the whole installation, only one fiber was found to be broken. Fortunately, it was part of an inside run of only 55 meters. The total amount of four-fiber cable used in the installation was 15½ km and required approximately 500 SMA connectors.

The equipment cabinets were fully tested at Guisborough before being shipped to Malvern for installation, commissioning, and system test. A special test unit was built to inject 100-ns squarewave or pulse signals into the computer interface cables and test the individual data paths between all the computers in the network. The on-site system and acceptance tests included the running of communications software and the transmission of test messages between all computers. The completed system provides RSRE Malvern with a secure, versatile and reliable fiber-optic communications system.

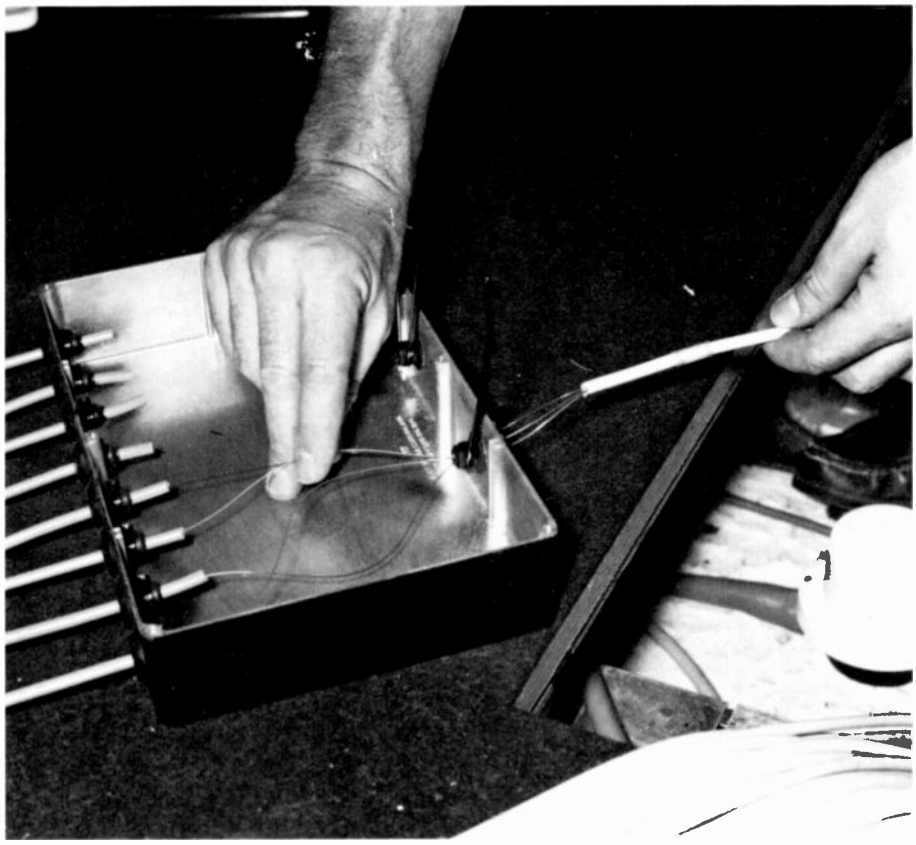

**Fig. 7. The cable-splitter box,** which splits the fibers from 2 four-way cables and clamps the outer sheaths.

In conclusion, the contract has been extremely valuable to the RCA Systems Services group, it has been a useful design exercise in a new area of technology, and it has provided the group with experience in a rapidly expanding field. Fiber-optic communications will be used on an increasing scale in both industrial and military applications, and the experience gained on this contract should provide RCA with similar business in the future.

**David Ainsbury** is Leader, Microsystems Development Group, RCA Systems Services Limited. He joined RCA in September, 1971, as a programmer analyst on the BMEWS system. He has worked on the software and hardware of a large variety of industrial and military microsystems, and has over 15 years of experience in the electronics and computer industry.

Contact him at:
**RCA Systems Services Limited**
**9a-11a Market Place**
**Guisborough, Cleveland (Great Britain)**
**TS14 6BN**

G.J. Ammon | C.W. Reno

# Data recording on optical discs at 300 Mb/s

*The tracks are 0.4-μm wide, the disc capacity is 6.25 gigabytes with each disc side holding the equivalent of 50,000 images, the data rates are 300 Mb/s, and the potential is being realized at the Advanced Technology Laboratories in Camden.*

**Typical trilayer optical disc.**

**Abstract:** *Optical disc recorder systems are being developed for ultra-high data rate, high-density storage applications. These systems use multiple, independently modulated laser beams to simultaneously record closely spaced tracks of data, with close to diffraction-limited performance.*

*The record-and-playback source for these systems is an argon laser whose output is efficiently split into the number of beams needed to achieve the desired data rates. The recording beams are passed through a multiple transducer A-O modulator to encode the information to be recorded. An optical system focuses the modulated beams onto the record disc. A second set of low-power unmodulated beams pass through the same optical system and are focused onto the optical disc to allow data verification playback while recording is in progress. These same beams are used for normal playback during subsequent data-retrieval operations.*

The optical disc has become a viable candidate for archival mass digital data storage systems. The write-once read-many-times characteristic of today's laser-ablated, thin-metal-film disc structures is well suited to data bases that must remain intact for many years. The materials used in optical discs allow for potentially long periods of storage without stringent environmental controls. The high storage densities associated with diffraction-limited optical systems provide a cost per recorded bit that is an order-of-magnitude lower than with any other media.

This article describes a design approach for a wideband optical disc data-recorder system. The approach is based on splitting the output of a single laser into multiple beams, which are independently modulated and used to simultaneously record multiple tracks of data at high rates onto a trilayer optical disc.

An engineering model has been developed to verify the feasibility of this approach. It can record $5 \times 10^{10}$ bits of data on one side of an optical disc at user rates of 300 Mb/s. This system has achieved a bit-error rate of one in $10^8$ while allowing access to any block of data in less than 0.5 s. Achievement of these results required the generation of multiple laser spots focused into a 0.4-μm diameter and spaced on 1.25-μm centers. These record spots had to be a minimum of 15 mW in amplitude and modulated at up to 50 Mb/s. In addition, a set of unmodulated collinear low-power spots were required for playback and data-verification purposes.

## The basic optical disc system

Figure 1 is a basic block diagram for an optical disc system. A modulated laser beam is focused onto a rotating disc to form a series of "pits" arranged into a circular track. The record process involves melting the thin metal film on the disc to permanently ablate the surface and store the desired information. Readout is accomplished by lowering the laser power to inhibit ablation, removing the modulation,


Final manuscript received March 2, 1982
Reprint RE-27-3-5

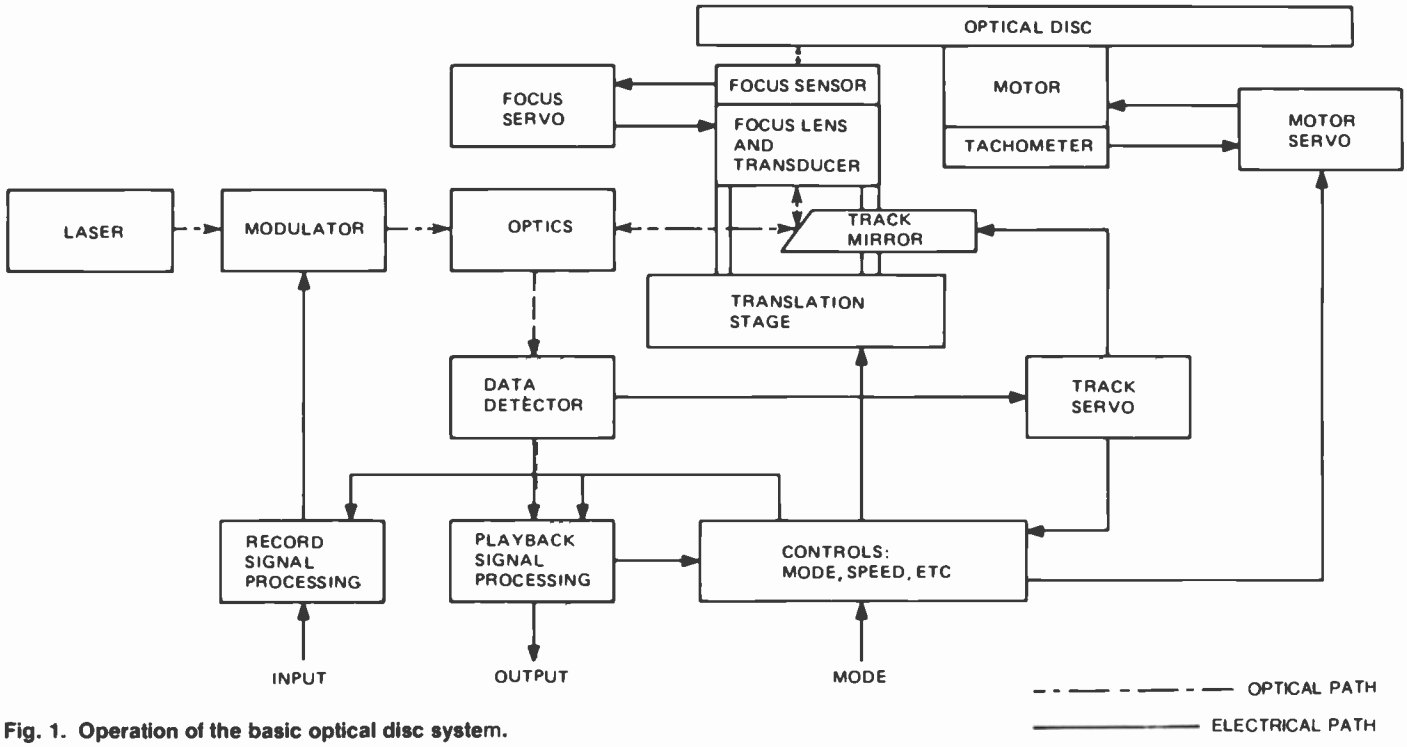


**Fig. 1. Operation of the basic optical disc system.**

and sensing the reflected light from the disc's surface.

Three servo systems are used. A focus servo keeps the laser beam focused, in the presence of surface uneveness, to a diffraction-limited spot on the disc's surface. A track servo follows the recorded tracks during readout, correcting for eccentricities due to imperfect centering. A motor servo maintains a constant disc speed, to record and play back at a fixed data rate.

The heart of the optical disc system is the unique "trilayer" optical disc.* This article's lead illustration (p. 36) is a photograph of this disc and a sectional view of its structure is shown in Fig. 2. The disc is formed by depositing a number of layers onto a substrate that is similar in size and shape to an ordinary audio-LP record. The trilayer section of the disc is designed as an antireflection structure and it absorbs almost all of the incident laser light. The thin-metal ablation layer is melted by the laser radiation to expose the reflector layer. The function of the transparent overcoat is to protect the trilayer section from handling, and to prevent optical blockage from dust particles and small scratches. The advantage of the trilayer optical disc is that recording can take place in a very thin (7.5-nm) layer that is completely encapsulated. This yields good signal-to-noise and playback contrast, as well as high sensitivity and immunity to environmental effects. The trilayer structure is also easily modified to accommodate lasers of various wavelengths (HeNe, GaAs). This is done by changing the thicknesses of the metal ablation and dielectric layers to achieve the antireflection condition at the laser wavelength.

*See article in this issue, "High density optical recording using diode lasers," R.A. Bartolini, *et al.* Also, see references 1 and 2.

## *Data path*

The data path of the digital optical disc system is illustrated in Fig. 3. User data is fed into the input-buffer portion of the system. This circuitry allows data to flow into the system on a continuous basis, and to be transmitted for addition of overhead information on a demand basis. Data from the input buffer goes to the record formatters in bursts called sub-blocks. Each sub-block is passed through an error-detection-and-correction (EDAC) encoder that adds parity bits for subsequent error protection during playback. The record formatter then groups the sub-blocks into address blocks onto which is added address information to facilitate data retrieval on playback. Finally, the record formatter groups the address blocks into user-oriented blocks that match a convenient subset of the data to be recorded and retrieved.

Formatted data from the record formatter is sent to the record electronics portion of the disc-drive unit. Here the data is encoded into the delay-modulation-recording code used to transfer data on and off the optical disc. The record electronics also adds special sync symbols to the encoded data pattern. These symbols are used to identify the start of the sub-blocks and address blocks on playback. The formatted and encoded data from the record electronics is fed to the laser modulator portion of the record/read station.

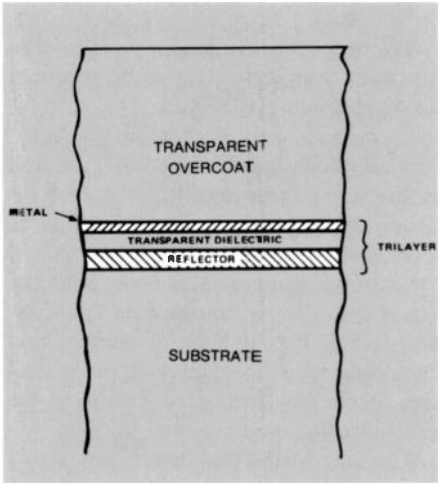


**Fig. 2 Sectional view of trilayer structure showing the protective overcoat.** The trilayer structure is composed of a metal recording-layer, spacer, and reflector, on the disc substrate.

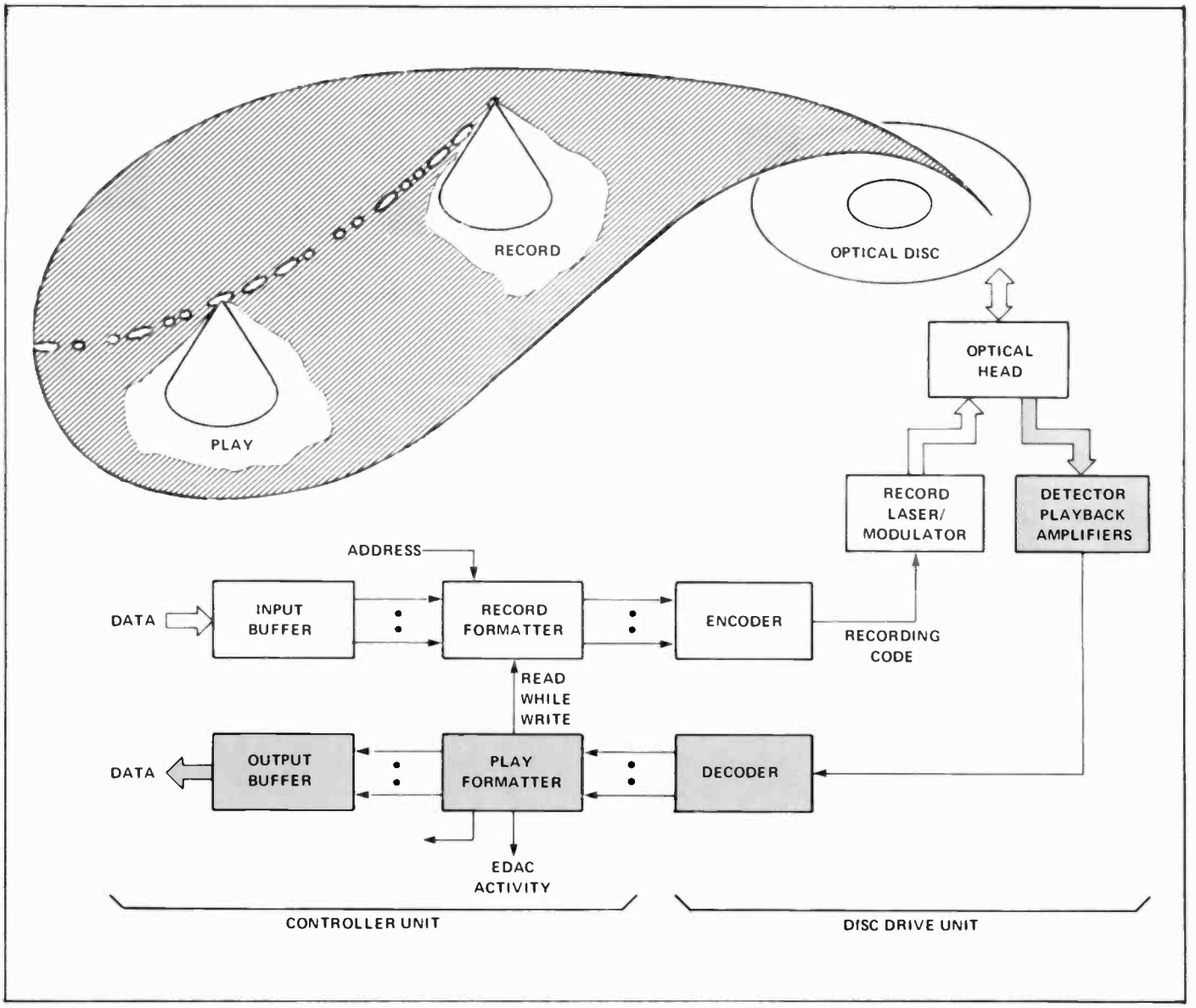


**Fig. 3. Digital optical disc data flow from data source to playback data.**

The record/read station provides the functions that allow data to be recorded onto a disc and played back. This includes the generation and modulation of the argon-laser beam used for recording, as well as the servo and optics functions for focusing the beam onto the optical disc to form data "pits." On playback, a second lower-power unmodulated beam from the argon laser illuminates the data "pits" on the disc. Reflected light is detected and demodulated in the play electronics and sent to the play-formatter portion of the controller unit.

The play formatter corrects any errors in the data and strips off the address overhead information used for track identification during high-speed access. The resultant playback data is fed to the output buffer for subsequent transfer to the user. This buffer "de-skews" the data and presents it to the user as a continuous stream.

## *Error control*

The integrity of the data stored in the digital optical disc system is maintained through the use of several error-control[3] measures, as illustrated in Fig. 4.

Because the major error sources are media related, the quality of the disc substrate and subsequent coatings must be controlled to minimize dropouts or voids in the coatings, and surface irregularities. The effects of dust particles and scratches can be minimized by the use of a protective overcoat that places them out of focus with respect to the active layers on the disc. The overcoat will also protect the active layers from contaminants that could speed aging of the disc. Additional control of the potential errors due to dust and mishandling is achieved through the use of a protective cartridge. The result is that only the very small particles are able to penetrate the cartridge and accumulate on the disc. Because of their small size, the effect of these particles is essentially eliminated by the overcoat.

The basic error-management philosophy that has been implemented at RCA involves a combination of write-verification (read-while-write), rewrite, and EDAC techniques. These techniques are augmented by specifically designed data formats, data-encoding techniques, equalization techniques, and the high signal-to-noise ratio (during playback) of RCA's trilayer disc structure.

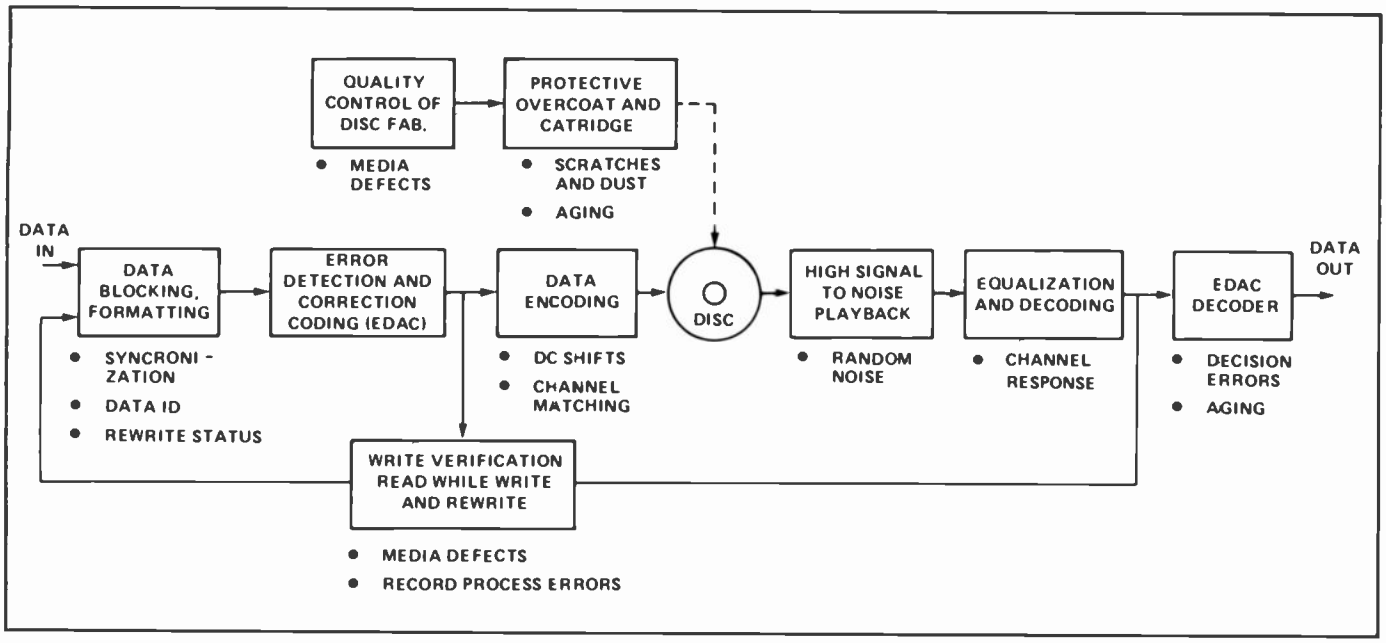


**Fig. 4. Flow diagram of error control approach.** This diagram shows the philosophy used to achieve ultimate bit-error rates of less than $10^{-8}$ and an archival lifetime.

As indicated in Fig. 4, the read-while-write and the rewrite functions are independent of the EDAC processing in that the written data is verified in its EDAC-encoded form, and rewrite decisions are made before the data is corrected by the EDAC circuitry. This approach was chosen so that at the time of recording, the bit-error-rate performance of the system would be met using only a fraction of the EDAC capability. The task of the EDAC subsystem then is to protect the data from aging or use-related problems, such as dust or "soft" errors caused by tracking- or focus-subsystem disturbances.

## A 300-Mb/s recorder/player system

### *Multibeam optical system*

Figure 5 shows the optical system for the engineering model of a 300-Mb/s nine-beam recorder system. Because of the need to record at high data rates and high packing density, an argon laser was selected as the recording source. Its high output power (approximately 2 W) and short wavelength (0.488 $\mu$m) are ideally suited to these requirements. This laser's output beam is first passed through a primary beamsplitter (BS) that allows 95 percent of the beam to be passed through to the record beamsplitter. The record beamsplitter efficiently divides the single high-power argon-laser beam into nine separate beams with equal amplitudes. The equal-amplitude beams are passed through a multichannel modulator that independently impresses each beam with the information ($m_1$ through $m_9$) to be recorded.

The modulated beams are passed through the beam-combiner optics, which merge them with an equal number of unmodulated lower-power beams to be used for playback. These playback beams are obtained by passing 5 percent of the argon laser's output through a play beamsplitter. The polarization of these beams is set to allow them to pass through the polarizing beamsplitter and quarter-wave plate ($\lambda/4$) to the beam-combiner optics with minimum attenuation.

The beam combiner aligns the record and play beams so that they can be passed through a common optical system to the optical disc. The beams are first expanded to collimate them and provide the magnification needed to fill the objective lens and allow the formation of diffraction-limited spots on the optical disc. As shown in the inset of Fig. 5, the record spots (R) are aligned on the disc to form closely spaced parallel circular tracks of data. These spots have sufficient power to ablate the optical disc to form pits with reflectivities much higher than the normally absorptive disc surface. The play spots (P) are aligned to be collinear with the recorded tracks at a point where they allow readout of the data just after it is recorded. Light from the playback spots is reflected by the recorded pits on the disc and passed back through the optical system to the polarizing beamsplitter. At this point, light polarization has been changed by 90 degrees (two passes through $\lambda/4$) and the light is directed to the nine-element detector array. The changes in disc reflectivity introduced during the recording are then converted back into electrical signals ($d$) containing the recorded information. Playback is used during recording to verify that the information has been recorded properly. When recording errors are detected, these data are re-recorded until no errors are detected.

The same play spots are used for playback subsequent to recording. Here though, a tracking servo is required to keep the play spots properly aligned to the data tracks. To accomplish this, the galvo is used to steer the play beams along the radial disc direction. A dither tracking servo[4] drives the galvo to lock the beams to the tracks. This, in combination with readout of the track's address, allows the play spots to be lined up with the proper set of recorded tracks.

A focus servo is required, also, for proper operation of this optical system. The focus servo is needed to keep the objective lens at the proper distance from the optical disc to form diffraction-limited spots during record and playback. The elements for this servo are not shown in Fig. 5, but the scheme employed involves using a separate laser beam (HeNe) passing through one side of the objective and reflecting back to a split detector. The detector is aligned such that at focus, the reflected spot is centered; out of focus,

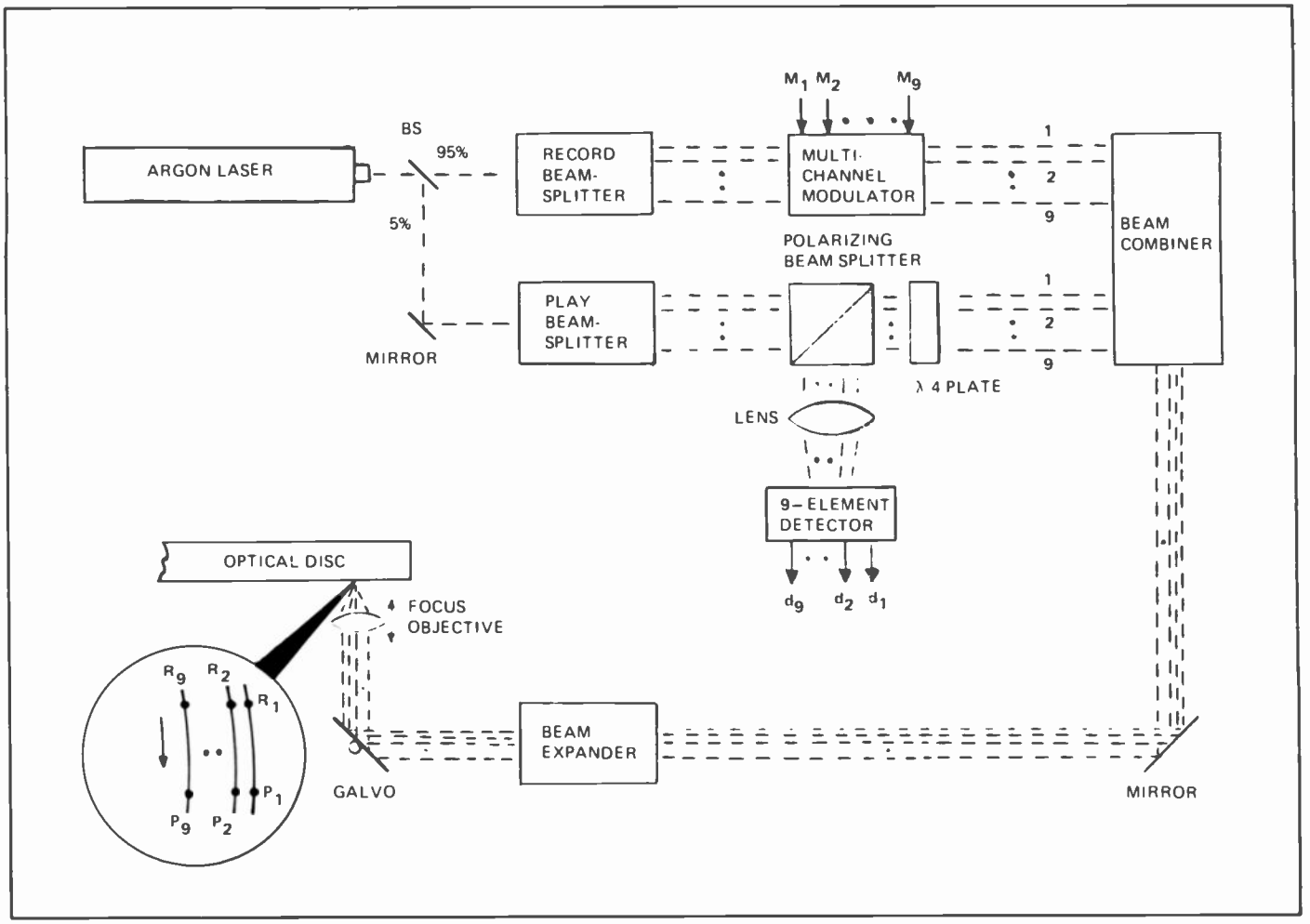


**Fig. 5. Functions of the multibeam recorder optical system** illustrating the techniques used to create read-and-write spots at the disc and also to play the disc.

the spot moves to one side of the detector.

## Key system components

Several key components were required to implement the multibeam optical disc recorder. A series of design trade-offs was conducted to select the best approaches for each component development. The most important selection criteria were optical efficiency, alignment stability, and ease of construction.

*Record/playback beamsplitters.* The optimum approach to beamsplitting was through the use of a complex phase grating. The phase grating was designed by adapting the techniques of Lee.[5] Beam patterns were calculated by summing the pattern from each portion of the grating lying within the beam and by considering each sector as a slit. The results of these calculations are shown in Fig. 6 for a nine-beam grating. The residual deviation between beams in the nine-beam case was reduced (theoretically) to ±1 percent from the average for a grating of 141-μm period and 39-, 28-, 9.5-, 27-, 9.5-, and 28-μm slit widths; all with a phase shft of 77.3 degrees.

The nine-beam grating was constructed using integrated circuit (IC) techniques. A metal master was made using the IC mastering equipment at the Solid State Division facilities in Somerville. This master was accurate to ±0.25 μm. Replication into a phase grating was accomplished in the silicon-on-sapphire processing facility in Princeton. An $SiO_2$ layer was grown on a sapphire window using chemical vapor deposition. Plasma etching of the photoresist was used to achieve very high accuracy in the final replication. A photomicrograph of the nine-beam grating is shown in Fig. 7, along with a photograph of the spots formed when a laser beam was passed through it. The relative intensities of the spots (488 nm) are within ±6 percent of the average, and the overall grating efficiency puts 68 percent of the input laser beam into the nine output beams.

*Multichannel modulator.* The multichannel modulator selected for the nine-beam system was developed by Harris,

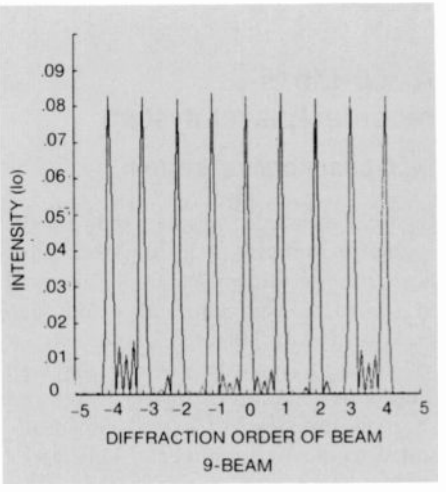


**Fig. 6. Calculated beam intensity distribution** for a phase grating having slit widths of 39-μm, 28-μm, 9.5-μm, 27-μm, 9.5-μm, and 28-μm. This pattern is repeated several times. The phase steps alternate ±77.3 degrees at the laser wavelength.

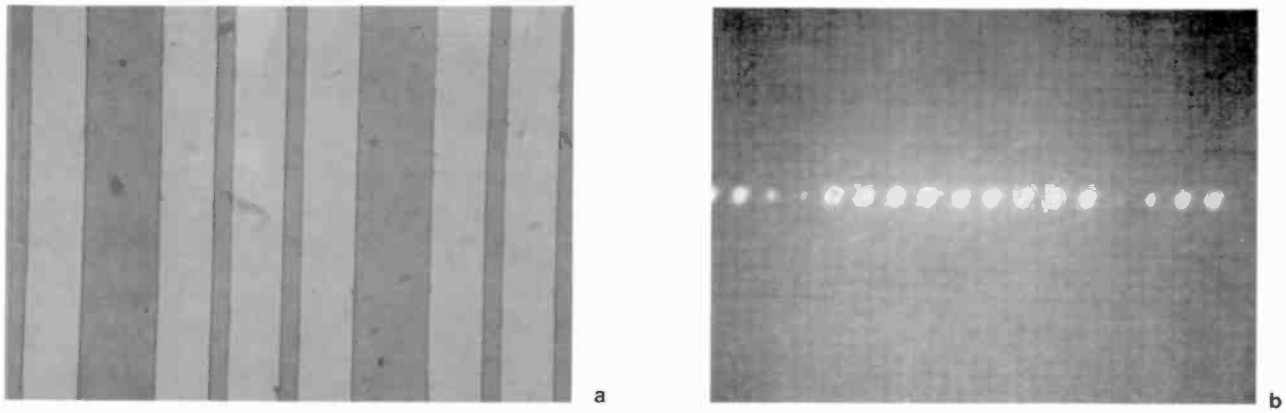

**Fig. 7. Nine-beam grating measurements. (a)** Photomicrograph illustrating construction. **(b)** Output spots showing nine nearly equal spots, plus lower-intensity higher orders.

Inc. It consists of a 3.5-inch by 3.5-inch by 1.75-inch head and a rack-mounted electronics enclosure. Specifications are summarized in Table I. The head, shown in Fig. 8, consists of a housing, the modulator crystal with transducers, transmission lines, matching networks, and 10 SMA connectors. The modulator crystal is fabricated with 10 separate transducers bonded to the crystal. Separations are 300 $\mu$m. Although light inputs and outputs are parallel, they are displaced by 18 mm because the crystal is fabricated with nonparallel input and output faces. This allows ease of access to a region close to the transducers without obstruction by the mount.

**Table I. Specifications for 10-channel modulator.**

| | |
|---|---|
| Operating wavelength | 488 nm |
| Number of channels | 10 |
| Risetime/falltime | <10 ns |
| Diffraction efficiency | >60% |
| Optical transmission (diffracted) | >50% |
| Transducer separation | 300 $\mu$m |
| Transducer width | 75 $\mu$m |
| Cross talk | 3.0 : 1 optical* |
| Optical beam waist diameter ($1/e^2$) | 30 $\mu$m |
| RF phase | Quadrature for adjacent channels |

* Operated at 100 : 1

The modulator driver consists of a single-oscillator power splitter and 10 rf modulators, followed by individual linear gain stages. Individual switches are supplied to enable each channel. A master switch on the rear panel provides a cw signal on each enabled channel for test purposes. Inputs are differential emitter-coupled logic (ECL) using Twinax, and each line is terminated in 50 ohms.

*Multi-element detector.* The multi-element detector selected for the nine-beam system is a nine-element hybrid avalanche photodiode array, shown in Fig. 9. This array, fabricated by RCA, Ltd., consists of nine chips normally fabricated as the C30817 avalanche photodiode. The chips are mounted on a custom hybrid sub-

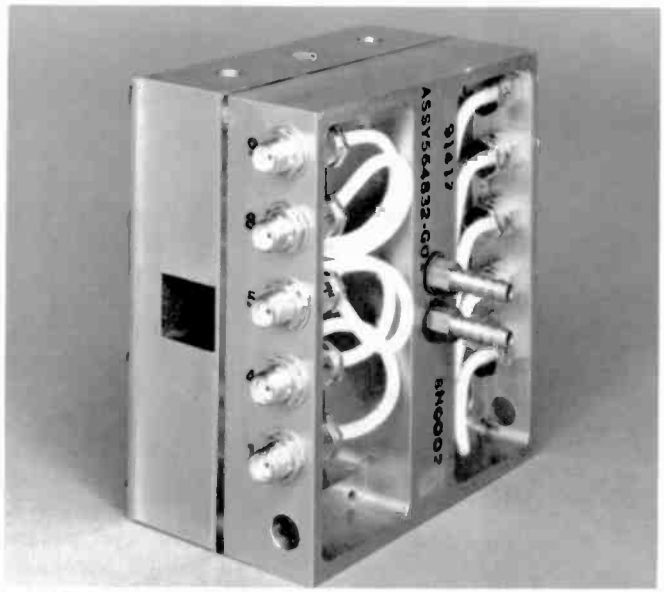

**Fig. 8. The 10-channel, 50-Mb/s/channel acousto-optic light-modulator head.**

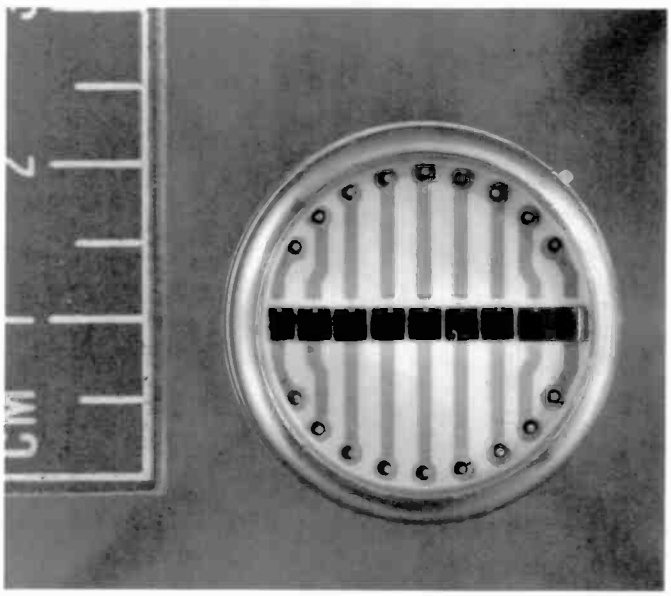

**Fig. 9. Nine-avalanche-diode-photodetector array used for playback detection in the system.**

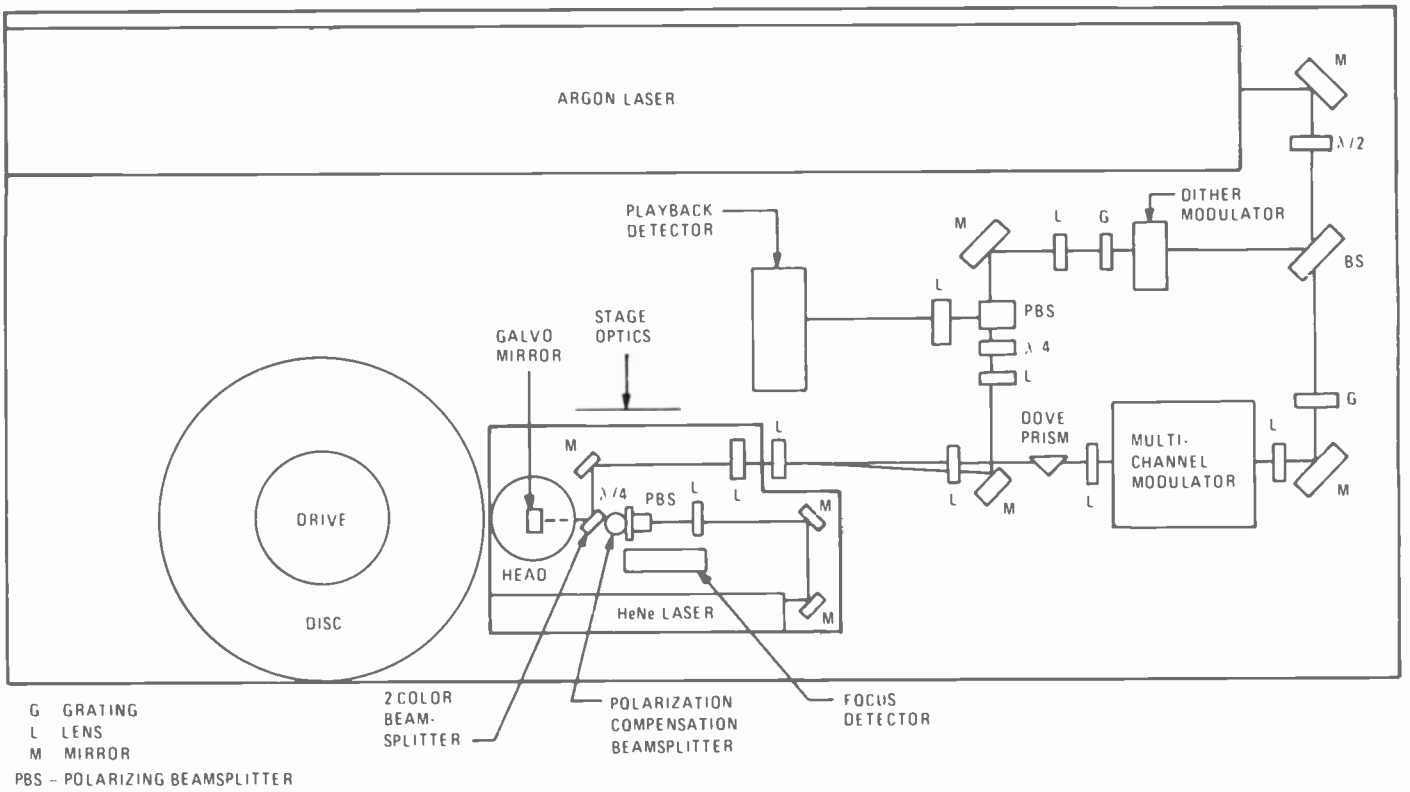


**Fig. 10. Nine-beam optical system layout with the laser-beam paths shown.**

strate. Leads are bonded and the package is hermetically sealed. This detector was selected because of its high bandwidth and sensitivity, which provides the greatest operational flexibility for the optical disc system.

## *System implementation*

The optical layout for the nine-beam 300-Mb/s optical disc recorder player is shown in Fig. 10. This system uses two nine-beam phase gratings for beamsplitting, the ten-channel acousto-optic modulator, and the nine-element avalanche detector array as key components. In addition, a HeNe laser and associated optics with a split detector are used in an optical focus servo system. An acousto-optic deflector is used to dither the play beams for closed-loop tracking during playback. The optical head and associated components are mounted on a high-speed translation stage that determines where the tracks are placed during recording and provides high-speed access during playback.

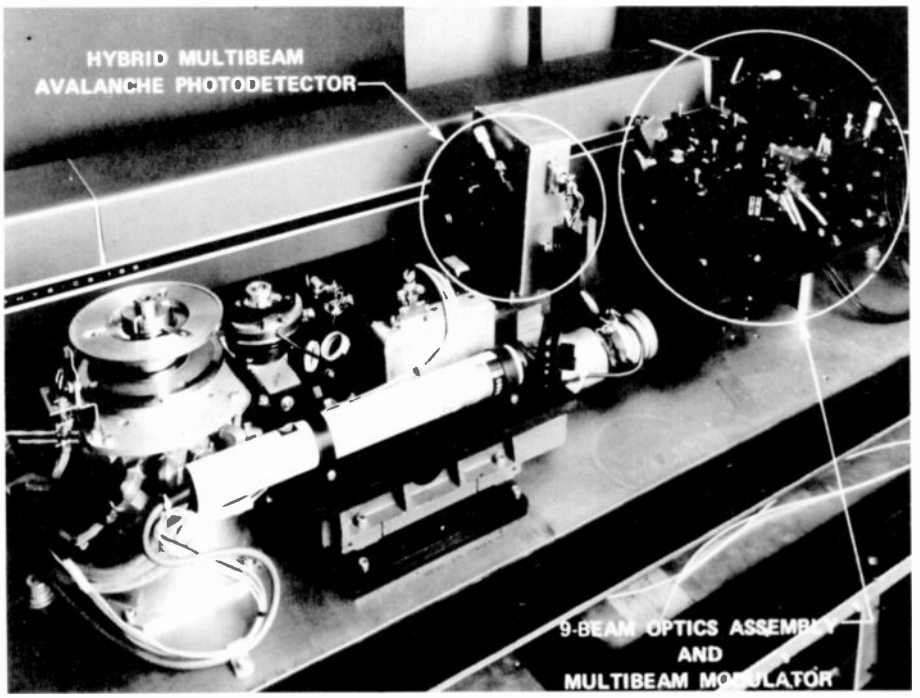


**Fig. 11. Wideband Recorder/Reproducer optics platform showing multibeam source and detector.**

Figure 11 shows the actual optical system. Figure 12 is a photomicrograph of tracks formed on an optical disc with this system. Track spacing is 1.0 μm and track width is about 0.4 μm. Figure 12 also shows playback waveforms. These waveforms were taken at a point in the system where the photodetector's outputs are equalized to correct for aperture response. The data being played back is a pseudo-random pattern at a user rate of 33 1/3 Mb/s per channel. This information is encoded using delay modulation that has transitions at selected intervals of one-half a bit period. This type of photograph is normally referred to as an "eye" pattern because it shows all possible transitions superimposed and provides a qualitative measure of system performance by the

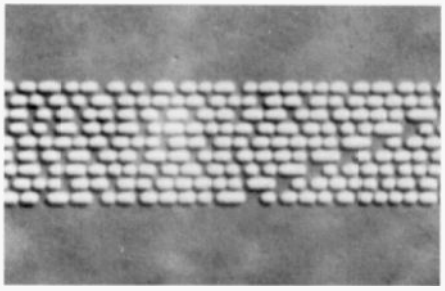


(a)

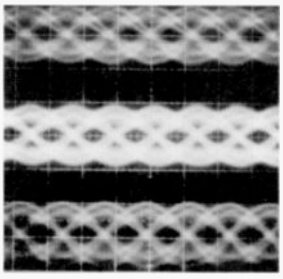


(b)

**Fig. 12. Performance results from nine-beam system. (a)** Photomicrograph of nine tracks with encoded data recorded on the optical disc. Tracks are 1-$\mu$m apart and the minimum hole size is about 0.4 $\mu$m. **(b)** Playback from three of the system's nine channels, showing the detection window used for decoding.

amount of clear space (eye) between half-bit cells.

## Conclusions

The 300-Mb/s optical disc recorder model has proven the feasibility of wideband digital recording on optical discs. The techniques for splitting the laser into multiple beams, the multichannel light modulator, and the photodetector array provide a reliable method for recording and playing multiple tracks through a single optical system. Optical disc recording systems similar to the one described here will become a key element in the collection, exploitation, and dissemination of wideband digital data.

**Authors Ammon (left) and Reno.**

**George Ammon** is Unit Manager, Optics and Electro-Optics Systems, in the Applied Physics Laboratory of the Advanced Technology Laboratories, Camden, New Jersey. As a Unit Manager, he has been responsible for the development of a 100-Mb/s optical disc recorder, the Air Force Wideband Recorder/Reproducer (a 300/Mb/s nine-beam optical system), and more recently, a multiple disc (jukebox) recorder/player. Mr. Ammon joined RCA in 1961 and became involved in the design of computer memories and digital control systems. He later joined the Applied Physics Laboratory and worked on the design of laser radars, illuminators, and tracker systems.
Contact him at:
**Advanced Technology Laboratories**
**Camden, N.J.**
**TACNET: 222-3879**

**Charles Reno** is a Principal Member of the Engineering Staff in the Advanced Technology Laboratories, Camden, New Jersey, where he has worked primarily with lasers and electro-optic systems. Since joining RCA in 1962, he has developed the optics for a precision laser sensor, designed a 40-to-1 spot-size zoom system for a laser recorder, designed the optics for the ESSWACS reconnaissance camera, developed the beamsplitting techniques for three and nine spots in multiple-beam optical disc recording, and has been responsible for the optics of the ODEM 100-Mb/s and the WDDR 300-Mb/s systems.
Contact him at:
**Advanced Technology Laboratories**
**Camden, N.J.**
**TACNET: 222-3129**

## References

1. Bell, A.E. and Bartolini, R.A., "High Performance Te Trilayer for Optical Recording," *Appl. Phys. Lett.*, Vol. 34, No. 275 (1979).
2. Bartolini, R.A., Bell, A.E., and Spong, F.W., "Optical Recording Structures for Use with GaAs Diode Lasers," *1979 IEEE/OSA CLEA Digest* (June 1979).
3. Corsover, S.L. and Thomas, C.H., "Error Management Techniques for Optical Disc Systems," *Proc SPIE*, Vol. 299 (1981).
4. Bricot, C., Lehureau, J.C., and Puech, C., "Optical Readout of Video Disc," *IEEE Transactions on Consumer Electronics*, p. 304 (November 1976).
5. Lee, W.H., "High Efficiency Multiple Beam Gratings," *Applied Optics*, Vol. 18, No. 14 (July 1979).

W. Altman | D.B. Hogan
E.C. Hutter | A. Rosenberg

# Space applications of lidar

*Lidar (LIght Detection And Ranging) is a laser radar that can* actively *measure atmospheric properties and constitutents, promising better resolution and accuracy than now obtained via passive remote sensing.*

**Abstract:** *Lidar (an acronym for LIght Detection And Ranging) systems consist of a laser source and appropriate receiver to detect and measure properties of scattered radiation. The particular property to be measured will depend upon the laser wavelength, detection mechanism, and parameters of the atmosphere. Ground-based and airborne systems have been developed since the mid-1960s to provide point measurement of parameters such as aerosol distribution, cloud height, pollution concentration, and wind speed. Due to the advancing state-of-the-art, lidar systems are presently being proposed as the next generation of satellite sensors providing meteorological and atmospheric constituent measurements on a global basis.*

*The basic principles involved will be described as well as system requirements for space application. Typical applications of lidar, for both terrestrial and spaceborne systems, will be provided with comparison to present non-lidar approaches to similar measurements. Emphasis will be placed on two specific systems, for wind sensing and for range-resolved constituent measurements, which have been analyzed as part of an in-house effort.*

As the manufacturer of low-earth-orbiting meteorological satellites, RCA Astro-Electronics has a vested interest in the payloads (sensors) of these spacecraft. The present sensor complement includes infrared sounders that measure temperature and water-vapor profiles of the atmosphere. Output data from these instruments are used as inputs into the present global circulation models to aid in weather forecasting. These sounders radiometrically measure the emitted and reflected radiation from the earth and its atmosphere in specific channels or bands chosen because of their absorption characteristics. The actual geophysical parameters are then obtained via an inversion technique that can in some cases require lengthy calculations and large amounts of "ground-truth" data.

The sounders are ultimately limited by atmospheric physics as to how accurately they can provide measurements of required parameters. Even a "perfect" instrument based on passive techniques would yield temperature measurements with a vertical resolution of only 4 to 8 km; for these broad layers, current accuracies in sounder-derived temperature measurments are on the order of 2.5 K. Spaceborne lidar (LIght Detection And Ranging) systems have the potential to measure profiles of temperature, water vapor, and ozone with finer vertical resolution and better accuracy than present sensors. They also have the capability of obtaining parameters heretofore unmeasurable via passive remote sensing. Ground-based and airborne lidars have been in development since the mid-1960s and have evolved into reliable systems capable of measuring a myriad of atmospheric properties and constituents. As the acronym implies, a lidar is, in effect, a laser radar that in general consists of a laser transmitter and an appropriate receiver (that is, a collecting mirror and detecting system).


Final manuscript received March 24, 1982.
Reprint RE-27-3-6

The basic equation relating the received power ($P_r$) to transmitted power ($P_t$) for a monostatic pulsed lidar is given by:

$$P_r = P_t \frac{ct}{2} \beta \frac{A}{R^2} \tau^2 \qquad (1)$$

Because the lidar is a radar, equation (1) is similar to the radar equation wherein $A$ is the collector area, $\tau$ is the atmospheric transmission, and $R$ is the range to the target. A major difference between this and typical radars is the $R^2$ dependence. The reason for lidar's $R^2$ dependence is that the illumination area is the same size as the lidar target, usually a portion of the atmosphere. If the target is smaller than the illumination area, as for conventional radars, an $R^4$ dependence appears instead. The pulse length is $t$, and the backscatter coefficient, $\beta$, has units of $m^{-1}$ $sr^{-1}$. The scattering is usually due to aerosols and/or molecules, depending on the wavelength and the state of the atmosphere. The product $\beta(ct/2)$ is equivalent to the scattering cross section of the atmosphere. The transmission term accounts for the round-trip losses due to molecular absorption and aerosol extinction. The finest vertical resolution obtainable for a lidar is given by $ct/2$ (typically 10 to 100 meters).

## Lidar applications

In 1977, NASA commissioned an international team of scientists and engineers to develop a series of experiments demonstrating the unique capabilities of lidar systems from spaceborne platforms. As a result of that effort, 26 experiments were defined for demonstration from the Space

**Table I. Shuttle multi-user lidar experiments.** A compilation of 26 experiments proposed for demonstration from a multi-user lidar system onboard the Shuttle. In general, the system complexity of the measurement follows the ordering of the experiment (from NASA SP-433).

| *Experiment* | *Wavelength Region* |
|---|---|
| Measure cloud top height | 530/1060 nm |
| Profiles of troposopheric clouds and aerosols | 530/1060 nm |
| Cirrus ice/water discrimination | 530 nm |
| Profiles of noctilucent clouds and circumpolar particulate layers | 530/1060 nm |
| Earth surface albedo measurement | 530/1060 nm |
| Stratospheric aerosol backscatter profiles | 530/1060 nm |
| Alkali atom density profiles | 589/671/770 nm |
| Ionospheric metal ion distributions | 280 nm and other resonance lines |
| Water-vapor profiles | Two, near 720 and 940 nm |
| Atmospheric species measurements—IR laser ground and cloud returns | Two, in the 9- to 11-$\mu$m range |
| Chemical release diagnostics | Several in the 400- to 600-nm range |
| Stratospheric ozone concentration profiles | 265 nm to 300 nm |
| Upper atmospheric trace species measurement using two-satellite earth occultation | Two, in the 9- to 11-$\mu$m region<br>Or scanning laser |
| Sodium temperature and winds | 589 nm |
| Surface pressure and cloud top pressure and height measurement | Two, near 760 nm |
| Vertical profiles of atmospheric pressure | Two, near 760 nm |
| Troposphere/tropopause temperature profiles | Two, near 760 nm |
| Altitude distribution of atmospheric constitutents IR DIAL | Two, in the 9- to 11-$\mu$m range |
| Measure cloud top winds to $\pm$5 m/sec | 350 nm to 1100 nm + 9 to 11 $\mu$m |
| Aerosol winds between ground and 30 km altitude | 0.35 to 11 $\mu$m |
| OH-density profiles 35 to 100 km | ~ 300 nm |
| Simultaneous measurement of metallic atom, ion and oxide profiles | 280, 285, 500 nm<br>(three simultaneous) |
| Tropospheric $NO_2$ concentration profile — total burden of $NO_2$ | 442 + 448 nm<br>(two simultaneous) |
| Stratospheric aerosol composition | 9 to 11 $\mu$m |
| NO density profiles between 70- and 150-km altitude | 215 to 227 nm |
| Abundance and vertical profiles of atomic oxygen | 225-nm transmit, 844.9-nm receive |

Shuttle. These experiments are listed in Table I.

As can be seen, lidar applications are varied and numerous. The simplest of all measurements is ranging to a "hard" target (for example, the earth) or a "soft" target (for example, clouds), because the large scattering from these targets contributes to a large return signal. By using polarization discrimination, the ratio of ice crystals to water droplets in clouds can also be determined. The vertical profile of aerosols is more difficult to measure, because of the smaller return signal from aerosol scattering. Even more difficult are measurements of temperature and pressure profiles, because they require a pulsed tunable laser with a narrow bandwidth and high stability. However, ground-based demonstrations have already been performed, and aircraft measurements are being planned by NASA for the near future.

Another application for lidar systems is atmospheric constituent detection/monitoring. The types of constituents that can be measured are limited only by the wavelengths of absorption lines and the availability of laser sources that coincide with those wavelengths. Typical constituents considered to date are ozone, pollutants (such as sulfur dioxide emanating from electric power plants), carbon monoxide, and chemical agents.

Among the other applications of lidars are those for oceanic research (for example, bathymetry, sea state, detection of oil spills), topography, and earth-resource detection. These include global geological surveys employing ranging to earth-based retroreflectors and, at the same time, studies of the earth's crustal dynamics and tectonic plate motions. Finally, certain satellites are expected to have laser range finders on board to topographically map the polar ice regions and monitor their long-term growth.

Determination of tropospheric winds offers a good example of a measurement that cannot be performed directly by present satellite remote sensors. The only current method of measuring winds from satellites is by correlating cloud inhomogeneities between geostationary-satellite imagery frames. The usefulness of the measurements is limited because of their dependence on cloud patterns and

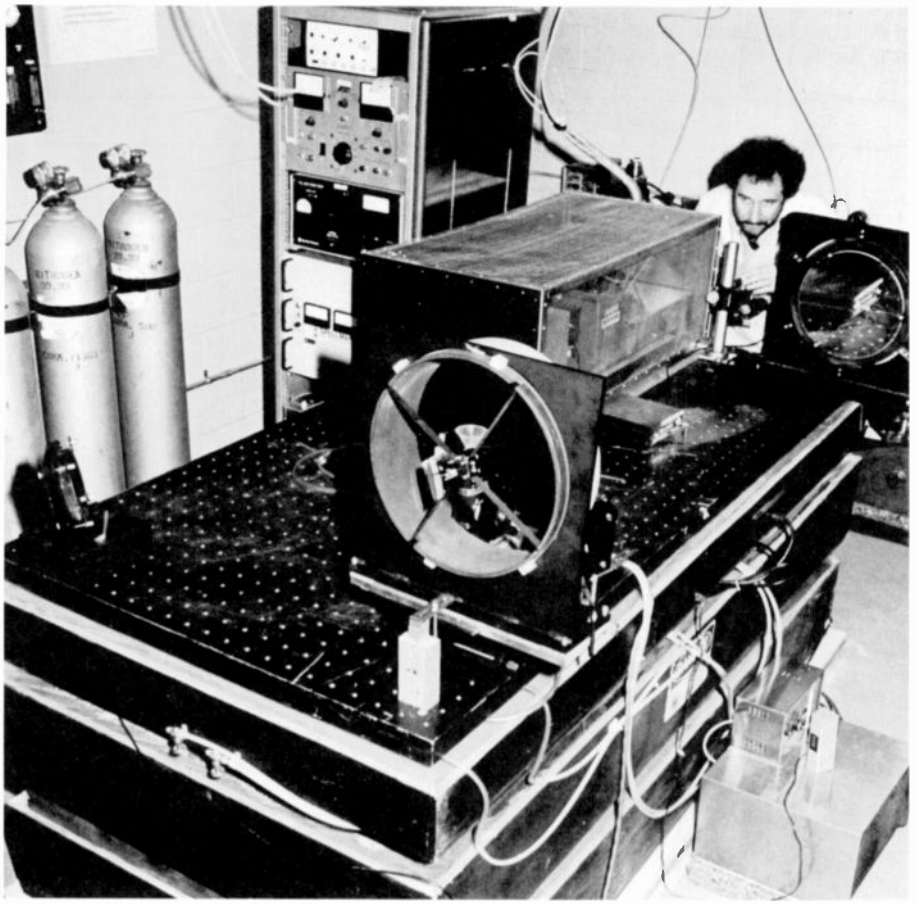

**The experimental lidar facility configured for aerosol-scattering measurements is shown.** The TEA laser is housed in a screen cage to reduce EMI to electronic circuits from the high-voltage discharge. A 30 cm receiving mirror is near the rear of the table. The detector is partially obscured behind the transmitter-optics mount, which is coaxial to the receiver.

the lack of adequate information on cloud heights. It has been suggested that remote global wind measurements in the lower 10 to 20 km of the atmosphere would impact weather forecasting in much the same manner as the integrated circuit affected computers. For this region of the atmosphere, lidars seem to be the only means by which these measurements can be made.

## Types of lidars

There are four major types of lidar, each suited to particular applications and regions of the atmosphere. These are DIAL (DIfferential Absorption Lidar), Doppler lidar, Raman scattering lidar, and laser-induced fluorescence lidar.

The DIAL system measures the absorption in a given atmospheric volume from which geophysical properties (for example, temperature and pressure) or constituent concentrations can be obtained. The technique involves the transmission of two or more wavelengths and measurement of the relative returns from the atmosphere. The wavelengths are chosen such that at least one lies on or near an absorption maximum, while another is nearby in a nonabsorbing spectral region of the atmosphere; the off-line wavelength then provides information on the background absorption while the on-line wavelength absorption provides information regarding both the background and the constituent of interest. The measured absorption coefficient can then be directly related to the parameters of interest (for example, constituent concentration or temperature).

DIAL systems can measure either a path-averaged absorption or a range-resolved absorption. In the path-averaged case, the laser can either be continuous wave (cw) or pulsed, and the basic measurement is of absorption of radiation scattered by a topographic target or a retroreflector. Because the scattering from these targets is much higher than that from aerosols and molecules, the laser-energy requirements are greatly reduced from those necessary when the molecules are the scatterers. However, because of the nature of the measurement, range resolution can only be achieved via wavelength-inversion techniques similar to those used by passive sounders, and hence the range resolution is limited by atmospheric physics. To achieve better range resolutions, a higher-energy pulsed laser must be employed, and thereby scattering from aerosols and molecules can be measured.

For measuring winds, Doppler lidar systems must be employed. These systems measure the Doppler shift from radiation scattered by aerosols, with the tacit assumption that these aerosols move with the wind. To achieve a high measurement accuracy—detecting 1 m/s winds, for example—engineers must assure that the frequency stability of the laser source is commensurately high.

Raman lidars rely on the measured shift of the incident wavelength caused by an exchange of energy between the scattering photon and the scattering species (the Raman effect). The Raman-shifted spectra collected by the lidar system can be processed to derive the temperature and concentration of the species being measured. The cross section for Raman scattering is usually smaller than that for the unshifted Rayleigh scattering by about three orders of magnitude. However, the Raman lidars are useful because they do not require a tunable laser source. Typical atmospheric molecules measured by Raman lidars are nitrogen and water vapor.

In a laser-induced fluorescence system, a laser pulse is absorbed by a constituent and re-radiated at a different wavelength by fluorescence. Efficient fluorescence relies on near coincidence with an absorption line of the species, which in turn implies precise control of the wavelength and high spectral stability, as compared to that necessary for the Raman scattering measurements. This technique has been used to measure oil spills, the hydroxyl radical (a by-product of ozone depletion), and uranium deposits.

## RCA lidar studies

Astro-Electronics has placed major emphasis on the analysis and development of Doppler lidar for wind detection, and DIAL systems for measuring temperature and humidity, because of the great meteorological need for these measurements. Descriptions of some of the specific requirements for these two systems, as presently projected, follow.

To measure winds, a spaceborne lidar must detect the Doppler shift introduced

by wind-carried aerosols. The majority of effort to date has concentrated on the use of the $CO_2$ transverse excited atmospheric (TEA) laser as the source. This laser is chosen for several reasons. First, the $CO_2$ laser has been well developed as a highly stable frequency device that can be used in heterodyne systems to measure frequency shifts. In addition, this laser has a relatively high efficiency (5 to 10 percent) which is very important for power-limited applications on satellites; moreover, the spectral output of the laser is in the range of 9 to 11 $\mu$m (discretely tunable), which coincides with the 8- to 12-$\mu$m atmospheric transmission window. Present requirements call for a 10 joule/pulse laser, operating at a repetition rate of 10 Hz; these requirements can be lowered, with a corresponding trade-off in velocity measurement accuracy and global coverage. The collecting mirror should be on the order of 1 meter in diameter and should be diffraction limited at 10 $\mu$m.

For heterodyne detection, a local oscillator must be available, and its frequency stability (and that of the transmitter laser) should correspond to less than the corresponding wind-velocity-measurement accuracy. Assuming a wind-velocity error of 1 m/s, the frequency stability should be better than 200 kHz.

The major absorption in this spectral region is due to water vapor and carbon dioxide. To reduce this absorption to a minimum and, in turn, enhance the signal-to-noise ratio, specific laser lines were examined. Minimum values of absorption were found to occur for lasers based on $CO_2$ isotopes; in particular, lines corresponding to low absorption are the 00°1-10°0 *P*-branch of $^{13}C^{16}O_2$ ($\lambda = 11.19$ $\mu$m), the 00°1-10°0 *R*-branch of $^{13}C^{18}O_2$ ($\lambda = 10.6$ $\mu$m), and the 00°1-02°0 *R*-branch of $^{12}C^{18}O_2$ ($\lambda = 10.6$ $\mu$m). The development of lasers based on these isotopes must then take into account the material composition to assure that no molecular interchanges occur.

Another system currently under analysis uses a doubled Nd:YAG laser operating with a fairly narrow spectral linewidth. In this case, the Doppler shift is detected by measuring fringe shifts from a Fabry-Perot interferometer rather than by use of heterodyne detection. The main reason for examining such an alternative system is that the aerosol scattering should increase as the wavelength decreases, and the overall system efficiency should benefit, even though the efficiency of Nd:YAG lasers is lower than that of $CO_2$ lasers. In addition, the value and variability of aerosol scattering at 10 $\mu$m is under close scrutiny, while at 0.5 $\mu$m the scattering is better documented and less in question. The key requirement, however, is the development of a narrowband Nd:YAG laser.

A simpler version of the Fabry-Perot detection system, which passively measures winds in the mesosphere and thermosphere, is currently on board an RCA satellite, Dynamics Explorer. It is determining wind fields with an accuracy of ±5 m/s by measuring the Doppler shift of thermal emission of oxygen atoms at 6300 angstroms. This passive technique

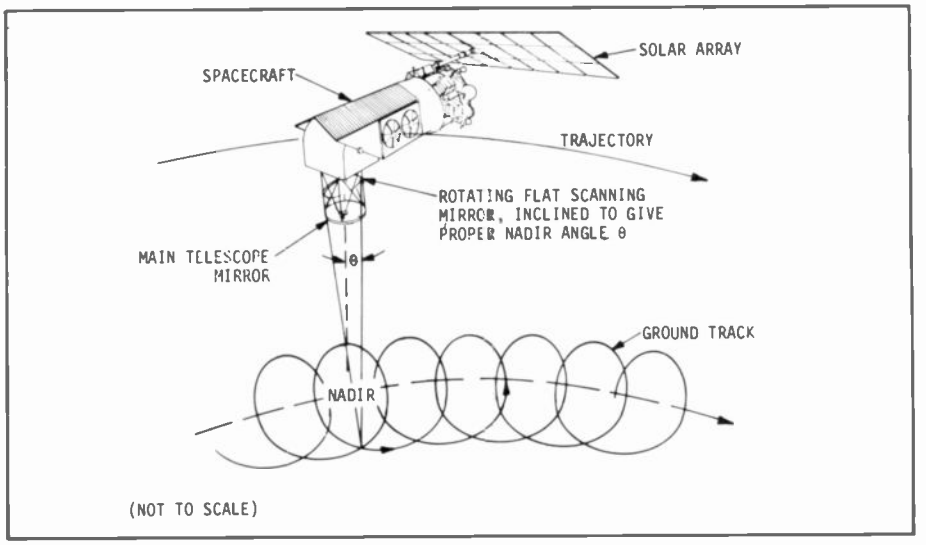


**Fig. 1. A spaceborne conical scan lidar system.** Pictured is an artist's conception of a typical Doppler lidar onboard a satellite. To measure horizontal winds, radial wind velocity measurements must be made, both fore and aft of the satellite position.

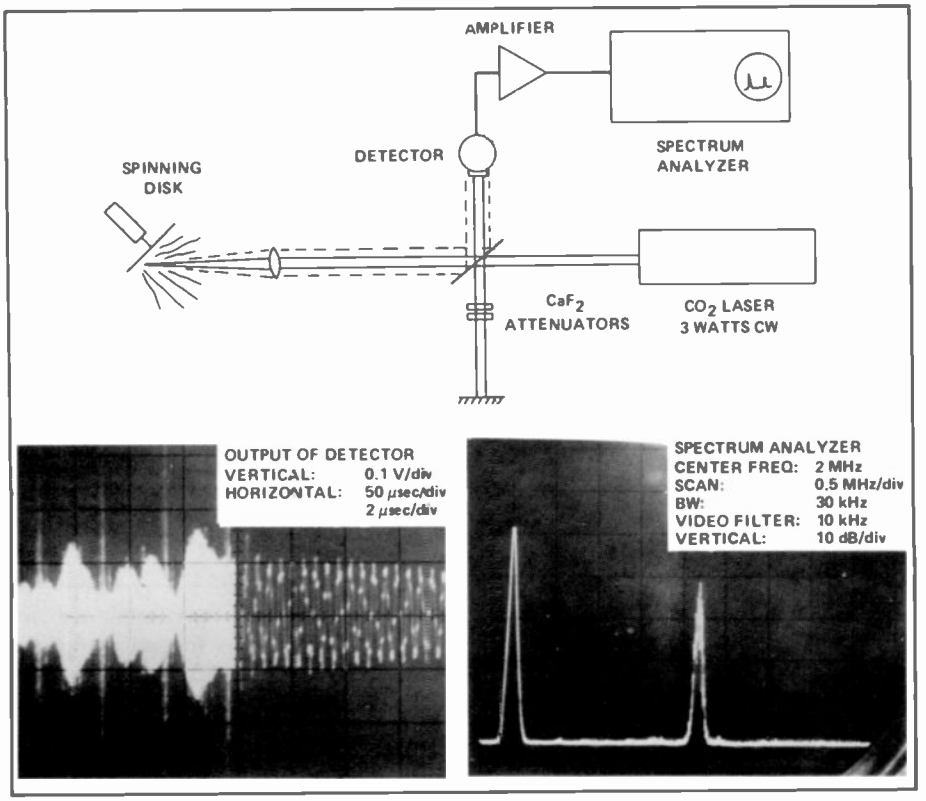


**Doppler measurement (spinning disk).** Shown is an experiment to demonstrate the typical heterodyne return signal expected from a diffusely scattering moving target; that is, a sinusoidal waveform with a random envelope. The detector output is shown in the left oscilloscope trace. The right oscilloscope photo is the spectrum-analyzer output and it indicates a 2.2 MHz shift or a radial velocity of 11 m/sec.

cannot be applied in the troposphere because of line broadening in this region; hence, active illumination is required.

An artistic conception of a spaceborne system is shown in Fig. 1. The Doppler lidar system, as described, measures the component of wind velocity along the line of sight. To actually measure horizontal winds, at least two measurements must be made to transform line-of-sight values to horizontal winds. To minimize angular perturbations to the spacecraft, the scanning mirror will probably perform a conical scan. Data will then be stored on board the satellite until the same area is illuminated from at least two scans. Since the satellite velocity also introduces a Doppler shift, it is essential to know precisely the spacecraft's velocity and pointing angle to achieve accurate wind measurements.

The second lidar system that has been extensively analyzed at Astro-Electronics is a DIAL system for measuring temperature and humidity. Present efforts have been concentrated on the water vapor band near 7200 angstroms. The requirements for this system are laser-pulse energies of about 100 to 300 millijoules per wavelength, at a repetition rate of 10 Hz. The collection aperture is 1 meter in diameter. The laser linewidth should be on the order of 0.01 to 0.03 angstrom—a very demanding requirement. In addition, the laser frequency should be controlled within a fraction of the linewidth to the line center of the absorbing molecule. Finally, detectors with higher quantum efficiencies would increase the measured return signal and enhance the measurement accuracy.

Actual wavelengths used in DIAL systems will depend on the species to be measured and the availability of laser sources. In the ultraviolet, visible, and near-infrared regions, the laser sources have been based on Nd:YAG lasers. Usually, the Nd:YAG laser output will be doubled in frequency to 5300 angstroms and used to pump a tunable dye laser. Dye lasers are complicated systems containing volatile liquids that have a limited lifetime and, as such, are not well suited for the space environment. New sources are therefore needed for space applications. One such system, based on alexandrite, is currently being evaluated by NASA. Alexandrite is a solid-state material which is continuously tunable in the 7000- to 8000-angstroms spectral region. It has the potential of providing an all-solid-state source that is compact, efficient, and long-lived.

**Authors (left to right) Hogan, Rosenberg, Altman, and Hutter.**


**Wolf Altman,** Principal Member Technical Staff, joined RCA in 1979 and is currently in the Advanced Missions Group at Astro-Electronics. His primary work has been to develop analytical and experimental capabilities in support of laser remote sensing. His previous experience includes laser optical design, holography, adaptive optics, and optical heterodyne detection. He is a member of the OSA and SPIE.
Contact him at:
**RCA Astro-Electronics**
**Princeton, N.J.**
**TACNET: 229-2270**

**David Hogan** received his BS in Physical Science, and MS in Meteorology from the University of Maryland. He joined Astro-Electronics in 1980 where, as part of the Advanced Missions Group, he has been studying space-based remote sensing of atmospheric parameters. His recent work has included developing a DIAL technique to simultaneously measure atmospheric temperature and humidity profiles, and investigations into new methods of determining atmospheric moisture structure using passive infrared instruments.
Contact him at:
**RCA Astro-Electronics**
**Princeton, N.J.**
**TACNET: 229-3355**

**Arieh Rosenberg** received his bachelor's and master's degrees in Science from the Israel Institute of Technology, Haifa, Israel, and his Ph.D. in Physics from the Weitzman Institute of Science, Rehovoth, Israel. He has been doing research in experimental and theoretical molecular spectroscopy and atmospheric physics. Recently, he has been concentrating on the analysis of active and passive spaceborne remote sensors. He joined Astro-Electronics in 1980 as a Staff System Scientist and is currently Manager of the Advanced Earth Observation System Group.
Contact him at:
**RCA Astro-Electronics**
**Princeton, N.J.**
**TACNET: 229-2691**

**Edwin Hutter** who received his Ph.D. in Physics from the University of Virginia, is a Staff Systems Scientist at Astro-Electronics, where he has been working since 1979 on studies for new meteorological satellite sensors. In earlier work with Astro-Electronics, he was Manager, Physical Research Laboratory. Subsequent work at RCA Laboratories and the Addressograph-Multigraph Corporation included direction of research on electrostatic imaging systems.
Contact him at:
**RCA Astro-Electronics**
**Princeton, N.J.**
**TACNET: 229-3475**


RCA has long had a commitment to developing technology for space applications. With respect to lidar systems, RCA is the first company to have flown a laser in space, and, in fact, it was a lidar. As part of the Apollo program, a laser altimeter was developed to provide accurate ranging to the lunar surface. By boresighting with a photographic camera, accurate topographic mapping of lunar features was made possible.

Remote sensing by lidars makes possible many important measurements that cannot be adequately carried out by presently used passive sensors. Lidar sensors are expected to play a major role in future meteorological spacecraft systems. However, current laser technology is a limiting factor in the implementation of these systems, and improvements in laser technology are needed.

W.F. Kosonocky | H. Elabd | H.G. Erhardt
F.V. Shallcross | G.M. Meray | R. Miller
T.S. Villani | J.V. Groppe | V.L. Frantz | F.J. Tams

# Schottky-barrier infrared image sensors

*High-quality infrared imaging was demonstrated with PtSi and $Pd_2Si$ IR-CCD image sensors. These monolithic silicon focal-plane arrays represent the first practical solution for many infrared imaging applications.*

**Abstract:** *Recent development of high-performance palladium silicide ($Pd_2Si$) and platinum silicide (PtSi) Schottky-barrier infrared charge-coupled-device (IR-CCD) image sensors make these monolithic focal-plane arrays attractive for many short-wavelength-infrared (SWIR) and thermal-imaging applications. PtSi Schottky-barrier detectors operated at 80 Kelvin (K) have a quantum efficiency of several percent in the 3- to 5-μm spectral range and a cut-off wavelength in excess of 6.0 μm. $Pd_2Si$ Schottky-barrier detectors operated between 120 and 140 K have a cut-off wavelength of 3.6 μm and quantum efficiency in the range of 1.0 to 8.0 percent in the SWIR band. High-quality thermal imaging has been demonstrated with a 64 × 128-element PtSi Schottky-barrier IR-CCD imager in a TV-compatible IR camera operated with 60 frames per second. Also, a reflective infrared imaging of very good quality was achieved with the $Pd_2Si$ Schottky-barrier IR-CCD image sensor.*

The work on Schottky-barrier IR-CCD imagers[1] began at RCA Laboratories in June 1973 with the support of and as a joint effort with Air Force Systems Command, RADC/ESE, Hanscom AFB, Mass.[2] The first operating Schottky-barrier IR-CCD (in 1974) was a 64-element line sensor with "thick" palladium silicide ($Pd_2Si$) detectors and a three-phase surface-channel aluminum-CCD readout register.[3, 4] The first platinum silicide (PtSi) Schottky-barrier IR-CCD arrays were developed at RCA Laboratories also with the support of RADC/ESE, Hanscom AFB, Mass., in 1977. They were 256-element line sensors[4] and 25 × 50-element area sensors.[2, 5, 6] These arrays were operated as thermal sensors at RADC/ESE and exhibited very promising performance, such as a noise-equivalent temperature of less than 1°C and a response nonuniformity of about 1 percent rms.[6-8]

The PtSi Schottky-barrier detectors (SBDs) in the first generation of IR-CCD arrays were made in the form of "thick" PtSi using about 600 angstroms of deposited platinum. The development of the high-performance, "thin" PtSi SBDs was started as a joint effort with RADC/ESE. Thin Schottky-barrier IR detectors were described in 1973 by Archer and Cohen.[9] The first thin-PtSi SBDs were made by RADC/ESE in 1978. These thin-PtSi SBDs (with about 100 angstroms of Pt) showed improvement in responsivity by a factor of two over the previous thick SBDs (with 600 angstroms of Pt). To further improve the responsivity of the thin SBDs, we had proposed in 1978 to fabricate the thin-PtSi SBDs with an aluminum reflector separated from the thin-PtSi film by a 2000-angstrom layer of deposited silicon dioxide ($SiO_2$). These first thin-PtSi detector arrays were implemented at RCA Laboratories on the 25 × 50-element IR-CCD arrays in the first part of 1979 as part of an Independent Research and Development (IR&D) project. A dramatic improvement in responsivity, by a factor of about 10, was first observed on these arrays at RCA Automated Systems, Burlington, Mass., in June 1979.[10-12]

As a result of this breakthrough in performance, our 1980 and 1981 IR&D effort on the Schottky-barrier IR-CCD image sensor in the support of Automated Systems was expanded. As part of this IR&D project, we have developed a 64 × 128-element IR-CCD image sensor with high-performance thin-PtSi detectors. A major part of this work, however, was devoted to the development of a reproducible process for fabrication of the thin PtSi detectors using 32 × 63-element IR-CCD arrays initially designed and fabricated under a contract with RADC/ESE.[13]

The quality of thermal imaging, in the 3.0- to 5.0-μm spectral range, achieved


Final manuscript received March 15, 1982.
Reprint RE-27-3-7

**Fig. 1. Thermal image of G.W. Hughes, detected by the 64- by 128-element PtSi IR-CCD TV camera.** This camera operates in a liquid-nitrogen Dewar at about 80 K with 60 frames/second and f/1.5 germanium optics. It is sensitive in the 3.0- to 5.0-$\mu$m spectral band and responds to the infrared radiation emitted by the scene. It can resolve minute temperature variations (a fraction of a degree Celsius) in the scene.

with the 64 × 128-element thin-PtSi IR-CCD image sensor is illustrated in Fig. 1. This imager is operated in a liquid nitrogen temperature at about 80 K. The IR-CCD TV camera used for the thermal imaging reported in this paper was developed at Automated Systems and is described by J. Klein, N. Roberts and G. Chin in another paper (pp. 60-66) of this issue. Although useful thermal imaging can be obtained with these IR-CCD imagers without any electronic uniformity compensation, in this case an additive type of uniformity compensation was used to improve the performance.

With the support of the RCA Advanced Technology Laboratories, Camden, N.J., in the second part of 1981 we have initiated the development of $Pd_2Si$ IR-CCD focal-plane arrays (FPAs) for shortwave-infrared (SWIR) satellite-borne applications. The passive cooling of such FPAs requires an operation at temperatures in the range of 100 to 140 K. This effort is described in this issue by F.B. Warren, D.A. Gandolfo, J.R. Tower, H. Elabd, and T.S. Villani.

## High-performance thin SBDs

### *Construction*

The infrared SBD consists of very thin layers (20 to 100 angstroms) of PtSi, $Pd_2Si$, or other metals or semi-metals formed on a *p*-type silicon substrate. This type of infrared detector can be integrated with silicon readout circuits, such as the charge-coupled devices (CCDs), to form monolithic silicon infrared-image-sensor arrays. The Schottky-barrier IR-CCD image sensors are fabricated by forming the silicide detectors near the end of the device-processing sequence after all of the high-temperature steps (900 to 1050°C) are completed.

The operation of the Schottky-barrier infrared detector is based on an internal photoemission of hot holes across the Schottky barrier, $\psi_{ms}$, that is formed between the silicide layer and the *p*-type silicon substrate (see box). The construction of recently developed high-performance thin-PtSi SBDs is illustrated in Fig. 2. In this structure a very thin and very uniform layer of PtSi, formed on the *p*-type silicon substrate, is separated from an aluminum reflector by a layer of a deposited $SiO_2$ dielectric. The optimal thickness of the silicide layer is in the range of 20 to 100 angstroms, while that of the $SiO_2$ layer is in the range of 2000 to 6000 angstroms. The *p*-type silicon substrate has resistivity in the range of 30 to 50 ohm-cm. This detector structure has been designed to optimize the photoresponse of the SBD.

To improve the injection, or emission efficiency, the thickness of the silicide layer is made comparable to, or smaller than, the attenuation length of the "hot" holes. This implies that the injection of the hot holes across the silicide-silicon interface is enhanced by scattering (reflection) from the silicide-$SiO_2$ interface. The reduced thickness of the silicide layer also is expected to reduce the reflection of the infrared radiation at the silicon-silicide interface. The aluminum reflector, separated from the thin-silicide layer by the $SiO_2$ dielectric layer, provides a further improvement of the coupling of the infrared radiation to the silicide layer. Our exper-

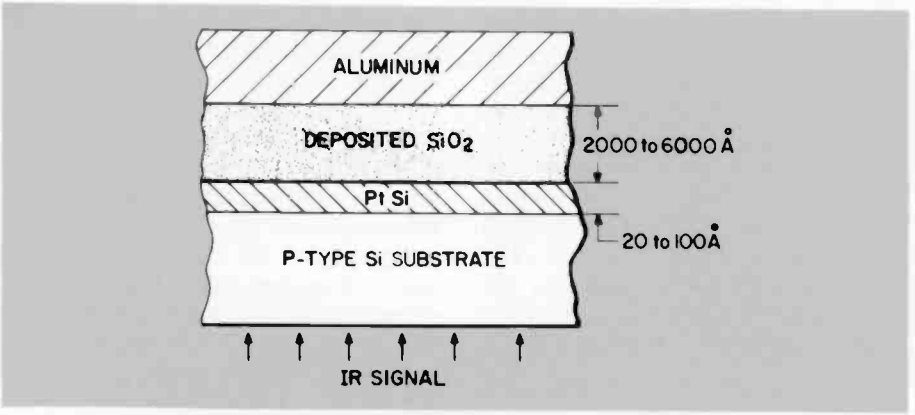


**Fig. 2. Cross-sectional view of a high-performance thin-PtSi SBD.** The crucial element in this structure is the very thin (20 to 100 angstroms) and very uniform layer of PtSi.

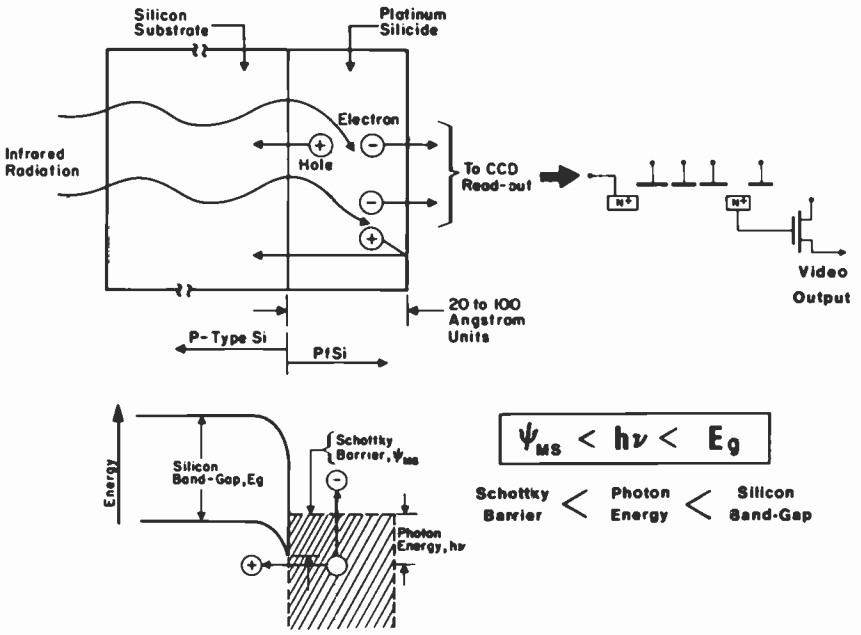


## Operation of the Schottky-barrier detector (SBD)

The above figure illustrates the basic construction and operation of a back-illuminated PtSi Schottky-barrier infrared detector integrated with a silicon-CCD readout. The infrared radiation with the photon energy less than the bandgap of silicon ($E_g$ = 1.1 eV) is transmitted through the substrate. The absorption of the infrared radiation in the silicide layer results in the excitation of photocurrent across the Schottky barrier ($\psi_{ms}$) by internal photoemission. The "hot" holes (those that have sufficient energy to go over the Schottky barrier, $\psi_{ms}$, formed between the silicide and the *p*-type silicon) are injected into the silicon substrate. Hence, a net negative charge will accumulate on the silicide electrode. Finally, the detection of the infrared optical signal is completed by the transfer into a CCD-readout structure of this negative charge formed at the silicide electrode. This transfer is carried out either by a periodic voltage-reset (vidicon-type) readout, or by a continuous (charge-skimming-type) readout. The spectral energy window of a back-illuminated SBD is $\psi_{ms} < h\nu < E_g$ where $\psi_{ms}$ is the metal-semiconductor Schottky barrier, $h\nu$ is the photon energy, and $E_g$ is the silicon bandgap energy (1.1 eV).

iments on the optimization of this detector structure showed that the choice of the thickness of the PtSi in the range of 20 to 100 angstroms has a major effect on the photoresponse of the SBD.

### *Photoemission characterization*

The responsivity, $R$, of the SBD can be approximated by a modified Fowler equation[14] as:

$$R = C_1\left(1 - \frac{\psi_{ms}\,\lambda}{1.24}\right)^2 \qquad (1)$$

where $R$ is the responsivity in A/W, $C_1$ is the emission coefficient in $eV^{-1}$, $\psi_{ms}$ is the metal-semiconductor Schottky barrier in eV, and $\lambda$ is the wavelength of the infrared radiation.

The responsivity, $R$, and the quantum efficiency, Q.E., of the recently developed high-performance thin-PtSi detectors are compared in Fig. 3 with the data obtained for thick-PtSi detectors (with the PtSi layers in the range of 500 to 1000 angstroms). The dramatic improvement in performance is due to the improvement of the emission coefficient, $C_1$, by an order of magnitude from 5.0 to 54.2 percent $eV^{-1}$, and the extension of the cut-off wavelength, $\lambda_c$, from 4.7 to about 6.0 $\mu$m. The cut-off

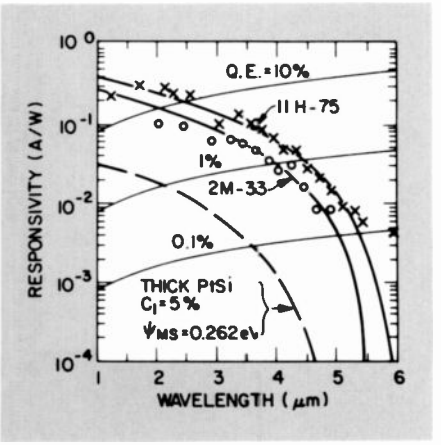


**Fig. 3. Measured responsivity and quantum efficiency (Q.E.) of two of the high-performance thin-PtSi SBDs are compared with that of a thick-PtSi detector.** This data was obtained with a 1000°C source, with an aperture diameter of 1.25 cm, and at a distance of 15.8 cm from the detectors. The devices 11H-75 and 2M-33 are thin-PtSi detectors. The device 11H-75 has $\psi_{ms}$ = 0.208 eV and $C_1$ = 54.2% $eV^{-1}$. The device 2M-33 has $\psi_{ms}$ = 0.219 eV and $C_1$ = 38.1 percent $eV^{-1}$. Note that the 11H-75 detector has quantum efficiency ranging from 7.0 to 1.0 percent in the spectral range from 3.0 to 4.5 $\mu$m.

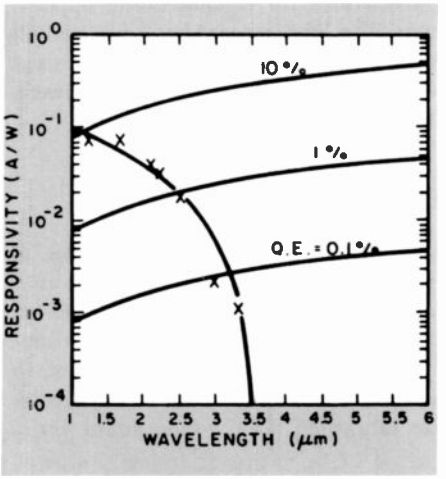


**Fig. 4. Measured responsivity and quantum efficiency of the first-generation thin-$Pd_2Si$ detectors under the same conditions as in Fig. 3.** This detector has $\psi_{ms}$ = 0.337 eV and $C_1$ = 19.1 percent $eV^{-1}$. It has a quantum efficiency of 10.0 to 2.0 percent in the spectral range from 1.0 to 3.0 $\mu$m.

wavelength $\lambda_c$, given in $\mu$m, is defined as:

$$\lambda_c = \frac{1.24}{\psi_{ms}} \qquad (2)$$

The responsivity obtained for a first-generation thin-$Pd_2Si$ SBD is shown in Fig. 4. These detectors were recently developed for a short-wavelength infrared (SWIR) system and for operation at intermediate

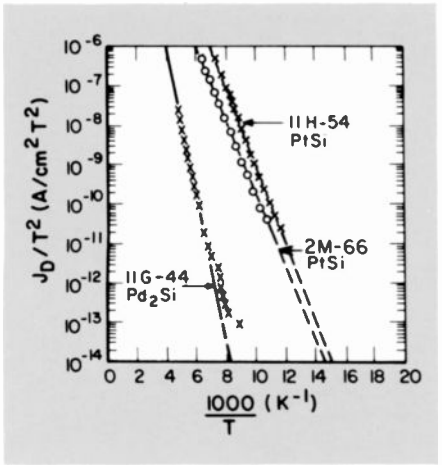


**Fig. 5. Comparison of the dark-current temperature characteristics of two PtSi SBDs and a $Pd_2Si$ SBD.** The PtSi and the $Pd_2Si$ detectors in this test were operated with a reverse-bias voltage of 4.0 and 5.0, respectively. Schottky-barriers of the two PtSi and the $Pd_2Si$ detectors determined from the slopes of the above curves are the $\psi_{ms}$ (PtSi, 11H-54) = 0.20 eV, $\psi_{ms}$, (PtSi, 2H-66) = 0.18 eV, and $\psi_{ms}$ ($Pd_2Si$) = 0.37 eV. Note, the value of $J_D/T^2 = 10^{-11}$ A/cm$^2$K$^2$ corresponds to an operating temperature of about 80 K for PtSi and about 140 K for $Pd_2Si$.

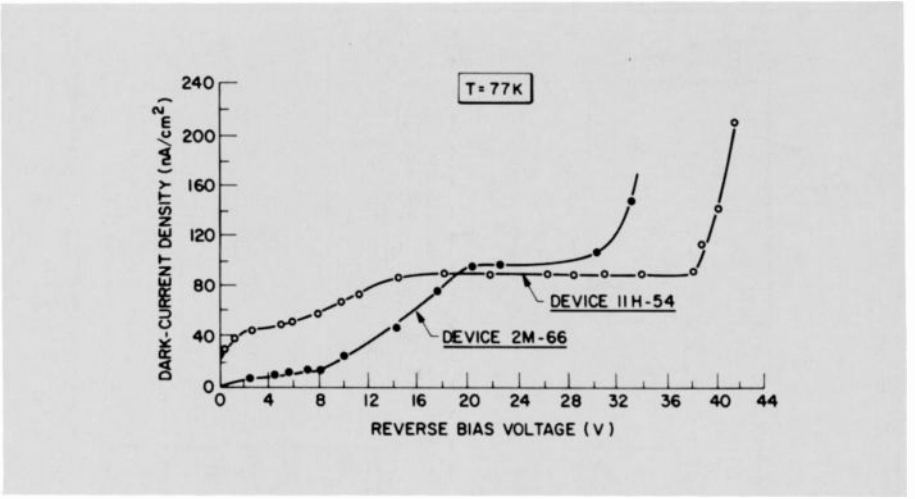


**Fig. 6. Measured dark-current density, $J_D$, of two types of thin PtSi SBDs as a function of the reversed-bias voltage at 77 K.** Both types of detectors can be operated in IR-CCD arrays at 77 K with optical integration times of 10 to 100 ms for the normal range of operating voltages of 4 to 10 V.

temperatures for satellite-borne applications. The $Pd_2Si$ imager has a wavelength range of 1.0 to 3.5 $\mu$m and can be used with passive coolers for operation between 100 and 140 K.

### *Dark-current characteristics*

Measured dark-current characteristics of the thin $Pd_2Si$ and PtSi detectors as a function of the operating temperatures are shown in Fig. 5. To provide greater uniformity of the dark current, that is, to avoid dark-current spikes, these detectors are fabricated with *n*-type guard rings.

The dark-current-versus-temperature characteristics follow the thermionic emission model, and the dark-current density, $J_D$, in A/cm$^2$ can be expressed as:

$$J_D = A^* T^2 \exp(-q\psi_{ms}/kT) \qquad (3)$$

where $A^*$is the Richardson emission constant for holes in silicon (which is ideally 32 A/cm$^2$K$^2$); $T$ is the detector temperature in K; $q$ is the electronic charge in Coulomb; $\psi_{ms}$ is the activation energy or the Schottky barrier in eV; and $k$ is the Boltzmann constant. The values for the Schottky-barrier, $\psi_{ms}$, determined as the activation energies from the dark-current versus temperature characteristics, are not necessarily the same as those determined by the photoemission measurements.

The dark-current density at 77 K of two types of thin-PtSi Schottky-barrier detectors as a function of the reversed-bias voltage is shown in Fig. 6. Device 2M is representative of detectors formed with a graded junction, while device 11H has a more abrupt junction. This dark-current data illustrates the excellent reversed-breakdown characteristics of the thin-PtSi detectors, and shows that, with liquid nitrogen cooling, the dark current of these detectors is sufficiently low to allow optical integration times in the range of 10 to 100 ms.

## IR-CCD focal-plane arrays

The IR-CCD image sensors or focal-plane arrays (FPAs) developed at RCA Laboratories are summarized in Table I. The 256-element line sensor was developed under a contract with RADC/ESE for the Infrared Fence Sensor Development Program.[4] This FPA has 40-$\mu$m (horizontal) $\times$ 200-$\mu$m (vertical) pixels and a fill factor, or detector-area efficiency, of 50 percent for SBDs with *n*-type guard rings and 78 percent for SBDs without the guard rings. This IR-FPA was designed for operation with the continuous-skimming type of detector readout.[4, 7]

The 25 $\times$ 50 interline-transfer (IT) IR-CCD,[2, 5, 7] the 32 $\times$ 63 series-parallel-series interline-transfer (SPS-IT) IR-CCD,[13] and the 64 $\times$ 128 SPS-IT IR-CCD[15] were designed for operation as staring FPAs with optical integration time for the full TV frame time of 1/60 or 1/30 s. However, they can also be operated as scanning-type TDI (time-delay-integration) image sensors with an optical integration time of up to 100 ms.

The SPS-IT organization is illustrated in Fig. 7. The SPS designation indicates that this type of IR-CCD array has an

**Table I. IR-CCD focal-plane arrays developed at RCA Laboratories.**

| Type of FPA | Chip Size (mil)$^2$ | Pixel Size ($\mu$m)$^2$ | Fill Factor | Type of SBD | Year |
|---|---|---|---|---|---|
| 256 x 1 Line Sensor | 438 x 71 | 40 x 200 | 50%<br>78% | Thick PtSi<br>Thin PtSi | 1977<br>1979 |
| 25 x 50 Interline Transfer | 230 x 230 | 160 x 80 | 17% | Thick PtSi<br>Thin PtSi | 1978<br>1979 |
| 32 x 63 SPS IT | 265 x 265 | 160 x 80 | 25% | Thin PtSi<br>Thin $Pd_2Si$ | 1980<br>1981 |
| 64 x 128 SPS IT | 364 x 364 | 120 x 60 | 22% | Thin PtSi<br>Thin $Pd_2Si$ | 1981<br>1982 |

input register. The input registers are used mainly for wafer-probe testing at room temperature to identify the arrays with operating CCD registers. As shown in Table I, the 64 × 128 array with the chip size of 364 × 364 mil is a rather large integrated circuit. All of the area-sensing IR-CCD FPAs have a similar design and are fabricated with two-level polysilicon, four-phase buried-channel CCD registers.

One limitation of the developed area-sensing IR-CCD FPAs are rather low fill factors (17 percent for the 25 × 50 array, 25 percent for the 32 × 63 array, and 22 percent for the 64 × 128 array). The fill factor is defined here as the ratio of the active detector area to the total pixel (picture-element) area. With the new process/design concepts now under development, we expect to have a fill factor of about 50 percent in the next generation of the IT IR-CCD arrays.

Returning to Fig. 7, note that the operation of the IT IR-CCD image sensor as a staring FPA with optical integration for the full time is as follows: During the vertical retrace time at the beginning of each frame, the detected charge signal is transferred from the SBDs to the vertical column registers; then during the blanking time of each horizontal line, the charge signal of one row of the parallel column registers is transferred to the serial output register. This line charge is then transferred in series to an on-chip output amplifier. A low-impedance output signal is obtained in these arrays from a two-stage source-follower on-chip amplifier with a floating-diffusion capacitance of 0.16 pF.

The 64 × 128-element IR-CCD image sensor bonded in a 32-lead ceramic package is shown in Fig. 8. The photograph in Fig. 9 illustrates that 37 of these IR-CCD arrays can be fabricated on a 3-inch silicon wafer.

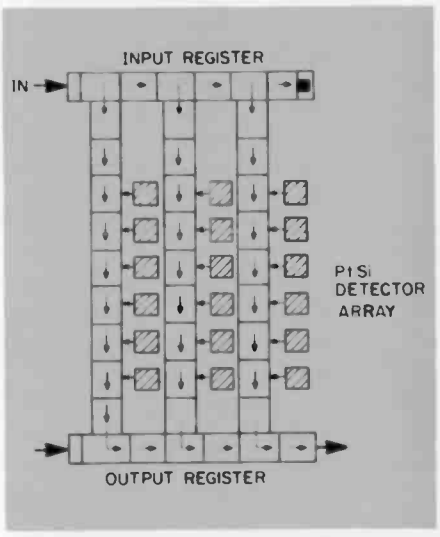


**Fig. 7. Organization of an interline-transfer (IT) IR-CCD image sensor.** The interline transfer implies that the IR detectors are placed between the vertical column registers. In the design shown here (that we have used for all of the area arrays), the serial input and output registers have two CCD stages for each column of detectors.

### *Construction of one pixel*

The construction of one pixel of the 64 × 128 array is illustrated by the pixel layout in Fig. 10, and a cross-sectional view is shown in Fig. 11 (a). As illustrated in these figures, the PtSi detectors as well as the buried-channel CCD (BCCD) registers are isolated by $p^+$-channel steps. To guarantee uniform dark-current characteristics, each detector is surrounded by an $n$-type guard ring formed by the BCCD implant. The coupling of the PtSi detectors to the CCD column register is accomplished by an $n^+$ diffusion in series with a surface-channel transfer gate ($V_T$). The four-phase BCCD column registers are bussed by aluminum lines shown in Fig. 10. Using 5- to 7-$\mu$m design rules for this layout, the active detector area is 40 $\mu$m × 40 $\mu$m and the pixel size is 120 $\mu$m × 60 $\mu$m, which gives the fill factor of 22 percent.

### *Schottky-barrier detector with CCD readout*

The charge readout from a PtSi detector of an IT IR-CCD array operated as a staring or vidicon-type sensor is accomplished in a voltage-reset charge-integration mode (Fig. 11). During the optical integration time, the surface-channel transfer gate is biased into accumulation. This isolates the Schottky-barrier detector from the BCCD register and also provides a blooming control mechanism for this detector. As shown in the potential diagram in part (b), the transfer gate is pulsed-on once at the end of the optical integration time (once per frame time). This transfers the detected charge signal (electrons) from the PtSi electrode to the BCCD register and resets the detector to the potential-2. Then, at the end of the transfer-gate pulse, a potential barrier (potential-1, that is equal to the substrate potential) is formed between the detector and the BCCD register, initiating the next optical integration

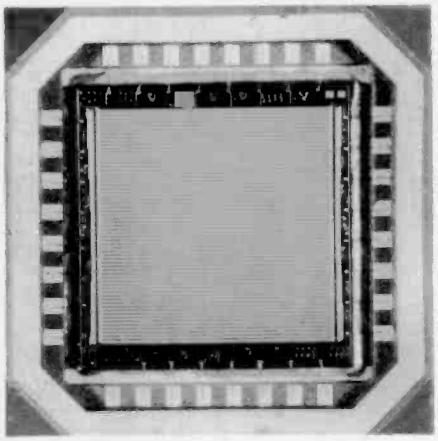

**Fig. 8. Photomicrograph of a 64- by 128-element IR-CCD image sensor** bonded in a 32-lead ceramic package custom-made by Kyocera.

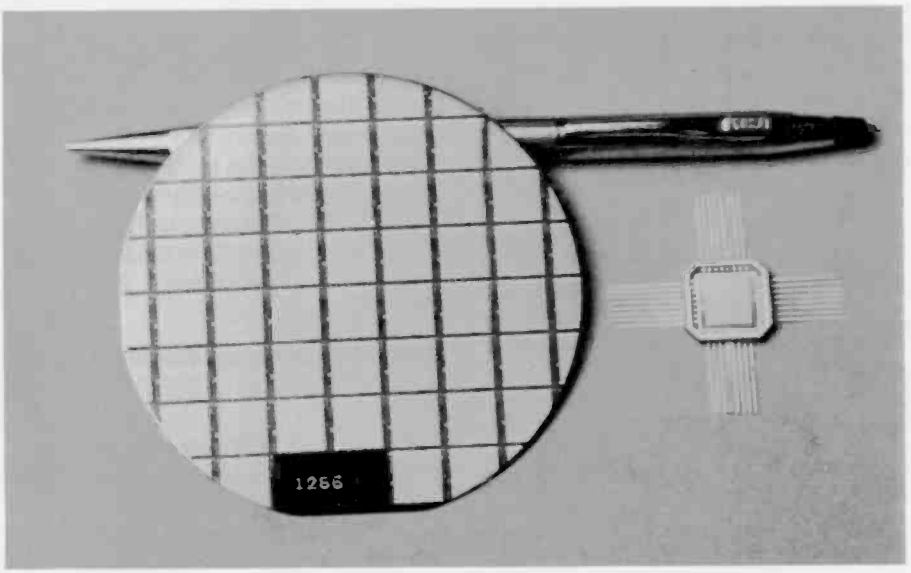


**Fig. 9. A processed 3-inch silicon wafer and a packaged 64- by 128-element IR-CCD array chip.**

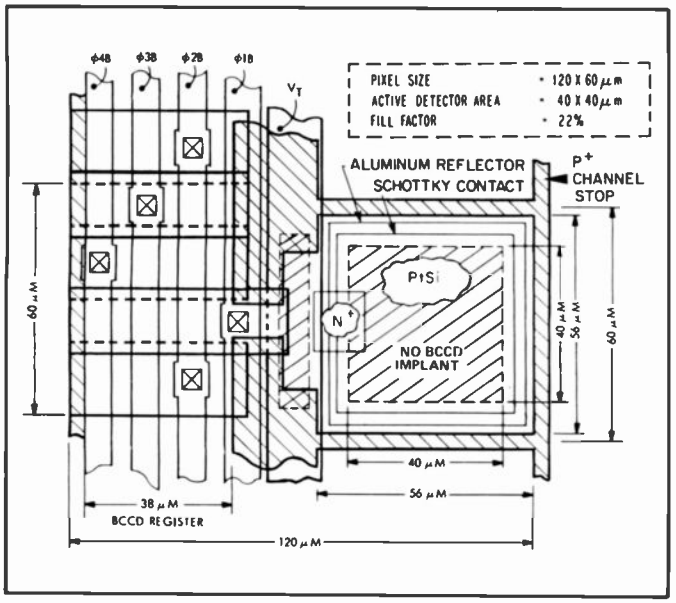


**Fig. 10. Pixel layout of the 64- by 128-element IR-CCD image sensor showing one stage of two-level-polysilicon vertical CCD column register,** with four-phase clock ($\phi_{1B}$, $\phi_{2B}$, $\phi_{3B}$, and $\phi_{4B}$), a transfer gate controlled by a voltage pulse, $V_T$, and the PtSi Schottky-barrier detector surrounded by an *n*-type (buried-CCD implant) guard ring and $p^+$ channel stops. The pixel size is 120 μm by 60 μm, the active detector area is 40 μm by 40 μm, and the fill factor is 22 percent.

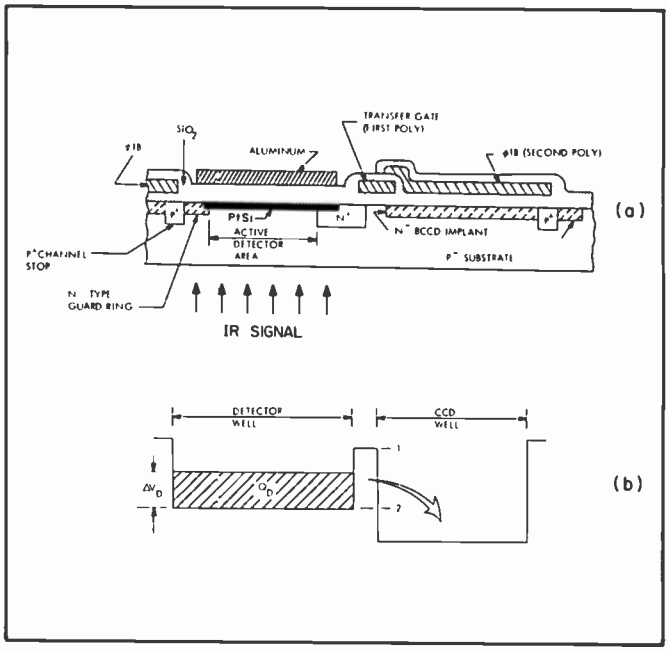


**Fig. 11. PtSi SBD with buried-channel CCD (BCCD) readout. (a)** Cross-sectional view of the structure. **(b)** Potential diagram illustrating the operation of this detector in the voltage-reset (vidicon) mode, where the detected charge signal, $\Delta Q_D$, is integrated for the full frame time of the imager, and the detector is reset once per frame time to the potential-2.

period. The change of the detector voltage, $\Delta V_D$, due to the detected charge signal can be expressed as:

$$\Delta V_D = Q_D / C_D \qquad (4)$$

where $Q_D$ is the detected charge signal, and $C_D$ is the effective capacitance of the detector.

The built-in blooming control of the SBD can be explained in a few steps. A strong optical signal forward-biases the SBD, and no further negative charge is accumulated at the PtSi electrode. The small negative voltage developed at the PtSi electrode is not sufficient to forward-bias the $n^+$ diffusion of the detector to inject a negative charge into the CCD register through the silicon region under the transfer gate driven into accumulation.

## Imaging with Schottky-barrier IR-CCD FPAs

### *Thermal imaging with a 64 × 128 PtSi IR-CCD TV camera*

The quality of thermal imaging obtained with the 64 × 128-element PtSi IR-CCD FPA was shown in Fig. 1. The performance achieved with this IR FPA is further illustrated by Figs. 12 and 13. These thermal images were obtained with an infrared TV camera developed by J. Klein of RCA Automated Systems, Burlington, Mass., using the 64 × 128-element IR-CCD image sensor with the high-performance thin-PtSi SBDs. This IR camera was operated with 60 frames per second and f/1.5 germanium optics. The FPA was cooled to about 80 K in a liquid nitrogen Dewar. Additive-type electronic response compensation (that corrects mainly for variation of the dark current of the detectors) was used to improve the overall performance. Figure 12 illustrates the blooming-control characteristics of the SBD array. The inset photograph shows one of the authors holding a glowing match. The enlarged picture shows a TV monitor with the detected thermal image. The sensitivity of this camera to very small temperature variations in the scene is illustrated in Fig. 13. Here, a thermal print of a hand on a notebook is detected by the infrared TV camera (thermal ghost effect).

### *Reflective infrared imaging with a 32 × 63 $Pd_2Si$ IR-CCD FPA*

The quality of reflective infrared images produced with the 32 × 63-element $Pd_2Si$ IR-CCD FPA is illustrated in Fig. 14. The $Pd_2Si$ image sensor in this case was operated at 60 frames per second with f/2.0 optics, at a temperature of 120 K. The inset photograph (part b), showing a man smoking a cigar, demonstrates the control of blooming due to an optical overload.

## Linearity, dynamic range, and sensitivity

A measured optical transfer curve of the 32 × 63-element IR-CCD image sensor is shown in Fig. 15. The numbers shown next to the data points correspond to the net optical transmission of neutral-density filters calibrated in the 3- to 5-μm spectral range. The experimental data points of the output voltage, $V_{out}$, represent the change of the net output voltage, $V_{out}$, above the 300-K background value. The transfer curve in Fig. 15 is drawn with a slope of 1.0, indicating that the responsivity of the PtSi SBD array is linear with the irradiance, or the photon flux, until the SBDs are driven into saturation. The measured temporal noise, $V_n$, of this array, for a 300-K background, is about 4.0 mV p-p (peak-to-peak) or 0.67 mV rms. Thus, the dynamic range of this array can be expressed as:

$$\text{Dynamic range} = \frac{H_I\,(\text{Saturation})}{\text{NE}\Delta H_I} = \frac{V_{out}\,(\text{Saturation})}{V_n\,(\text{rms})} \qquad (5)$$

where $\text{NE}\Delta H_I$ is the noise-equivalent ir-

**Fig. 12. Demonstration of the control of blooming in a Schottky-barrier IR-CCD image sensor.** Thermal image of Walter Kosonocky holding a glowing match detected by a 64-by 128-element PtSi IR-CCD TV camera (right). Visible photograph of the scene (left).

**Fig. 13. Demonstration of the sensitivity of the 64 by 128 PtSi IR-CCD image sensor.** In this experiment Walter Kosonocky is holding in front of the IR-CCD camera a notebook on which he previously formed a print of his hand. The thermal image of the handprint is shown on the TV monitor. The IR camera is operated by Harry Erhardt.

radiance corresponding to the temporal noise of the FPA, $V_n$ (rms). On the basis of equation (5), the dynamic range of this FPA is $4 \times 10^3$. When the above array was operated with f/2.0 optics, it had a measured response of 8 mV/°C. Therefore, noise-equivalent temperature, NE$T$, of this array is 0.084°C for f/2.0 optics, and 0.19°C for f/3.0 optics. The above values are in good agreement with the minimum detectable temperature of 0.15°C measured for a similar 32 × 63 FPA

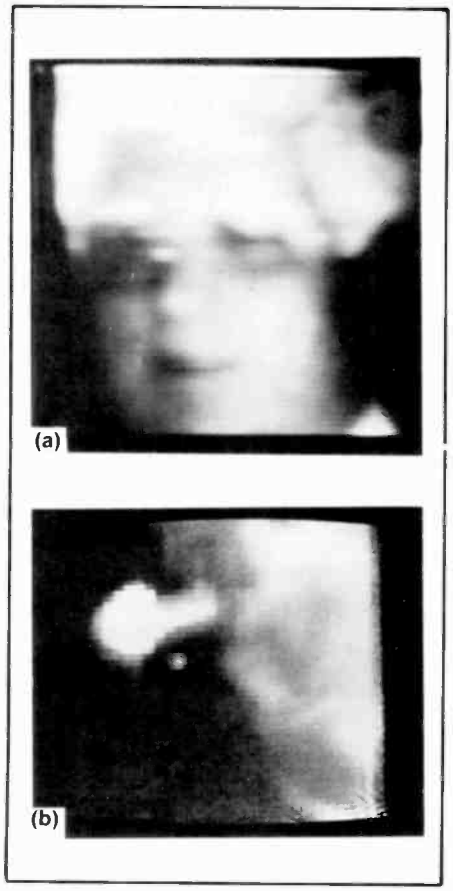


**Fig. 14. Reflective infrared images** detected with the $Pd_2Si$ IR-CCD TV camera. In **(a)** is the detected image of Hammam Elabd; in **(b)** is the image of Rod Angle smoking a cigar.

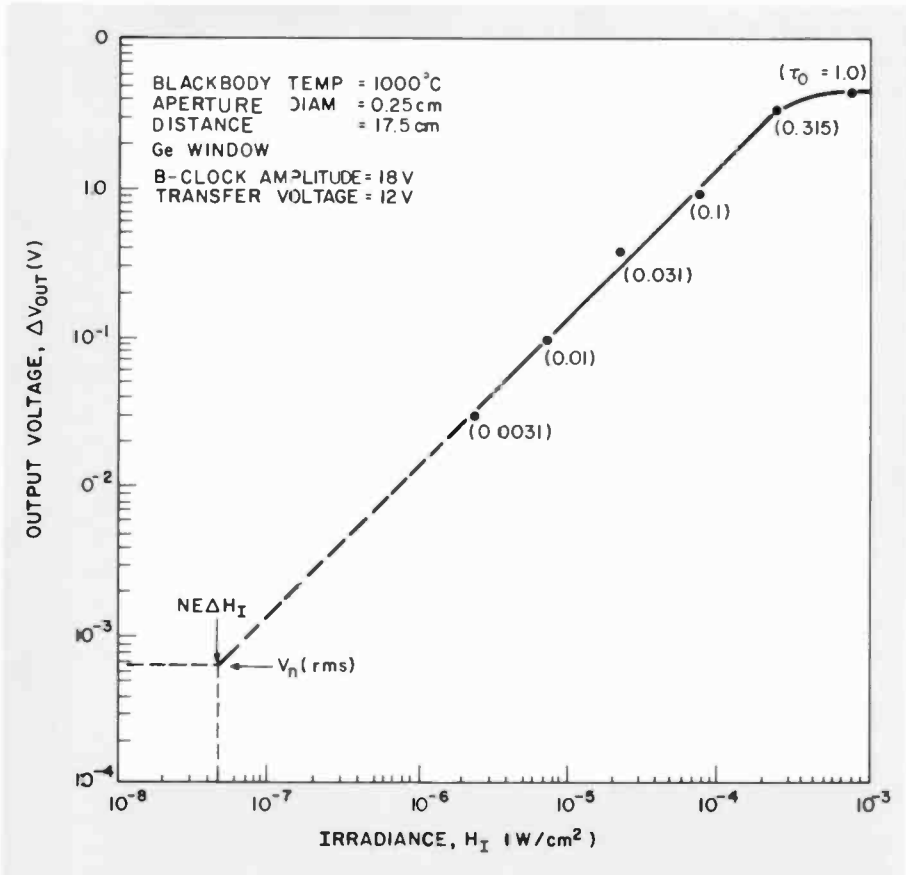


**Fig. 15. Optical transfer characteristics of the 32- by 63-element IR-CCD image sensor showing the measured change of the output voltage,** $\Delta V_{out}$, as a function of irradiance above 300°C thermal background. The noise-equivalent irradiance, NE$\Delta H_I$ of $5 \times 10^{-8}$ W/cm$^2$ is estimated from the projection of the transfer curve to the value of the measured noise voltage $V_n$ (rms) for a 300-K background.

operated with f/3.0 optics. These data were obtained by M.J. Cantella of RCA Automated Systems, Burlington, Mass.

## Uniformity and fixed-pattern noise

PtSi Schottky-barrier IR-CCD technology represents the only known FPA technology that can be used without uniformity compensation. However, to achieve performance limited only by the temporal noise of the array, some form of electronic compensation for the fixed-pattern noise is required. The fixed-pattern and temporal noise measured for the 32 × 63-element IR-CCD FPA is shown in Fig. 16.[16] This illustrates the measured fixed-pattern noise and the temporal noise as a function of exposure in photons/pixel (bottom horizontal coordinate) or in mV (top horizontal coordinate), representing the detected output for a given exposure level. The inspection of the measured fixed-pattern noise curve shows that the 2M-37 array has about 0.3 percent multiplicative fixed-pattern noise and an additive fixed-pattern noise of about 700 rms electrons/pixel, corresponding to a 0.3-mV (rms) fluctuation of the output voltage. The additive fixed-pattern noise in this array is attributed to the small dark-current variations of the PtSi detectors (operating in this case at 80 to 85 K). The curve of the fixed-pattern noise in Fig. 16 was obtained without any electronic compensation for the array uniformity.

The curve of the temporal noise was measured as a random response variation of an individual pixel from frame to frame. Note that the 300-K background corresponds to an exposure level of about $2.7 \times 10^5$ photons/pixel. The data points for exposures below that value were obtained by placing cooled objects in front of the IR camera. Also shown, in Fig. 16, is the background-shot-noise level representing the background-limited performance (BLIP) for this array.

Examination of the temporal noise curve indicates that the total additive temporal noise of the system corresponds to about 250 rms electrons/pixel. This includes the reset noise and $1/f$ noise of the detectors, the reset noise of the floating-diffusion amplifier, and the $1/f$ and white noise of the on-chip amplifier. At a 300-K background exposure of $2.7 \times 10^5$ electrons/pixel, the fixed-pattern noise is only 60 percent above BLIP, and the temporal noise is only 30 percent above BLIP.

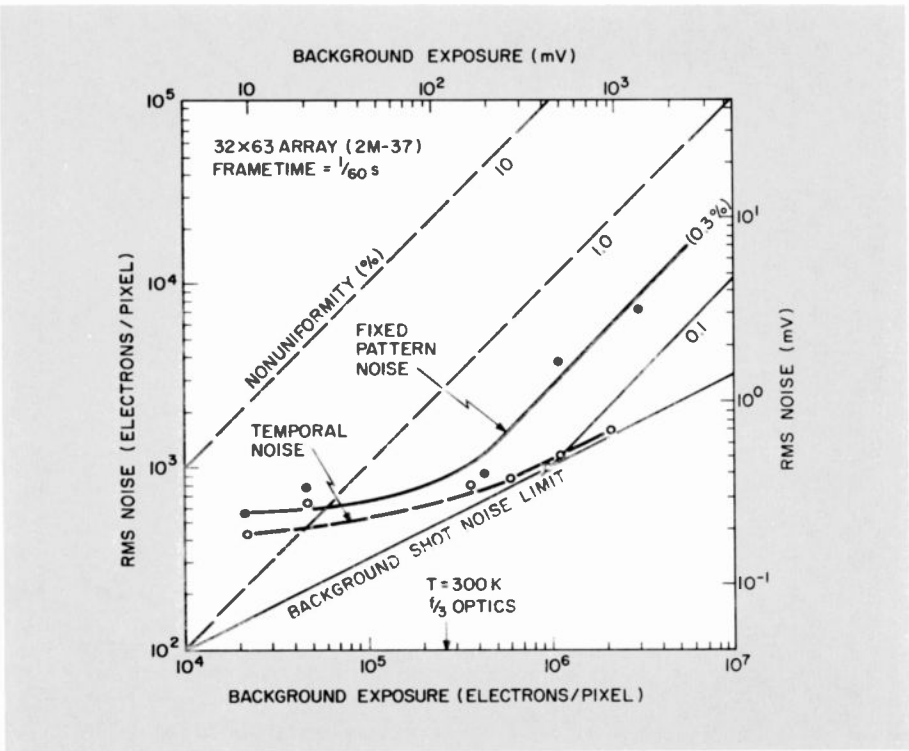


**Fig. 16. Noise-data analysis for 32- by 63-element IR-CCD image sensor (2M-37) measured at RCA Automated Systems, Burlington, Mass.** The measured noise curve indicates that this FPA has 0.3 percent of multiplicative fixed-pattern noise and an additive fixed-pattern noise of 700 rms electrons/pixel, which corresponds to 0.3 mV (rms) fluctuation of the output voltage.

## Characteristics of Schottky-barrier IR-CCD image sensors

In conclusion we will summarize the general characteristics of the Schottky-barrier IR-CCD image sensors.

- *Monolithic silicon construction.* The monolithic Schottky-barrier IR-CCD FPAs represent the only infrared-array technology that is compatible with standard IC processing. Therefore, these devices potentially can be made in large volume at low production cost. Also, they represent the most attractive approach for the development of large-area high-density FPAs. A 160 × 244-element IR-CCD FPA presently under development with the support of RADC/ESE is an example of the next step towards achieving a Schottky-barrier IR-CCD FPA with full-TV resolution.
- *Spectral response and operating temperature.* The high-performance thin-PtSi Schottky-barrier detectors made by our standard process have response in the spectral range from 1.0 to 6.0 μm, and quantum efficiency of several percent in the 3- to 5-μm thermal IR band. They can be operated as staring imagers with optical integration times of 10 to 100 ms at about 80 K.

  The thin-$Pd_2Si$ SBDs have response from 1.0 to 3.5 μm and are well suited for SWIR applications with passive cooling at apertures in the range of 100 to 140 K.
- *High element uniformity.* The Schottky-barrier IR-CCD FPAs were made with photoresponse nonuniformity of less than 0.3 percent rms, which is about an order of magnitude lower than the competing HgCdTe IR FPAs.

  Useful thermal imaging can be obtained with the PtSi FPAs without any electronic compensation for the uniformity. However, to achieve the best performance with minimum resolvable temperature (MRT) in the range of 0.1 to 0.2°C, a simple additive type of uniformity compensation is needed to compensate for the dark-current variations. The $Pd_2Si$ SBDs, even at operating temperatures of 140 K, have dark currents that are lower by more than an order of magnitude than the PtSi SBDs at 80 K. Therefore, the $Pd_2Si$ FPAs produce excellent reflective IR imagers without any uniformity compensation.
- *Linearity, large dynamic range, no blooming, and no cross talk.* The Schottky-barrier IR-CCD FPAs have linear

response over a dynamic range of $10^3$ to $10^4$. Under strong infrared irradiation, their response saturates without blooming and without lag. The SBD IR-CCD FPAs also have no observable cross talk; this assures that the MTF of these FPAs is determined by the geometric dimensions of the detectors.

## Acknowledgment

The authors would like to express their appreciation to D.E. O'Connor and G.W. Hughes for their support of this project, to I.M. Bijaczyk and A.J. Bijl for their effort on processing of the devices, and to R.J. Paff and R.T. Smith for their help on the diagnostics of the silicide structures.

## References

1. Shepherd, F.D. and Yang, A.C., "Silicon Schottky Retinas for Infrared Imaging," *1973 Int. Electron Devices Meeting, Tech. Dig.*, pp. 310-313.
2. Kohn, E.S., Kosonocky, W.F., and Shallcross, F.V., "Charge-Coupled Scanned IR Imaging Sensors," RADC-TR-77-303 (September 1977).
3. Kohn, E.S., Roosild, S.A., Shepherd, F.D., and Yang, A.C., "Infrared Imaging with Monolithic, CCD-Addressed Schottky-Barrier Detector Arrays, Theoretical and Experimental Results," Int. Conf. on Application of CCDs (October 29-31, 1975).
4. Kosonocky, W.F., Kohn E.S., and Shallcross, F.V., "256-Element Schottky-Barrier IR-CCD Line Sensor," RADC-TR-77-304 (September 1977).
5. Kosonocky, W.F., Kohn, E.S., and Shallcross, F.V., "Optimization Study of IR-CCD Array," RADC-TR-78 (July 1978).
6. Capone, B.R., Skolnik, L.H., Taylor, R.W., Shepherd, F.D., Roosild, S.A., Ewing, W., Kosonocky, W.F., and Kohn, E.S., "Evaluation of a Schottky IR-CCD Staring Mosaic Focal Plane," 22nd Int. Tech. Symp. Society of Photo-Optical Instrumentation Engineers, San Diego, Calif. (August 28-29, 1978).
7. Kosonocky, W.F., Kohn, E.S., Shallcross, F.V., Sauer, D.J., Shepherd, F.D., Skolnik, L.H., Taylor, R.W., Capone, B.R., and Roosild, S.A., "Platinum-Silicide Schottky-Barrier IR-CCD Image Sensors," 1978 Int. Conf., on CED Applications, pp. 2-7 to 2-38 (October 25-27, 1978).
8. Shepherd, F.D., Taylor, R.W., Skolnik, L.H., Capone, B.R., Roosild, S.A., Kosonocky, W.F., and Kohn, E.S., "Schottky IR-CCD Thermal Imaging," *Adv. Electron. Phys.*, Vol. 22, 7th Symp. Photo-Electron Image Devices, pp. 495-512 (1979).
9. Archer, R.J. and Cohen, J., "Schottky-Barrier Monolithic Detector Having Ultra-thin Metal Layer," U.S. Patent 3,757,123 (September 4, 1973).
10. Taylor, R.W., Skolnik, L.H., Capone, B.R., Ewing, W., Shepherd, F.D., Roosild, S.A., Cochrun, B., Cantella, M., Klein, J., and Kosonocky, W.F., "Improved Platinum-Silicide IR-CCD Focal Plane," SPIE's Tech. Symp., Advances in Focal Plane Technology, Los Angeles, Calif. (February 4-5, 1980).
11. Kosonocky, W.F., Erhardt, H.G., Meray, G.M., Shallcross, F.V., Elabd, H.A., Cantella, M.J., Klein, J., Skolnik, L.H., Capone, B.R., Taylor, R.W., Ewing, W., Shepherd, F.D., and Roosild, S., "Advances in Platinum-Silicide Schottky-Barrier IR-CCD Image Sensors," *SPIE*, Vol. 225, IR-Image Sensor Technol., pp. 69-71 (1980).
12. Cantella, M.J., Klein, J., Skolnik, L.H., Capone, B.R., Taylor, R.W., Ewing, E., Shepherd, F.D., Roosild, S.A., Kosonocky, W.F., Erhardt, H.G., and Cochrun, B., "A High Sensitivity Schottky IR-CCD Focal Plane Array, IRIS Meeting (May 1980).
13. Kosonocky, W.F., Elabd, H., Erhardt, H.G., Levine, P.A., Shallcross, F.V., and Villani, T.S., "Improved IR-CCD Area Sensor," Final Report, RADC-TR-81-F, (August 1981).
14. Cohen, J., Vilms, J., and Archer, R.J., "Investigation of Semiconductor Schottky-Barriers for Optical Detection and Cathodic Emission," Air Force Cambridge Research Labs, Report No. 68-0651 (1968).
15. Kosonocky, W.F., Elabd, H., Erhardt, H.G., Shallcross, F.V., Villani, T., Meray, G., Cantella, M.J., Klein, J., and Roberts, N., "64- × 128-Element High-Performance PtSi IR-CCD Image Sensor," 1981 IEDM, Washington, D.C. December 7, 1981.
16. Cantella, M.J., "IR Focal Plane Array System Performance Modeling," *Proc. SPIE Technical Symposium*, Los Angeles, Calif. (January 1982).

**Walter Kosonocky** is a Fellow of Technical Staff at RCA Laboratories, Princeton, N.J. He joined RCA Laboratories in 1955 and, since 1970, has been working on the design and process development of charge-coupled devices for signal-processing and image-sensing applications. Since 1975, he has been involved in the development of the Schottky-barrier infrared image-sensing arrays.
Contact him at:
**RCA Laboratories**
**Princeton, N.J.**
**TACNET: 226-2017**

**Grazyna Meray** joined RCA Laboratories in 1969. Since 1972, she has been working on the layout and programming of CCD arrays.
Contact her at:
**TACNET: 226-2664**

**Frank Shallcross** joined RCA Laboratories as a Member of Technical Staff in 1958. Since 1972, he has been engaged in the process development and fabrication of CCD arrays for signal-processing and imaging applications.
Contact him at:
**TACNET: 226-2307**

**Frederick Tams, III,** joined RCA Laboratories in 1953. Since 1967, he has been working in the area of thin-film deposition.
Contact him at:
**TACNET: 226-3010**

**Verne Frantz** joined RCA Laboratories in 1958. Since 1972, he has been working on various aspects of processing CCD image-sensing arrays.
Contact him at:
**TACNET: 226-2308**

**Robert Miller** joined RCA Laboratories in 1965. Since 1972, he has been working on CCD processing for comb filters, and for visible and infrared image sensors.
Contact him at:
**TACNET: 226-2350**

**Joseph Groppe, Jr.,** joined RCA Laboratories in 1967. He has worked mainly in testing and characterizing various types of MOS and CCD circuits.
Contact him at:
**TACNET 226-2681**

**Tom Villani** joined RCA Laboratories ir. 1980. Since that time, he has been working on testing and characterizing Schottky-barrier infrared CCD arrays.
Contact him at:
**TACNET: 226-2686**

**Harry Erhardt** is a Member of Technical Staff at RCA Laboratories. He joined the Laboratories in 1978 and since then, has been involved in the development of the Schottky-barrier focal-plane arrays for infrared-imaging applications.
Contact him at:
**TACNET: 226-2674**

**Hammam Elabd** is a Member of Technical Staff at RCA Laboratories. He joined the Laboratories in 1980 and has since been involved in the technology, development, and characterization of the PtSi and $Pd_2Si$ Schottky-barrier detector arrays.
Contact him at:
**TACNET: 226-2687**

**Authors (left to right) Groppe, Villani, Erhardt, and Elabd.**

**Authors (left to right) Tams, Shallcross, Frantz, and Miller.**

# What's New in Microwave? A special issue of the *RCA Review*

The *RCA Review* (Vol. 42, No. 4) covers current work by RCA scientists and engineers on microwave devices and systems. Subjects covered in over 400 pages of articles include advanced microwave materials, hybrid and monolithic circuits, millimeter-wave sources, computer-aided design techniques and special components, including amplifiers, phase shifters, filters, and applicators used in cancer research. The issue's guest editor was Markus Nowogrodzki.

Fred Sterzer, Director of the Microwave Technology Center at RCA Laboratories, wrote an article on his research (see contents page) and also wrote the foreword to the issue. For additional information, contact Ralph Ciafone, Editor, *RCA Review*, RCA Laboratories, TACNET: 226-3222.


## Contents Page

J.J. Klein | N.L. Roberts | G.D. Chin

# Infrared-camera system developed to use the Schottky-barrier IR-CCD array

*Unlike a parallel-scan IR camera, which requires a TV camera to multiplex its parallel video output to a serial video output, the focal plane array with its on-chip signal-processing CCDs provides an output that is compatible with standard serial TV imagery.*

**Abstract:** *An advanced infrared camera system that offers significant reductions in size, cost, reliability, and complexity has been developed. The heart of the camera system is a tiny monolithic Schottky-barrier focal plane array with over 8000 infrared detectors and a corresponding number of signal-processing charge-coupled devices. Unlike conventional infrared cameras, which mechanically scan a scene by an arrangement of oscillating or rotating mirrors, the focal plane array views the entire scene all at one time. Thus, it is referred to as a "staring array," as opposed to the "scanning" of the mechanical-optical type. The staring array camera has greater sensitivity than current-generation IR cameras and, therefore, can resolve temperatures in a scene to a fraction of a degree.*

A complete infrared (IR) camera system has been developed for field test, demonstration, and evaluation of a 32 × 64 and a 64 × 128 Schottky-barrier infrared charge-coupled device (IR-CCD) focal plane array. The overall system consists of a camera head with its associated lens and signal-processing electronics, a 12-bit video data converter and a 12-bit digital scan converter.

This IR-camera system offers significant reductions in size, cost, and complexity while increasing its reliability. The heart of the camera system is a tiny monolithic Schottky-barrier focal plane array (FPA) with over 8000 infrared detectors (64 × 128 array) and a corresponding number of signal-processing charge-coupled devices. Unlike conventional IR cameras, which mechanically scan a scene by an arrangement of oscillating or rotating mirrors, the focal plane array views the entire scene all at one time. Thus, it is referred to as a "staring array," as opposed to the "scanning" mechanical-optical type.

The staring-array camera has greater sensitivity than the current generation of IR cameras and, therefore, resolves temperatures to a fraction of a degree. Unlike a parallel-scan IR camera, which requires a TV camera to externally multiplex its parallel video output to a serial video output, the focal plane array contains on-chip signal-processing CCDs that provide a serial output which is convertible to standard serial TV imagery.

## IR-camera system

A simplified block diagram of the overall IR-camera system is shown in Fig. 1. The system consists of a camera head with its

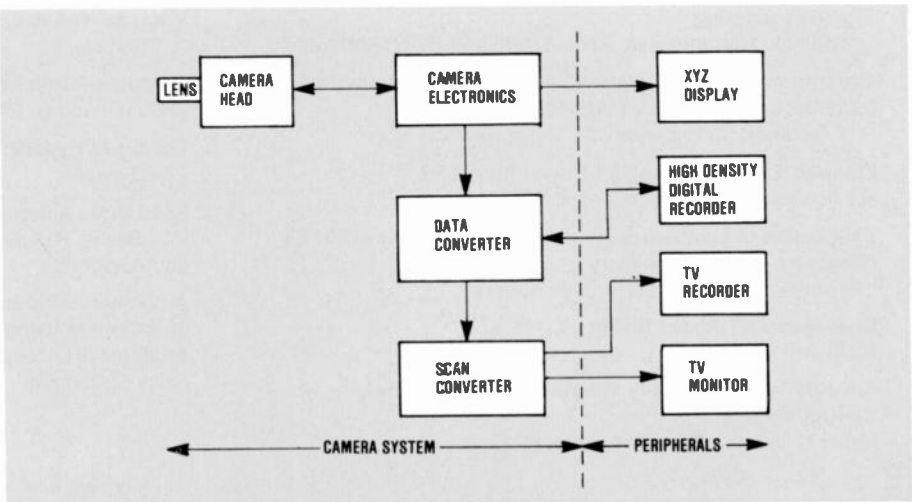


**Fig. 1. IR camera system.** Camera, data converter, scan converter, recorder and displays are required for observation and recording of IR signature data.


Final manuscript received March 18, 1982.
Reprint RE-27-3-8

associated lens and signal-processing electronics, a 12-bit, high-speed data converter, and a 12-bit scan converter.

The camera features include video double-correlated sampling, automatic black-level control, logarithmic compression and video pixel-to-pixel nonuniformity and shading correction. To preserve the wide dynamic range of the camera's video output, the video is processed by the data converter's analog-to-digital (A/D) converter into 12-bit digital words. These 12-bit digital words are recorded by a high-density digital recorder for later analysis or viewing. Data gathered during field tests may be studied at leisure when the information from the digital recorder is played back through the data converter's 12-bit digital-to-analog (D/A) converter. The data converter's digital output is also used as the input to a 12-bit scan converter. The converter changes the 64-line or 128-line output of either focal plane array to a standard 525-line interlaced-TV-raster format, which can be displayed on a standard TV monitor or can be recorded on a standard video cassette recorder. The XYZ display is used for direct viewing of the camera's video output. A photo of the camera system and related equipment is shown in Fig. 2.

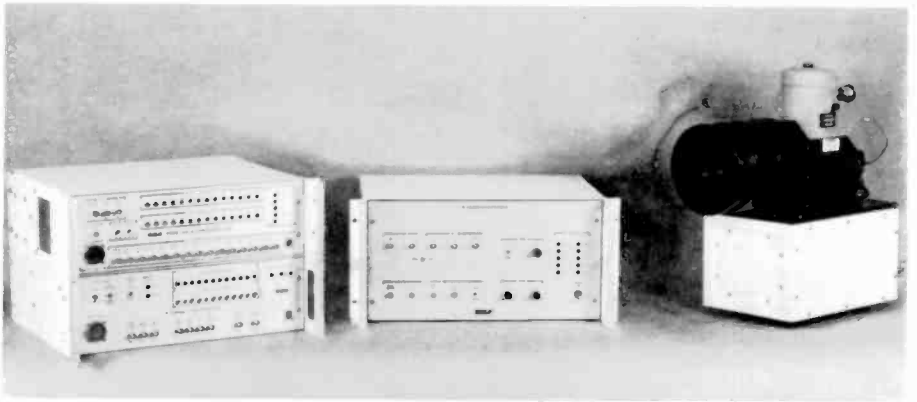

**Fig. 2. Schottky-barrier array camera system.** Data converter, scan converter, camera-control electronics and camera head with optics are shown.

## Focal plane array (FPA)

The basic construction of the IR-CCD focal plane array (FPA) is shown in Fig. 3. The area array uses an interline-transfer system, which consists of a vertical parallel array of illuminated IR Schottky detectors with non-illuminated CCD (B) registers all leading in parallel into a single output CCD (C) register. The IR optical image is detected by the vertical lines of 128 Schottky detectors. The vertical line detectors are separated from each other by opaque vertical 128-element B registers. Once every frame, the signals from the IR detectors are transferred into the vertical B registers by applying a 1-$\mu$s pulse to the transfer gate. Then, the entire detected image is shifted down—row by row in unison—by a B clock, and it is transferred into a 128-element output C register, one line at a time. The horizontal lines are then transferred out from the register by a high-frequency C clock before the next horizontal line is shifted in. Since the output horizontal CCD register has 128 bit positions, only the even-numbered bit positions are loaded during the line shift from the B to the C register.

The output C register is designed to be operated with a dc-biased charge-preset input, also referred to as a fill-and-spill input. This electrical input allows for the introduction of adjustable amounts of bias charge (fat-zero) into all bit positions of the C register to improve the transfer efficiency of the C register. The bias-charge packets are introduced into one end of the C register in sequence with the read-out of signal plus bias charge at the other end.

The 128-by-1 A register, a non-output stage, is designed with a dc-biased charge-preset input. This electrical input allows for the introduction of adjustable amounts of bias charge, clocked in synchronism with the C clock, into all 128 bit positions of the A register. These bias charges can then be transferred, line by line, from the A to the B registers to provide bias charge (fat-zero) for all bit positions in the B registers.

The addition of this register enhances the overall performance capability of the FPA as follows:

- The addition of bias charge into the B registers improves their transfer efficiencies;
- The overall array operation can be checked, at room temperature, by introducing a fixed digital pattern of biased-charge signal packets into the A and C registers;
- The FPA can be used for moving-target indication (MTI) by taking the signal output of the C register, and inverting

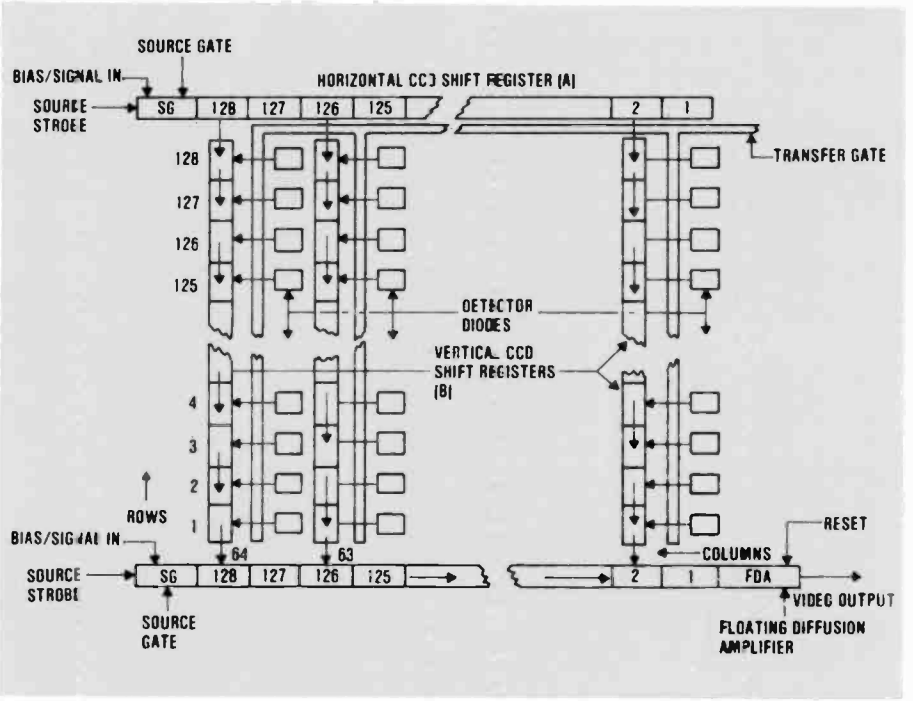


**Fig. 3. Construction of Schottky-barrier IR-CCD array.** The readout organization of the area IR image sensor is patterned after the interline transfer geometry.

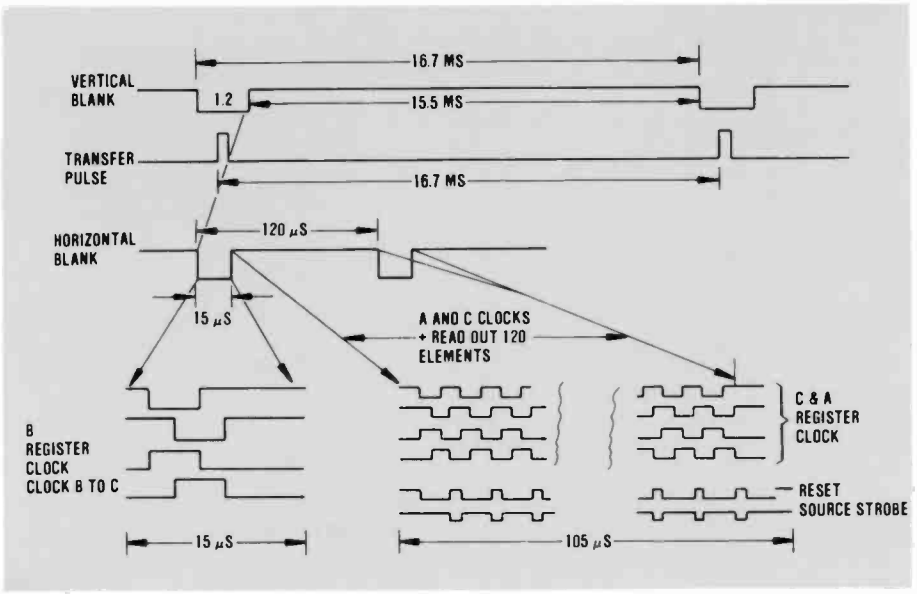


**Fig. 4. Simplified timing diagram.** The IR image charge is transferred to the B register from the Schottky diodes (60 times per second), and then it is clocked row by row from the B to the C register and out of the chip through the C register.

and recirculating it back into the B register by way of the A register. The first frame out of the array will contain all video. The second frame minus the first will contain all video information from objects that are moving within the scene.

A simplified timing diagram is shown in Fig. 4. As shown, the detected IR signals are transferred to the B registers, once every 1/60 second, during the vertical blanking interval.

Immediately following this transfer, 128 horizontal lines of video have left the FPA via the B and C registers and the output-floating-diffusion amplifier. The horizontal line period is approximately 120 μs, which consists of 15 μs of "blank time" allotted for B-to-C and A-to-C transfer and 105 μs of active line time. During the active line time, the A and C clocks, running at 1.2 MHz, allow for readout of the C register, and for introduction of bias-charge packets into both the A and C registers.

For normal operating situations, the resulting signal output waveform is shown in Fig. 5. As shown, the real-zero output level of the FPA is at 8.6 volts. The fat-zero C level (level of charge packets injected into C register only) is at 8.2 volts and the fat-zero B-plus-C level is at 8.0 volts. The level due to detected IR-signal charges extends from 8 volts to 6 volts for a total signal range of 2 volts. Since the RMS noise is typically less than 0.2 millivolts and the sensitivity is 10 to 15 millivolts for scene temperature differences of 1°C, the overall dynamic range of the FPA is greater than 10,000 to 1.

## IR camera design

A block diagram of the IR camera is shown in Fig. 6. The camera-head electronics, consisting of the A, B, and C clock generators, the video preamp, and the FPA-electrode voltage-adjustment panel, have been located as close as possible to the FPA to minimize noise pickup and to reduce the number of wires going from the camera-electronics box to the camera head.

The camera-electronics package consists of: a synchronizer, a power converter, a video preprocessor, an automatic black-level controller, a video mixer/image-compressor, an output video buffer, vertical and horizontal sweep-voltage generators, and a pixel corrector.

The synchronizer is crystal-controlled to produce jitter-free video output. The video preprocessor accepts the video from the camera-head preamp and provides a sampled video-signal output with an absolute minimum of noise. The automatic black-level control circuit automatically adjusts the preprocessor signal output to a

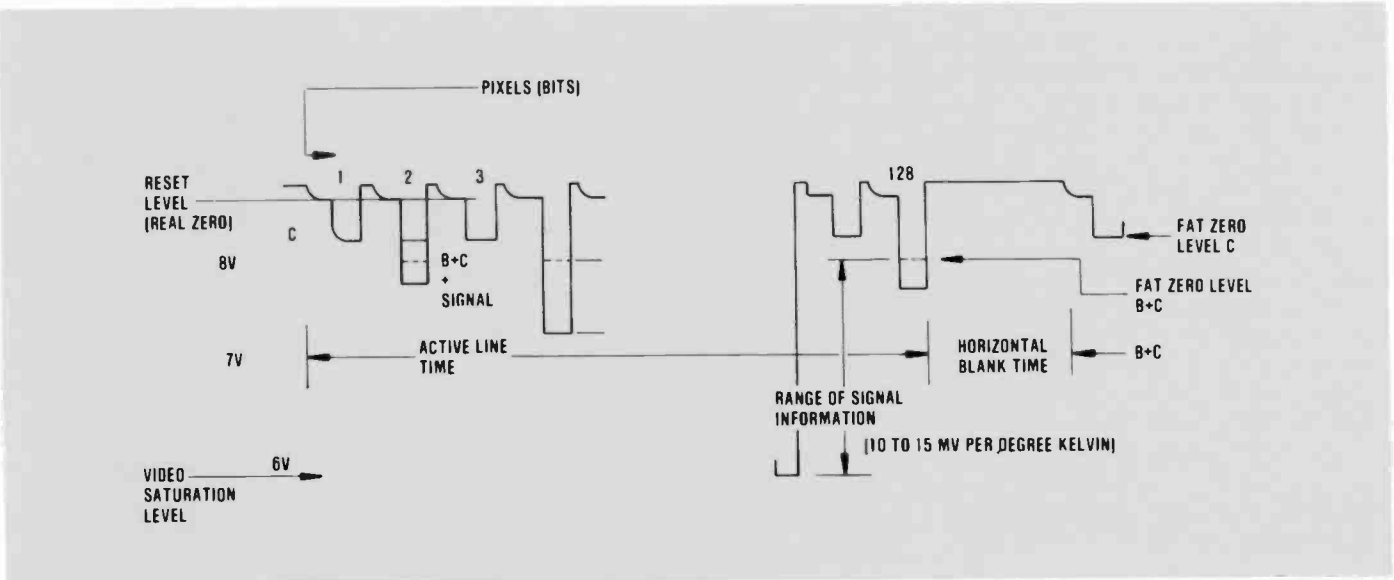


**Fig. 5. Signal output of a focal plane array (one horizontal line).** The output of the focal plane array covers a tremendous dynamic range of approximately 10,000 to 1.

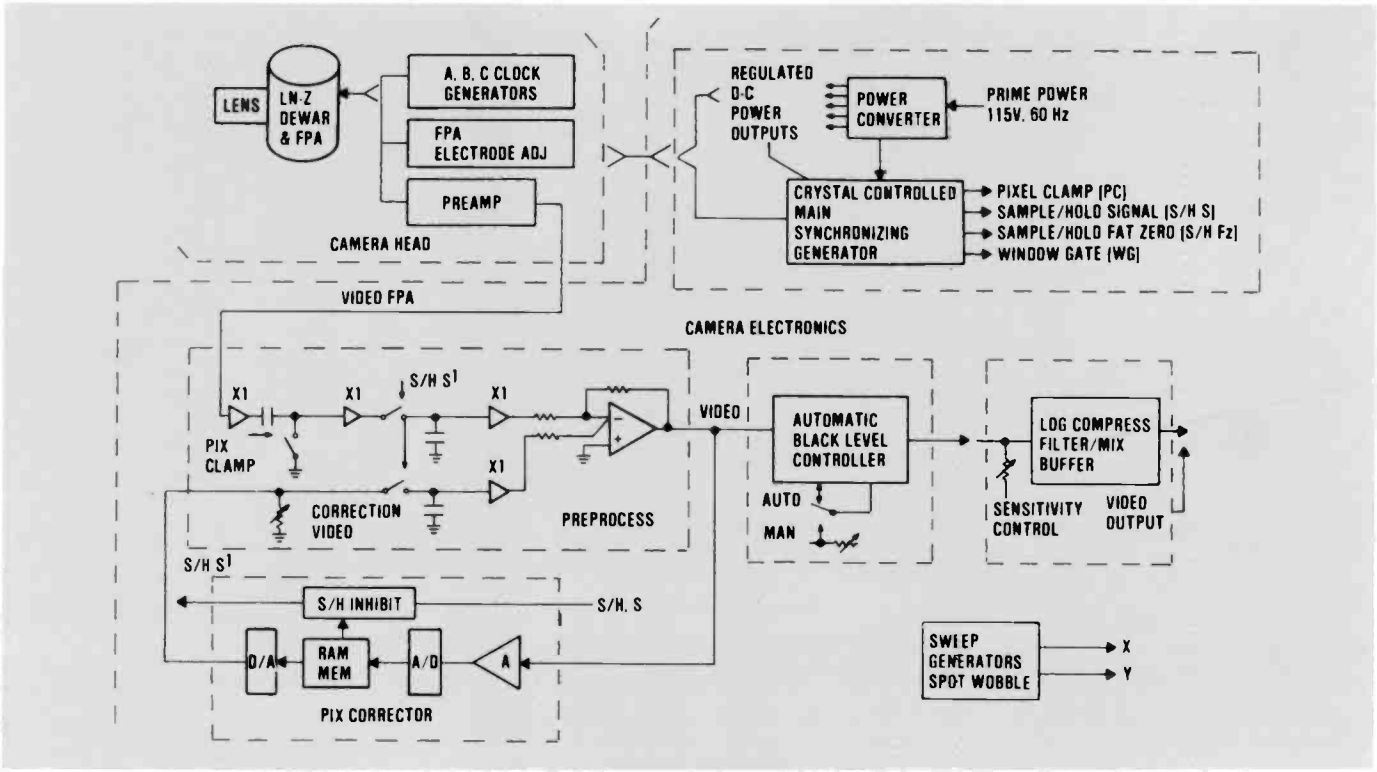


**Fig. 6. IR Focal Plane Array camera.** The camera features are: double-correlated sampling, automatic black-level control, pixel correction, and logarithmc compression.

dc level that places the scene's background-level signal at the black reference setting. An automatic/manual switch is also provided for manual setting of black level. The video output processor consists of a video compressor, a video mixer, a filter, and an output buffer amplifier. The logarithmic video compressor is needed to handle the very wide signal dynamic range. The sensitivity control, by varying the input signal to the video compressor, allows for the enhancement of a target with a specific temperature within an overall scene. The video mixer allows for the summation of mixed blanking with the video signal information. A two-pole video filter optimizes the video bandwidth.

The pixel correction is used to provide a correction signal for improving both the shading and pixel nonuniformity due to fixed offsets in the array. A correction signal is generated by capping the lens and loading a frame of uncorrected video into the RAM memory by way of the A/D. The RAM-memory correction signal is summed back into the video by the D/A and a sample/hold switch on the preprocessor board. Sensor diodes that are either shorted or open will generate correction signals that are either all zeros or all ones. For either condition the sample-and-hold circuits are inhibited. Picture quality is unaffected because, typically, fewer than 10 diodes are bad. Horizontal sweep, vertical sweep, and Z video outputs are also provided in the camera electronics for use with an XYZ display.

## Data converter

The data converter, depicted in the block diagram of Fig. 7, contains both a high-speed A/D converter and a high-speed D/A converter, each capable of processing at a rate from dc to 5 mega-conversions per second. Designed to be operationally compatible with a particular high-density digital recorder, it is a self-contained, general purpose subsystem to support the IR-CCD camera electronics in storing and recovering video data on magnetic tape. To preserve the dynamic range of the IR-CCD signal on tape for post-analysis, all video data is 12-bits long. Recorded with the video data are the data clock, horizontal sync and vertical sync for pixel, line and frame-timing references.

The A/D converter uses the data clock to identify the pixel location in the input video and to serve as the encode-command signal. To compensate for the sequential processing delay in the A/D converter, both the horizontal and vertical sync signals are delayed four data-clock periods before they are provided for recording. A total of 15 data lines—consisting of 12 magnitude bits, 2 timing bits, and a data clock—are provided to the digital recorder and, simultaneously via parallel output connectors, to other support or signal-processing equipment, such as the scan converter. In the latter case, immediate TV-monitor viewing from the IR-CCD camera is obtained.

The D/A converter receives data from the digital data recorder and reproduces the IR-CCD video signal along with the horizontal and vertical sync signals for driving an x-y monitor. To simplify testing of both converters, the output of the A/D section can be sent to the D/A converter via a 15-bit-wide multiplexer. All data lines are buffered by differential interface circuits to minimize common-mode grounding problems.

## Scan converter

To view the IR-CCD video signal on a standard TV monitor, the processed video from the sensing-array electronics is modified by a scan converter to provide the required NTSC waveform signal. The scan converter accepts 12-bit parallel video data, plus frame and line reference timing, from a high-density digital recorder or directly from the camera via a video A/D convert-

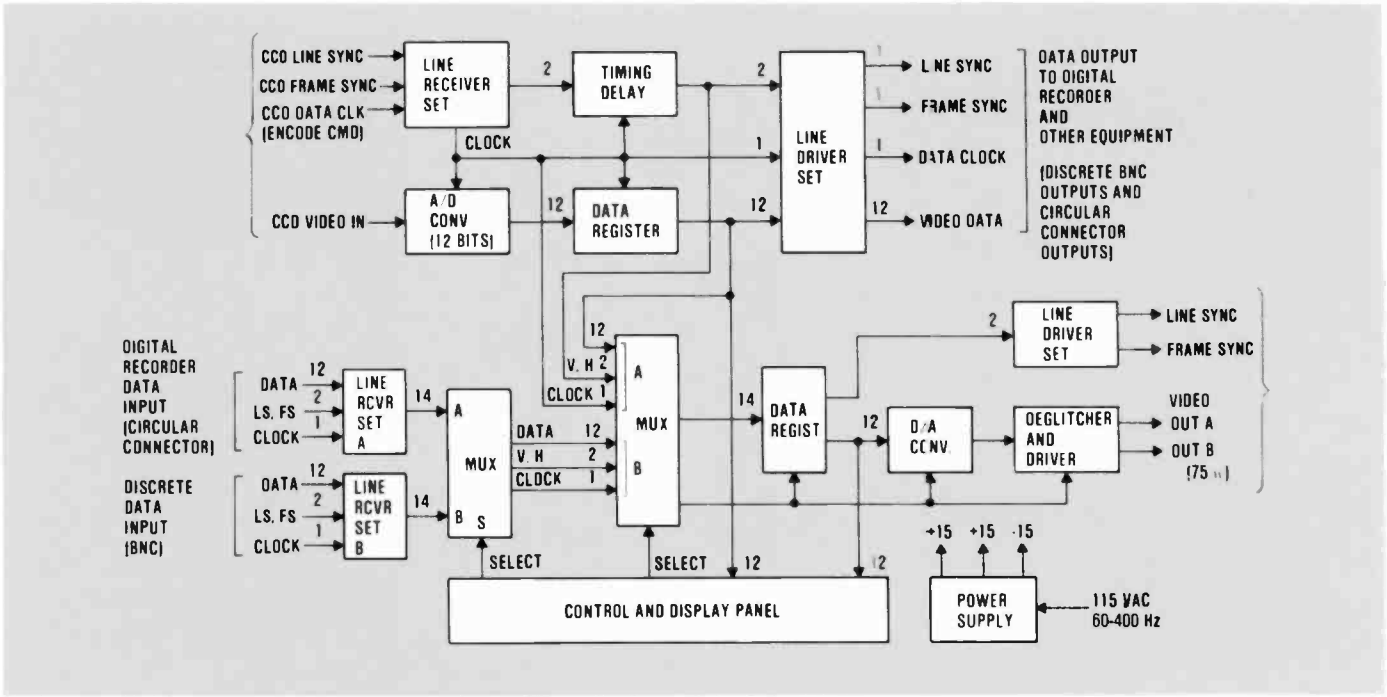


**Fig. 7. Data converter block diagram.** This multi-function support unit provides a signal conversion interface between the IR-CCD camera and a magnetic tape recorder or NTSC scan converter for real-time recording and/or standard TV viewing. It also can be used to convert recorded data back to electrical signals for driving an X-Y CRT monitor.

er for real-time viewing. Two parallel, 75-ohm composite video outputs as well as selected sync and test signals are available.

The primary function of the scan converter is to increase the IR-CCD data rate needed for reconstructing the video portion of the NTSC composite signal. It adjusts the rate to produce a square picture (the view seen by the staring array), and aligns the picture to the center of the TV screen. To improve picture quality, the scan converter can perform interpolation (a modified moving-average scheme) in the vertical dimension. Smoothing in the horizontal line is controlled by *LC* integration. The scan converter can handle either the 32(H) × 64(V) or the 64(H) × 128(V) IR-CCD sensing array.

A block diagram of the scan converter is shown in Fig. 8. The frame-sync signal is re-referenced to the internal clock frequency of 13.104 MHz to minimize frame-to-frame coupling jitter. The crystal-controlled clock is counted down to 3.27 MHz for the line-interpolator control section and to 504 kHz for the NTSC

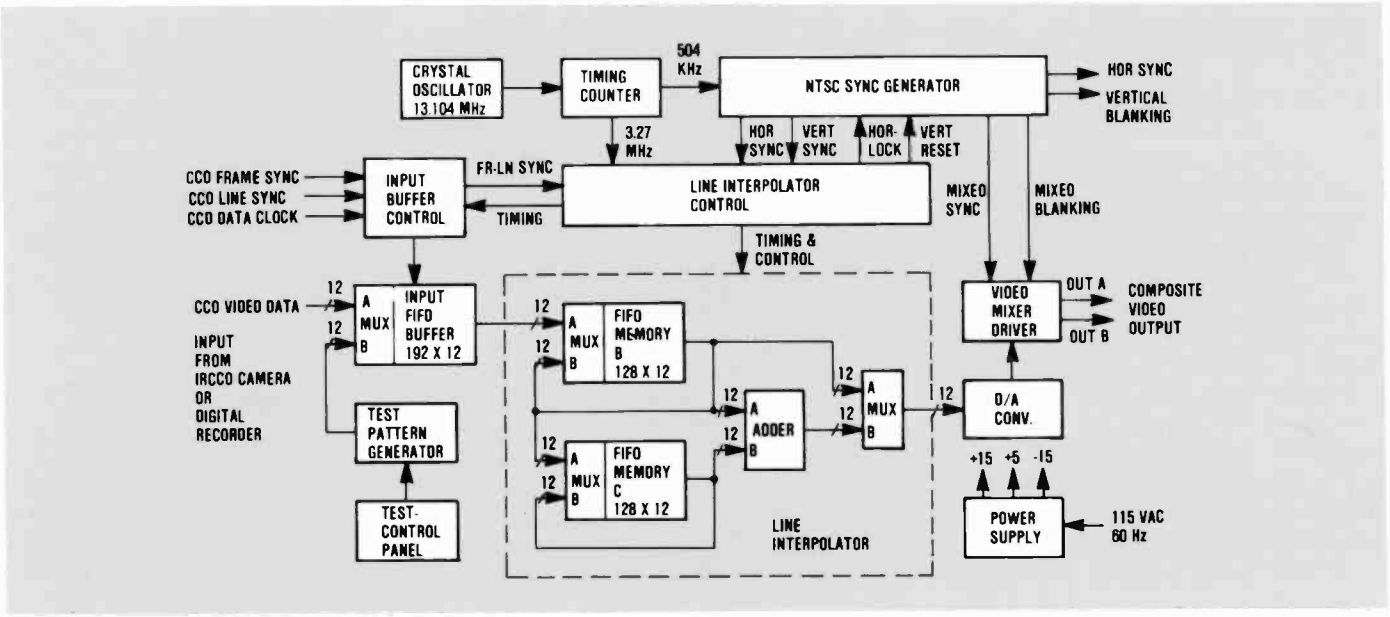


**Fig. 8. Scan converter block diagram.** This support unit translates digital data and timing signals from either a magnetic recording or a data converter to a NTSC composite video signal.

**Fig. 9. Walter Kosonocky, RCA Labs, holding** hot (left hand) and cold (right hand) cups.

**Fig. 10. A TV close-up of a man's face.** Note his cold nose.

sync generator. To isolate the two different video data rates between the external data source and the internal processing logic, a 192-word, 12-bit-wide FIFO (first-in, first-out) input buffer memory is used. The input buffer provides data storage for up to three 64-pixel IR-CCD lines. For the 32 × 64 array, the input data rate is 163,800 words per second; for the 64 × 128 array, the rate is 655,200 words per second. To facilitate a system self-check, a data set for a "checkerboard" test pattern can be sent to the input FIFO buffer via the input multiplexer.

The NTSC sync generator provides the standard horizontal and vertical timing signals for constructing the composite video signal as well as for synchronizing the line-interpolator-control logic. Within the line-interpolator section are two FIFO memories, each with a capacity of 128 words, 12 bits wide. While operating, FIFO memories B and C store a word group for exactly one line. If line interpolation is not desired, the output data from FIFO memory B is sent directly to the D/A converter. When line interpolation is selected, the data stream to the D/A converter alternates between the output of FIFO memory B and the output of the 12-bit adder, which adds one pixel (12 bits) in a current line from memory B to a same-column pixel in a previous line from memory C as the data groups are recirculated within each FIFO memory. The divide-by-two function is obtained by shifting the data connections to the D/A input multiplexer by 1 bit, the result being an averaged value between two same-column pixels in adjacent lines. The schedule of unmodified and interpolated lines for a 240-line field is controlled by two PROMs, one for each size sensing array serviced.

The ratio of IR-CCD lines to TV lines is selected to have all array pixels visible on the viewing screen. As implemented, a ratio of 4 IR-CCD lines to 15 TV lines was chosen for the 32 × 64 array and a ratio of 8 IR-CCD lines to 15 TV lines was chosen for the 64 × 128 array. The 240-line screen is divided into 16 blocks of 15 TV lines.

The word rate to the D/A converter is automatically determined by the array size being handled by the scan converter. For the smaller array, the D/A converter input data rate is 819,000 words per second; for the larger array the rate is 1,638,000 words per second. To produce the composite video signal, the video mixer-driver combines the mixed sync and mixed blanking signals from the sync generator and the "de-glitched" output from the D/A con-

**Fig. 11. U.S. Army Jeep.** IR image of jeep taken with 64 × 128 array sensor. Note the (black) windshield and (white) hot grill and the reflection of exhaust system on the ground.

**Fig. 12. U.S. Army Armored Personnel Carrier (APC).** Note the exhaust (white spot) and the driver image.

verter. The scan converter operates as a self-contained unit with its own ac-dc power-supply system.

## Summary

The overall IR-camera system has been tested during day and night operations, and it has obtained excellent IR signatures of tanks, trucks, jeeps, armored personnel carriers, helicopters and high-performance aircraft. The sensor has successfully demonstrated that it can "see" through smoke, haze and dust. Examples of the imagery obtained with this camera system are shown in Figs. 9, 10, 11, and 12.

## Acknowledgments

Many people within RCA have been contributing to the development and use of the modeling, simulation, design, and automated-testing techniques described in this paper. Team participation has involved engineers and management principally at RCA Automated Systems and RCA Laboratories. Their dedication to technical excellence in high-quality imaging systems has provided the inspiration and technical guidance needed for this work.

## References

1. Steckl, A.J., "Infrared Charge Coupled Devices," *Infrared Physics*, 16, 65 (1976); Steckl, A.J., Nelson, R.D., French, B.T., Gudmundsen, R.A., and Schechter D., "Application of Charge-Coupled Devices to Infrared Detection and Imaging," *Proc. IEEE*, Vol. 63, No. 64 (1975).
2. Tegnelia, J.A., "DARPA Unveils Staring Focal Plane Array," *Defense Electronics*, Vol. 12, No. 101 (1980).
3. Cantella, M.J., "IR Focal Plane Array System Performance Modeling," *Proc.*, SPIE Technical Symposium, Los Angeles, Calif. (January 1982).
4. Hudson, R.D., Jr., *Infrared System Engineering*, Wiely Interscience (1969).
5. Wolfe, W.L., *The Infrared Handbook*, Office of Naval Research, Washington, D.C. (1978).
6. Ratches, J.A., "Static Performance Model for Thermal Imaging Systems," *Optical Engineering*, Vol. 15, No. 6, pp. 525-530 (November/December 1976).
7. Schade, O.H., Sr., "An Evaluation of Photographic Image Quality and Resolving Power," *Jour SMPTE*, Vol. 73, No. 2, pp. 81-119 (February 1964).
8. Schade, O.H., Sr., "Image Quality—A Comparison of Photographic and Television Systems," RCA Laboratories (1975).
9. Cantella, M., Honickman, H., Kim, K., "IR Focal Plane Array Noise Characterization and Measurement," *Proc.*, IRIS Detector Specialty Group Meeting (June 1981).
10. Shepherd, F.D., Yang, A.C., Roosild, S.A., Bloom, J.H., Capone, B., Ludington, C., and Taylor, R.W., "Silicon Schottky-Barrier Monolithic IRTV Focal Planes," *Advances in Electronic and Electron Physics*," Vol. 40B, No. 981 (1975).
11. Shepherd, F.D., Taylor, R.W., Skolnik, L.H., Capone, R.R., Roosild, S.A., Kosonocky, W.F., and Kohn, E.S., "Schottky IR-CCD Thermal Imaging," *Advances in Electronics and Electron Physics*, Vol. 52, 7th Symposium on Photo-Electronic Image Devices, Vol. 495 (1979).
12. Kosonocky, W.F., Erhardt, H., Meray, G., Shallcross, F., Elabd, H., Cantella, M., Klein, J., Skolnik, L., Capone, B., Taylor, R., Ewing, W., Shepherd, F., and Roosild, S., "Advances in Platinum Silicide Schottky-Barrier IR-CCD Image Sensors," *SPIE Vol. 225 - IR Image Sensor Technology*, No. 69 (1980).
13. Capone, B., Skolnik, L., Taylor, R., Ewing, W., Cantella, M., Klein, J., and Kosonocky, W.F., "A TV Compatible Schottky Barrier Monolithic IRCCD Focal Plane," SPIE Meeting, Los Angeles, Calif., 197, 134 (August 1979).
14. Taylor, R., Skolnik, L., Capone, B., Ewing, W., Shepherd, F., Roosild, S., Cochrun, B., Cantella, M., Klein J., and Kosonocky, W.F., "Improved Platinum Silicide IR-CCD Focal Plane," SPIE's Technical Symposium, *Advances in Focal Plane Technology*, Los Angeles, Calif., Vol. 217, No. 103 (February 4-5, 1980).
15. Kosonocky, W.F., Elabd, H., Erhardt, H., Shallcross, F., Villani, T., Meray, G., Cantella, M., Klein, J., and Roberts, N., "64- × 128-Element High Performance Pt Si IR-CCD Imager Sensor," 1981 IEEE International Electron Devices Meeting, (December 1981).
16. Martin, F.F., "An Anti-tank Seeker Employing an Infrared Schottky Barrier Focal Plane Array," SPIE Meeting, Los Angeles, Calif. (August 1981).

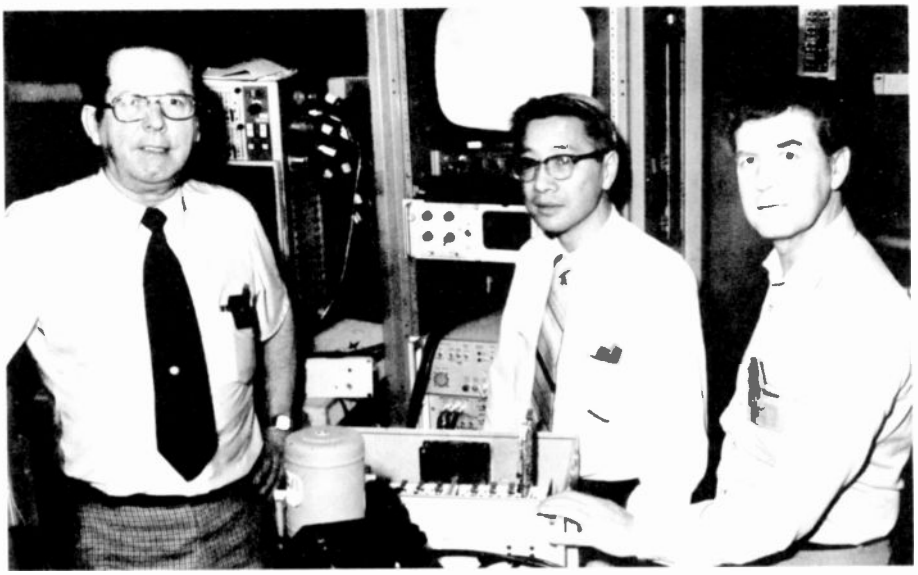

**Authors (left to right) Klein, Chin, and Roberts.**

**Jack Klein** is a Manager Design Engineering and is a member of the Radiation Systems Engineering section at RCA Automated Systems. Since joining RCA in 1956, his assignments have included the design of multi-sensor scan-converter displays, surveillance television systems, high-efficiency switching power supplies for the Lunar Module, and a 10,000-TV-line airborne camera system for the U.S. Air Force.

During the past two years, Mr. Klein has been given the responsibility of designing an IR-camera system which uses an IR-CCD focal plane array imager with over 8,000 platinum silicide Schottky-barrier detectors.

Contact him at:
**Automated Systems**
**Burlington, Mass.**
**TACNET: 326-3697**

**Gep Chin** is a member of the Radiation Systems Engineering section at RCA Automated Systems. From 1955 to 1964 he worked at RCA Missile and Surface Radar, Moorestown, New Jersey, where he was a digital and analog circuits designer on the land-based Talos project, the AN/FPS-16 and AN/FPQ-6 radar programs and BMEWS. Transferred to RCA Burlington in 1965, he has been involved in the Lunar Module Rendezvous Radar program, the AN/ALQ-127 Tail Warning Radar, the Electronic Solid State Wide Angle Camera System (ESSWACS), REMBASS and various IR&D projects. Since 1975, he has had hardware design responsibility on three microprocessor-based systems.

Contact him at:
**Automated Systems**
**Burlington, Mass.**
**TACNET: 326-2044**

**Norman Roberts,** Senior Project Member, Technical Staff at Automated Systems, received his BSEE degree from the Milwaukee School of Engineering in 1965 and has been with RCA since January of 1966 as a design and development engineer. Since 1967, he has designed electronic circuits design for electro-optical equipment, particularly laser rangefinders.

Contact him at:
**Automated Systems**
**Burlington, Mass.**
**TACNET: 326-2401**

M.J. Cantella

# Design and performance prediction of infrared sensor systems

*The sky's the limit for applications of these temperature-sensitive imagers.*

**Abstract:** *Effective modeling for infrared (IR) systems requires an orderly integration of diverse technologies and languages associated with radiation physics, solid-state sensors and circuits, optics, pointing-and-tracking mechanisms, signal processors, display hardware, and human factors. This paper describes the procedures, computer models and software, and the signal- and data-processing facilities used successfully for performance assessment, design iteration, and performance prediction. Examples of IR Schottky-barrier-array sensor systems demonstrate that current and future hardware offers high potential for military, industrial (monitoring and automation), medical, and energy applications.*

Electro-optical hardware is playing an increasingly important role in Government and commercial systems. The key to the performance of these systems is the availability of sensors of high resolution and high data rate covering a wide spectral region. In tactical and strategic military applications, these systems can be used to detect, locate, identify, track, and destroy targets with unprecedented speed and accuracy. The sensors can operate passively or in conjunction with laser illuminators to provide not only high performance, but high resistance to countermeasures. Commercial areas of application span surveillance, inspection, diagnostics, automation, and all types of data handling including entry, processing, and retrieval. Compared to other technologies, electro-optics offers high operational capability in small, lightweight, low-cost packages.


Final manuscript received March 30, 1982.
Reprint RE-27-3-9

## System design methodology

The design of electro-optical systems requires an orderly integration of diverse technologies. These include device physics, optics, circuit design, signal and data processing, gimbal and servo design, structural and thermal technology, target- and background-radiation phenomenology, atmospheric physics, and operational scenario strategies.

A typical flow diagram of military-sensor system design parameters is presented in Fig. 1. The hardware design elements, shown in the central block, include the opto-mechanical assembly, sensor configuration, signal- and data-processing function, and weapon characteristics. Constraints on the hardware design are shown on the left and include operational re-

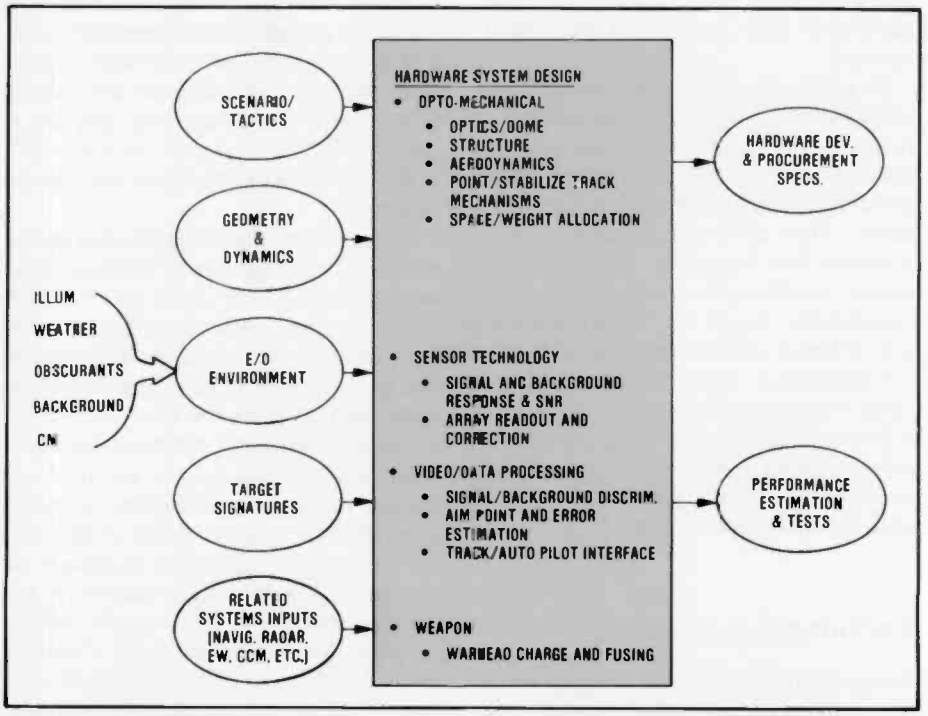


**Fig. 1. Methodology for military sensor system design-and-performance assessment.** Cost-effective electro-optical sensors can be designed to meet complex military requirements.

quirements, the military environment, and related hardware-system characteristics. Shown on the right are the principal outputs of the hardware-system design process: development/procurement specifications and performance estimates. The complexity of most systems usually requires an iterative procedure to produce an optimum system configuration.

Recently, the development of solid- state infrared (IR) focal plane arrays (FPAs) has been pursued intensively by several laboratories within the IR community.[1] These devices are expected to permit sensors to be designed for unprecedented performance at a fraction of the size and cost of currently available mechanical-scanning sensors.[2] RCA Laboratories has been especially successful in the development of Schottky-barrier FPAs that operate in the 1- to 5-$\mu$m spectral region and that have sufficiently high uniformity to yield high sensitivity without elaborate signal processing. Their monolithic silicon construction makes obvious the future potential for high resolution, high yield, and low cost. Because of the importance of this new RCA-developed technology, it has been chosen as a theme for exemplifying the sensor-system-design process described in this paper. A description of the Schottky-barrier FPAs is presented in the companion paper by W.F. Kosonocky, *et al.*, RCA Laboratories, and a description of associated sensor and signal conversion hardware is presented in the companion paper by J. Klein, *et al.*, RCA Automated Systems.

To permit quantitative trade-off of FPA and hardware design-and-performance parameters, a comprehensive model was developed.[3] This model has been extremely useful for the establishment of Schottky-barrier FPA- and hardware-development priorities that harmonize with emerging military requirements. It has also yielded considerable insight into future application potential of this technology in medical diagnostics, energy conservation, security systems, and industrial controls and robotics. A brief description of this model follows, along with facilities for its use and examples of system-performance predictions and demonstrations.

## Performance model

Electro-optical image-forming systems have wide application. Vacuum-tube and solid-state sensors are available and under development to cover spectral radiation from the ultraviolet to the far infrared. Sensor outputs can either be displayed for direct interpretation by a human observer, or they can be processed for automatic and semiautomatic functions such as detection, moving-target indication, tracking, and pattern recognition. Most of these systems are complex, and systematic and accurate analytic methods are needed for their design and for computation of performance. The technical community has developed a wide variety of standards that involve various test patterns and threshold performance criteria. These standards require interpretation on a common analytic base, especially when various spectral regions are employed simultaneously to achieve a satisfactory system performance.

A common standard, resolving power, is the highest periodic-bar spatial frequency ($f$) at which the bars are discernible. Technologists working in the visible spectral range have generally adopted a three-bar chart as a standard. The infrared community generally uses four bars, and they have extended their standards to include Minimum Resolvable Temperature (MRT), which is a plot of differential temperature versus spatial frequency. A related standard is Minimum Resolvable Contrast (MRC), which is a plot of required contrast versus spatial frequency for a family of exposures. This standard is mostly applicable to reflected-illumination, low-contrast imagery. Periodic-bar-pattern standards include various threshold (S/N) imaging criteria based on visibility statistics, operator viewing-distance and fatigue, and so on. These standards provide a particularly good measure of a system's ability to reproduce changes in small image details.

Aperiodic bar patterns provide a useful measure of reproduction of isolated image details. These details can be well resolved by the imaging system or can be too small to be resolved. Standards for detection of this type of pattern have application to image and point-source detection, adaptive-gate tracking, and pattern recognition.

One standard, evolved by the IR community, is Minimum Detectable Temperature (MDT), which is a plot of differential temperature versus the reciprocal of the size of a square input pattern. A related standard, used in the visible spectral range, is Minimum Detectable Contrast (MDC), which is a plot of threshold contrast versus the reciprocal of the size of a square input pattern, for a family of exposures.

The recent progress in development of IR FPAs and the great multiplicity of IR-imaging applications have presented a challenge for bridging the gap between FPA and system performance. The key to the attainment of this objective is the proper modeling and measurement of various FPA noise components.

In many infrared applications, earth background produces such low contrast that to achieve satisfactory performance, system responsivity uniformity must be extremely good.[4,5] As a result, most equipments developed in the past employ a combination of mechanical scanning and a small number of cells to allow practical compensation of cell-to-cell differences. Some excellent performance models have been generated for these systems.[6] However, for staring, solid-state FPAs, there has been a need to extend previous performance modeling and measurement techniques to include fixed-pattern noise.

Especially in high-contrast imaging situations, additive noise (video preamplifier, dark current, and so on) often dominates system performance. This type of noise can have a wide range of amplitude and spatial characteristics that require proper description for sensor-system performance computation.

The model depicted in Fig. 2 was developed for computation of imaging-system signal-to-noise ratios for aperiodic and periodic rectangular input patterns of arbitrary shape, size, and orientation. Expressions are formulated in terms of electron-density exposure so that they can be applied to any spectral region through straightforward radiometric calibration. This model includes exposure level and contrast; aperture response functions; quantum, fixed-pattern and peaked-amplifier noise components; and visual and automatic system threshold criteria. Maximum use is made of space-domain, noise-equivalent aperture functions to permit efficiency of computation and direct assessment of the effect of alternative linear and nonlinear hardware design-and-performance parameters. A smooth and accurate transition between resolved and unresolved image-forming situations permits application of the model to a broad range of system problems, including variable range and/or variable magnification. This model differs from most in its ability to quantify the effects of fixed-pattern noise, so it is especially useful for assessment of IR FPA systems.

The central computational block in Fig. 2 (solid lines) contains the image-pattern

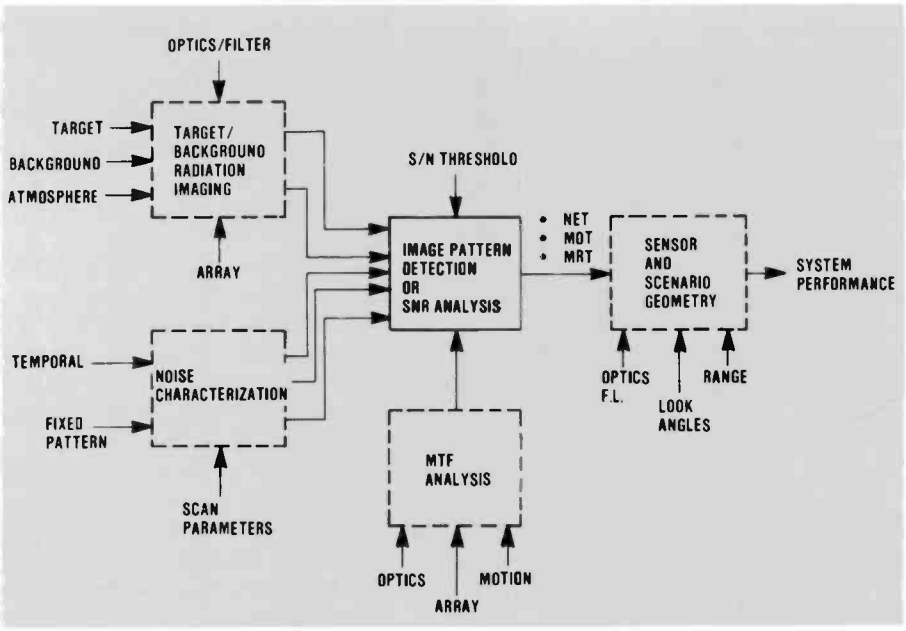


**Fig. 2. System performance model.** Image pattern signal-to-noise ratio is the key to effective system-performance modeling.

SNR models. These models provide a space-domain measure of SNR that can be interpreted directly in terms of the input geometric pattern of interest and of the output processing criteria. Computation of SNR is pivotal to the achievement of accurate results from the model. The basic approach, introduced and used successfully by Schade,[7, 8] uses the geometry of the pattern and an assumption of white-noise electron density to form a S/N quotient. Each noise component is then corrected by a factor that accounts for non-white characteristics caused by such phenomena as MTF filtering and amplifier peaking. These correction factors contain space-domain spread factors that are summed appropriately. Working in the space-domain as much as possible preserves visibility of the effect on overall SNR performance of the various parameters. The image-pattern S/N theory, which is the basis for this model, is described in the literature.[3]

As shown in the last block, performance quantities obtained from the central block and referred to the image plane can be translated to system performance by straightforward scaling using optics focal length and scenario geometry. The noise-characterization block provides quantum, additive and multiplicative components obtained from hardware design-and-performance quantities. The MTF-analysis block represents standard static- and dynamic-response functions cascaded to provide overall system MTF and noise-equivalent bandwidth. The exposure-computation block uses input radiation, spectral responsivity, and integration time to provide image contrast and signal.

A high degree of validation of this model has been achieved with TV and IR FPA sensors. Accurate prediction of system performance has been accomplished with a consistent methodology even for complex situations that contain both thermal emission and reflected components of radiation from object and background. Therefore, the model can be used to analyze alternative hardware designs and to predict performance of systems used for detection, autonomous acquisition, and tracking. Examples of its use are presented later in this paper under the "IR Schottky-barrier array systems" heading.

## Data processing and recording facility

The capability of modern data-acquisition and computing equipment has provided unprecedented speed and accuracy for prediction of performance and for synthesis of IR systems. A comprehensive computer-analysis-and-simulation capability has been under development at RCA Automated Systems. The overall concept for this facility is presented in Fig. 3, and the capabilities embodied are listed in Table I.

The system has high utility for both hardware and software designers and can be applied to contract and to new business activities. The modular structure and universal language permit interchange of theory, hardware performance measurements, and actual hardware to provide realistic simulation of system performance. Application to IR Schottky-barrier sensor systems has produced accurate performance assessment and design iteration.

Input data can be obtained from either live camera video or video previously re-

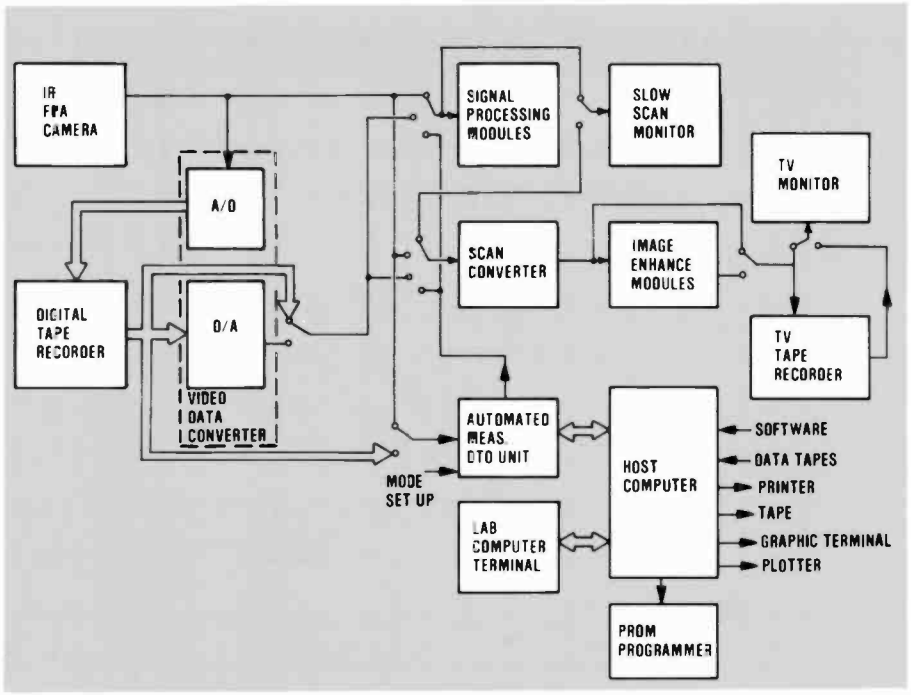


**Fig. 3. Sensor data-processing and recording capability.** Analog and digital equipments have been integrated into a sensor data-processing and recording facility.

**Table I. Analysis and simulation capability.**

*RCA-generated programs*

- System-performance analysis
- Missile-trajectory simulation
- Automated focal-plane-array testing
  - Array characterization
  - Defect data generation and PROM-compensation data transfer

*Government-furnished programs and databases*

- System-performance models
- Atmospheric-transmission and path-radiance model
- Target and background signature data

*Hardware data manipulation*

- Field-data assessment and recording
- Camera/display optimization
- Processor/tracker algorithm evaluation

corded digitally on tape. This video is at slower line rates than standard TV and can be displayed on a slow-scan monitor directly, or after video processing. In addition, it can be converted to standard TV format for display or recording on TV tape. The slow-scan IR data can also be transferred to a digital computer via a microprocessor. This microprocessor has been tailored for use in this system primarily for automation of IR FPA performance measurements and for generation of defect-correction PROMS. It also can transfer and display image data sent to and received from the host computer.

The host computer could be of any type, either dedicated or time-shared; but application of the system with actual imagery and/or with RCA and Government-furnished performance and simulation models demands the speed and storage capacity of a large, dedicated computer. To permit rapid iteration of the system design, interactive programs and a graphic display and plotter are used. Performance records are stored on magnetic tape.

## IR Schottky-barrier array systems

### *Attributes of array technology*

Schottky-barrier IR charge-coupled devices (CCDs) have been under development at RCA Laboratories partly under Air Force sponsorship since 1972. These devices cover the 1- to 5-$\mu$m spectral region and are of monolithic silicon construction. Fabrication procedures have permitted reduction of cell-to-cell nonuniformities to below 0.5% rms, providing the potential for high-sensitivity earth background (300 K) imaging without need for complex signal processing. The silicon construction allows low-cost production and the fabrication of large high-density arrays using relatively standard integrated circuit processing technology.[10-15]

A perspective on the requirement for array uniformity for IR imaging in a 300-K background can be obtained from Fig. 4. This figure shows the % rms nonuniformity permitted versus the noise equivalent $\Delta T$ desired for the sensor system. The characteristics were derived from blackbody functions for the 3- to 5-$\mu$m and 8- to 14-$\mu$m spectral bands. Note that the requirement is somewhat more stringent for the 8- to 14-$\mu$m band, and that to achieve good performance in either band, nonuniformity must be less than one percent. As indicated on the figure, currently fabricated Schottky-barrier arrays with inherent nonuniformity in the 0.1% to 0.5% rms range make it possible to attain excellent ($\approx$0.1°C) thermal sensitivity without the use of video processing for uniformity correction. This can permit concentration of processor design on the important problems of image interpretation and tracking-signal generation. An example of imagery obtained with a 64 × 128-element Schottky-barrier array is presented in Fig. 5. Note the thermal detail in the human face and clothing and the very large signals produced by the cold drink and hot pipe. Even much hotter objects can be imaged without bloom because of the inherent self-limiting properties of Schottky-barrier photodetection.

Superimposed on Fig. 4 is the approximate range of nonuniformities reported for competing array technologies. A substantial amount of processing tailored to an individual array is necessary to achieve adequate performance with alternative approaches.

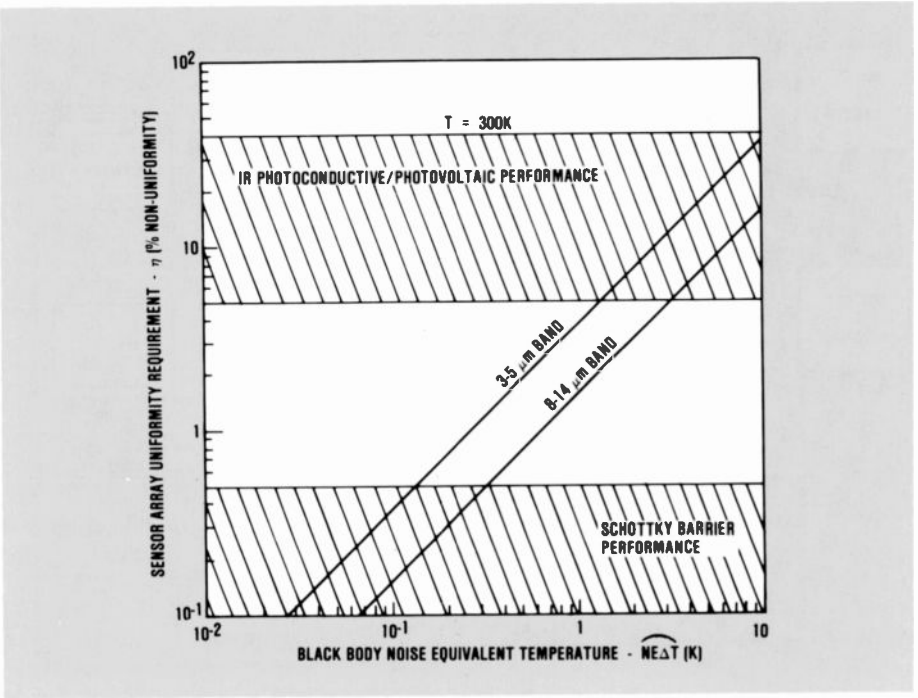


**Fig. 4. IR sensor array uniformity.** The excellent uniformity of Schottky-barrier arrays provides high thermal sensitivity without the need for complex signal processing.

### *Application thrusts*

The outstanding characteristics of Schottky-barrier FPAs provide the potential for many new applications. Presented in Fig. 6 are the anticipated thrusts for these applications as driven by the special properties of the hardware and the imaging phenomenology.

The monolithic silicon construction of Schottky-barrier FPAs is the most fundamental attribute. The close similarity to integrated circuits provides the basis for low-cost, high-volume production of arrays of high resolution and high uniformity. This can make economically feasible the manufacture of military weapons; security systems; and inspection, monitoring, and diagnostic systems for industry and medicine.

Operation of these arrays in the staring mode eliminates the need for mechanical scanning and permits observation of transient phenomena. This staring mode can be used not only for acquisition of imagery but for radiometry and heat-seeking applications. Compared to previous nonimaging instrumentation, which use chopping reticules, these imaging radiometers can provide unprecedented levels of sensitivity and background discrimination because of the inherently high spatial discrimination.

For some important applications, it is desirable to supplement a narrow-angle, high-frame-rate, staring mode of operation with a very-wide-angle, low-frame-rate mode. This dual mode can be implemented conveniently by addition of slow-speed mechanical scanning while operating the two-dimensional array in a Time-Delay-Integration (TDI) mode. In TDI, information stored in the array is shifted (clocked) continuously, one line at a time, in the direction of scanning to provide continuous, high-sensitivity acquisition of imagery. Transition to the frame mode is accomplished when desired simply by clocking the information at the frame rate. This dual mode of operation is applicable to many search-and-identification scenarios associated with weaponry, defense systems, search-and-rescue operations, and inspection and monitoring systems.

The realization of future applications of Schottky-barrier arrays is dependent on appropriate utilization of phenomenology associated with the 1- to 5-$\mu$m spectral region. For high-performance thermal imaging, the 8- to 12-$\mu$m band has been used almost exclusively in the past. The fundamental reason for this stems from the fact that for earth-background (300 K) imaging, thermal contrast is very low (less than 1 percent for 0.1°C differential temperature). This low thermal contrast demands detector uniformity that is so good that the preferred sensor implementation has been the use of one or a limited number of detectors, scanned mechanically. Scanned detectors can intercept only a small fraction (typically $10^{-4}$) of the photons collected by the optics, so operation in the 8- to 12-$\mu$m is preferred since photon flux is approximately 100-times higher. The achievement of practical staring-mode operation, made possible by the high uniformity of Schottky-barrier arrays, has recently produced demonstrated high thermal sensitivity in the 3- to 5-$\mu$m band.

This new thermal-imaging capability will permit exploitation of several phenomena in the 1- to 5-$\mu$m band. For images that are reasonably warm ($\Delta T > 10°C$), black-body theory predicts that thermal contrast and signal-to-clutter ratios are higher in the 3- to 5-$\mu$m band than in the 8- to 12-$\mu$m band. This provides enhanced capability for military systems for autonomous target acquisition. For long-range detection and acquisition requirements, this enhanced thermal contrast combined with the higher optics resolution inherent to the 3- to 5-$\mu$m band will permit significant improvement in the capability of threat-warning and weapon-seeker sys-

**Fig. 5. High quality IR imagery obtained from a 64- by 128-Schottky-barrier FPA.** IR imagery of high sensitivity and wide dynamic range has been obtained from 64 × 128 Schottky-barrier FPAs.

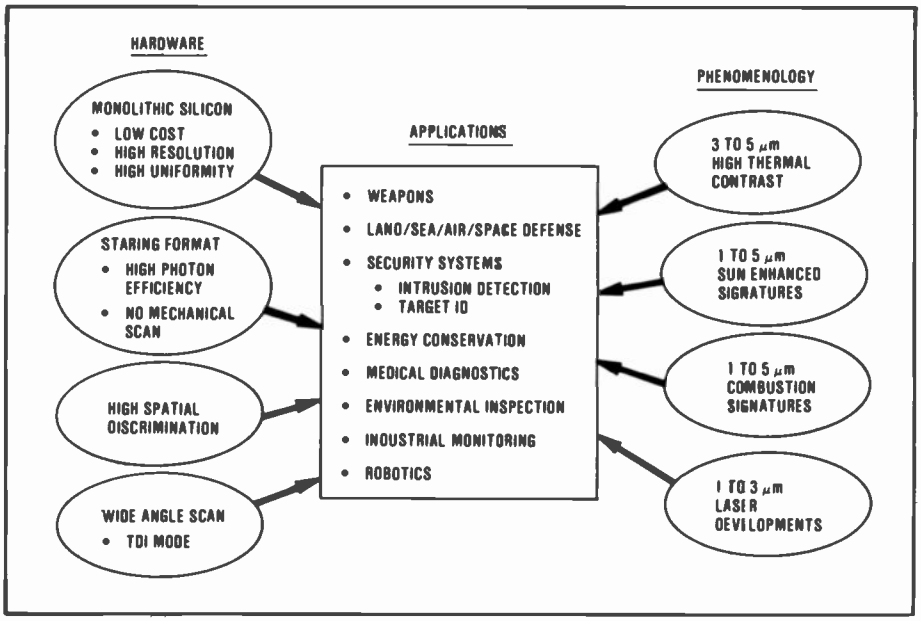


**Fig. 6. Schottky-barrier array application thrusts.** In future applications, the attributes of Schottky-barrier FPA technology can exploit a multiplicity of radiation phenomena.

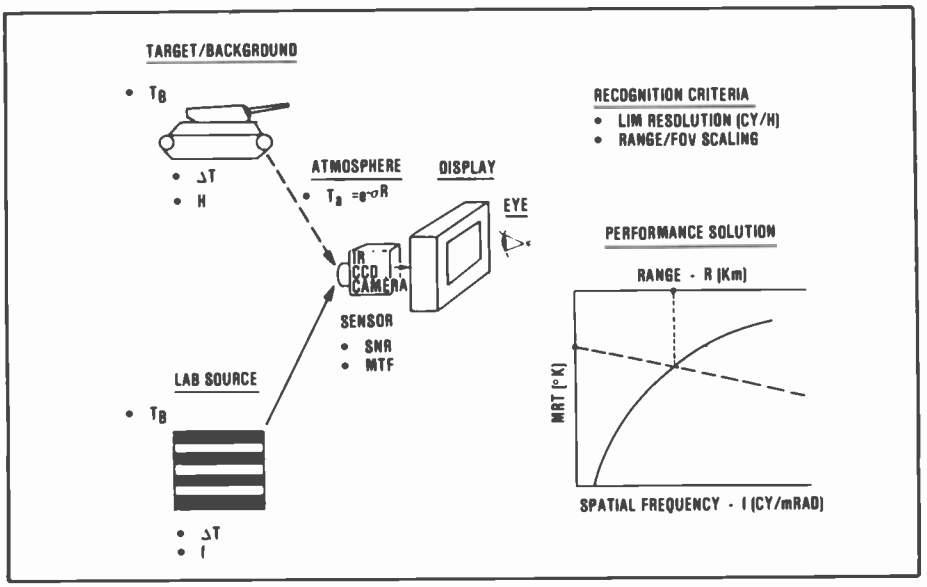


**Fig. 7. Methodology for recognition-range-performance prediction.** The basis for prediction of recognition range is visual performance data established for targets and sensor test charts.

tems. An example of use in industrial automated machining operations is the automatic detection of overheated drills or tool bits.

Although thermal imaging systems can yield impressive levels of performance under most day and night conditions, there are certain periods in which thermal washout (very low contrast) can occur. This happens mostly during daylight hours due to the relative heating and cooling, between object and background, which occurs as part of the normal diurnal cycle. Recent field tests have shown that it is possible to improve viewing conditions substantially during this period by a shift in spectral filtering toward shorter wavelengths to admit sunlight. These and related techniques are expected to greatly extend the capability of future staring-FPA systems, which use the basic 3- to 5-$\mu$m band for thermal imaging.

Another form of image enhancement results from the presence of strong emissions in the 1- to 5-$\mu$m band from combustion products. This greatly enhances the visibility of operating vehicles in military engagements and makes practical the autonomous acquisition of targets. It also can provide the basis for air-pollution monitoring and control.

Lasers that operate in the 1- to 3-$\mu$m band are currently under development for military target surveillance, acquisition, and weapon control. Many of these systems could be enhanced by a staring-type imaging capability. A Schottky-barrier array is ideally suited for this function, and a number of dual-mode (thermal plus laser) systems are expected to emerge in the future.

The schedule for evolution of the applications cited in Fig. 6 will be determined largely by the total resolution of available arrays. This development has progressed rapidly. Within approximately two years, 25 × 50, 32 × 64, and 64 × 128 element arrays have been operated successfully, and these are ideally suited for inexpensive weapon applications.

A 160 × 244 array is currently under development, and that will provide approximately one-half standard-TV-quality images within the next two years. This resolution level will be adequate for many viewing and monitoring systems. Development of full TV resolution is expected to require an additional two years, and this capability will permit replacement of many currently deployed 8- to 12-$\mu$m viewing systems.

## *Tank recognition performance*

An important application of the performance model pertains to the recognition of military ground targets. The overall methodology is presented in Fig 7 for a tank target. IR-imaging hardware performance is expressed in terms of Minimum Resolvable Temperature (MRT), and this performance is matched geometrically to empirically derived tank-recognition sta-

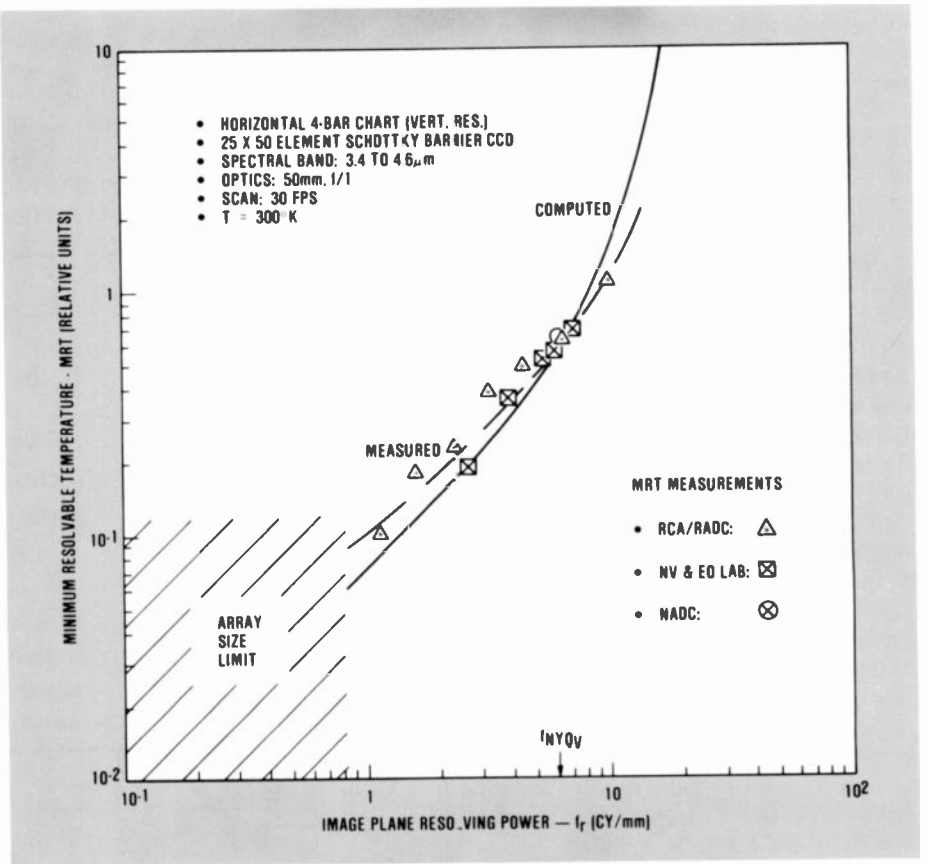


**Fig. 8. Minimum Resolvable Temperature characteristics.** Minimum Resolvable Temperature computation has been validated experimentally.

tistics measured in cycles/height. The difference temperature (target temperature relative to background) of the tank along with its size represent the IR signature.

A graphical method for determination of range performance is also illustrated in Fig. 7. The MRT scale is logarithmic, and the spatial frequency and range scales are linear. Range is scaled to frequency via the tank-recognition criterion expressed as a dimensional spatial frequency. At zero range, target difference temperature is equated to MRT, and this difference is attenuated by the atmosphere (linearly on semi-log paper for exponential attenuation). The intersection of the attenuated temperature signature with the MRT characteristic yields the desired range performance.

The solution for range can be obtained alternatively with a computer, usually using iterative procedures. More exactly, nonexponential atmospheric attenuation functions may be included to represent not only homogeneous atmosphere, but a variety of natural and man-made obscurants. Using the general method previously outlined and a periodic-bar SNR computation, MRT for a FPA can be computed.

This MRT model has been validated repeatedly with experimental measurements. One such example (expressed in unclassified relative units) is presented in Fig. 8 for a Schottky-barrier IR focal plane array. The camera parameters used in the model are listed in Fig. 8. This MRT model has been included in a digital computer for recognition-range-performance computation. A graphically illustrated example for a Schottky-barrier FPA seeker is presented in Fig. 9.

An outgrowth of this design methodology has been the successful hardware design, fabrication, and field-test of an anti-tank missile seeker.[16] This seeker was designed for an advanced single-man-portable missile, and its compact construction includes refractive optics, a two-axis gyrostabilized gimbal, a 64 × 128-element Schottky-barrier array, and cryostat-cooled dewar assembly. This package has demonstrated the potential for an important new FPA application.

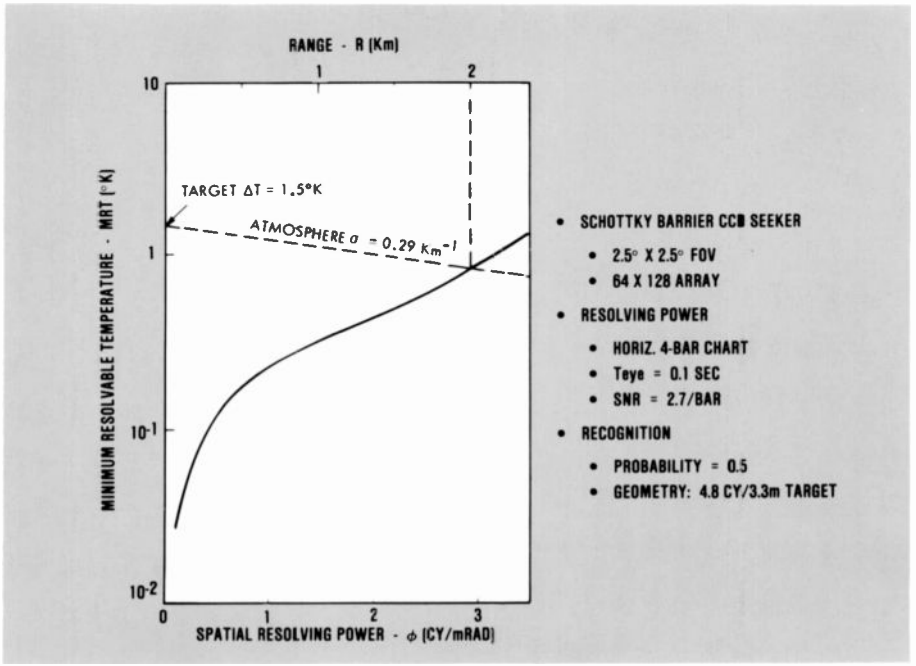


**Fig. 9. Target-recognition range.** A graphical solution for recognition range can be derived from characteristics of the target, atmosphere, and sensor.

## *Aircraft detection range*

The range for detection of aircraft can be obtained by modeling it as an aperiodic bar and by using the general methodology described in the performance model. Using a suitable SNR-threshold criterion, a solution for range performance can be obtained in much the same way as presented for recognition-range solutions. However, recent experience in the use of IR FPAs for detection of aircraft has shown that this methodology must be extended for the following main reasons:

- Thermal signatures due to skin heating and engine exhaust can be large enough to violate differential temperature approximations;
- Contributions of solar irradiance to both target and background radiance can be significant and must be included;
- An aircraft can provide a significant specular component of radiation;
- Background clutter represents an important noise source and must be combined appropriately with FPA noise.

An appropriate methodology for computation of aircraft range performance is presented in Fig. 10. Difference radiance

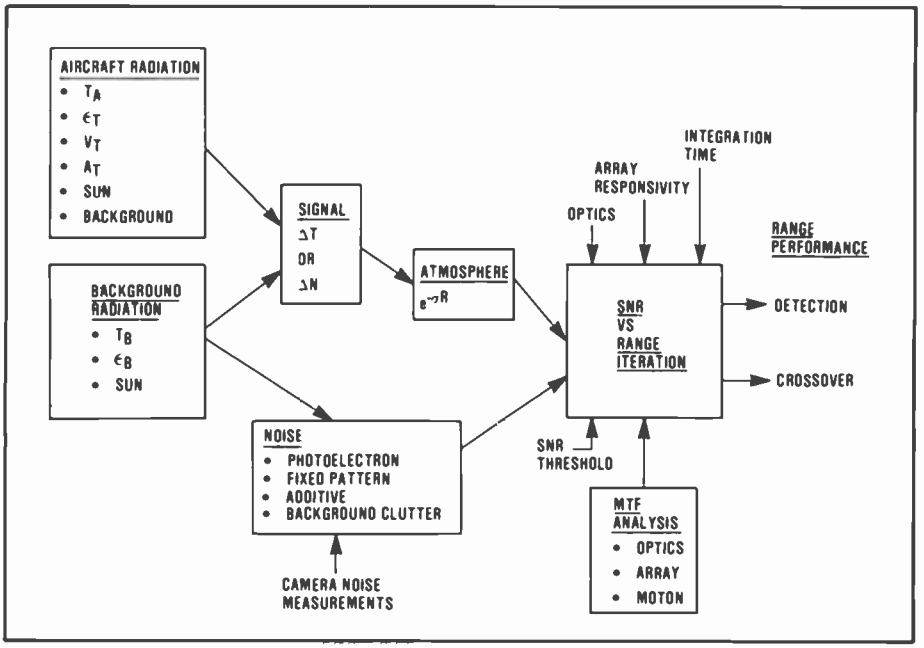


**Fig. 10 Aircraft range-performance methodology.** Prediction of aircraft detection range is highly dependent on complex radiation signatures of the aircraft and the background.

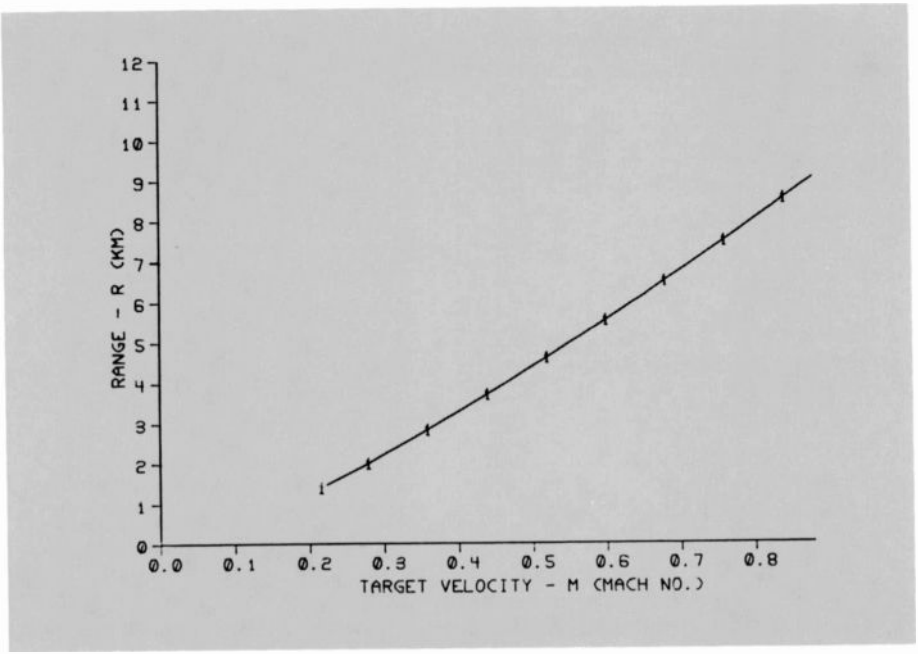


**Fig. 11. Computer-generated aircraft-detection range performance.** Aircraft detection range characteristics can be computed accurately and plotted automatically.

between target and background is attenuated by the atmosphere to obtain signal exposure. Noise contributions obtained from FPA and background measurements are summed appropriately to obtain SNR for the system-hardware parameters shown. An SNR threshold is chosen to satisfy detection-probability and false-alarm-rate requirements, and a solution for range is obtained by iteration.

Computation of exposure for the aircraft is accomplished by adding solar, thermal, and specular components. The solar component is obtained from the solar irradiance and the Lambertian component of reflectivity. The thermal component is obtained from the emissivity and air-friction-induced heating.

The specular component of exposure is obtained by use of the specular reflectance component and the background behind the aircraft (terrain, sky, and so on).

The background exposure is obtained in a similar manner, assuming Lambertian behaviour for both solar reflection and thermal radiation. Background clutter is difficult to characterize in a way that permits combining it with FPA noise components. This has been accomplished by introducing factors derived empirically from threshold-exceedance characteristics of the background and from the characteristics of signal-processing hardware.

A typical range-versus-velocity characteristic generated by a computer is presented in Fig. 11. This type of characteristic has been validated with field tests. Adjustment of the parameters of the analysis can permit studies of various sensor hardware-design parameters and of changes in such environmental characteristics as ambient illumination, air temperature, and aircraft altitude. The methodology has been extended to the assessment of adaptive, tracking-gate algorithms used after autonomous acquisition is accomplished.

## Summary

The design and performance characterization of electro-optical sensor systems has been enhanced by the development and use at RCA Automated Systems of a comprehensive performance model. The modular structure of the model and the use of universal language and units has permitted its successful employment in the development of hardware components and systems that cover a wide spectral region. The parallel development of a computer-based analysis, simulation, and automated measurement capability has facilitated and enhanced its use.

Of special significance has been the use of the modeling techniques in the development of IR sensor systems associated with the Schottky-barrier FPAs developed by RCA Laboratories. It has been possible to interpret military system requirements expressed in conventional units and translate them into array and hardware development requirements and priorities within the constraints imposed by the phenomenology of the environment and the physics of the sensor. These modeling techniques have been validated through extensive field testing with both resolved and unresolved radiation sources.

Theoretically and experimentally demonstrated characteristics of Schottky-barrier FPAs indicate great potential for Government and commercial applications. Development thrusts are likely to start with moderate-resolution weapon seekers because of compact size and low-cost production requirements. Development of arrays of TV quality is progressing rapidly, and this is expected to foster additional applications of surveillance, medical diagnostics, industrial automation, and energy conservation.

## Acknowledgments

Many people within RCA have been contributing to the development and use of the modeling, simulation, design, and automated testing techniques described in this paper. Team participation has involved engineers and management principally at RCA Automated Systems and RCA Laboratories. Their dedication to technical excellence in high-quality imaging systems has provided the inspiration and technical guidance needed for this work.

## References

1. Steckl, A.J. "Infrared Charge Coupled Devices," *Infrared Physics*, Vol. 16, No. 65 (1976).
2. Tegnelia, J.A., "DARPA Unveils Staring Focal Plane Array," *Defense Electronics*, Vol. 12, No. 101 (1980).
3. Cantella, M.J., "IR Focal Plane Array System Performance Modeling," *Proc. SPIE Technical Sysnposium*, Los Angeles, Calif. (Jan. 1982).
4. Hudson, R.D., Jr., *Infrared System Engineering*, Wiley Interscience (1969).
5. Wolfe, W.L., *The Infrared Handbook*, Office of Naval Research, Washington, D.C. (1978).
6. Ratches, J.A., "Static Performance Model for Thermal Imaging Systems," *Optical Engineering*, Vol. 15, No. 6, pp. 525-530 (November/December 1976).
7. Schade, O. H., Sr., "An Evaluation of Photographic Image Quality and Resolving Power," *Jour. SMPTE*, Vol. 73, No. 2, pp. 81-119 (February 1964).
8. Schade, O. H., Sr., *Image Quality—A Comparison of Photographic and Television Systems*, RCA Laboratories, (1975).
9. Cantella, M., Honickman, H., and Kim, K., "IR Focal Plane Array Noise Characterization and Measurement," *Proc. IRIS Detector Specialty Group Meeting*, (June 1981).
10. Shepherd, F.D., Yang, A.C., Roosild, S.A.,

Bloom, J.H., Capone, B., Ludington, and Taylor, R., "Silicon Schottky Barrier Monolithic IRTV Focal Planes," *Advances in Electronics and Electron Physics*, Vol. 40B, No. 981 (1975).

11. Shepherd, F.D., Taylor, R.W., Skolnik, L.H., Capone, R.R., Roosild, S.A., Kosonocky, W.F., and Kohn, E.S., "Schottky IR-CCD Thermal Imaging," *Advances in Electronics and Electron Physics*, Vol. 52, 7th Symposium on Photo-Electronic Image Devices, 495 (1979).
12. Kosonocky, W.F., Erhardt, H., Meray, G., Shallcross, F., Elabd, H., Cantella, M., Klein, J., Skolnik, L., Capone, B., Taylor, R., Ewing, W., Shepherd, F., and Roosild, S., "Advances in platinum Silicide Schottky-Barrier IR-CCD image sensors," *SPIE Vol. 225—IR Image Sensor Technology*, Vol. 69 (1980).
13. Capone, B., Skolnik, L., Taylor, R., Ewing, W., Cantella, M., Klein, J., and Kosonocky, W.F., "A TV Compatible Schottky-Barrier Monolithic IRCCD Focal Plane," SPIE Meeting, Los Angeles, Calif., 197, 134 (August 1979).
14. Taylor, R., Skolnik, L., Capone, B., Ewing, W., Shepherd, F., Roosild, S., Cochrun, B., Cantella, M., Klein, J., and Kosonocky, W.F., "Improved Platinum Silicide IR-CCD Focal Plane," SPIE's Technical Symposium, Advances in Focal Plane Technolcoy, Los Angeles, Calif., 217, 103 (February 4-5, 1980)
15. Kosonocky, W.F., Elabd, H., Erhardt, H., Shallcross, F., Villani, T., Meray, G., Cantella, M., Klein, J., and Roberts, N., "64- × 128-Element High Performance PtSi IR-CCD Imager Sensor," 1981 IEEE International Electron Devices Meeting (December 1981).
16. Martin, F.F., "An Anti-tank Seeker Employing an Infrared Schottky-Barrier Focal Plane Array" SPIE Meeting, Los Angeles, Calif. (August 1981).

**Michael Cantella** joined RCA, Automated Systems in 1959 and is a Senior Engineering Scientist responsible for electro-optical systems development. He has made major contributions in the development of an optical surveillance system for automatic detection of satellites, low-light-level visual and IR TV systems, the first laser target-designation system, and high-resolution (10,000 TVL) TV systems for reconnaissance and automatic test. Recently he has promoted development and field test of Schottky-barrier FPA technology and systems. Mr. Cantella received his B.E.E. from RPI and SM in E.E. from MIT and is a member of Tau Beta Pi, Eta Kappa Nu, Sigma Xi, and SPIE. Contact him at:
**RCA Automated Systems**
**Burlington, Mass.**
**TACNET: 326-3303**

F.B. Warren | J.R. Tower
D.A. Gandolfo | H. Elabd | T.S. Villani

# Space applications for RCA infrared technology

*A unique detector technology developed by RCA may be crucial to the next generation of spaceborne sensors.*

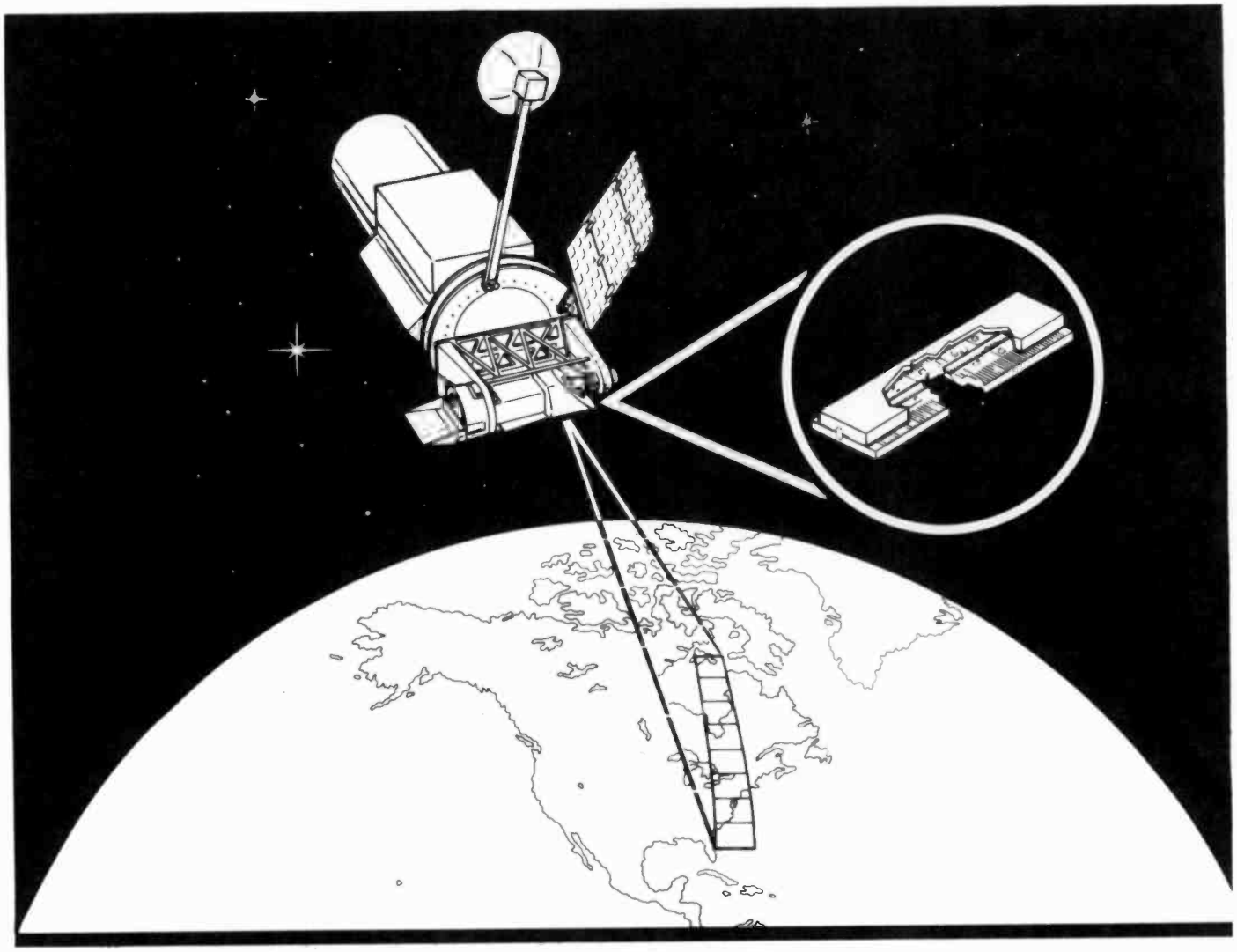

**Fig. 1. "Pushbroom" scanning.** Surveillance and earth resources satellites can make use of very large linear detector arrays (6,000 to 12,000 elements) to gather high-resolution ground data.


Final manuscript received March 1, 1982.
Reprint RE-27-3-10

**Abstract:** *A high-performance shortwave infrared sensor technology based on silicon IC technology has been developed. The maturity of the basic technology and the high yield of blemish-free focal planes make Schottky-barrier IR-CCDs an excellent choice for future spaceborne sensors.*

NASA earth-resources applications such as Landsat require multispectral data in the visible, near-infrared (near-IR), and shortwave-IR (SWIR) spectral regions to assess land usage, crop yields, and mineral deposits. A next-generation project, the Multispectral Linear Array (MLA) program, plans to implement large focal planes of up to 12,000 elements in each of four visible and near-IR bands, and two SWIR bands (1 to 3 $\mu$m). Imagery will be obtained by using a "pushbroom" scan, letting the satellite's motion scan these large line arrays in a 185-km-wide swath on the earth's surface (Fig. 1).

RCA Laboratories has developed a silicon-based detector technology that can in many ways outperform visible and infrared detectors made from more exotic materials. This technology uses the internal photoemission effect from a metal silicide to a silicon diode, and conventional charge-coupled-device (CCD) multiplexing registers to provide a single serial video output. The result is a monolithic integrated-circuit chip, based on mature silicon processing, that can contain thousands of individual detectors. To date, area arrays as large as 64 × 128 elements (>8,000 detectors) and 1 × 256 line arrays have been fabricated and successfully used in military applications. These applications have included an imaging missile seeker (area array)* and a physical security intrusion sensor (line array).**

## Responsivity and cooling

All sensors with useful sensitivity rely on the photoelectric effect, whereby a photon striking the detecting material has a high probability of exciting an electron into a signal circuit. These sensors are called quantum detectors. The most familiar imaging sensors are those used in the visible spectrum, such as the television vidicon. A photon of visible light is sufficiently energetic to displace electrons from relatively stable materials, such as silicon. As photon energy decreases for the longer IR wavelengths, detector materials that release electrons more easily must be used. Unfortunately, these materials are also more susceptible to the release of electrons due to ordinary thermal excitation. These electrons take the form of random noise that competes with the video signal.

Vidicons and silicon CCDs perform well as visible imagers at room temperature. However, it has not been possible to develop a vidicon equivalent for IR wavelengths. Single detectors of many different materials have been used in the conventional IR spectrum (roughly 2 to 12 $\mu$m) with images being formed by mechanically scanning a few small individual detectors over the field of view. Advancing requirements in IR imaging are encouraging the use of large arrays of many elements to reduce or eliminate the need for mechanical scanning. The leading material now used in this attempt is mercury cadmium telluride (HgCdTe) compound. HgCdTe is responsive across the entire IR spectrum with good quantum efficiency (Q.E. equals the number of electrons per photon, and it varies from 0 to 1), and the material is typically cooled to temperatures ranging from 77 Kelvin (K) to 185 K (dependent upon application).

IR quantum detectors have well-defined areas of the spectrum to which they are designed to respond. Intrinsic detector technologies specify definite cut-off wavelengths by tailoring the energy bandgap (HgCdTe varies the ratio of the mixture of HgTe and CdTe to obtain the desired spectral response). Schottky-barrier detectors can be given different cut-off wavelengths by changing the metal used for the metal silicide photodiodes. With platinum, for example, the detector gives a cut-off below 6 $\mu$m; with palladium, it cuts off at 3.5 $\mu$m.

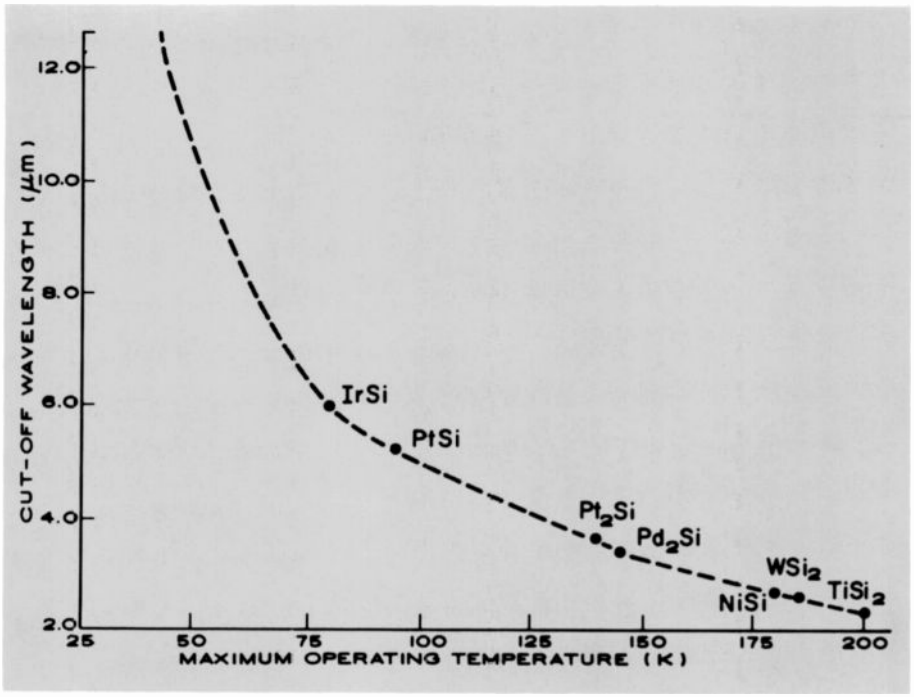


**Fig. 2. A diversity of cut-off wavelengths is possible with Schottky-barrier technology.** Longer cut-off wavelengths require metals with lower electron-work function.

Regardless of the metal, Schottky detectors exhibit increasing sensitivity (quantum efficiency) as wavelengths shorten toward visible light (actually, sensitivity peaks at 1 $\mu$m when the detectors are back-illuminated through the silicon chip, which will not pass shorter wavelengths). Optical bandpass filters are used to constrain the spectral band to less than a range from 1 $\mu$m to the cut-off wavelength, if this is desired. Longer cut-off wavelengths require metals with lower electron-work functions, which release electrons more easily, and they require operation at lower temperatures. Figure 2 shows the cooling required for various cut-off wavelengths with Schottky detectors.

For infrared focal planes, satellite designers prefer to use passive coolers, which cool the detector area by radiating into cold space. Although platinum silicide devices will outperform palladium silicide at any given wavelength up to 6 $\mu$m, the platinum silicide cooling requirement is more stringent. A passive cooler can cool these large focal planes to a temperature between 100 K and 120 K. Because palla-

* Work done at RCA Automated Systems, Burlington, Mass.

** Work done at RCA Advanced Technology Laboratories, Camden, N.J.

**Fig. 3. Uncompensated imagery,** from a recently produced 32 × 64 palladium array at 130 K (reproduced from video tape).

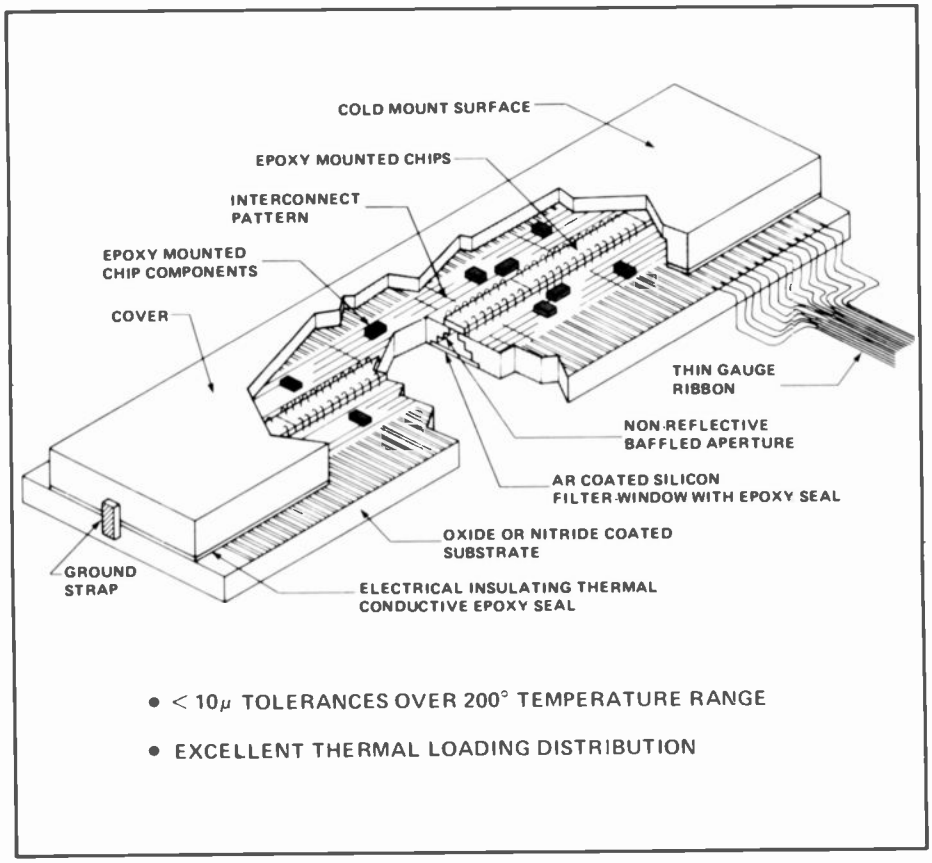


**Fig. 4. The instrument focal plane.** Large dual-band focal planes are made possible by end-to-end abutment of individual detector chips.

dium-based detectors can operate at 120 K or warmer without experiencing excessive thermally generated noise current, and platinum-based detectors cannot, palladium is the material of choice for short-wave-IR satellite applications.

## RCA technology advantages

NASA is currently investigating the competing infrared technology to assess the best choice for the Multispectral Linear Array Instrument and other future land observation satellites. Early this year, RCA Advanced Technology Laboratories and RCA Laboratories submitted a solicited proposal to NASA to build a prototype Schottky-barrier infrared focal plane.

The Schottky-barrier technology offers a number of advantages when compared to the widely accepted HgCdTe technology. Perhaps the greatest advantages of the IR-CCD technology are its high yield of defect-free focal planes and its reproducibility. Defect-free 64 × 128 focal planes have been produced in the mature platinum silicide (PtSi) technology, as well as defect-free 32 × 64 focal planes in the developmental palladium silicide ($Pd_2Si$) technology. Each of these technologies offers high yield along with a photoresponse uniformity on the order of 99.5 percent rms. Figure 3 demonstrates defect-free, uncompensated performance of a 32 × 64 $Pd_2Si$ focal plane. This high yield and excellent uniformity have not been approached by HgCdTe technology.

The IR-CCD is a silicon-based, monolithic technology. This is a distinct advantage when compared to the hybrid construction typically used to produce HgCdTe focal planes. In the HgCdTe technology, a separated CCD multiplexer chip is indium-bump bonded to the HgCdTe detector array. This adds complexity to the manufacturing process and attendant loss in yield.

**Table I. Schottky-barrier technology characteristics.**

| *Characteristics* | *Schottky IR-CCD* |
|---|---|
| Yield (largest defect-free FPA shown) | 8192 detectors |
| Nonuniformity | 0.2 to 0.5% rms |
| Construction | Monolithic |
| Operating temperature | 77 to 140 K ($Pd_2Si$) |
| Quantum Efficiency ($\lambda$ = 1.65 μm, AR Coating) | ≈9% ($Pd_2Si$) |
| Blooming | No blooming and low cross talk |

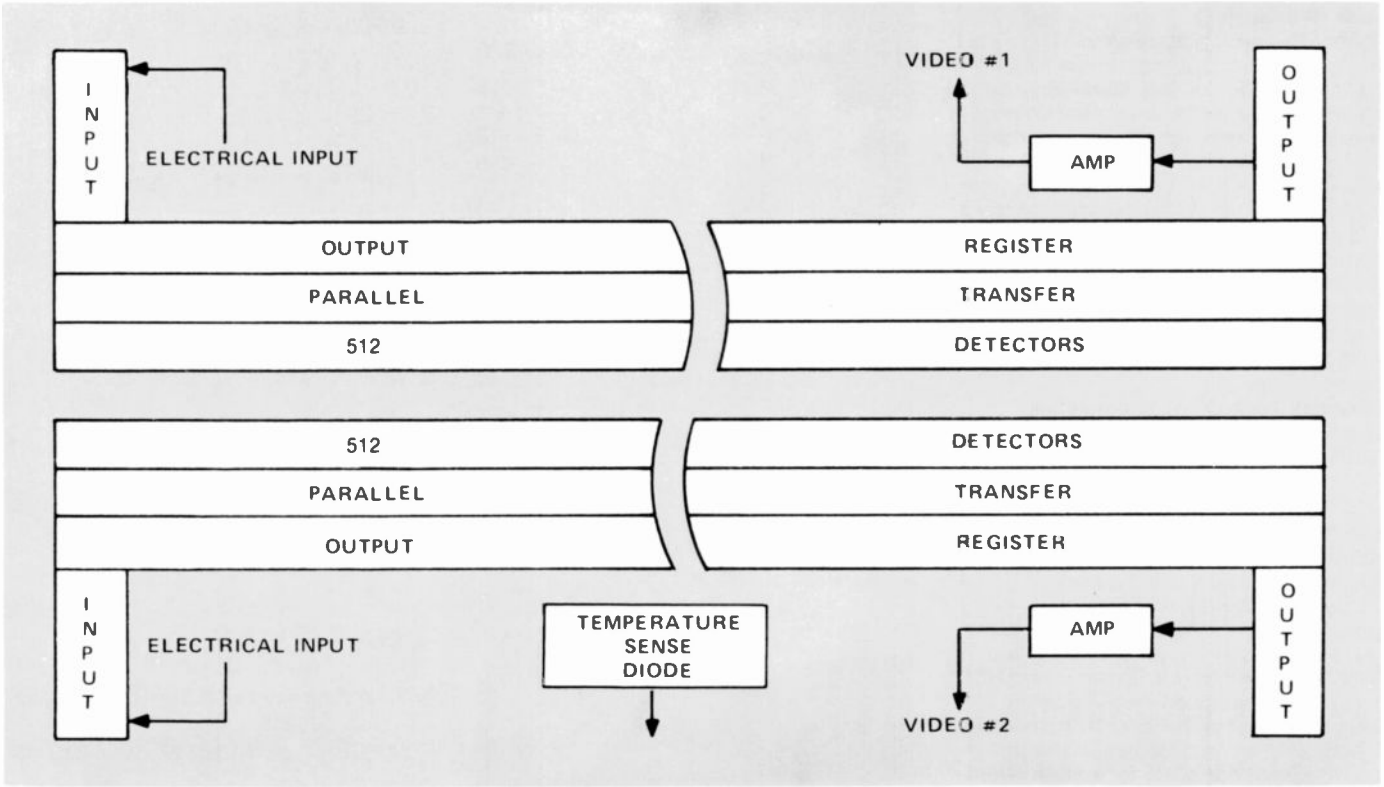


**Fig. 5. Dual-band 2- by 512-detector chip architecture.** The arrangement provides precise band-to-band alignment of multispectral linear array shortwave-infrared (MLA-SWIR) sensors.

A summary of the characteristics of the Schottky-barrier IR-CCD technology is given in Table I. The currently attained quantum efficiency of $Pd_2Si$ detectors is approximately 9 percent at 1.65 $\mu$m (one of the MLA spectral bands). This compares with 75 percent to 95 percent quantum efficiency for HgCdTe. This means that more signal electrons will be produced for a given irradiance by a HgCdTe detector than by a $Pd_2Si$ detector. However, the system performance of an imaging technology does not depend upon quantum efficiency as much as it does on signal-to-noise ratio. It has been shown that the detector noise of the HgCdTe complex-compound technology is significantly greater than that of $Pd_2Si$. Thus, the benefit of the greater sensitivity is partially consumed by the larger noise component inherent in HgCdTe detectors.

Measurements have shown that the $Pd_2Si$ IR-CCD exhibits low noise characteristics and also very good stability. The stability requirement is important because it is hoped that the satellite will not require recalibration more than once every 25 seconds. Indeed, calculations have shown that the $Pd_2Si$ technology will be capable of meeting or exceeding the NASA-specified signal-to-noise ratio for the MLA instrument.

## Focal plane architecture

RCA has developed an MLA focal plane architecture that permits the realization of high-density, high-performance SWIR focal planes with thousands of defect-free detectors. The design for the MLA instrument is based on an appropriately sized chip with a dual-band capability, thus providing precise band-to-band alignment of the two shortwave infrared arrays. The technology yield is high enough to permit two linear arrays of 512 detectors each. These chips will utilize end-to-end abutment to produce larger arrays of contiguous, in-line detectors. For the MLA instrument, twelve of these chips would be placed end-to-end to produce two linear arrays of 6,000 detectors each. A concept view of an instrument focal plane is shown in Fig. 4.

The architecture for the dual-band chip is shown in Fig. 5. Each detector array has its own CCD parallel-to-serial multiplexer and NMOS output amplifier. The device will thus provide two serial output signals with a minimum of clock and control waveforms. The operating mode chosen guarantees no blooming, an important reliability feature. The calculated on-chip power dissipation is only 11 mW. Thus, a full dual-band SWIR focal plane with 12,000 detectors ($2 \times 6000$) may be achieved with only a 132-mW power dissipation. This power dissipation is well within the 120-K operating capability of satellite passive coolers.

## Conclusions

The $Pd_2Si$ Schottky-barrier technology offers performance that is an excellent match to the infrared imaging requirements of earth-resources remote-sensing systems. Indeed, the high yield and maturity of this silicon-based technology may make it the only viable choice for the next generation of NASA earth-resource satellites.

## Acknowledgment

The authors wish to acknowledge the contributions of Dr. F.V. Shallcross, R. Miller, V.L. Frantz, and J.V. Groppe, RCA Laboratories, for processing and preparation of test devices; B.M. McCarthy, R.T. Strong, and L.D. Elliott, Advanced Technology Laboratories, and L. Pellan, RCA Laboratoraies, for assistance in device evaluation; and Dr. W.F. Kosonocky, RCA Laboratories, for many helpful discussions.

**Frank Warren** is Manager, Systems and Electro-Magnetic Laboratory, in the Advanced Technology Laboratories, Camden, N.J. As manager of this laboratory, he is responsible for infrared-systems development and millimeter-wave imaging research. Prior to joining RCA in 1979, Mr. Warren was employed by Martin-Marietta Aerospace where his work included analysis and design of infrared seekers, development of a laser seeker, design of prototype sensor and missile systems, and the mechanical concept and signal-processing design for a hybrid infrared/millimeter-wave sensor.

Contact him at:
**Advanced Technology Laboratories**
**Camden, N.J.**
**TACNET: 222-2771**

**John Tower** is Unit Manager, Electron Device Systems, in the Systems and Electro-Magnetic Laboratory of the Advanced Technology Laboratories, Camden, N.J. He is currently responsible for investigating system applications for the Schottky-barrier IR-CCD technology. Mr. Tower joined RCA in 1976 and has been involved in the development of a number of CCD correlators. In particular, he participated in the design of a 512-stage correlator for antijam radios, and a high-speed CMOS/NMOS/CCD correlator for communication modems. During 1981, he worked at RCA Laboratories, Princeton, N.J., on the development of time-delay-and-integration (TDI) CCD imagers for high-speed electronic mail applications.

Contact him at:
**Advanced Technology Laboratories**
**Camden, N.J.**
**TACNET: 222-3883**

**Dave Gandolfo** is Unit Manager, Millimeter Wave Applications, in the Systems and Electromagnetic Laboratory of the Advanced Technology Laboratories, Camden, N.J. As a Unit Manager, Dr. Gandolfo has been directing the design of signal-processing CCDs, and the development of CCD-based visible and infrared imaging systems. He has been involved in the investigation of surface acoustic wave filters, microwaves, cryogenics, plasma physics, and radiation damage. He has been responsible for several custom-CCD applications such as programmable transversal filters, analog-scan converters, and high-data-rate line-scan imagers. His group was also responsible for ESSWACS and the IR-CCD Fence Sensor System.

Contact him at:
**Advanced Technology Laboratories**
**Camden, N.J.**
**TACNET: 222-3791**

**Authors Villani (left) and Elabd.**

**Authors (left to right) Tower, Warren, and Gandolfo.**

**Hammam Elabd** received the BSc degree in Electrical Engineering from Cairo University, Egypt, in 1969, and MSc degrees from the University of Arkansas, Fayetteville, Ark., and Rensselaer Polytechnic Institute, Troy, N.Y., in 1975 and 1979, respectively. He received the PhD degree in Electrical Engineering from Rensselaer Polytechnic Institute in 1979. Currently, a Member of Technical Staff at RCA Laboratories, Princeton, N.J., he is involved in the development of Schottky-barrier IR-CCD arrays. This work has led to contributions in the following areas: detector-process development for the platinum silicide and palladium silicide Schottky-barrier detectors, and detector and IR-CCD image-sensor characterization (responsivity, spectral response, dark current, noise, and fixed-pattern noise).

Contact him at:
**RCA Laboratories**
**Princeton, N.J.**
**TACNET: 226-2687**

**Tom Villani** received the BS degree in Electrical Engineering in 1980 from Fairleigh Dickinson University, Teaneck, N.J.

He joined RCA Laboratories, Princeton, N.J., in the same year, where he worked on the testing and evaluation of platinum silicide and palladium silicide Schottky-barrier focal-plane arrays for thermal and SWIR imaging applications. Presently, he is pursuing, on a part-time basis, postgraduate studies at Rutgers University, New Brunswick, N.J.

Contact him at:
**RCA Laboratories**
**Princeton, N.J.**
**TACNET: 226-2686**

R.G. Neuhauser

# The Saticon* photoconductor: The latest in color-camera-tube photoconductors

*The Saticon photoconductor—with improved resolution, lack of flare, freedom from blemishes, very low lag, and long life—is being introduced into the larger high-performance studio cameras.*

**Abstract:** *The history of the Saticon photoconductor is traced and RCA applications of the device are given, with an eye to the primary features of the device: high resolution, lack of flare, freedom from blemishes, very low lag, and long life. Brief mention is given to the latest Saticon photoconductor technology, the Saticon III.*

The original Saticon photoconductor was introduced into production and extensive camera use in 1977, making it the first new photoconductor suitable for color-TV-camera use since the lead-oxide photoconductor was introduced in 1966. The Saticon photoconductor, first applied in small electronic-journalism cameras and in color cameras used for reproducing film on TV, is now being introduced into the larger high-performance studio camras. Tubes employing the Saticon photoconductor are now used in the overwhelming majority of three-tube color cameras being sold in North America.

## Acclaimed by the IEEE

Dr. Nahiro Goto of the NHK (Japan Broadcasting Corporation) Research Laboratory was recognized with the prestigious Vladymir K. Zworykin Award of IEEE for the year 1981 for his leadership in advancing state-of-the-art television technology by development of the Saticon photoconductor. The photoconductor developed by Dr. Goto's team consists of a sophisticated combination of Selenium, Arsenic, and Tellurium, the "SAT" in Saticon photoconductor. It is one of those rare, useful, solid-state semiconductors that is amorphous (glassy) instead of crystalline.

The basic photoconductor is a 4- to 6-μm-thick amorphous selenium layer doped with arsenic to produce stability in the glassy phase and carefully doped in one region with tellurium to produce adequate response in the red portion of the visible spectrum. The success of the photoconductive layer, which must be produced to exacting standards, is the result of the sophisticated formulation of its constituents; its manufacture is successfully accomplished by a unique computer-controlled deposition method that controls the doping concentration profiles throughout the layer. A cross section of the photoconductor is shown in Fig. 1.

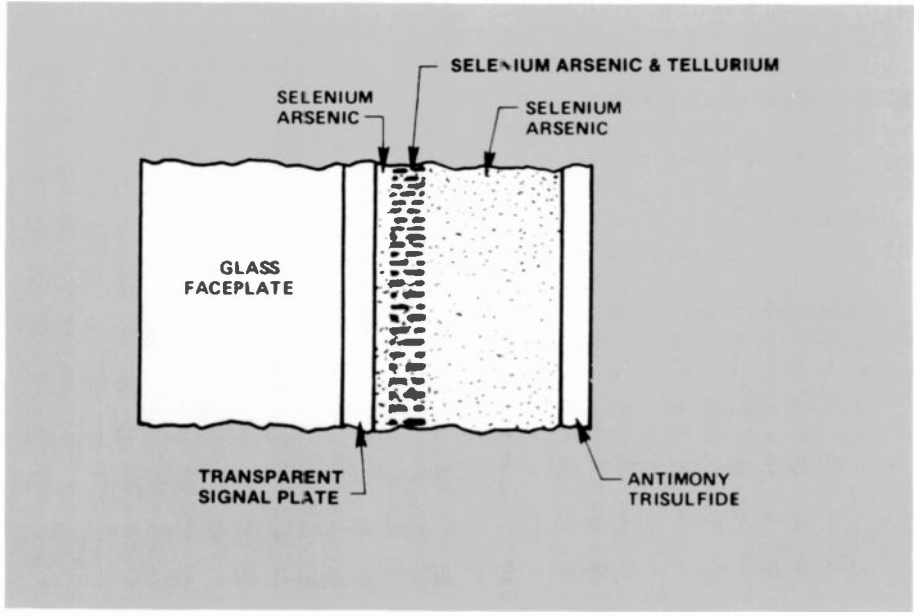


**Fig. 1. The Saticon photoconductor.** A schematic cross section.

* Used with permission of trademark owner.


Final manuscript received April 21, 1982.
Reprint RE-27-3-11

### *Selenium photoconductors—a long history in television*

Selenium, the primary ingredient of the Saticon photolayer, has been known and used as a photoconductor or light detector for more than 100 years. Many early experiments, using TV scanning-disc systems, employed selenium as the light detector. In fact, the first commercial photoconductive camera tube, the vidicon, was developed by RCA and employed an amorphous selenium photolayer. This layer was quickly replaced by the antimony trisulphide photoconductor, which had longer life and stability and higher red response, although the superiority of selenium, because of its low lag* and high resolution, was clearly recognized. Later, RCA Laboratories researchers substantiated the ability of arsenic to stabilize the selenium in its amorphous form at practical working temperatures and the ability of tellurium doping to extend the red response.

Concentrated work by Dr. Goto and his colleagues at NHK eventually resulted in the sophisticated layer design of the present Saticon photoconductors. The manufacturing techniques necessary to produce this superior-performing photoconductor were finally developed in the laboratories of Hitachi, until now the sole source of Saticon tubes.

## Chronology

The chronology of developments in Saticon tubes in the four short years of their use is briefly noted below:

**1977:** The first Saticon tube in three-tube electronic journalism cameras (BC4408/H8397) is introduced.

**1978:** Low-beam-impedance (low-lag) gun employing Saticon photoconductor is introduced in the 18-mm diameter tubes, type BC4908/H8397A.

**1979:** Low-capacitance Saticon photoconductor further reducing lag with no loss in resolution or sensitivity (BC4395) is introduced.

**1980:** Low-output target capacitance (shunt capacitance) target structure improving tube signal-to-noise ratio is combined with the low-capacitance photoconductor for low lag in types BC4391/ H9366 and BC4396/H9369.

**1981:** Saticon II photoconductor that reduces specular-highlight memory (the trails or smears that follow bright spots on the screen) is announced. A single-doped modification of the photoconductor produced these results.

The first RCA-made Saticon tube, the 13-mm diameter Saticon tube, is produced for the Hawkeye recording camera.

**1982:** Saticon III photoconductor, a modified version of the low capacitance photoconductor with even less specular-highlight memory, resulting from a double-doping process, is introduced.

The first diode-gun 18mm diameter Saticon III tube is introduced. The diode gun reduces the beam impedance and, accordingly, the low-light lag.

A wide variety of the Saticon-tube types introduced in this time period were applied in a number of areas of color broadcast and medical television.

The more recently developed group of tubes are the "low cap" tubes having both a low-storage-capacitance photoconductor (6 instead of 4 $\mu$m thick) and a low-capacitance target output. The low-storage-capacitance photoconductor lowers the lag, and the low shunt capacitance of the target output improves the signal-to-noise ratio of the picture. Both characteristics contribute to better performance at low light levels; that is, they lead to a higher effective camera sensitivity. The 18- and 25-mm-diameter versions of these tubes—BC4391 and BC4386, respectively—are now available.

The 13-mm (1/2-in) diameter BC4398 Saticon tube (Fig. 2) was introduced in 1981 as the heart of the revolutionary RCA Hawkeye recording camera. The lower weight, lower power requirements, and smaller size of this tube contribute substantially to the smaller size and high performance of the camera system. The very low output capacitance and low photoconductor capacitance of the tube combine to reduce noise and lag at low light levels, and both contribute to the excellent low-light-level sensitivity and performance of the Hawkeye camera. The Hawkeye tubes will, of course, incorporate the Saticon II photoconductor when it is put into full production.

Saticon photoconductors are also being used in the higher-grade color VTR (video tape recorder) cameras for home and educational use. These cameras are single-tube types that employ internal color stripes to produce the necessary color-information signals. The high resolution and low lag of the Saticon photoconductor are the primary features in these cameras leading to better color pictures.

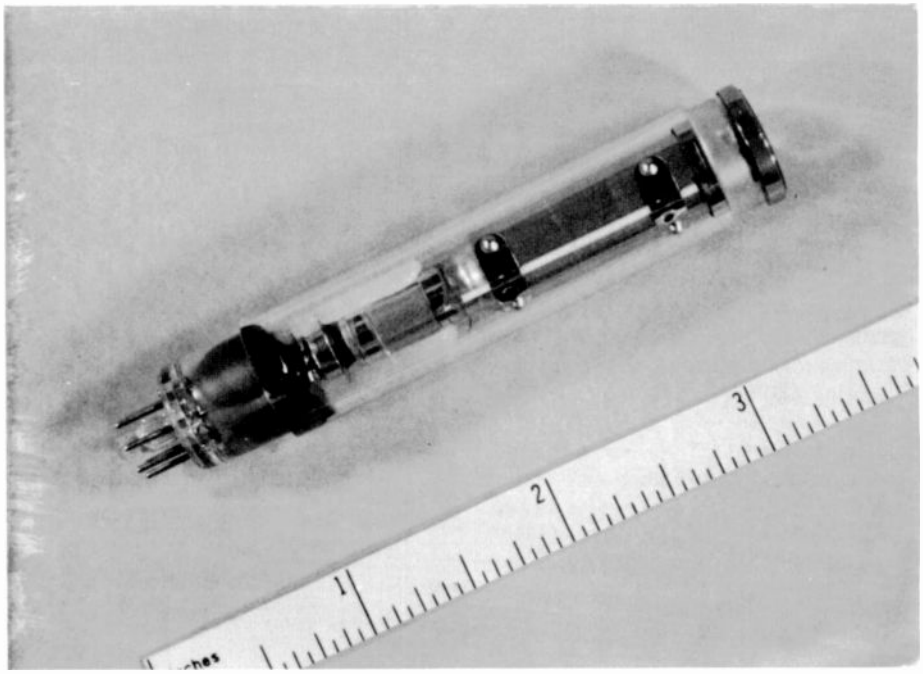


**Fig. 2. For the RCA Hawkeye recording camera.** The 13-mm (1/2-in) diameter BC4398 Saticon tube.

* Lag in a television camera tube is the measure of the rate of decay of the video signal when the illumination is changed or cut off. The lag is usually measured as a percentage of the original signal level after an interval of time following the removal or changing of the illumination.

**Fig. 3. Photograph comparing Saticon (right) and lead-oxide-photoconductor reflectivities.**


**Fig. 4. The new low capacitance Saticon tube (BC4391)** showing the low-output-capacitance target contact.

## Features of a Saticon photoconductor

### *Resolution*

Improvement in resolution is the key offering of a Saticon photoconductor. The resolution of a Saticon tube is substantially better than that of any tube, of similar size by actual measurement, equipped with a lead-oxide photoconductor. The key to this higher resolution is the glassy nature of the photoconductor; it does not scatter light, but absorbs it almost completely in the front surface of the layer. As a result, storage capacitance and lag can be decreased by increasing the thickness of the layer without compromising resolution. The resolution of a Saticon tube is also independent of the color channel or the wavelength of light.

### *Flare*

Unlike lead-oxide photoconductors, which are highly reflective (Fig. 3), the Saticon photoconductor does not reflect light back through the optical system. The result of the Saticon tube's almost total absorption of light at the photoconductor and, hence, its low reflectivity (lack of flare), is clear distortion-free colors, even low-light colors, and clear color transitions with no discoloration at all levels of the picture, even when large areas of the picture are of high contrast or consist of highlights.

### *Freedom from blemishes*

Blemishes on a Saticon-tube picture are a rarity both initially and after long use. The glassy photoconductive layer is virtually immune to the fracturing and other breakdown defects that produce conducting white spots in other tubes.

### *Very low lag*

The ability to capture motion at low light levels and to avoid color shifts during motion is greatly improved by three Saticon-tube features: the low-lag, low-impedance gun used in all broadcast-grade Saticon tubes, the low-capacitance target (Fig. 4), and the low charge-carrier trapping effect inherent in the Saticon photolayer. This latter effect avoids the low-contrast long-persistence image that trails moving objects in other cameras. The diode gun in the new BC4399 18-mm Saticon tube produces even lower low-light lag.

Two highly effective operational techniques also further reduce the low-light lag. The first is the use of bias light,* now used in all three-tube color cameras. The second is the use of dynamic beam-type controls that maintain the beam at a low level for normal scene content and automatically increase it when excessive highlights are encountered.

### *Long life*

The glassy impervious Saticon photolayer is not subject to gas doping from the inevitable residual atmosphere in the tube, nor does it decompose or outgas and "poison" the cathode of the electron gun. Therefore, the performance of the photoconductor does not change with time. Both the photoconductor and the electron gun in the Saticon tubes exhibit extremely long life compared to any other broadcast camera tube with a similar operating-temperature range.

Tube shelf life is no problem; spares, which can be used in any channel of the camera, can be stored for very long peri-

* In bias lighting, a small amount of uniform illumination is applied on the photoconductor. The amount of bias light usually used is enough to develop a uniform dark-level signal equal to 5 to 10 percent of the normal highlight signal current (5 to 10 nA). Bias lighting as a technique to reduce lag was discovered accidentally by the author and T. Shipferling when they were experimenting with early versions of the Vistacon tubes. The charge voltage developed by the bias light raises the voltage on the photoconductor scan side in the absence of scene light to a voltage that is near the effective velocity spread of electrons within the beam. The beam lands more fully on the lowest charges developed by light from the scene image. Under these conditions, the beam has, effectively, a low resistance, and the lag is substantially reduced. Bias light does not reduce the contrast, since the added dc signal is subtracted out in the signal-processing amplifier.

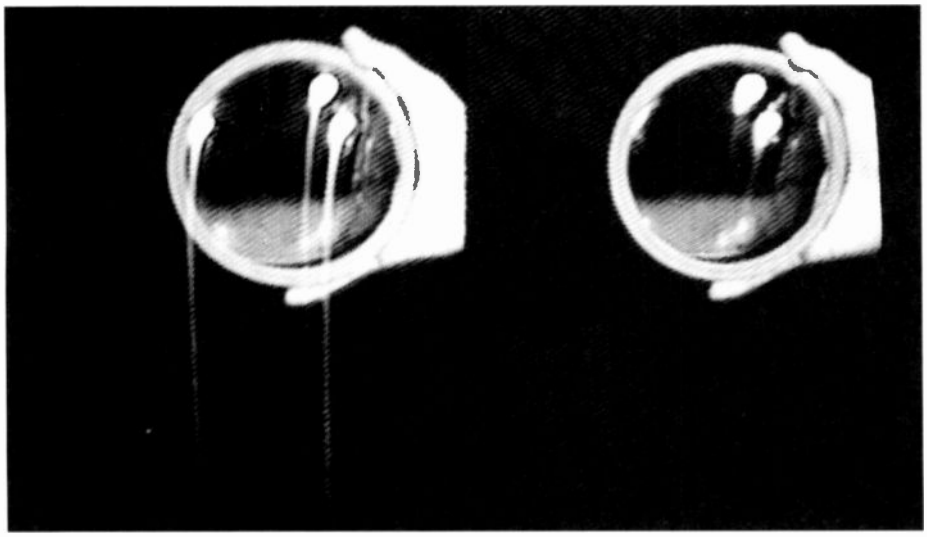

**Fig. 5. The new Saticon II layer (right) and its predecessor.** A comparison of the memory reduction of extremely high specular highlights (courtesy Hitachi Corporation).

ods without conditioning. The long operating and storage-life claims for the Saticon tube are backed by a six-month full-replacement warranty and a twelve-month prorated warranty starting from the date of installation of the tubes.

## Saticon II

One of the latest developments in the television camera-tube photoconductors is the Saticon II photoconductor. This new advance in photoconductor technology substantially reduces the retention or "memory" of specular highlights (bright spots) in the television picture; that is, it effectively eliminates most of the smear or trail that these highlights can produce as they move across the screen (Fig. 5). In addition, the Saticon II photoconductor performs better than the original Saticon photoconductive layer at the high end of its operating temperature range.

### *Saticon II features*

The Saticon II photoconductor was developed, as already mentioned, to greatly reduce the memory of specular highlights. Specular-highlight memory occurs when a high concentration of carriers drops into deep traps in the tellurium-doped region of the photoconductor, when that portion of the photoconductor experiences an excessively bright portion of an image. The band gap of the photoconductor is constricted at the region where tellurium doping occurs, and this allows generation of electronic carriers from lower-energy "red" photons of light (Fig. 6).

Excessive light generates a large number of electronic charge carriers that distort the field in the region of the doped layer and reduce the field across the photoconductor (Fig. 7). The carriers that are normally swept out by the electric field to be stored as the video signal charges, fall into traps from which they slowly escape, producing the memory of the highlight.

The Saticon II formulation reduces the number and depth of available trapping states in the tellurium-doped region and, as a result, reduces the memory of specular highlights by as much as 75 percent.

The Saticon II formulation also produces the added benefit of better performance at the upper end of the operational-temperature range. Image retention produced by long-term exposure of stationary scenes is minimized, and the retained image disappears very rapidly. These improvements have been made in the Saticon photolayer without compromising any of its other excellent performance characteristics, except blue sensitivity, which is reduced by an approximate average of 5 percent.

### *Saticon II tube introduction and availability*

The Saticon II photoconductor became available in all of the 50-volt-target broadcast versions of the Saticon tube (BC4908 and BC4390) in January 1982. These tubes are identified by the Saticon II brand.

Saticon II tubes can be used to replace earlier Saticon tubes; however, tube replacement should be done by the set so that old and new tubes are not intermixed in any one camera. Saticon tubes can also directly replace tubes of other types. For example, the 18-mm (2/3-in), 7-pin Saticon tube with glass faceplate extender, the BC4390, was introduced as optically and pin-base compatible with the 18-mm Plumbicon/Leddicon tubes.*

* Plumbicon is a trademark of N.V. Philips.

Leddicon is a trademark of English Electric Valve.

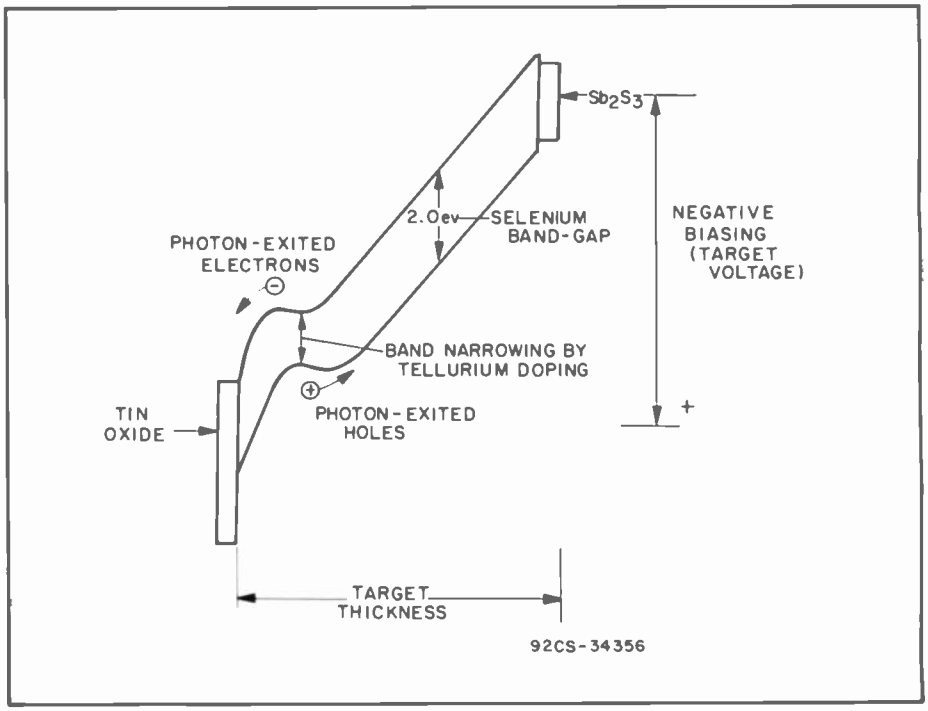


**Fig. 6. Band-structure schematic** of a Saticon photoconductor.

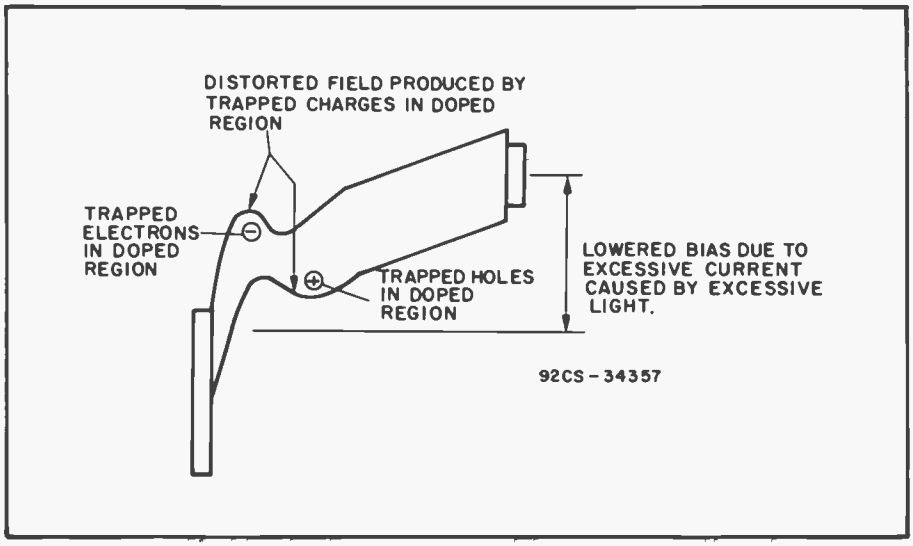


**Fig. 7. Distortion of the field** of a Saticon photoconductor by a specular highlight.

## Saticon III

The latest Saticon photoconductor technology, the Saticon III technology, was developed in the low-capacitance versions of the Saticon tube. The Saticon III photoconductor is the product of a very sophisticated development program relying on the computer-controlled deposition of two additional doping agents. The process is fine-tuned for the different color channels in which the tubes are to be used. Saticon III tubes are, therefore, not interchangeable in the different channels of a color camera.

This new photoconductor produces even greater resistance to memory of specular highlights and stationary long-term images. The Saticon III photoconductor requires a slightly higher target voltage than the earlier low-capacitance Saticon tubes, that is, 75 volts instead of 65 volts.

The Saticon III photoconductor is available now in two newly announced types, the 18-mm-diameter diode-gun, type BC4399 (H9386B), and the 25-mm-diameter low-output-capacitance tube, type BC4386 (H9379A), which will replace the BC4396 (H9369) Saticon tube.

## Saticon-tube manufacturing schedule

RCA entered into an agreement to use Saticon tubes in its broadcast cameras in 1977, and the Electro-Optics activity began to distribute broadcast color-camera Saticon tubes and to service the broadcast camera industry in North America and Europe. An agreement covering mutual exchange of Saticon-tube and photoconductor technology was a part of this agreement. In 1981, RCA entered into its first venture in Saticon-tube manufacture when it developed the 13-mm (1/2-in) Hawkeye camera tube—the BC4398. Other new broadcast-type Saticon tubes are also under active development.

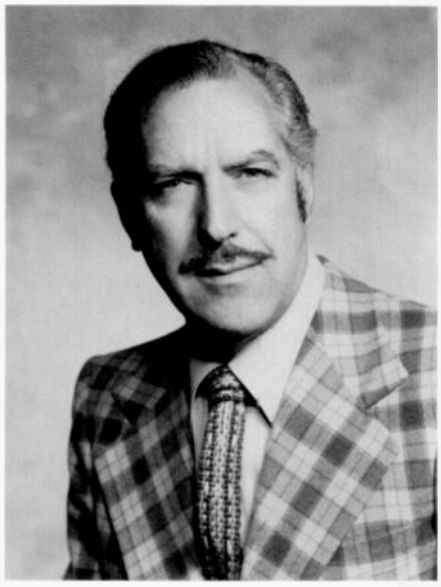

**Robert Neuhauser,** Senior Member of the Technical Staff, RCA Electro-Optics and Power Devices, Lancaster, Pa., is a graduate of Drexel University with a B.S. in electrical engineering. Since 1949, he has been employed continuously at RCA in various engineering and supervisory capacities in the design, production, and applications engineering of vidicon, image orthicon, Vistacon, and Saticon television camera tubes. He is a Fellow Member of the Society of Motion Picture and Television Engineers, and recipient of the David Sarnoff Award of that Society for his leadership in developing camera tubes for color television cameras. He has published more than thirty papers on television camera tubes and tube technology.
Contact him at:
**RCA Electro-Optics and Power Devices**
**Lancaster, Pa.**
**TACNET: 227-2223**


## Publication from the *RCA Engineer*

According to the RCA Engineering Information Survey conducted in 1977, the *RCA Engineer* is the second most important source of technical information about RCA (the most important information source is the engineer's associates). The back issues of the *Engineer*—150 of them—provide a record of RCA's progress in invention, development, and manufacturing. To make this wealth of technical information accessible to the engineers, a *25-Year Index to the RCA Engineer* has been published.

The *Index* can help you find specific information that is needed in your work. Or the *Index* might provide a vital contact in another RCA business, someone who has related experience and who would be willing to consult with you. The *Index* gives you the opportunity to profit from RCA's technical heritage—to reuse knowledge, to build on past accomplishments.

The *25-Year Index to the RCA Engineer* is available in all RCA Libraries. Recipients of the *RCA Engineer* can obtain their personal copies by writing to:

*RCA Engineer*
Building 204-2
Cherry Hill, N.J.

## Got an electro-optics question?

If you still can't find what you need in this comprehensive update on electro-optics at RCA, we have another resource: a collection of 28 articles on electro-optics by RCA engineers and scientists. Compiled in 1977, this collection nevertheless represents the foundations of much of the business that RCA is pursuing today. The 144-page volume contains articles on light sources; light transmission media and devices; light detectors; electro-optics systems; electro-optics for inspection and detection; and television for display, surveillance, and reconnaissance. Your copy will cost $2.00. Send your order to:

*RCA Engineer*
Bldg. 204-2
Cherry Hill, N.J.

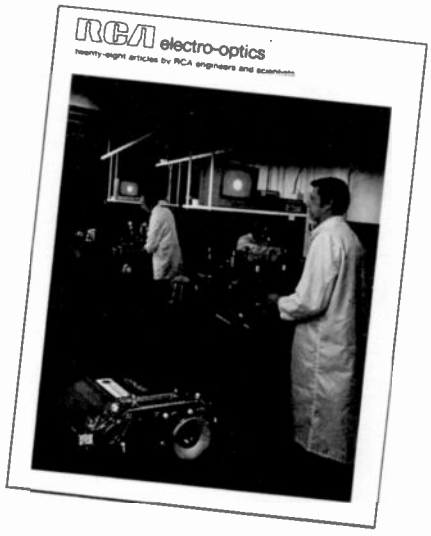


## Correction note:

March/April *RCA Engineer*

"Custom and Quantity Manufacturing: An Engineering Comparison," an article by J.A. D'Arcy and R. Miller published in the March/April 1982 *RCA Engineer*, contains two errors. The last line of type in column 1 on page 6 is missing. That missing line should begin a new paragraph with the words: "We will describe both custom manu-." On page 11, two photos are reversed. The photo in Fig. 8 should appear above the caption for Fig. 9, and the photo in Fig. 9 should appear atop the caption for Fig. 8.

L. Arlan

# A high-performance TV camera for target-acquisition and laser-designator systems

*Through electro-optics and associated circuitry, the image of the enemy can be captured on a 1-inch vidicon television camera.*

**Abstract:** *Television sensors are used in target-acquisition and laser-designator systems to provide remote imagery and tracking signals when used as a daylight TV sensor or as the modular FLIR readout with parallel-to-serial electro-optical multiplexing. The design of a television sensor for this application entails stringent requirements pertaining to imaging-tube parameters, weight, size, ruggedization, power, raster stability, electromagnetic compatibility, and video processing. A high-performance miniaturized TV sensor was developed for use on the Target Acquisition and Designation System/ Pilot's Night Vision System (TADS/ PNVS). Extensive use of hybrid circuitry and low-power design resulted in a 1-inch vidicon camera weighing less than 1.0 kg with a power dissipation of less than 7 watts. The raster boresight was stabilized to within 0.1% of the raster dimension by the use of circuit compensation techniques. This stability was maintained under adverse conditions of temperature, vibration and earth's magnetic-field effects. A ruggedized ceramic vidicon was used to achieve less than 3 percent microphonics in a high-vibration environment.*


Final manuscript received March 30, 1982.
Reprint RE-27-3-12

**Fig. 1. This high-performance miniaturized TV sensor was developed for use on the Target Acquisition and Designator System/Pilot's Night Vision System (TADS/PNVS).** Extensive use of hybrid circuitry resulted in this compact design (less than 1.0 kg).

Television sensors employing vidicon imaging devices are being used in target-acquisition-and-designation systems to extend the range and accuracy at which crew members of a weapon system can acquire (detect, recognize, and lock-on) targets and launch offensive weapons against an enemy threat. A typical system combines long-focal-length direct-view optics, a forward-looking infrared (FLIR) with remote TV-readout display for night operation, a high-resolution television system for day operation, a laser target designator and ranger, and a laser tracker all on a stabilized platform. Modular component development for parallel-scan FLIR systems and daylight TV acquisition-and-tracking applications have led to RCA's development of the miniaturized television sensor shown in Fig. 1.

The sensor assembly is a 1-inch vidicon television camera, which is the second generation of a camera originally developed by RCA for the U.S. Army Night Vision Laboratory. The camera serves a dual function when integrated with a direct-view imaging system. It functions as an electro-optical multiplexer by imaging the output of a common-module FLIR having a 180-parallel-channel LED-scanned display and providing a serial video for remote imaging and contrast tracking, and it works as a daylight TV imaging device by providing daytime acquisition and low-contrast tracking of long-range targets by means of an optical system as depicted in Fig. 2.

The sensor can employ either a 1-inch silicon diode array or antimony trisulfide

target in a highly ruggedized all-magnetic ceramic vidicon. Extensive use of thick-film hybrid circuitry has resulted in a high-performance, compact and reliable design. Careful attention to design techniques that stress low power consumption, minimizes internal temperatures with a total power dissipation of 6.5 watts. Stringent requirements in regard to vidicon blemishes, shading, noise, microphonics, resolution and sensitivity directly affect the ultimate long-range performance of the target-acquisition-and-designation system.

## General requirements

The TV sensor is required to be configured for minimal size and weight to optimize the gimbal-load requirements without sacrificing performance. This was accomplished by extensive use of thick-film hybrid circuitry and by "remoting" the power supply, synchronizer and some video-processing circuitry. The principal electrical and mechanical requirements achieved with this sensor are summarized in Table I.

## Electrical and mechanical performance

Raster stability was accomplished using temperature-compensation circuit techniques while maintaining the specified total power dissipation. Minimization of internal power dissipation is an important factor in preventing excessive thermal build-up. Vidicon dynamic range is limited by dark current, which approximately doubles for every 10°C rise in temperature. Closed-loop horizontal deflection circuits normally employed to achieve this tight stability would typically consume much higher power levels. Raster stability is achieved by careful attention to deflection-circuit design, tube-potting techniques, mechanical configuration, materials used, and magnetic shielding employed to attenuate effects of the earth's field or other ambient magnetic-field sources.

Shading caused by vidicon target nonuniformity and beam-landing errors is another important factor to be considered. Video-shading components limit the dynamic range of automatic contrast control circuits under conditions of high dark current or high haze pedestals where long-range, low-contrast target tracking is required. A shading criteria of 15 percent over the entire image surface is very stringent but can be achieved with proper vidicon selection and beam-landing error correction. Dynamic focus correction, using horizontal and vertical parabolic correction on the focus electrode, resulted in corner resolution in excess of 500 TVL/RH and shading within 15 percent for the silicon C23262 B/H tube.

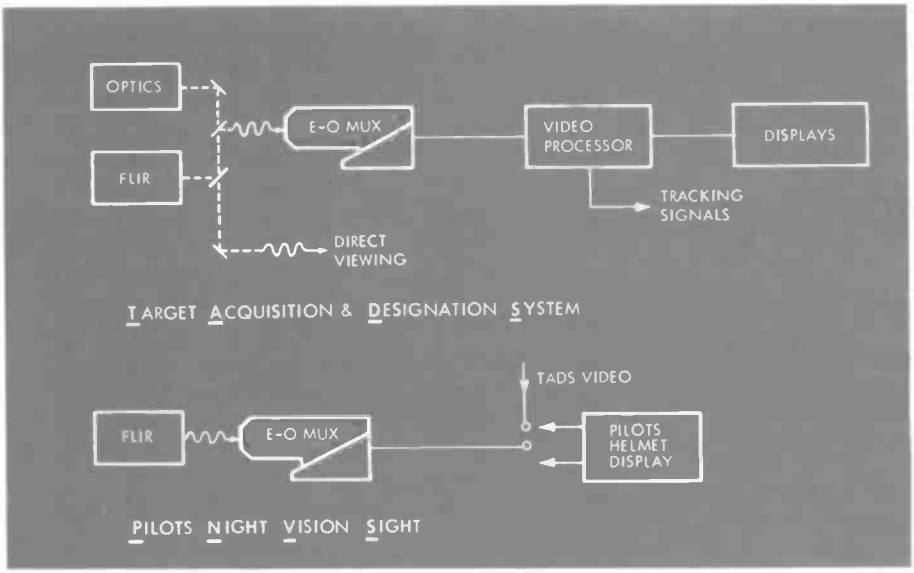


**Fig. 2. The dual function of the miniaturized TV sensor is illustrated in this block diagram of the TADS/PNVS system.** The TV sensor serves as either a FLIR electro-optical multiplexer or as a day TV sensor in the TADS system.

A unique hybrid preamplifier located in close proximity to the vidicon target, shown in Fig. 3, was developed, and it resulted in outstanding performance. This close proximity to the vidicon target minimizes input capacitance and enables decoupling of the mesh lead, brought from the front of the tube, at the preamplifier. This results in a video signal that is free of pickup and deflection-ringing, and an equivalent input noise current of 6 nanoamperes (nA). This noise performance, coupled with tube selection providing 500-nA operation (silicon), results in a better than 30 dB signal-to-noise ratio with a high Modulation Transfer Function (MTF) response.

The MTF of the multiplexer can be boosted by using an aperture-corrector circuit that provides a controlled amplitude response as a function of frequency with linear phase characteristic. The linear phase characteristic is necessary to prevent distortion in the wideband video signal. Figure 4 shows the MTF of a typical FLIR, the aperture-corrected response of the electro-optical multiplexer, and the resulting overall MTF of the coupled system.

Assuming that the aforementioned elec-

**Table I. Electrical and mechanical requirements.**

| | |
|---|---|
| Power consumption | 6.5 W |
| Weight | <1 kg with ± 1% control |
| Center of gravity | Controlled within ± 1.3 mm |
| Aperture-corrected MTF | 95% @ 400 TLV/RH |
| Target current (silicon) | 500 nA nominal, 600 nA peak |
| Geometric distortion | ≤2% |
| Image format | 12.8 × 9.6 mm |
| Shading | ≤15% |
| Noise with aperture correction | ≤16 nA rms |
| Raster stability @ 25°C ± 25°C | ≤1 TVL in center |
| Scan rate | 875/60 |
| Operating temperature | −32°C to +55°C |
| Microphonics | ≤12.5 nA @ 5 g to 2,000 Hz |
| Video output | 0.5 V differential into 62 Ω @ 1mv/nA |
| Blemishes | Tube-selection dependent |

trical and mechanical design criteria have been considered, the ultimate performance of the sensor as a long-range day TV or as a FLIR electro-optical multiplexer in regard to video tracking of low-contrast targets is highly dependent on the imaging device performance.

Parameters such as shading, resolution, dark current, microphonics, geometric fidelity and spectral sensitivity are all important, but they are generally controlled by a specific design and vidicon selection. Another highly important criterion that limits system performance is fixed-pattern noise. Vidicon manufacturers employ state-of-the-art manufacturing techniques in silicon bulk-material growth and target fabrication to control the size and number of blemishes, but a very stringent requirement for video-tracking applications results in a low-yield device. This is generally accomplished with silicon targets by careful selection from a high-volume production line. Antimony trisulfide surfaces are made by a deposition process on the vidicon faceplate, and they generally exhibit fewer and smaller blemishes.

The choice of vidicon target material is dependent on the system use. Silicon is the usual choice for daylight TV cameras because of the extended near-IR response enabling operation in the 0.7- to 1.1-micrometer spectral region for optimum atmospheric transmission and also because of silicon's immunity to solar burn. Antimony trisulfide vidicons are commonly employed for electro-optical multiplexer use with FLIRS because the dielectric lag reduces an interference pattern resulting from the instantaneous coincidence of the readout beam and the LED image.

A typically very stringent blemish requirement for a silicon target vidicon is given in Table II where zone 1 is a raster-centered circle with a diameter equal to one-half of the raster height within which most of the target-tracking performance is required. Zone 2 is a concentric circle with a diameter equal to the raster height, and zone 3 is the remaining area.

## Environmental

Extensive environmental testing was conducted on the TV sensor, related to use in a flight vehicle. Environmental test results are listed in Table III. A prime feature of the TV sensor is the low microphonic performance achieved by use of a highly ruggedized ceramic vidicon employing a target bonded to the faceplate. This tube has survived shock levels in excess of 250

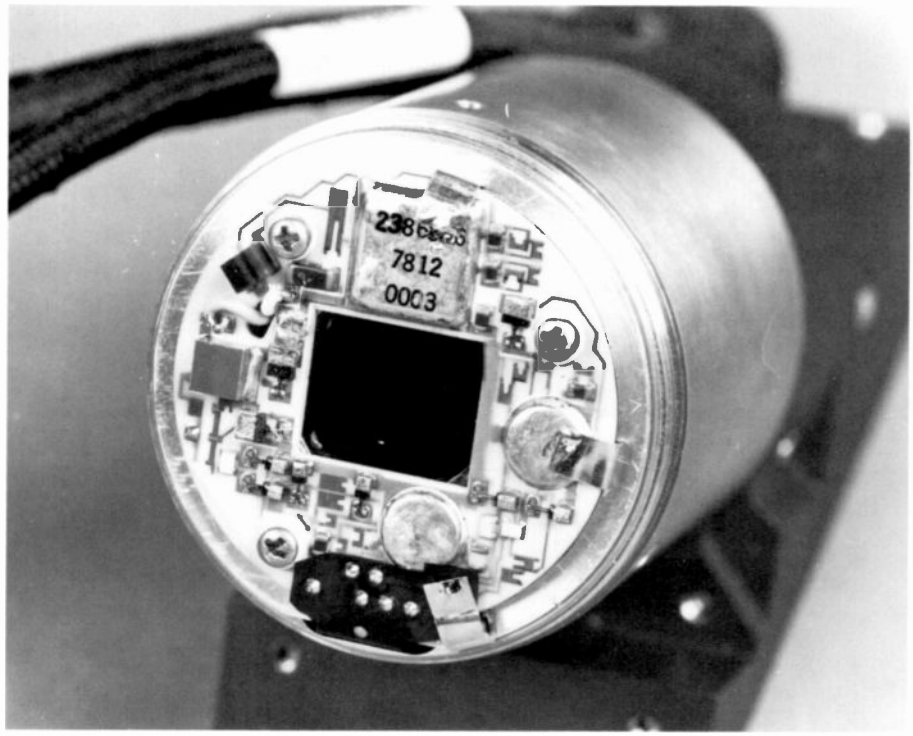


**Fig. 3. A unique hybrid preamplifier located in close proximity to the vidicon target was developed.** This device exhibits excellent noise performance and immunity to external noise sources.

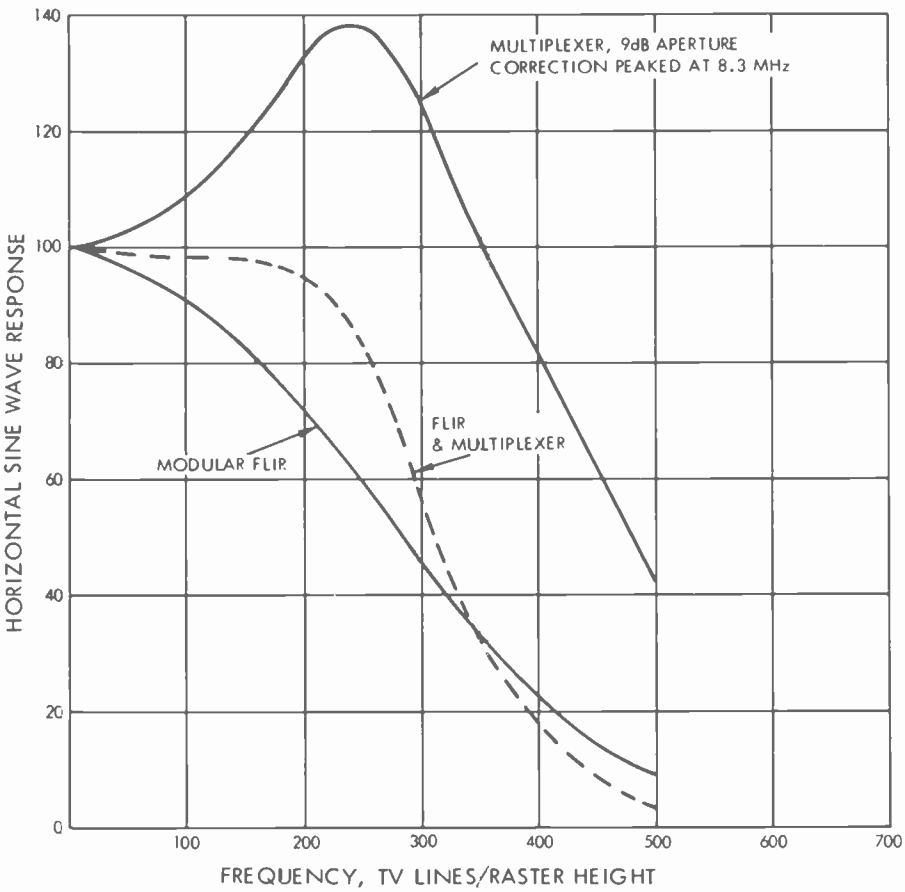


**Fig. 4. The effect of aperture correction on the modulation transfer characteristic of the multiplexer is shown by the upper curve.** When this response is coupled with that from the FLIR, an improved overall response is achieved as shown by the broken curve.

**Table II. Tube-blemish criteria.**

| *Blemish size (in equivalent 875 TV raster lines)* | *Allowed spots (Zone 1)* | | *Allowed spots (Zones 1 & 2)* | | *Allowed spots (Zones 1, 2 & 3)* | |
|---|---|---|---|---|---|---|
| | *Bright* | *Total* | *Bright* | *Total* | *Bright* | *Total* |
| Over 7 | 0 | 0 | 0 | 0 | 0 | 0 |
| Over 4 | 0 | 0 | 2 | 2 | 2 | 5 |
| Over 2 | 0 | 0 | 2 | 4 | 3 | 5 |
| Over 1 | 0 | 2 | 3 | 6 | 4 | 12 |
| 1 or smaller | * | * | * | * | * | * |

**Table III. Environmental performance.**

| *Environmental test* | *Test results* |
|---|---|
| Vibration: 10 g's 5-50 Hz<br>5 g's 50-2000 Hz | Less than 3% microphonic signal in video |
| Shock: 44 g's, 15 ms | No detectable microphonics |
| Temperature/altitude: −32°C to +55°C, at 50,000 feet | Tested up to 71°C with only degradation due to dark current |
| EMI: RS01, RS03 | Met requirements at all frequencies up to 180 MHz |
| RE02, RE02.1 | Met requirements |

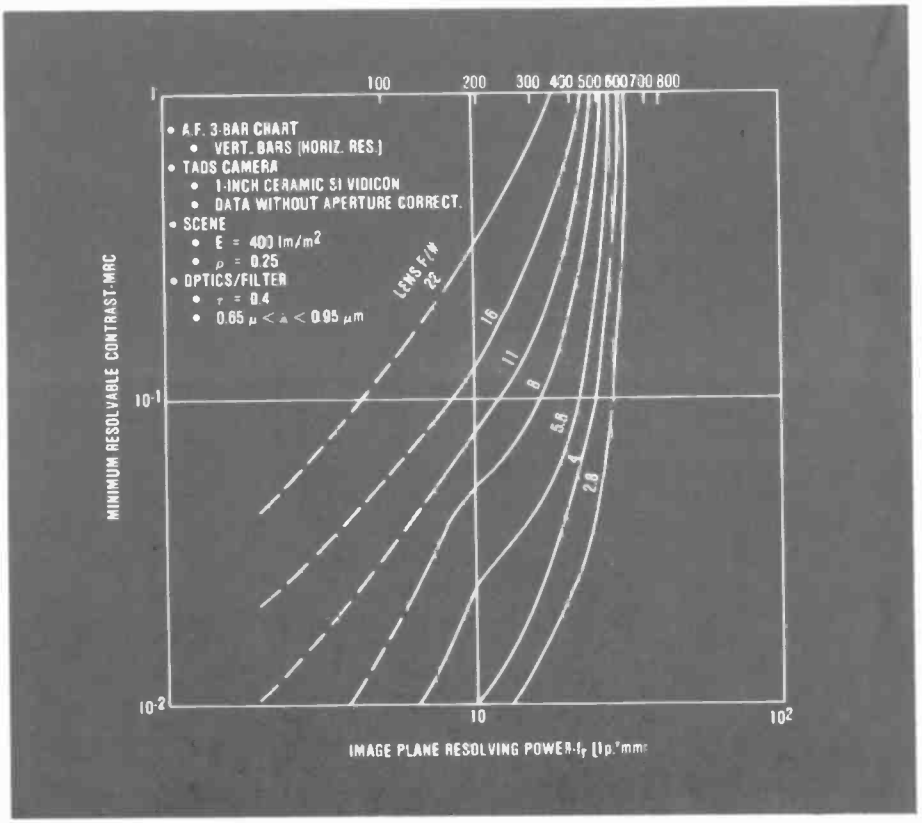


**Fig. 5. The measured Minimum Resolvable Contrast (MRC) is shown as a function of horizontal resolution.** The data, plotted for various exposure levels, shows excellent low-contrast performance well below the $10^{-2}$ level.

g's, and no microphonics were reported during the TADS/PNVS development-phase flight test.

## Functional performance

The major performance parameters contributing to the success of this TV sensor as a viable target-acquisition-and-tracking device are:

- Low microphonics;
- High MTF with linear-phase aperture correction;
- High signal-to-noise ratio;
- Low shading and stringent blemish criteria;
- Minimum size and weight;
- Low power dissipation; and
- Boresight stability.

The high image quality with the TV sensor is apparent when a moderate contrast scene is displayed. The ultimate usefulness as a long-range daylight TV image sensor, however, involves the Minimum Resolvable Contrast (MRC), which is defined as the image contrast needed to resolve a periodic bar chart (usually a three-bar or four-bar chart). Silicon vidicons are generally used for this application because the near-IR response enables operation in a spectral region with improved atmospheric transmission compared to the visible region and also because these vidicons have a linear (unity gamma), wide-dynamic-range transfer characteristic. These characteristics provide good image performance under low-contrast, high-background conditions that are controlled by other than preamplifier noise.

The MRC for the silicon target TV sensor is dependent upon the MTF and various noise sources. The principal noise sources are preamplifier noise, fixed-pattern noise and quantum-photoelectron noise. Preamplifier noise is usually the dominant component in high-contrast applications but in low-contrast imaging the complexity of the mechanisms involved makes theoretical performance modeling difficult. It is, therefore, important to determine performance empirically.

The TV sensor has been measured, by means of a beam splitter, to superposition background and test charts with independent sources of illumination to obtain variable low-contrast images, with an observer positioned at an optimum distance from the display determining the resolvable contrast.

The measured image-plane MRC data is presented in Figs. 5 and 6 for horizontal and vertical bar orientations respectively, with a 300-angstrom bandpass spectral filter centered at approximately 8010 angstroms. These data were obtained without aperture correction, which can provide additional vertical-bar MRC performance. The slight bulge in the family curves observed at slightly below MRC = 0.1 represents the presence of a low-level fixed-pattern noise component in the target structure that is exposure dependent. In any case, excellent low-contrast performance has been demonstrated down to contrasts well below the $10^{-2}$ level shown on the graph.

The data in Figs. 5 and 6 are plotted for various values of system f/# required for a minimum scene exposure of 400 $1m/m^2$. The radiometric calibration curve is given in Fig. 7 and assumes a 5900-Kelvin (K) black-body illumination with a scene reflectivity $E = 0.25$.

## Electrical design

A simplified functional diagram of the TV sensor is shown in Fig. 8. Video from the vidicon target is first amplified in a low-noise transimpedance preamplifier hybrid. The signal is then fed, via the flexible printed wiring circuit, to the video board where the signal is aperture-corrected, bandwith-limited and converted to a differential drive output on a twisted, shielded pair.

The control board contains all of the vidicon-gun voltage filters and bleeder networks. Potentiometer controls are provided for adjustment of beam current (G-1) and electrostatic focus (G-3). A dynamic focus signal, consisting of adjustable horizontal and vertical parabolic waveforms, is generated on the focus board and summed with the G-3 voltage through a capacitor on the control board. The focus board also contains a focus-current regulator that feeds a focus coil in the deflection assembly. The input differential horizontal and vertical drive signals are converted to single-ended outputs for use by the deflection and dynamic focus circuits. The drive signals are also combined to form the cathode-blanking signal for the vidicon.

The deflection board contains the horizontal and vertical deflection circuits that drive the deflection assembly. Each deflection circuit also has a sweep-failure circuit to protect the vidicon via the cathode signal in the event of loss of either sweep waveform. Test points are available at the external connector to provide for fault isolation to a board or modulator assembly for field maintenance.

## Tube-yoke assembly

The tube-yoke assembly consists of a custom-designed precision magnetic-deflection-yoke assembly with a C23262BH ceramic vidicon in a RTV potted configuration. Potting of the tube within the yoke assembly is accomplished with a precision fixture to maintain overall faceplate perpendicularity to within ± 8 arc-minutes. The potting technique also allows for tube replacement and was designed and verified for minimal vibration-induced microphonics and high thermal stability.

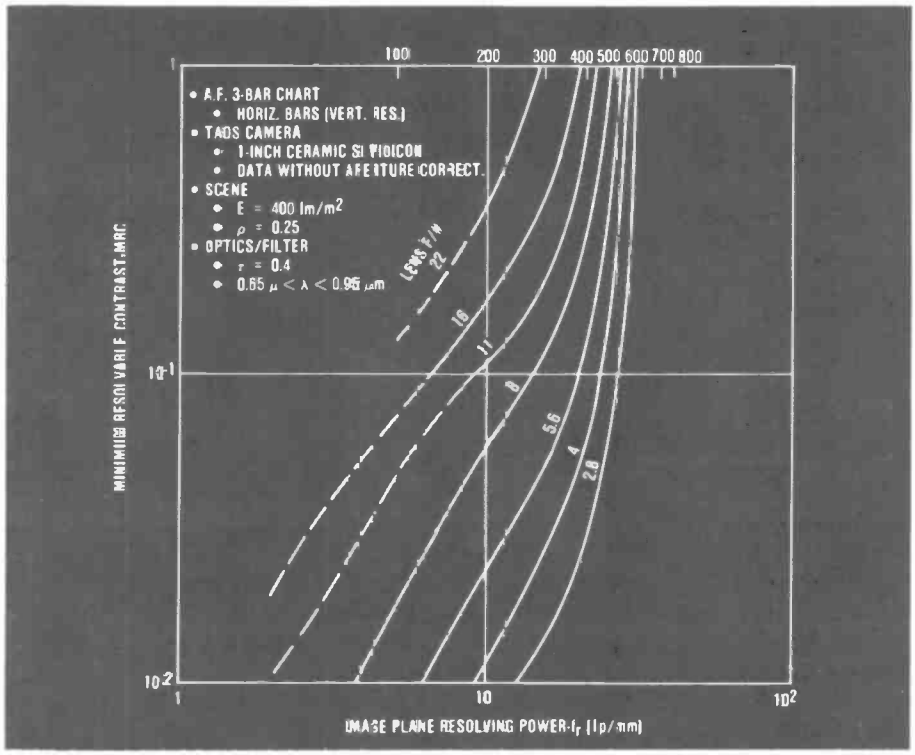


**Fig. 6. Minimum Resolvable Contrast is shown as a function of vertical resolution.** A horizontal oriented 3-bar chart was used for these measurements.

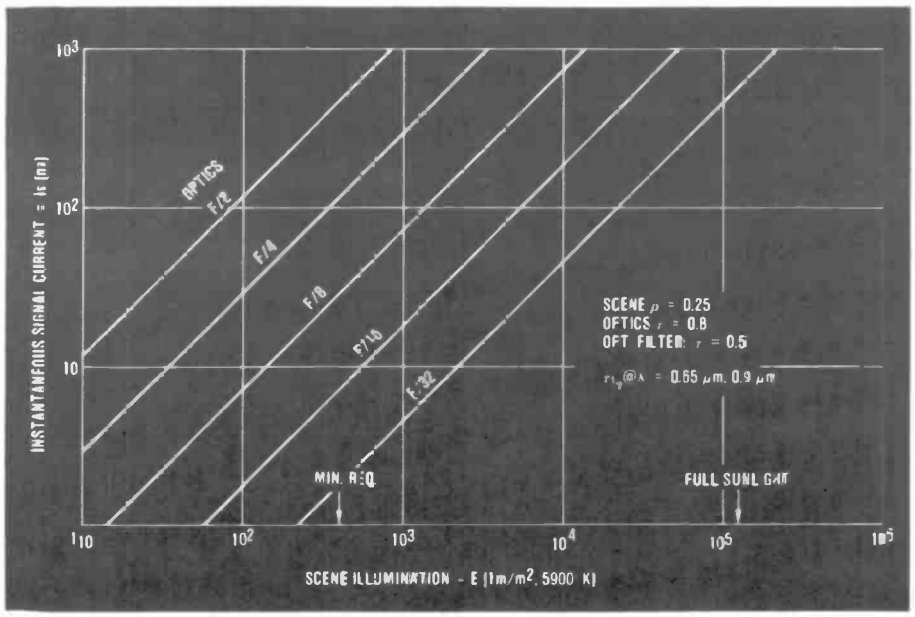


**Fig. 7. The radiometric callibration curves are shown as a function of lens speed.** A 5900 Kelvin black-body illumination source is assumed.

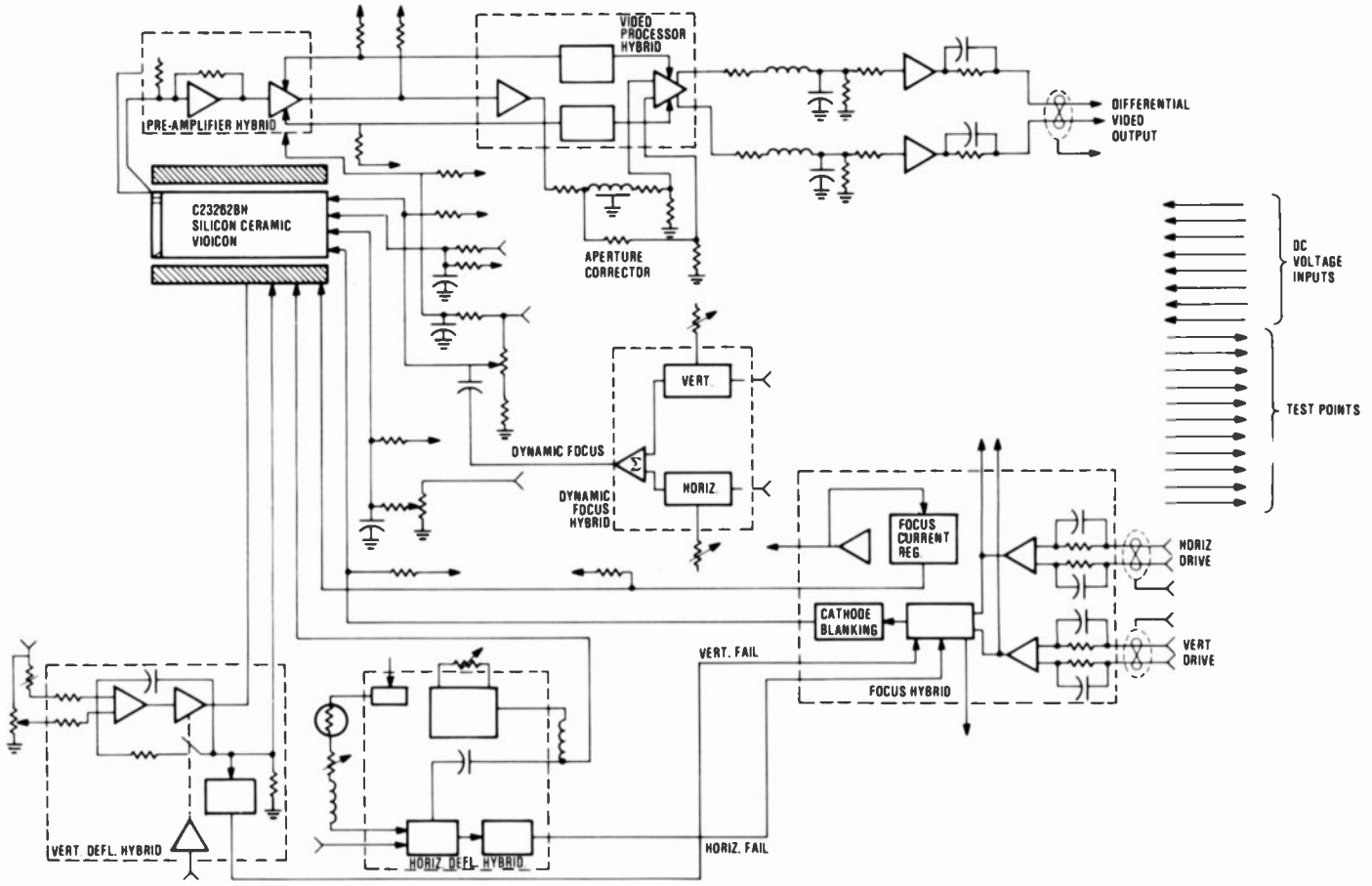


**Fig. 8. A simplified block diagram of the TV sensor** shows the major elements of the assembly and the functional interrelationship between them.

A mu-metal shield covers the entire tube-yoke assembly within the aluminum housing to shield against electromagnetic interference and to provide excellent boresight stability within the earth's magnetic field at any attitude.

The yoke was designed with an inverted technique using deflection coils on the outside of the focus coils. This provides a more uniform field, which has resulted in a good beam-landing characteristic. As a result, corner resolution is improved and shading characteristics are far superior to those previously achieved with printed-circuit yokes. The horizontal deflection coil was designed to minimize power and to provide good linearity with a flyback-type deflection circuit.

## Video preamplifier hybrid

The complete preamplifier, shown in Fig. 3, is packaged on a circular ceramic substrate and positioned directly over the front faceplate of the tube. A rectangular hole in the preamplifier allows imaging onto the tube faceplate.

The preamplifier circuit consists of a low-noise transimpedance amplifier with a 100-kΩ feedback resistor, a wideband amplifier and a video-output buffer. A transimpedance amplifier is used to present a low-impedance load to the video signal current. This eliminates the need for peaking compensation and minimizes noise pickup and parasitic oscillations. The circuit and packing techniques have resulted in a low-power design with noise performance that approaches theoretical values.

## Video, deflection, focus and control boards

The video signal from the preamplifier is fed to the video board for partial processing. The video board consists of a video-processor hybrid, aperture corrector, bandwidth filters and differential line drivers as shown in Fig. 8. The aperture corrector is not included in the video-processor hybrid; therefore, the adjustments of frequency and amplitude can be made or disabled to fit the application. The bandwidth filters provide a two-pole roll-off with the noise bandwidth limited to 17 MHz at the -3 dB point.

The delay-line aperture corrector compensates for vidicon spot size or optics response by increasing the definition of abrupt transitions in video tone, through the introduction of controlled overshoots and undershoots as previously described.

The deflection board has both the horizontal and vertical deflection hybrids, shown in Fig. 8, with associated components to provide full beam deflection and sweep-failure protection. The horizontal hybrid consists of a high-efficiency resonant flyback circuit with centering control. The vertical hybrid consists of a very stable feedback-controlled linear deflection circuit. As previously mentioned, thermal stabilization through circuit compensation resulted in an overall raster boresight stability of better than 1 TVL.

The focus board consists of two hybrid circuits and peripheral adjustment parts. One hybrid, shown in Fig. 8, generates a composite signal for dynamic focus consisting of individually adjustable horizon-

tal and vertical parabolic waveforms. This waveform is added to the quiescent dc focus voltage, which increases the focus voltage as the beam position increases from the tube raster's center position. The second hybrid contains a highly stable 2.5-V reference source internally used by the focus-current regulator and also used by the deflection circuits. This hybrid also converts the differential input drive signals to single-ended outputs and provides the cathode-blanking signal with sweep-failure protection control.

The control board is a small printed wiring board (PWB) containing filters, shown in Fig. 8, for the filament, G-1, G-2, G-3. The +550-V filtered output is then sent to the preamplifier for local filtering prior to application to the vidicon mesh (G-4). Controls are provided for G-1 and G-3 voltages. The +550 V is also applied to a bleeder network, which provides the G-3 focus voltage. In this manner, the G-3 and G-4 voltage track each other so that focus is optimized for small changes in the +550 VDC supply.

## Mechanical design

The TV camera comprises four plug-in printed-circuit modules, a ceramic vidicon tube, a microelectronic preamplifier, a magnetic-deflection-yoke assembly and flexible wiring interconnections packaged within a two-piece structure plus a branch cable with two connectors. Fig. 9 shows the assembly with cover removed so that the four PC boards are exposed. The front of the camera—which contains the tube, yoke, and preamplifier assembly—is machined from aluminum and has a nominal barrel outside diameter of 55 mm, a total length of 152 mm and a height of 86 mm. Behind the tube-yoke assembly is the flexible circuit termination/interwiring board area shown in Fig. 10 and below that are mounted the four plug-in modules. Most chassis wiring is accomplished by means of the flexible printed circuitry, shown in Fig 11, attached to the PC-module connectors before installation. A seven-conductor branch of flexible circuit is mounted in the machined recess in the bottom of the barrel and provides the electrical connections to the microelectronic preamplifier as shown in Fig. 3.

## Preamplifier

Figure 3 shows a closeup of the front of the camera with the electromagnetic inter-

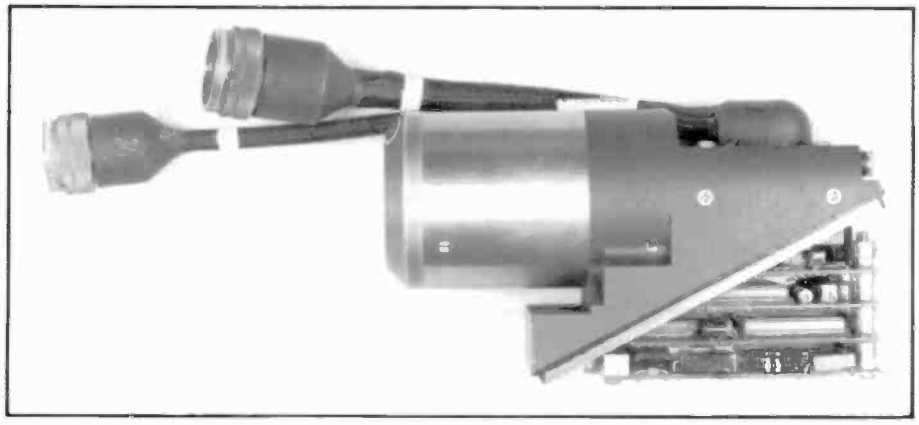

**Fig. 9. This view of the TV sensor, with a cover removed, reveals the plug-in board assemblies.** A dense packaging was achieved while providing a high degree of maintainability.

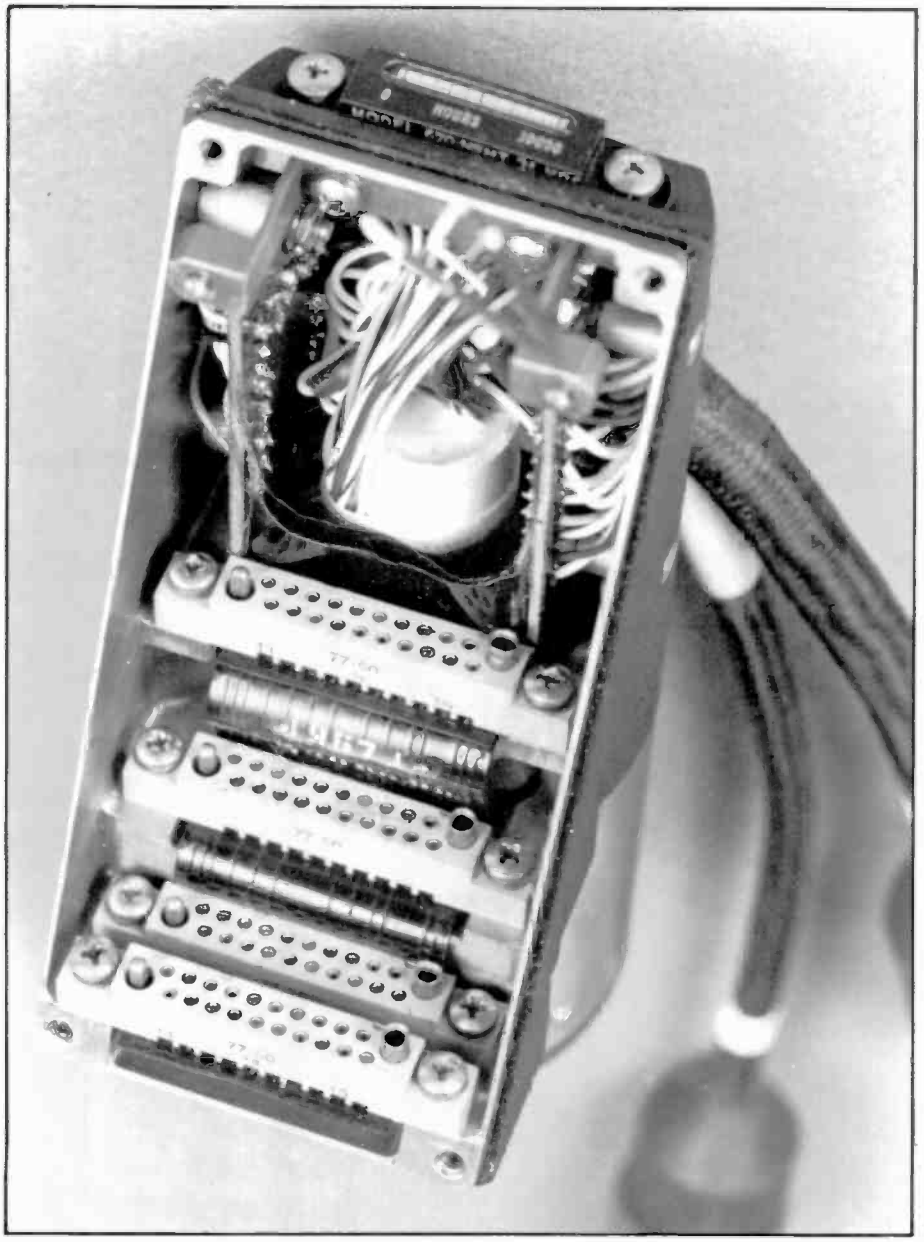

**Fig. 10. In this view, the plug-in boards are removed** to reveal the flexible printed wiring that interconnects the board connectors and wires from the tube/yoke assembly.

ference (EMI) screw-on shield removed. The preamp contains all microelectronics on a 1-mm-thick ceramic substrate with many of the resistors, and so on, deposited directly. The two short insulated wire connections from the tube target and G-4 can be seen attached to terminals. Behind the preamp is a 0.13-mm thick, plated copper ground plate that connects to two of the hybrid cans and also the preamp circuit ground.

The ceramic substrate is much stronger in compression than in tension. For this reason, small teflon (cushion) washers (0.076-mm thick) are mounted under the ceramic where it mounts to the yoke, and under the head of the screw that holds down the top surface of the ceramic substrate. The screws are also torqued down to eliminate over-stressing at assembly. There have been no problems or refinements required of this design as a result of the environmental tests conducted.

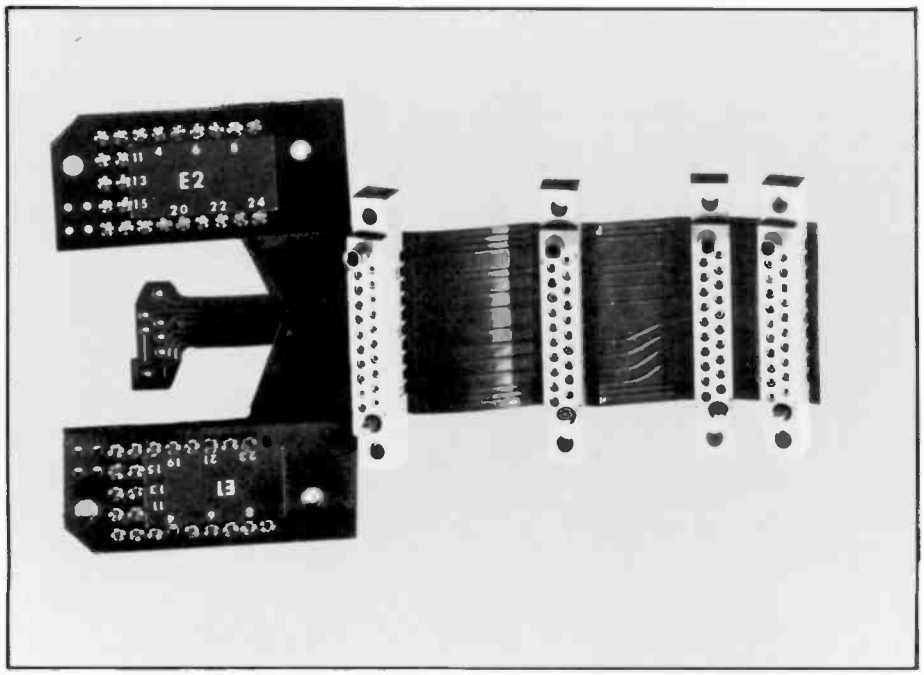


**Fig. 11. Most of the chassis wiring is accomplished by a flexible printed wiring assembly.** The flexible wiring is assembled with connectors prior to installation in the chassis.

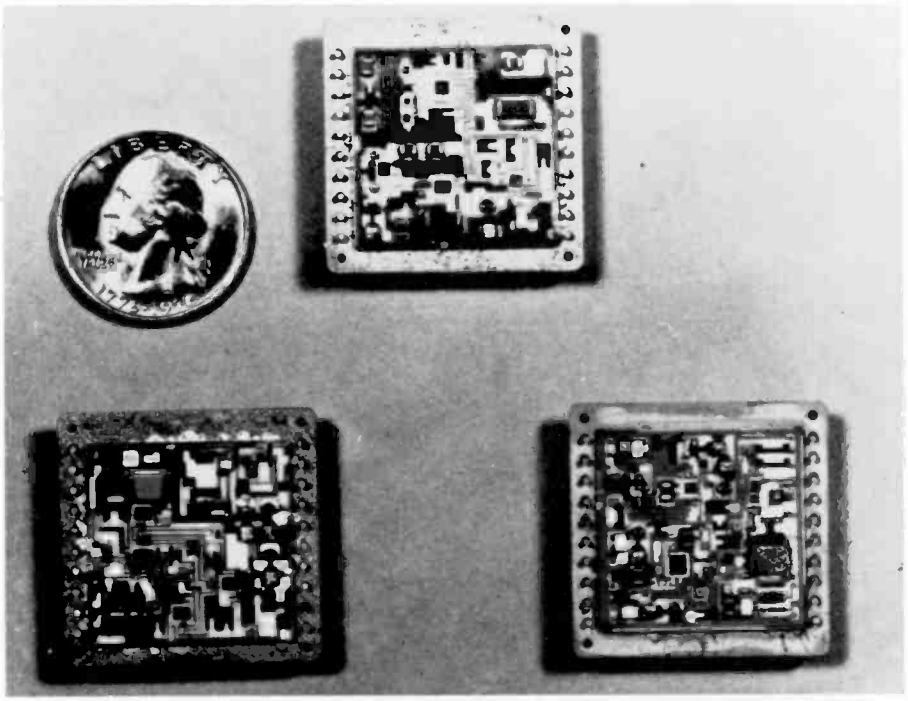

**Fig. 12. Most of the TV sensor circuits are contained within six custom-designed hybrid microcircuits.** Three of these rugged packages are shown with covers removed.

## Printed circuit modules

The four PC modules use 1.2-mm thick by 50-mm wide glass epoxy boards and contain both microelectronic (hybrid) packages and discrete parts. An Airborne™ 20-pin male PC connector mounts on one end of the module and plugs into the female chassis-mounted connector (Fig. 10).

Each module is a different length due to optimum circuit-layout requirements and the need to use available space as efficiently as possible. The ends of the modules opposite the connector all lie in the same plane and are sandwiched together with two screws plus spacers that secure the boards to the chassis structure. The connector on the other end of the module provides sufficient restraint so that additional extraneous supports (and thus extra weight) are not required.

## Chassis/cover assembly

Figures 1 and 10 show how the triangular cover is assembled to the chassis. This design provides optimum accessibility because, by removing just four cover-mounting screws, all trim pots are accessible and the PC modules can be easily removed for servicing. When the four cover screws are securely tightened, the compression of the RTV "formed-in-place gasket" will be approximately 20 percent. This design has proven adequate for sealing against moisture.

## Hybrid design

Most of the TV-sensor-assembly electronic circuits have been constructed using custom-designed hybrid microcircuits. When compared with alternative circuit-fabrication methods that use discrete parts and cased integrated circuits mounted and solder-connected on printed-circuit boards, this approach has reduced the size and weight, lowered volume production costs, simplified system assembly and increased the reliability.

There are six different types of thick-film hybrids used in the camera system.

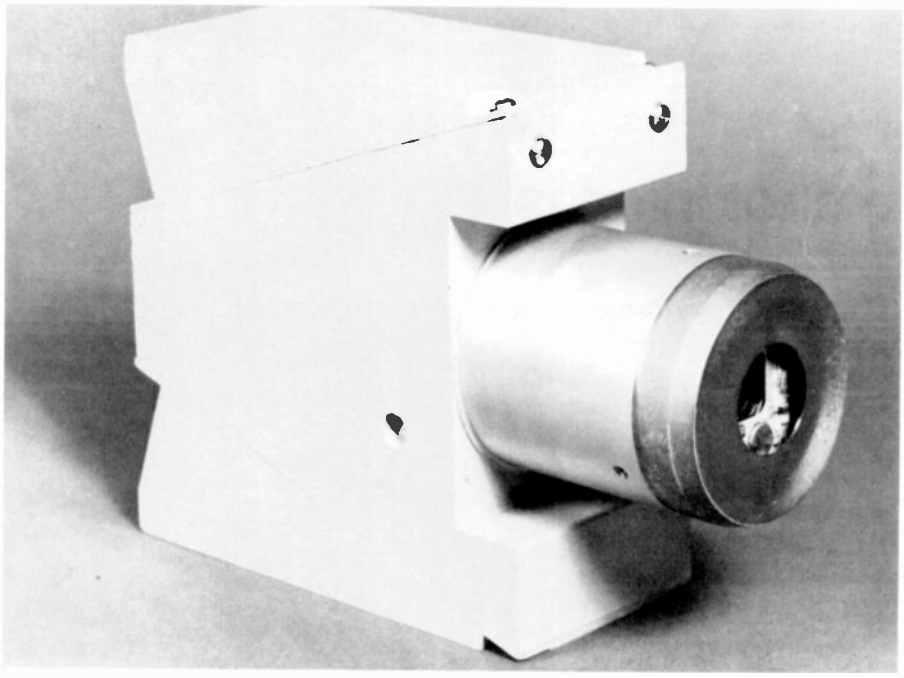

**Fig. 13. A similar TV sensor that features a built-in power supply and improved producibility has been developed for the U.S. Navy Seafire Program.** This camera is capable of performing under high levels of shock and severe EMI conditions.

All are hermetically sealed in the same-style, rugged, platform package shown in Fig. 12 except for the preamplifier previously shown in Fig. 3. Because the circuits were designed and partitioned under disciplines sensitive to production costs, all six hybrids are being manufactured to the same sequence of well-documented process operations and controls. The hybrids meet the screening requirements of MIL-STD-883A, Method 5004, for Class-B devices.

Three representative hybrids used in the camera system ("Interface & Focus," "Dynamic Focus" and "Vertical") are shown in Fig. 12 at a stage of assembly up to the point of sealing the covers. The 25 × 25 mm substrates, with thick-film resistors and metallization, are solder-mounted to the platform base.

Some processing highlights relative to the standard RCA manufacture of these hybrid microcircuits are:

1. Eutectic solder-chip mounting of all transistors and diodes to gold-plated moylbdenum tabs
2. Solder mounting of chip-tab assemblies and chip capacitors
3. Approved epoxy mounting of integrated circuit chips (no current passage in backside of silicon chip)
4. Ultrasonic gold-ball bonding of wires with automatic wire bonding for production.

The first-generation electro-optical multiplexer developed for the U.S. Army Night Vision Laboratory formed the basis for a low-power, miniaturized, high-performance TV sensor. The TADS/PNVS sensors improved the previous design and showed better airborne performance, meeting all size, weight and environmental requirements. RCA has also developed a similar TV sensor, for the U.S. Navy Seafire Program, that features built-in power supply, improved producibility, a high degree of maintainability, and is capable of the same high performance under extreme EMI conditions. This unit is shown in Fig. 13.

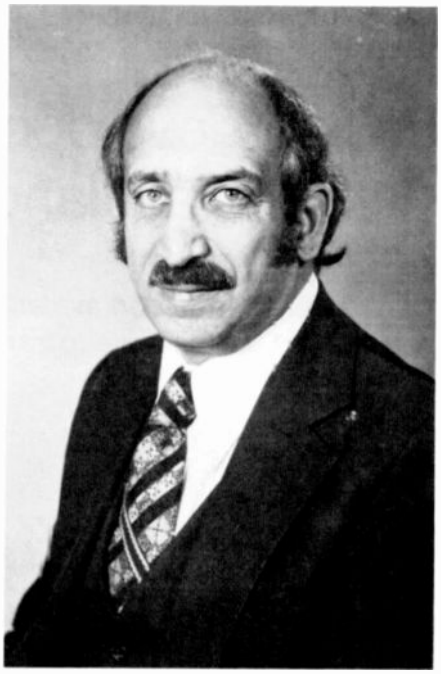

**Lionel Arlan** is a Design Engineering Manager in the Radiation Systems Engineering at RCA Automated Systems, Burlington, Massachusetts. From 1954 to 1962, he worked in Camden on several infrared and television systems including the advanced Ranger Television cameras. Transferred to Burlington in 1962, he has been involved in the development of many electro-optical systems such as LCSS, LLL TV cameras, miniaturized fire-control-system TV cameras, and a high-resolution computerized television system for automated hybrid inspection.

Contact him at:
**Automated Systems**
**Burlington, Mass.**
**TACNET: 326-3729**

## Acknowledgment

The author wishes to acknowledge the valuable contributions made to this program by P. Arntsen, M. J. Cantella, J. Klein, E. P. Lea, R. E. Rooney, R. G. Spiecker, and M. W. Stewich.

P.P. Webb | R.J. McIntyre

# Recent developments in silicon avalanche photodiodes

*Improvements in silicon avalanche photodiode performance are summarized, with an eye toward electro-optic system applications.*

**Abstract:** *Recent developments in silicon avalanche photodiodes (APDs), of potential interest to the electro-optic system designer, are reviewed. These developments include:*

- *Devices with enhanced ultraviolet response (quantum efficiency (Q.E.) greater than 80 percent at 4000 angstroms);*
- *Devices with enhanced infrared response (Q.E. up to 50 percent at 1.06 μm);*
- *Low-noise APDs (effective k value reduced from 0.02 to 0.006);*
- *Faster devices (for optical communications at greater than 1 Gbit/s);*
- *Linear and two-dimensional arrays of APDs (dead space reduced to 0.003 inch); and*
- *APDs designed for single-photon counting (single-photon-counting efficiencies of 50 percent at a gain of $10^9$, but with some remaining problems).*

The reach-through avalanche photodiode (RAPD) pioneered by RCA[1-5] has found wide use throughout the world in many electro-optic systems, particularly for optical rangefinding, optical communications, optical recording, point-of-sale equipment, and so on. This paper reviews recent developments in avalanche photodiodes that should make them prime candidates for many other applications, some of which may not have been possible previously.


Final manuscript received January 27, 1982
Reprint RE-27-3-13

## Devices with extended spectral response

One advantage of the RAPD structure is that it can be made with a high quantum efficiency for wavelengths ranging from the near ultraviolet to beyond one micron. Recently, devices with enhanced responsivity at both the short- and long-wavelength limits have been developed.

### *Ultraviolet-enhanced diodes*

Since most applications of APDs are in the wavelength range of 0.8 μm to 1.06 μm, standard production diodes have an antireflection (A/R) coating that minimizes the reflective losses in this range. With

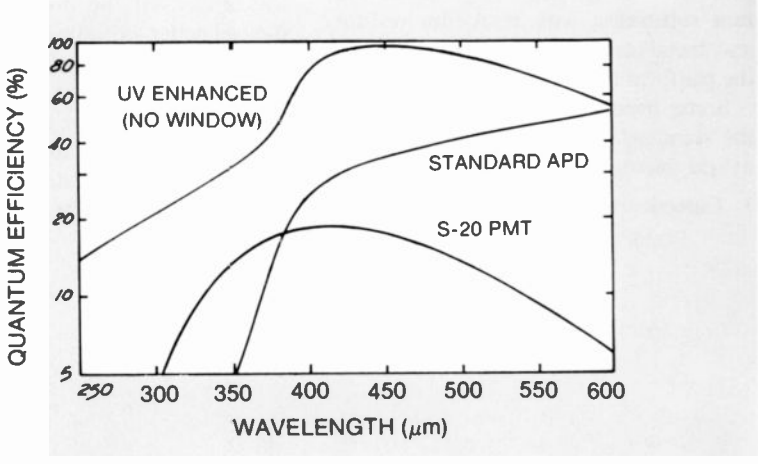


**Fig. 1. Quantum efficiency** of an ultraviolet-enhanced APD compared with a standard APD (optimized for 900 nm) and a standard photocathode having an S-20 photoresponse.

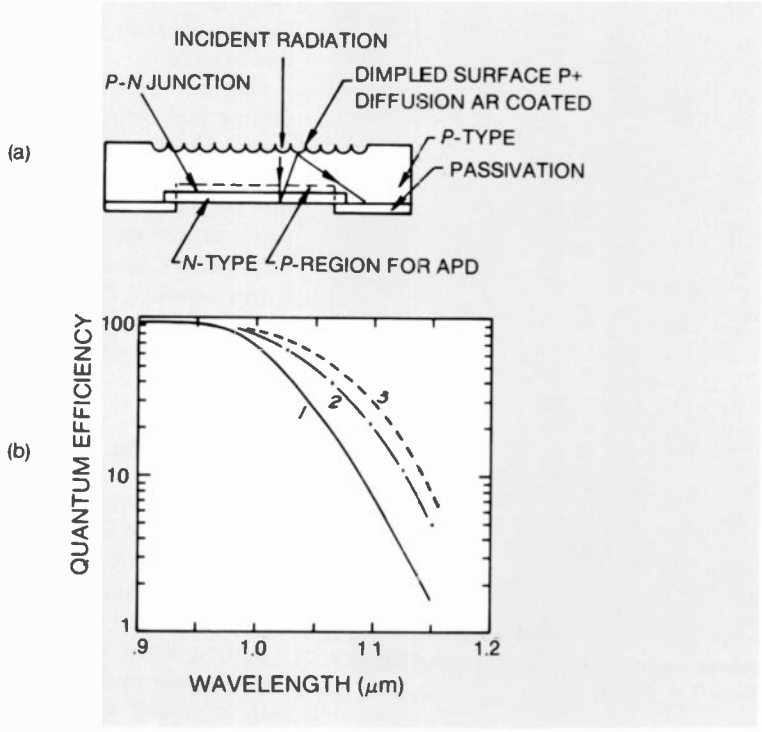


**Fig. 2. Improving IR response. (a)** Structure of APD with "dimpled" top surface to improve IR response. **(b)** Quantum efficiencies of APDs beyond 1 μm. Curve 1: standard, or plane surface diode; Curve 2: dimpled 1-mm-diameter diode; Curve 3: dimpled 3-mm diode.

these devices, the reflective losses in the blue and the near ultraviolet can be quite high. Additional losses also occur in standard devices by recombination of the photogenerated electrons at the surface or in the heavily diffused $p+$ layer before they are collected and multiplied.

By changing the impurity distribution in the $p+$ layer to minimize recombination, and by optimizing the A/R coating for shorter wavelengths, it is possible to make RAPDs with quantum efficiencies greater than 80 percent at any desired wavelength from about 0.40 μm to 0.95 μm. Figure 1 shows the spectral response of a blue-enhanced APD. Also shown for comparison is the spectral response of our standard device and that of a photomultiplier tube (PMT) with an S-20 response. Blue-enhanced APDs are well-suited for use in scintillation counting, low-light-level spectroscopy, and other applications.

## *Infrared-enhanced diodes*

Although standard RAPDs have an active region up to 110-μm thick, the response starts to fall off at wavelengths beyond about 0.95 μm where the silicon becomes more and more transparent. At 1.06 μm, for example, the absorption coefficient of silicon is only about 13 $cm^{-1}$ so that the average photon travels about 700 μm in silicon before being absorbed. Although, in the standard device, a reflective coating on the back-side ensures that a photon must traverse the active region twice before escaping, the achievable quantum efficiency with this structure is only about 20 percent.

Recently, this number has been roughly doubled by configuring the top surface of the diode (Fig. 2a) so most of the light that makes it back to the top surface without being absorbed will strike it at an angle greater than the critical angle and be reflected back into the active region, often at a large angle. To escape without being absorbed, a photon must then make it all the way out to the edge of the active region. Thus, this approach is even more effective for large diodes than for small ones. In Fig. 2b, the measured quantum efficiency of 1-mm and 3-mm diameter "dimpled" diodes is compared with that of standard devices.

Another approach to extending the quantum efficiency at long wavelengths, useful in optical communications or other applications requiring only a small sensitive area, is illustrated in Fig. 3a. In this approach, the light enters the diode parallel to the depletion layer instead of perpendicular to it and could be absorbed at any point along the whole length of the diode (2 mm in the case illustrated). The spectral response of this device is shown in Fig. 3b.

The effective quantum efficiency with this approach is poor for wavelengths less than 1 μm, because electrons generated by light absorbed between the light en-

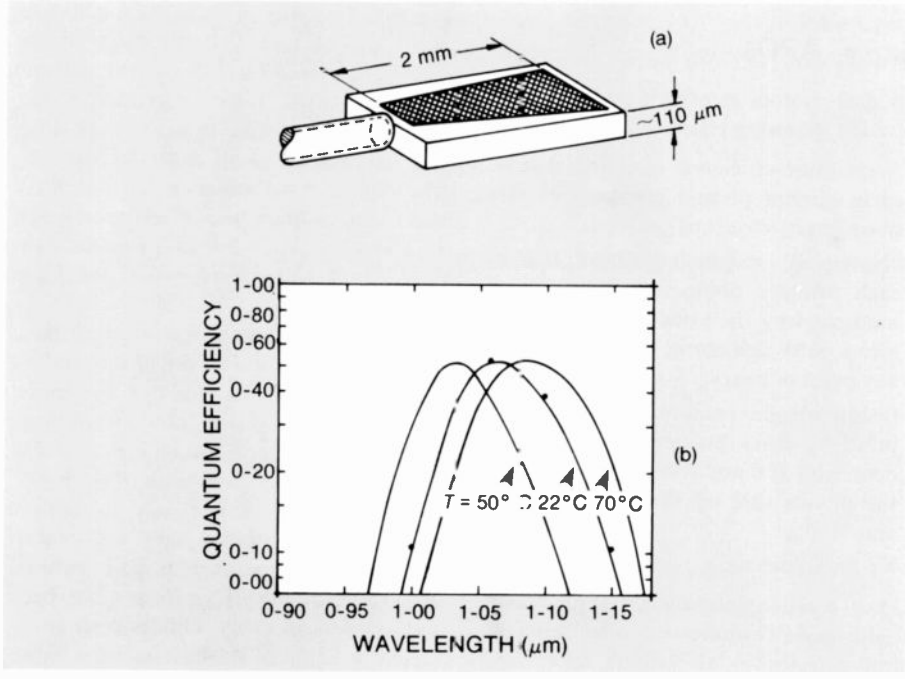


**Fig. 3. Edge-entry diodes. (a)** Schematic of edge-entry diode coupled to an optical fiber. **(b)** Quantum efficiency of edge-entry diode at three different temperatures. Curves are calculated; points are measured at room temperature.

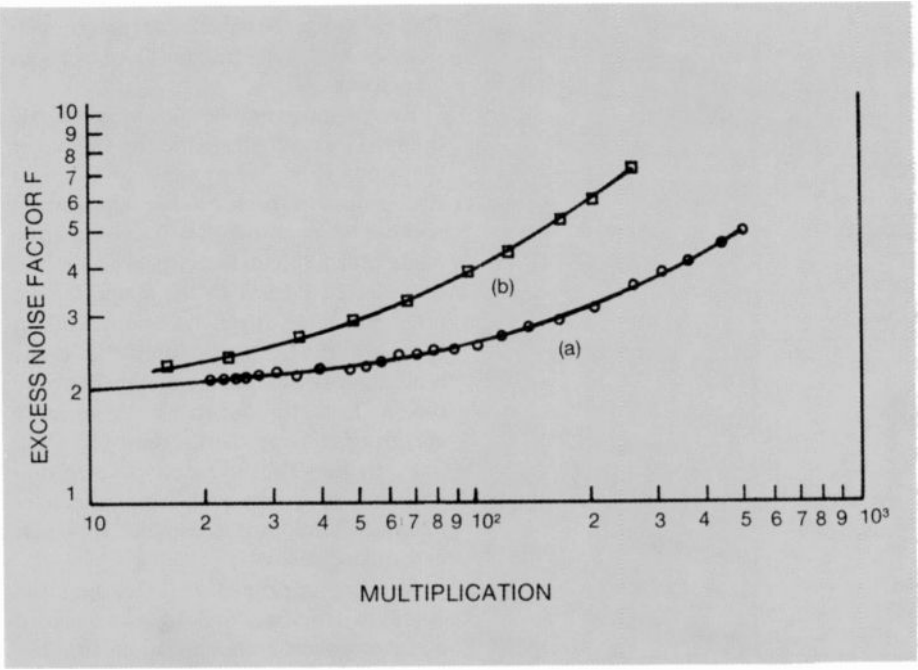


**Fig. 4. Excess noise factor.** Calculated and measured values of the excess noise factor $F$ as a function of diode gain. Curve a: $k = 0.006$; curve b: $k = 0.02$.

trance edge and the high-field region do not get multiplied; nevertheless, Q.E.s as high as 50 percent can be obtained at 1.06 $\mu$m. Another advantage is that the quantum efficiency at 1.06 $\mu$m varies only by about ±15 percent over the temperature range −40°C to +71°C. Special fiber-pigtail packages are being developed for use with this device and with other diodes requiring close coupling to an optical fiber.

## "Lo-$k$" APDs

An ideal photodetector, if it existed, would have the following characteristics:

- A quantum-efficiency of unity, that is, each incident photon generates exactly one primary electron;
- "Noiseless" high multiplication, that is, each primary photoelectron then gets multiplied by the same larger factor to give a pulse well above the noise level of any other circuitry;
- Instantaneous response so that each pulse is a delta function in time, coincident with (or uniformly delayed from) the arrival time of the signal photon; and
- No dark current.

For most high-frequency applications, a silicon APD comes close to being an ideal detector in all aspects except the second; its usable gain is limited and the multiplication process is a noisy one. As a result, the multiplied noise-in-signal is greater than it would be with a noiseless multiplier by an excess noise factor $F$ given by

$$F = kM + (1 - k)(2 - 1/M) \quad (1)$$

where $M$ is the gain and $k$ is an effective ratio of the ionization coefficients of holes and electrons.[4, 6] Typical values of $k$ are ≈ 0.01 to 0.04 for silicon APDs and 0.5 to 1 for most other materials.

For those applications requiring high gain, a lower $k$ would obviously be advantageous. One way of reducing $k$ is to fabricate diodes with a lower value of the electric field (and therefore higher voltage) in the avalanche region. Conradi, *et al.*,[7] showed that using our present $p$-type dose, but varying diffusion times to vary $V_A$ (the voltage in the avalanche region), there was a one-to-one trade-off between $k$ and $V_A$ given by $kV_A \approx 2.3$. Our present standard line of APDs has $k \approx 0.02$ and $V_A \approx$ 120 volts.

Recently, optimization studies have shown that it should be possible to reduce the $kV_A$ product by a factor of 2 or more, provided the impurity concentration in the avalanche region can be introduced in an ideal fashion. Although the "ideal" impurity profile is not easy to achieve experimentally, diodes have been fabricated which approximate its main features. As expected, the $kV_A$ product has been reduced considerably. Diodes with an effective $k$ value of 0.006 have been fabricated with $V_A \approx 200$ volts in a wide depletion-layer device and ≈160 volts in a thin device, giving a $kV_A$ product of from 1 to 1.2. Figure 4 shows the measured and theoretical excess noise factors as a function of gain.

One can show that in applications requiring high gain, the optical power required to give a desired signal-to-noise ratio is proportional to $k^{1.2}$. Thus, a reduction of $k$ from 0.02 to 0.006 should improve the detectivity by a factor of up to 1.8. Another advantage is that the gain is a less sensitive function of the doping nonuniformity, so that higher average gains can be expected in "lo-$k$" devices.

## Faster APDs

The RAPD structure is well-suited to high-bit-rate optical communications because, being fully depleted, virtually all of the photo-generated carriers are collected quickly. In most other structures at least a portion of the signal can be absorbed in the substrate material beyond the depletion layer and the carriers collected by diffusion only, giving a long tail following an initial fast response. This long tail can play havoc with the bit-error rate.

In the RAPD structure, the speed of response is determined by a combination of two components: the carrier transit time, and the multiplication time. Since the latter sets a maximum gain-bandwidth product of about 400 GHz, it is rarely a limit except at very high gains. At most practical gain levels in silicon RAPDs (<200) the response time is determined by the transit time only.

RCA's fastest production APD, the C30902E, has been optimized for optical communications at 0.83 $\mu$m and has an impulse response function with a full width at half maximum (FWHM) of about 600 ps, useful for data rates up to about 1

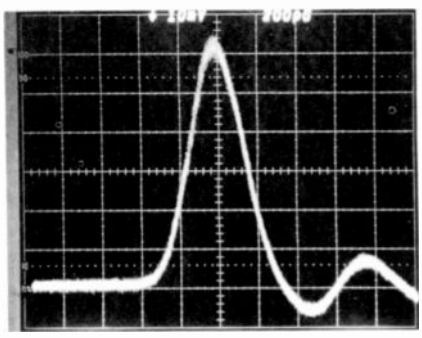

**Fig. 5. Pulse response of a "Lo-$k$" APD designed for high speed.** The FWHM is 330 ps when measured using the 900-nm source having a FWHM pulsewidth of 80 ps. The diode should be slightly faster at 530 nm.

Gbit/s. The device could be speeded up, by reducing the depletion layer width $w$ *below its present 30* $\mu$m, but at the cost of reducing the quantum efficiency. For optical communications through space at shorter wavelengths (such as using a doubled yttrium-aluminum-garnet (YAG) laser at 0.532 $\mu$m) the Q.E. does not suffer by reducing the depletion-layer thickness. Figure 5 shows the pulse response measured on a "lo-$k$" APD in which $w$ is less than 15 $\mu$m. As is evident, the FWHM has been reduced to about 330 ps.

## Multi-element APDs

In general, the desirable features for a useful multi-element APD would include the following:

- high gain;
- low noise;
- low or zero dead region between elements;
- low element-to-element cross talk; and
- high element-to-element isolation.

As will be seen in subsequent discussion, depending on the approach used in fabricating the array, certain conditions can be met, but always at the expense of one or more other factors.

The standard reach-through avalanche photodiode is fabricated with a high-field region, in which the avalanche multiplication occurs, surrounded by a low-field *pin* region. This can be seen in Fig. 2, where the $n$-layer overlaps the $p$-region. Thus, the problem of edge breakdown due to high surface fields or junction curvature is avoided. Fields in the interior of the diode are typically as high as $3.3 \times 10^5$ volts/cm, whereas fields in the surrounding *pin* region are lower by about an order of magnitude or so. In principle, a multi-element array can be made this way, but spacing of the multiplying regions would necessarily be very great if each element is to be surrounded by a *pin* region to avoid the edge-breakdown problem.

An alternative approach is one in which a single multiplying junction is used, and the $p$+ surface opposite the junction is separated into the desired array pattern by appropriate masking techniques. This method is shown in Fig. 6. Isolation of the elements is achieved when sufficient bias voltage is applied to fully deplete the device. The most desirable feature of this technique is that no decrease of gain occurs in the transition regions, and a smooth transition of signal occurs in going from one element to the next. Moreover, high gains can be achieved easily. A problem arises, however, due to the uncertain nature of the oxide-silicon interface at the crossover region. Normal oxide growth will cause an inversion layer in this area due to the high resistivity $p$-type substrate. This inversion layer can give rise to high noise and erratic behavior as any electrons generated are swept directly into the multi-plying region.

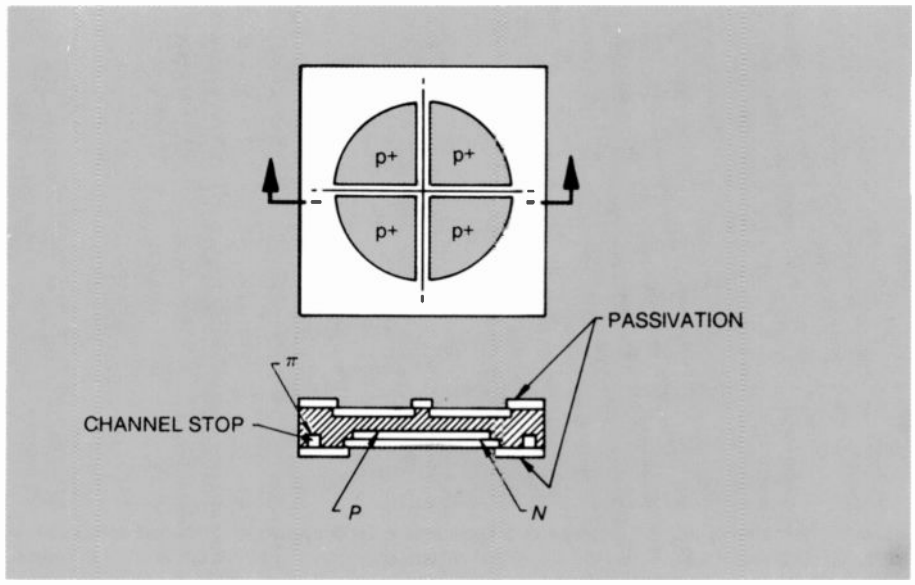


**Fig. 6. RAPD quadrant,** with elements divided on $p$+ side and a single common multiplying region.

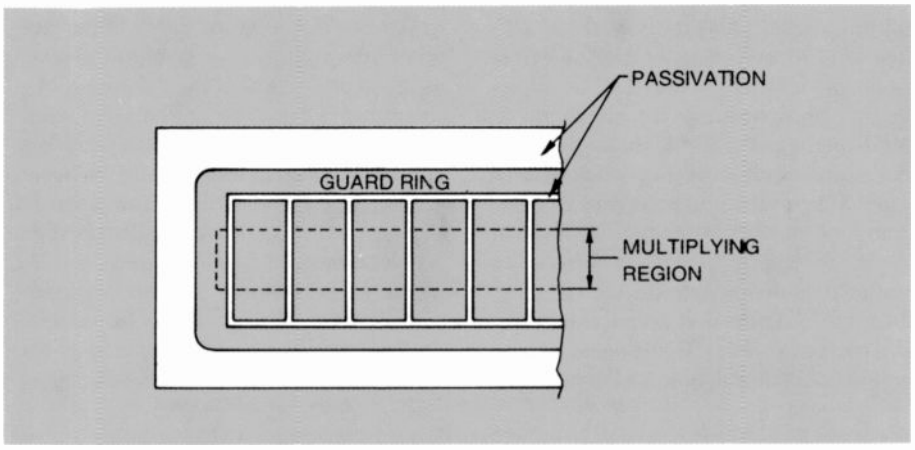


**Fig. 7. $N$+ and avalanche doping patterns on linear APD array with elements divided on $n$+ side of junction.** Center-to-center spacing is 300 $\mu$m.

In an attempt to overcome this problem, a very lightly doped $p$-layer was introduced to avoid the inversion problem. Although this technique stabilizes the array and reduces or eliminates injection from the transition-region oxide-silicon interface, the process also results in poor isolation between elements—typically about 10 k$\Omega$ to 20 k$\Omega$—severely limiting the amplifier design if unacceptable electrical cross talk and noise is to be avoided.

In yet another approach to the multi-element array, separate $n$-regions are allowed to approach each other very closely to reduce the width of the low-gain region between elements. There are certain conditions in which close spacing of the elements is possible, without resulting in edge breakdown. Under these conditions, each element is "guarded" by its neighboring elements, while the outside of the array is guarded by a *pin* region or a non-multiplying guard-ring. A portion of such an array is shown in Fig. 7. The close spacing of the elements causes the field to remain relatively high in the transition region between elements, thus minimizing the width of the low-gain region between elements.

The fabrication of such a device is made possible by the use of a self-aligning tech-

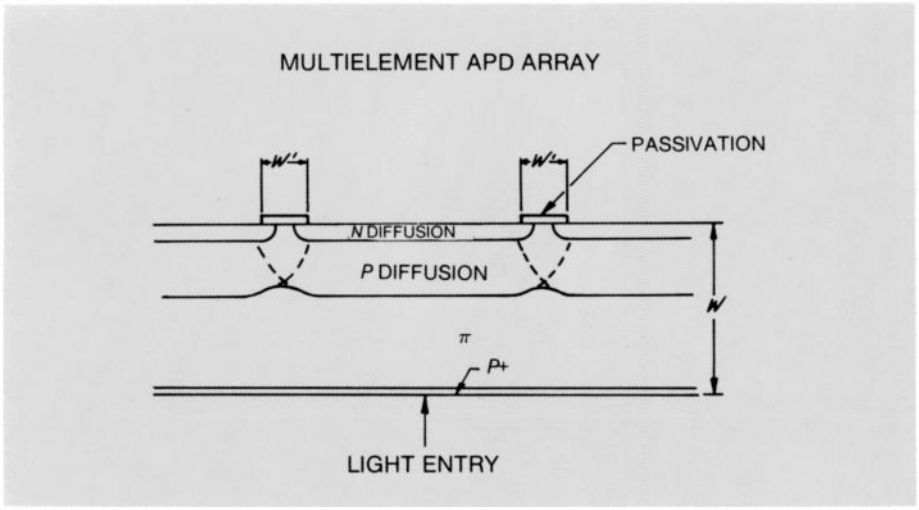


**Fig. 8. Schematic of doping profiles of *p*-type and *n*-type impurities diffused through the same self-aligning mask.** Diffusion depth for *p*-type impurities is sufficient so that diffusion fronts from adjacent elements overlap.

nique for the introduction of the required diffusion sources. A combination of oxide and photoresist masking is used to "self-align" boron and phosphorus sources in the central area of the array, while allowing only phosphorus in the peripheral or guard-ring regions. Thus, the multiplying area is surrounded by low-field regions. Figure 8 shows the relative depths of penetration of the *n*- and *p*-type diffusions. For the *n*-type diffusion, the line shows the junction depth, that is, the depth at which the acceptor and donor concentrations are equal. In order to maintain element-to-element isolation, this depth must be less than half the width of the masking passivation stripe (of width $w'$).

The line denoting the depth of penetration of the *p*-diffusion is (arbitrarily) taken as the depth at which the diffused-*p* concentration is equal to the bulk-*p* concentration. This is typically 20 $\mu$m to 25 $\mu$m, which is considerably greater than $w'$. Thus, the *p*-type diffusions from adjacent elements overlap, as shown. Provided the concentrations, diffusion depths, and the width $w'$ are chosen appropriately, the desired APD profiles can be achieved without having the electric field exceed the breakdown field in the transition region.

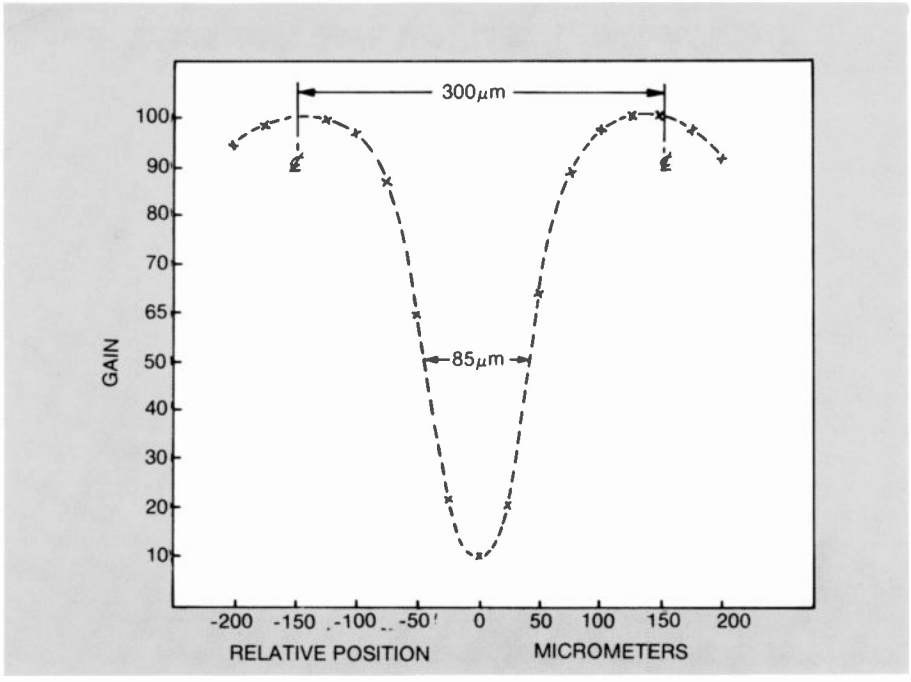


**Fig. 9. Responsivity as a function of position for two adjacent elements in diode linear array.** "Dead" width (distance between 50-percent points) is 85 $\mu$m.

Note that in operation, the diffused *p* region is completely depleted.

Experiments with a linear array, in which $w'$—the width of the passivating stripe between elements—was chosen as 14 $\mu$m, yielded inter-electrode resistances of the order of 10M$\Omega$ or more at normal operating bias voltages. Average gains of up to about 100 were achieved easily. The design of the device results in a region of low gain between elements, the width of which is dependent to some extent on the parameters of the fabrication process. For the process conditions used, Fig. 9 shows a plot of the signal in the transition region between two elements that were connected together. As noted for the diodes operating at a gain of about 100, the width of the region at the half-gain points is about 85 $\mu$m. Similar results were obtained for other arrays, and other values of gain between 20 and 100.

## Detecting single photons with APDs

If cooled sufficiently, the dark current of an APD goes essentially to zero. The voltage can then be raised above the breakdown voltage without the APD breaking down because there are no electrons or holes around to initiate the avalanche. In this state, an avalanche can be triggered by a single photon. Moreover, the breakdown current will quickly quench itself[8] provided the recharging current is limited to about 100 $\mu$A or less during the breakdown pulse. Thus, there exists the possibility of a single-photon-counting detector with high sensitivity, low-noise (all electrons multiplied equally), and with a high counting-rate capability. Such a device has been under investigation for the past few years.

Even when the voltage is above the breakdown voltage, not every electron will trigger an avalanche.[9, 10] Some electrons manage to cross the junction with no ionizing collisions; others start chains of ionizations that happen to peter out before they really get going. (It's like throwing a match in a fireplace. Not every match starts the fire.) The probability that the electron *does* initiate a breakdown pulse (the breakdown probability $P_b$) is in fact zero at the breakdown voltage and increases at higher voltages, gradually approaching unity when the maximum electric field in the avalanche region ($E_M$) exceeds the field required for breakdown ($E_B$) by an adequate amount.

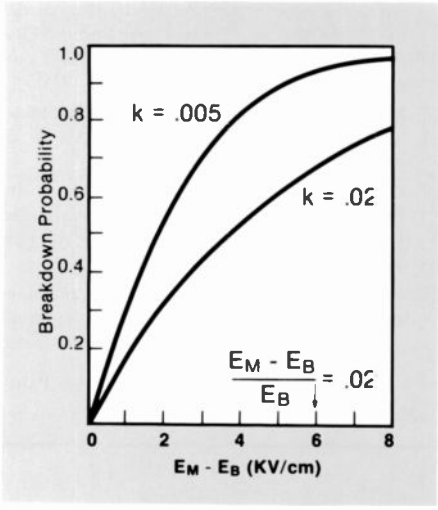


**Fig. 10. Calculated single-photon breakdown probability.** The probability is given as a function of how much the maximum field exceeds that required for breakdown.

Figure 10 shows the calculated dependence of $P_b$ on $E_M - E_B$ for diodes in which $k$ equals 0.02 and 0.005. Obviously, "Lo-$k$ devices are to be preferred for this application.

Figure 11 shows the probability $P(m)$ of an electron experiencing a gain $m$ in one of our standard APDs ($k = 0.02$) in three cases: right at the breakdown voltage ($E_M = E_B$), and at voltages above and below the breakdown voltage sufficient for $E_M$ to be greater or less than $E_B$ by 1000 V/cm (about 0.3 percent). For the case $E_M = E_B - 1000$, the average gain $M = \langle m \rangle$ is about 400. As can be seen, the vast majority of electrons experience a gain much less than 400; it is only because a few electrons experience a gain much higher than 400 that the average gain is as high as it is. It is easy to see why the excess noise factor, which is equal to $\langle m^2 \rangle / \langle m \rangle^2$, is high. When $E_M = E_B$, the only significant change is that the tail of the probability distribution now goes off to infinity. At $E_M = E_B + 1000$, the distribution is similar to the case for $E_M = E_B - 1000$, except that it is roughly 15 percent lower. That 15 percent represents the electrons that were successful in initiating a true breakdown pulse (that is, $P_b = 0.15$). The "gain" for these pulses is determined by the charge required to reduce the diode voltage to the breakdown voltage (in fact, to slightly below the breakdown voltage, due to inductance effects), and is given roughly by $(V - V_B)\,C/q$, where $C$ is the sum of the diode and stray capacitances. Typical gain values are in the $10^8$ to $10^9$ range.

Unfortunately, there is a fly in the ointment. Experimentally, although a photon is detected with a probability in good agreement with the curves shown in Fig. 10, one often gets not only one but two or more pulses, with the additional pulses occurring at times ranging from micro-seconds to kiloseconds after the first pulse and with the probability of re-ignition varying roughly as $1/t$ from the initial pulse. The number of additional pulses increases with $V - V_B$ until a critical voltage is reached at which the pulse rate gets very large even with no illumination.

While the mechanism of this phenomenon is not entirely understood, it is believed to occur as illustrated in Fig. 12. A photon is initially absorbed in the drift region (Fig. 12a) and swept into the avalanche region where a breakdown occurs, creating something like $10^8$ or $10^9$ electron-hole pairs (Fig. 12b). Also created, with low efficiency, is a light pulse consisting of roughly $10^{-4}$ photons per electron. Some of these photons (Fig. 12c) have energies greater than the bandgap and are re-absorbed in the diode, thus creating new electron-hole pairs. Most of these are collected immediately (ensuring that the whole diode breaks down, and not just one localized region). But a few (about 1 in $10^4$) are trapped (Fig. 12d), only to be released sometime later, depending on the depth of the trap. It is these trapped and re-emitted electrons which are thought to be responsible for the false pulses. The critical voltage is that voltage at which the diode gain is adequate to make the overall feedback efficiency greater than unity.

Although the device can be used in its present state with single-photon-detection efficiencies of up to 50 percent, particularly for applications where gating can be used to eliminate or reduce the false count rate, the false counts certainly limit the attractiveness of the device for general applications. Work is continuing to find ways of eliminating, reducing or circumventing this undesirable feedback effect.

## Conclusions

As the rapidly expanding field of electro-optics continues to grow, the variety of applications for which the silicon RAPD is the most suitable detector will also increase, and devices optimized for different applications will be required. In this paper we have tried to summarize some of the solutions found to date for other people's

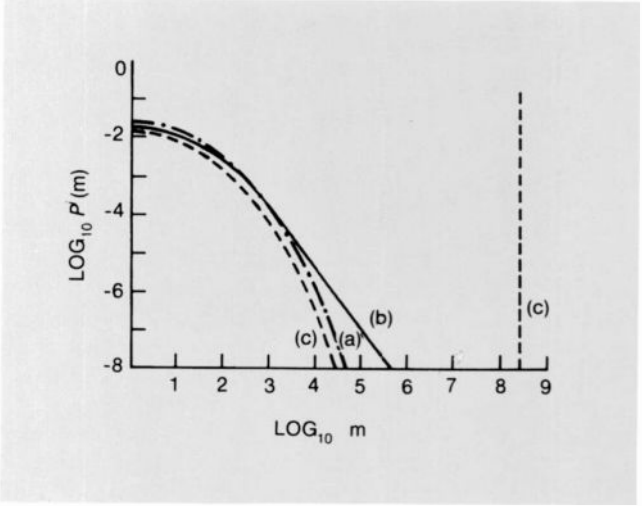


**Fig. 11. Probability $P_1(m)$ that a single electron will experience a gain $m$ for a diode with $k = 0.02$. (a)** $E_M = E_B - 1000$ V/cm; average gain = 400. **(b)** $E_M = E_B$. **(c)** $E_M = E_B + 1000$ V/cm.

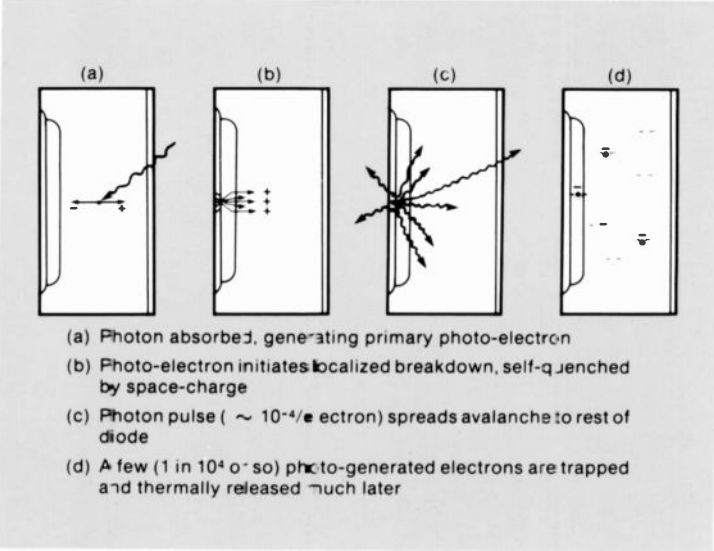


**Fig. 12. Schematic showing possible model for false-pulse generation.**

problems, with the hope that they might also be useful for yours.

## References


1. Webb, P.P. and McIntyre, R.J., "A Silicon Avalanche Photodiode for 1.06μm Radiation," Solid State Sensors Symposium, Minneapolis, Minn. (June 1970).
2. McIntyre, R.J., Sprigings, H.C., and Webb, P.P., "Solid State Detectors for Laser Applications," *RCA Engineer*, Vol. 15, No. 5, p. 32 (Feb./Mar. 1970).
3. Webb, P.P. and McIntyre, R.J., "An Efficient Low-Noise Avalanche Photodiode for Visible to 1.06 μm," *Proceedings*, Electro-Optical Systems Design Conference, East, p. 51 (1971).
4. Webb, P.P., McIntyre, R.J., and Conradi, J., "Properties of Avalanche Photodiodes," *RCA Review*, Vol. 35, No. 2, pp. 234-278 (June 1974).
5. McIntyre, R.J. and Webb, P.P., "Avalanche Photodiodes: No Longer a Laboratory Curiosity," *RCA Engineer*, Vol. 22, No. 4, pp. 52-55 (Dec. 1976/Jan. 1977).
6. McIntyre, R.J., "Multiplication Noise in Uniform Avalanche Junctions," *IEEE Trans. Electron Devices*, Vol. ED-13, p. 164 (1966).
7. Conradi, J., Webb, P.P., and McIntyre, R.J., "Silicon Reach-Through Avalanche Photodiodes for Fiber-Optic Applications," *Proceedings*, First European Conference on Optical Fiber Communications, p. 128, London (Sept. 16, 1975).
8. McIntyre, R.J., "Theory of Microplasma Instability in Silicon," *J. Appl. Phys.*, Vol. 32, No. 6, pp. 983-995 (June 1961).
9. Oldham, W.G., Samuelson, R.R., and Antognetti, P., "Triggering Phenomena in Avalanche Diodes," *IEEE Trans. Electron Devices*, Vol. ED-19, pp. 1056-1060 (Sept. 1972).
10. McIntyre, R.J., "On the Avalanche Initiation Probability of Avalanche Diodes Above the Breakdown Voltage," *IEEE Trans. Electron Devices*, Vol. ED-20, pp. 637-641 (July 1973).


**Authors (left to right) McIntyre and Webb.**


**Paul Webb** is a Senior Member of the Research & Development (R&D) Staff in the Electro-Optics Photodetectors Department at Ste-Anne-de-Bellevue. He joined RCA in 1958 and since then has been involved in a number of areas, including the study of breakdown phenomena in silicon-diffused junctions, and the development of various types of silicon and germanium nuclear-radiation detectors, and silicon photodiodes. In 1979, he was awarded, jointly with Bob McIntyre, the David Sarnoff Award for Outstanding Technical Achievement for work in photodiode development.

Contact him at:
**Solid State Division, Electro-Optics**
**Ste-Anne-de-Bellevue, Quebec, Canada**
**Phone: 514-457-9000**

**Bob McIntyre** is Manager of the Research & Development section of the Electro-Optics Photodetectors Department at Ste-Anne-de-Bellevue, where he is responsible for new device development. He joined RCA in 1956 and has spent most of his career in various types of detector development, including far-infrared detectors, sil-icon and germanium nuclear-particle detectors, and silicon *pin* and avalanche photodiodes. His main contributions have been to the theory of noise in avalanche devices. As Director of the Semiconductor Electronics Laboratory from 1967 to 1976, he was also involved in work on the design of microwave integrated circuits, computer-aided design, and surface acoustic wave devices. A Fellow of IEEE, in 1979 he was awarded, jointly with Paul Webb, the David Sarnoff Award for Outstanding Technical Achievement for work in photodiode development.

Contact him at:
**Solid State Division, Electro-Optics**
**Ste-Anne-de-Bellevue, Quebec, Canada**
**Phone: 514-457-9000**

# Pen and Podium

**Recent RCA technical papers and presentations**

**To obtain copies of papers, check your library or contact the author or his divisional Technical Publications Administrator (listed on back cover) for a reprint.**

## Astro-Electronics

D. Chu
**An Overview of Finite Element**—RCA Solid State Division, Lancaster, Pa. (1/21/82)

K. Oey | S. Teitelbaum
**SCP-050, The Next Generation CMOS/SOS LSI Spaceborne Computer**—Space Electronics Conference, Los Angeles, Calif. (1/26/82)

A. Schnapf
**Development of the TIROS Global Environmental Satellite System**—AIAA 20th Aerospace Sciences Conference, Orlando, Fla. (1/11/82)

E. Talley
**Applications of Advanced Composite Materials in RCA Satellites**—New Jersey SAMPE, Somerville, N.J. (3/18/82)

C. Voorhees
**Application 16-Channel Software Modal Test at RCA Astro**—(3/4/82)

## Automated Systems

L. Arlan | G.T. Burton | M.J. Cantella
**Performance of the Schottky-Barrier IR FPA Against Smoke Obscurants**—20th IRIS Symposium on Infrared Countermeasures, Huntsville, Ala. (3/82)

O.T. Carver
**The Need for AATPG (Analog Automatic Test Program Generation)**—IEEE AATPG Workshop, Philadelphia, Pa. (3/82)

D.J. Cushing
**Undersea Surveillance**—Maine Student Chapter IEEE, Univ. of Maine, Orono, Maine (2/82)

J.J. Klein
**IR Camera Systems for Tests, Evaluation and Demonstration of the Schottky-Barrier IR-CCD**—Electro-Optics Symposium, Princeton, N.J. (2/82)

F.F. Martin
**IR Missile Seeker System**—Electro-Optics Symposium, Princeton, N.J. (2/82)

F.P. McGurk | J.B. Perry
**Safety Considerations in the Manufacturing and Testing of Military Electronic Products**—61st Annual Massachusetts Safety and Health Conference, Boston, Mass. (3/82)

R.J. McLaughlin
**Products Developed and Manufactured at Automated Systems, Burlington**—Burlington Rotary Club, Burlington, Mass. (3/19/82)

J.D. Rickman
**Magnetic Methods of Sensing Shielded Part Motion**—1982 SAE Congress & Exposition, Detroit, Mich. (2/82)

F.R. Shirak
**Applications of General-Purpose ATE to Automated Test**—American Defense Preparedness Association, Electronic Test Equipment Symposium, Arlington, Va. (3/82)

J.H. Woodward
**Ten-Twenty Pulse per Second Nd : YAG Laser Modules**—Electro-Optics Symposium, Princeton, N.J. (2/82)

## Laboratories

R.C. Alig | S. Bloom | M. Inoue
**Optical-Mode Deformation Potential**—*Journal de Physique* (12/81)

M.T. Gale | H.W. Lehmann | E. Heeb | K. Frick
**A Simple Optical Thin Film Deposition Monitor Using LEDs and Fiber Optics**—*J. Vac. Sci. Technol.*, Vol. 20, No. 1 (1/82)

E.S. Kohn
**Scrambling and Cable-Ready TV Receivers**—Presented at the Western Cable Cable-TV Convention, Anaheim, Calif. (12/3/81)

A.G. Kokkas
**Notes: Minimum Value of the Low-Frequency Space-Charge Capacitance of MOS Structures**—*Solid State Electronics*, Vol. 25, No. 3 (1982)

A.R. Moore
**Collection Length of Holes in *a*-Si:H by Surface Photovoltage Using a Liquid Schottky Barrier**—*Appl. Phys. Lett.*, Vol. 40, No. 5 (3/1/82)

D. Redfield
**Silicon-Silicon Interfaces**—*Appl. Phys. Lett.*, Vol. 40, No. 2 (1/15/82)

H. Schade | J.I. Pankove
**Electron-Beam Induced Centers in Hydrogenated Amorphous Silicon**—*Journal de Physique*, (10/81)

## Missile & Surface Radar

O.G. Allen
**Control Charts Revisited**—American Society for Quality Control (Akron-Canton Section), 24th Annual Spring Conference, Akron, Ohio (3/20/82)

F.J. Buckley
**Software Quality Assurance**—American Society for Quality Control (Delaware Section), 9th Annual Symposium on Quality Control, University of Delaware, Newark, Del. (3/20/82)

F.J. Buckley
**Software Quality Assurance**—Society of Reliability Engineers, Portland, Ore. (3/11/82)

C.L. Christianson
**Next Generation Surface Radar Fire Control—Meeting Multifunction Needs with Modular Evolution**—American Institute of Aeronautics and Astronautics, Washington, D.C. (3/4/82)

C.L. Christianson
**Survivable SHORADS Weapons Control**—American Defense Preparedness Association, 1982 Symposium on Fire Control, White Oak, Md. (3/23/82)

T. Murakami
**Detection of Asymmetric Sideband Signals in the Presence of Noise**—*IEEE Special Issue: Historical/Classical Papers on Consumer Electronics* (2/82)

W.T. Patton
**Low-Sidelobe Phased Array Antennas for Tactical Radars**—IEEE Antennas and Propagation Society, Los Angeles Chapter, UCLA Campus, Los Angeles, Calif. (3/16/82)

L.C. Pickus
**Professional and Technical Writing**—IEEE SOUTHCON '82, Orlando, Fla. (3/23/82)

R.L. Schelhorn
**New Porcelain Coated Metal Core Substrate Materials for Chip Carrier Circuit Applications**—NEPCON WEST, Anaheim Convention Center, Anaheim, Calif., (2/23/82); NEPCON *Proceedings* (1982)

## Solid State Division

R.H. Zeien
**Design, Handling and Assembly, and Utili-**

**zation of the 0.040" Chip-Carrier Family**—Presented at NEPCON Cental '81, Rosemont, Ill. (9/23/81)

R.H. Zeien
**JEDEC Standardization of the 0.040" Chip-Carrier Package Family**—Presented at EIA/JEDEC VHSIC Packaging Seminar, Arlington, Va. (5/18/82)

R.H. Zeien
**Manufacturing Technology for Hermetic Chip-Carrier Packaging—0.040" Family**—Presented at VHSIC Packaging Workshop, U.S. Army ERADCOM, Ft. Monmouth, N.J. (9/15/81)

# Engineering News and Highlights

## Decker is Director of ATL

**Dr. C. David Decker** has been appointed Director of the Advanced Technology Laboratories of RCA's Government Systems Division. He is responsible for all activities of the organization, which develops technologies in computer systems, applied physics, solid-state circuits, electro-optics, signal processing, and systems development.

Prior to joining RCA, Dr. Decker was Research Manager of GTE Laboratories' Advance Technology Laboratory in Waltham, Massachusetts. He initiated and supervised basic and applied research programs in non-linear optics, intelligent robotics, applied mathematics and statistics, laser chemistry, organic chemistry, biochemical control mechanisms, polymer science, and electro-magnetic phenomena.

From 1973 to 1979, Dr. Decker was employed by GTE Sylvania's Electro-Optics Organization (EOO) in Mt. View, California. As Research and Development Department Manager, Dr. Decker was responsible for research and development efforts leading to new products and systems for government and commercial markets. He initiated and managed GTE Sylvania's high-power ultraviolet excimer laser business. Dr. Decker also was program manager for several tunable-laser and nonlinear-optics contracts.

Dr. Decker received his bachelor's degree, *cum laude*, in physics from Wabash College in 1967, and his master's degree in applied physics from Harvard University in 1969. Dr. Decker received his doctorate degree in electrical engineering from Rice University in 1974. From September 1969 to June 1971, Dr. Decker served as a lieutenant in the U.S. Army, first as a physicist at Edgewood Arsenal, Maryland, later in Vietnam as a communications officer and battery commander with the 52nd Artillery Group. His military decorations include the Bronze Star and Army Commendation Medals.

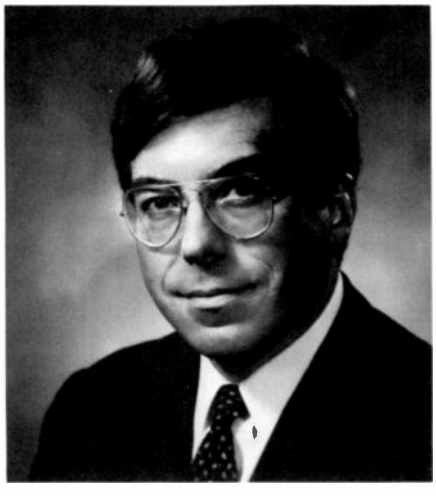

Decker

Dr. Decker is a member of Phi Beta Kappa, IEEE, Optical Society of America, American Physical Society, and Sigma Xi. From 1973 through 1978, he published nine research papers in American Physical Society and IEEE research journals.

## Former *Engineer* editor joins Service Company

Appointment of **John C. Phillips** as Manager of Business Development Planning was announced by Philip J. Martin, Division Vice-President, Business Development and Strategic Planning, RCA Service Company.

Mr. Phillips is responsible for developing ways to communicate new business concepts and features to prospective customers through proposals and presentations. He will also be working with all levels of Service Company management on internal business plans, presentations, and communications.

Prior to the appointment, Mr. Phillips was Manager of Marketing Communications and Administration for RCA Automated Systems, Burlington, Massachusetts, since October 1978. Mr. Phillips started his career with RCA in 1962 at the Astro-Electronics Division. In 1967, he was promoted to RCA's Corporate Staff to work on the *RCA Engineer*. He became Editor of the *RCA Engineer* in 1974.

## Staff announcements

### Commercial Communications Systems Division

**Dennis J. Woywood,** Division Vice-President, Broadcast Video Systems, announces the appointment of **Dr. Robert Hopkins** as Managing Director, RCA Jersey Ltd.

### Consumer Electronics

**Jack K. Sauter,** Group Vice-President, announces the appointment of **D. Joseph Donahue,** Division Vice-President and General Manager, Consumer Electronics Division.

**D. Joseph Donahue,** Division Vice-President and General Manager, Consumer Electronics Division, announces his organization as follows: **William E. Boss,** Division Vice-President, Distributor and Commercial Relations; **David I. Brenner,** Division Vice-President, Finance; **James E. Carnes,** Division Vice-President, Engineering; **Keith U. Clary,** Division Vice-President, Industrial Relations; **David E. Daly,** Division Vice-President, Product Planning and Industrial Design; **Frances V. McCann,** Division Vice-President, Public Affairs; **Charles A. Quinn,** Division Vice-President, Materials and Facilities; **Leonard J. Schneider,** Division Vice-President, Manufacturing; **James R. Smith,** Division Vice-President, Product Assurance; **Arnold T. Valencia,** President, RCA Distributing Corporation; and **Arnold T. Valencia,** President, RCA Sales Corporation.

**Peter C. Hill,** Manager, Ferrite Operations, announces the organization of Ferrite Operations as follows: **Wolfgang M. Binder,** Manager, Process Engineering; **Robert D. Cunningham,** Manager, Ferrite Quality Control; **Don Roberts,** Superintendent, Manufacturing and Test Operations; **William L. Vroom,** Manager, Ferrite Engineering; and **William C. Zenor,** Manager, Plant Maintenance.

## Corporate Engineering

**William C. Hittinger,** Executive Vice-President, announces the appointment of **George A. Kiessling,** Director, Product Safety. Mr. Kiessling will report to **Howard Rosenthal,** Staff Vice-President, Engineering.

## Solid State Division

**Larry J. French,** Division Vice-President, Solid State Technology Center, announces his organization as follows: **Philip K. Baltzer,** Head, LSI Systems; **Ronald C. Bracken,** Director, Computer-Aided Design and Photomask Operations; **John M. Herman III,** Director, IC Design & Process Development; and **David S. Jacobson,** Director, Custom LSI Products.

**Ronald Bracken,** Director, Computer-Aided-Design and Photomask Operations, announces his organization as follows: **Henry S. Miiller,** Manager, CAD Operations; **Walter F. Lawrence,** Manager, Photomask Technology and Operations; and **Lawrence M. Rosenberg,** Manager, Design Automation.

**David S. Jacobson,** Director, Custom LSI, announces the appointment of **William J. Paicius,** Manager, Quality and Reliability Assurance.

## Technical excellence

### Automated Systems Technical Excellence Achievements

The Burlington Technical Excellence Committee has selected for awards **G.R. Edgar,** Member Technical Staff, and **C.F. Matthews,** Senior Engineering Scientist, Technical Staff.

*Individual award for software development for Fighting Vehicle System vehicle*

**Glenn Edgar** contributed to improved means of program development on the Simulated Test Equipment (STE) projects through creative and innovative work, which he independently developed in response to complex technical problems. Glenn was assigned to develop the special tests for the Fighting Vehicle System (FVS) vehicle. Glenn's first contribution was the invention of a set of macro instructions, similar in many cases to standard measurement and control constructs of the STE application programming language. These macro instructions generate code that resides in the measurement processing unit of the STE test sets, and therefore the instructions execute at an order of magnitude faster than conventional DFL code. Nearly all of the special tests for the FVS applications programs were coded using this macro code.

In addition to the macro language, Glenn also conceived and implemented a pair of measurement constructs, LOGICHECK and CASE, which have revolutionized the testing and diagnostic capabilities of the STE-M1/FVS test system. Glenn was presented with the problem of making multiple measurements on different vehicle test points, many of them digital logic signal levels. Conventional measurement of one signal at a time required expansive flowchart representation and memory. Glenn developed two new "measurement" constructs that were added to the DFL software system.

The benefits to RCA from both of these software developments have been considerable. First, Glenn was able to produce all of the special test code for FVS without programming assistance, which is estimated to have saved 12 man months of coding and validation. Second, the documentation for this code is easy to prepare and understand, making maintenance of this code far easier than conventional assembly-language coding. Third, these software innovations have already saved computer memory through more efficient use of code and constructs. The saving to date on FVS is at least 20 kbytes of memory. Fourth, the constructs have made possible the expansion of diagnostics on the FVS program far beyond that previously considered practical.

**Automated Systems Technical Excellence:** From left to right, **D.M. Priestley,** Chief Engineer; **A.T. Hospodor,** Vice-President and General Manager, Automated Systems; **Glenn R. Edgar;** and **R.T. Cowley,** Manager, Vehicle Test Systems Engineering.

*Individual award for tactical information functional flow analysis*

**Fred Matthews** achieved outstanding technical results in the systems-analysis work that he carried out on a study contract for the Air Force. Fred was responsible for the day-to-day technical direction on the pro-

**Automated Systems Technical Excellence:** From left to right, **D.M. Priestley,** Chief Engineer; **Mrs. Matthews; A.T. Hospodor,** Vice-President and General Manager, Automated Systems; **C.F. Matthews;** and **E.M. Stockton.**

gram. The functional analysis that he performed required:

- An extensive understanding of similarities and differences in Air Force organizations, regulations and procedures in Europe and the Pacific, and for the Tactical Air Command/Rapid Deployment Forces;
- Judicious application of the Functional Flow Diagrams and Description ($F^2D^2$) top-down analysis methodology; and
- Use of operational analysis skills and logic to fill the data gaps, resolve differences, and determine the logical flow of information and procedures.

Particularly outstanding was Mr. Matthews' generation of tables and figures that facilitated the understanding of the text material in the report. Also, he personally wrote most of the final report volumes.

In addition to the RCA recognition of the technical excellence of this accomplishment, letters of commendation were sent by several of the Air Force Commands using the study results, including RADC Griffiss AFB, TAC Headquarters Langley Field and USAF Eu• pe.

## GCS team receives Technical Excellence Award

**GCS team (left to right): Glenn D. Adair, James Y. Higashi, Allen L. Starr, Debra Hamilton, Mark L. Grande, Clement C. Montgomery, Rebecca Paladino, George D. DeRosa,** and **Fredric Moeller.** Ms. Paladino is the Unit Manager of the group that won the award.

The Government Communications Systems Technical Excellence Committee has made a team award to the group responsible for the software development phase of the Integrated Radio Room Trainer Program. The members of this team are:

**Glenn D. Adair**
**George D. DeRosa**
**Mark L. Grande**
**Debra Hamilton**
**James Y. Higashi**
**Fredric Moeller**
**Clement C. Montgomery**
**Allen L. Starr**

During the extremely tight but contractually required 13-month development cycle, the team conceived a common design for convenient flexibility and control of both Trainers, developed a general purpose software architecture for supporting classroom training, and designed a syntax language through which the instructor can define the simulator stimuli and required trainee responses. Over 12,000 lines of code were written and no software trouble reports were written during the customer's final acceptance testing.

## GCS gives Technical Excellence Award

The Government Communications Systems has made an award to **Don Comninos** of Systems Engineering for his outstanding achievement in the total system design of the Integrated Radio Room (IRR) operational trainer and the maintenance trainer. These equipments are used to train line Naval personnel in the operation and maintenance of the IRR system and are extremely cost effective in that the training hardware cost less than 10 percent of the operational equipment.

One of the major contributions Don provided to the maintenance trainer was to develop a scheme to train in test-equipment use with simulated probes, simulated test points, and software-simulated oscilloscope waveforms. Several innovative CAI (computer-aided-instruction) features were developed by Don to enhance the trainer's scope and utility. This was RCA's first contract with this customer and since the customer is extremely pleased with the results, we not only enhanced our image, but can now qualify as a bidder for further procurements.

# Professional activities

## Astle, Staras, and Woodward named Fellows of Technical Staff

Appointment of **Brian Astle, Harold Staras,** and **Oakley M. Woodward** as Fellows of the Technical Staff has been announced by William M. Webster, Vice-President of RCA Laboratories, in Princeton. In naming the new Fellows, Dr. Webster said that the designation is comparable to the same title used in universities and technical societies. It is given by RCA in recognition of a record of sustained technical contributions in the past and in anticipation of continuing technical contributions.

A native of England, **Mr. Astle** received a B.A. degree in physics, with honors, in 1960. and an M.A. degree in 1964, both from

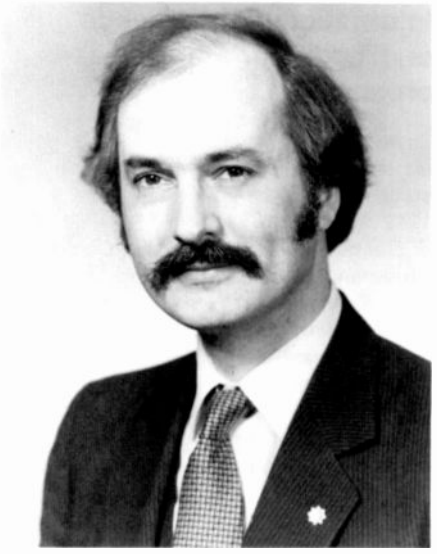

Astle

Staras

Woodward

Cambridge University. He has also taken postgraduate work at Oxford and Purdue Universities. Mr. Astle worked for RCA in Indianapolis, from 1967-1970. He returned to RCA in 1974 as a member of the technical staff in the Advanced Systems Research Laboratory. In 1978 he received an RCA Laboratories Outstanding Achievement Award for his contributions to the automatic set-up part of the RCA TK-47 broadcast camera.

**Dr. Staras,** a native of New York City, received a B.S. degree in 1944 from the City College of New York, an M.S. degree in 1948 from New York University, and a Ph.D. degree in 1955 from the University of Maryland, all in physics. After joining RCA Laboratories in 1955, Dr. Staras was engaged in research primarily in radio wave propagation through many different media. Later, as head of the radio systems research group from 1967 to 1973, he directed development of several automobile electronic systems, including a collision avoidance radar. Since 1973, Dr. Staras has been a staff scientist engaged in system analysis and planning of satellite communication systems. Dr. Staras was a Guggenheim fellow in 1961-1962 studying radio communications appropriate for developing countries. He is a member of the Consultative Committee on International Radio, the International Radio Scientific Union and the FCC advisory committee on direct broadcast satellites.

**Mr. Woodward,** a native of Davis, Oklahoma, received a B.S. degree in electrical engineering in 1938 from the University of Oklahoma. He joined the RCA Manufacturing Co. in 1941 and transferred to RCA Laboratories in Princeton the following year, where he worked primarily on antenna research and development. In 1961, Mr. Woodward transferred to RCA Missile and Surface Radar in Moorestown. He returned to RCA Laboratories in 1977 as a member of the Consumer Electronics Research Laboratory. Mr. Woodward has received six RCA Outstanding Achievement Awards for his development of various types of antennas. He has authored or co-authored 17 technical papers and has been issued 38 U.S. patents. He is a life member of the Institute of Electrical and Electronics Engineers and a member of IEEE groups on antennas and propagation and on microwave theory and techniques.

## Thirty-seven scientists honored at RCA Labs

**Dr. William M. Webster,** Vice-President, RCA Laboratories, Princeton, announced that thirty-seven scientists have received RCA Laboratories Outstanding Achievement Awards for contributions to electronics research and engineering during 1981. Recipients of individual awards are:

**Hammam A. Elabd,** for contributions to the science and technology of Schottky-barrier infrared detectors that have led to the development of high-performance infrared CCD imagers.

**Karl F. Etzold,** for the development of interferometric techniques that allow direct measurement of VideoDisc cutterhead motions.

**Edward C. Fox,** for significant contributions to the design of the TR-800 Broadcast Video Tape Recorder.

**Allan A. Guida,** for contributions to the optimization of traffic capacity in multicarrier satellite transponders.

**Karl G. Hernqvist,** for the development of a method of prevention and recovery of blocked apertures in color kinescopes.

**Stuart S. Perlman,** for the development of a mathematical model and computer program to calculate the overall transient response of a color TV system from light image input to light image output.

Recipients of team awards are:

**Stanley Bloom, Eric F. Hockings,** and **Donald J. Tamutus,** for contributions to the invention and development of electron-optic designs leading to a high-transmission focus mask for color picture tubes.

**Francis J. Campbell** and **Norman D. Winarsky,** for contributions to the development of comprehensive techniques for the computer modeling of television deflection systems.

**Pabitra Datta, Richard W. Nosker, Richard Williams,** and **Chih Chun Wang,** for contributions leading to environmentally stable VideoDisc surfaces.

**Louis A. DiMarco, Victor S. Dunn, Mohamed E. Labib,** and **J. Roy Nelson,** for contributions in optimizing the structure and chemistry of carbon black used in VideoDiscs.

**Robert A. Dischert, Warren H. Moles, Glenn A. Reitmeier,** and **James M. Walter,** for contributions leading to the establishment of a world-wide standard sampling rate for digital-television processing distribution.

**Robert M. Evans, Stanley P. Knight, Gerald E. Theriault,** and **Albert F. Young,** for contributions to the development of a novel TV tuner.

**Ralph C.J. Ferrara, Richard M. Peterson, Anthony D. Robbi,** and **Joseph O. Sinniger,** for contributions to the development of an effective system for electronic control of four-cylinder-engines.

**Lawrence A. Goodman** and **Lubomir L. Jastrzebski,** for contributions in analyzing the origin of process-induced defects in silicon power devices and integrated circuits and developing methods to minimize their effects on device performance and yield.

**Paul Hashfield** and **Ansley W. Jessup, Jr.,** for their contributions to techniques for detection and diagnosis of communications networks.

**Edward J. Holub** and **Pierre Valembois,** for contributions in improving VideoDisc stylus micromachining.

## Cardinal named Montreal IEEE Chairman

**Rene E. Cardinal,** Engineering Specialist with the Electro-Optics Photodetectors Department, Solid State Division, Ste. Anne-de-Bellevue, Quebec, was recently elected Chairman of the Montreal Section of IEEE for 1982-83. The Montreal section comprises approximately 1900 engineers and 11 professional groups. Mr. Cardinal has been a very active member of the IEEE in the Montreal area for years, previously having held the offices of Chairman, Joint Professional Group on Microwave Theory and Techniques/Antennas and Propagation; and Secretary, Treasurer, and Vice-Chairman of the Montreal section.

## IEEE Energy Committee briefs Senate staff on photovoltaics

**David Redfield** of RCA's David Sarnoff Laboratory in Princeton helped the IEEE Energy Committee brief Senate staff members for hearings on the Department of Energy's photovoltaics program. Three other IEEE members participated in the briefing, which was put together by William G. Herrold, IEEE Energy Committee Secretary, under the guidance of the Committee Chairman, John A. Casazza. Redfield gave an overview of photovoltaics technology, described a photovoltaic power system, and discussed the trade-off between the cost and efficiency of solar cells.

## International Conference on Consumer Electronics organized

Several RCA employees are key organizers of the International Conference on Consumer Electronics being held June 9 - 11, 1982 at Arlington, Illinois. At RCA Consumer Electronics, **Eugene Lemke,** Conference Chairman, **James E. Carnes,** Program Chairman, **Kenneth Barr,** Publicity and Promotion, and **Bernie Greenstein** are active. From the Solid State Division, **Steven Chapman,** Treasurer, and **Robert Dawson** are contributing. At RCA Laboratories, scientists **Dalton Pritchard** and **Michael D. Ross** are helping to organize sessions for the conference.

## Licensed Engineer

**Charles F. Smollin,** RCA Laboratories, Princeton, recently earned a New Jersey Professional Engineer's License. He also holds an Indiana P.E. license.

---

### DO WE HAVE YOUR CORRECT ADDRESS?

If not, please return the mailing label from the back cover and write your new address below. Mail to: C.A. Gardner, *RCA Engineer*, Bldg. 204-2, Cherry Hill, NJ 08358.

Name _____ Code * _____

Street or Bldg. _____

City, State and ZIP Code, or Plant _____

_____

_____

*Please indicate the code letter(s) that appear next to your name on the mailing label.

# Editorial Representatives

**Contact your Editorial Representative at the TACNET numbers listed here to schedule technical papers and announce your professional activities.**

## Commercial Communications Systems Division (CCSD)

| | | TACNET |
|---|---|---|
| **Broadcast Systems** | | |
| *Bill Sepich | Camden, New Jersey | 222-2156 |
| Krishna Praba | Gibbsboro, New Jersey | 222-3605 |
| Andrew Billie | Meadowlands, Pennsylvania | 228-6231 |
| **Cablevision Systems** | | |
| *John Ovnick | Van Nuys, California | 534-3011 |

## Consumer Electronics (CE)

| | | |
|---|---|---|
| *Clyde Hoyt | Indianapolis, Indiana | 422-5208 |
| Francis Holt | Indianapolis, Indiana | 422-5217 |
| Chuck Limberg | Indianapolis, Indiana | 422-5117 |
| Don Willis | Indianapolis, Indiana | 422-5883 |
| Byron Taylor | Indianapolis, Indiana | 426-3247 |

## Government Systems Division (GSD)

| | | |
|---|---|---|
| **Advanced Technology Laboratories** | | |
| *Merle Pietz | Camden, New Jersey | 222-2161 |
| Ed Master | Camden, New Jersey | 222-2731 |
| **Astro-Electronics** | | |
| *Frank Yannotti | Princeton, New Jersey | 229-2544 |
| Carol Klarmann | Princeton, New Jersey | 229-2919 |
| **Automated Systems** | | |
| *Paul Seeley | Burlington, Massachusetts | 326-3095 |
| Dale Sherman | Burlington, Massachusetts | 326-2985 |
| **Government Communications Systems** | | |
| *Dan Tannenbaum | Camden, New Jersey | 222-3081 |
| Harry Ketcham | Camden, New Jersey | 222-3913 |
| **GSD Staff** | | |
| *Ed Moore | Cherry Hill, New Jersey | 222-5833 |
| **Missile and Surface Radar** | | |
| *Don Higgs | Moorestown, New Jersey | 224-2836 |
| Jack Friedman | Moorestown, New Jersey | 224-2112 |
| Graham Boose | Moorestown, New Jersey | 224-3680 |

## National Broadcasting Company (NBC)

| | | |
|---|---|---|
| *Bob Mausler | New York, New York | 324-4385 |

## Patent Operations

| | | |
|---|---|---|
| Joseph Tripoli | Princeton, New Jersey | 226-2992 |

## Picture Tube Division (PTD)

| | | |
|---|---|---|
| *Ed Madenford | Lancaster, Pennsylvania | 227-3657 |
| Nick Meena | Circleville, Ohio | 432-1228 |
| Jack Nubani | Scranton, Pennsylvania | 329-1499 |
| J.R. Reece | Marion, Indiana | 427-5566 |

## RCA Communications

| | | TACNET |
|---|---|---|
| **American Communications** | | |
| *Murray Rosenthal | Princeton, New Jersey | 258-4192 |
| Carolyn Powell | Princeton, New Jersey | 258-4194 |
| **Global Communications** | | |
| *Dorothy Unger | New York, New York | 323-7348 |

## RCA Limited (Canada)

| | | |
|---|---|---|
| Bob McIntyre | Ste Anne de Bellevue | 514-457-9000 |

## RCA Records

| | | |
|---|---|---|
| *Greg Bogantz | Indianapolis, Indiana | 424-6141 |

## RCA Service Company

| | | |
|---|---|---|
| *Joe Steoger | Cherry Hill, New Jersey | 222-5547 |
| Ray MacWilliams | Cherry Hill, New Jersey | 222-5986 |
| Dick Dombrosky | Cherry Hill, New Jersey | 222-4414 |

## Research and Engineering

| | | |
|---|---|---|
| **Corporate Engineering** | | |
| *Hans Jenny | Cherry Hill, New Jersey | 222-4251 |
| **Laboratories** | | |
| Eva Dukes | Princeton, New Jersey | 226-2882 |

## "SelectaVision" VideoDisc Operations

| | | |
|---|---|---|
| *Nelson Crooks | Indianapolis, Indiana | 426-3164 |

## Solid State Division (SSD)

| | | |
|---|---|---|
| *John Schoen | Somerville, New Jersey | 325-6467 |
| **Power Devices** | | |
| Harold Ronan | Mountaintop, Pennsylvania | 327-1633 or 327-1827 |
| **Integrated Circuits** | | |
| Dick Morey | Palm Beach Gardens, Florida | 722-1262 |
| Sy Silverstein | Somerville, New Jersey | 325-6168 |
| John Young | Findlay, Ohio | 425-1307 |
| **Electro-Optics and Power Devices** | | |
| John Grosh | Lancaster, Pennsylvania | 227-2077 |
| **Solid State Technology Center** | | |
| Judy Yeast | Somerville, New Jersey | 325-6248 |

***Technical Publications Administrators, responsible for review and approval of papers and presentations, are indicated here with asterisks before their names.**

RCA Engineer

**A technical journal published by Corporate Research and Engineering "by and for the RCA engineer"**

Bldg 204-2, Cherry Hill, NJ 08358
Forwarding and return postage guaranteed

BULK RATE
US Postage
**PAID**
Phila., Pa.
Permit No. 2906

EM MUSSELMANN
PO BOX 9
STRASBURG
PA 17579

LCTT

Printed in the U.S.A.
Form No. RE-27-3